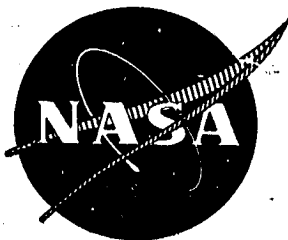# CLOSED-CYCLE GAS DYNAMIC LASER DESIGN INVESTIGATION

FINAL REPORT

by G. W. Kelch and W. E. Young

**UNITED TECHNOLOGIES CORPORATION
PRATT & WHITNEY AIRCRAFT GROUP
GOVERNMENT PRODUCTS DIVISION**

Prepared for the
NATIONAL AERONAUTICS AND SPACE ADMINISTRATION

NASA Lewis Research Center
Contract NAS3-19705

36

1. Report No. CR-135130	2. Government Accession No.	3. Recipient's Catalog No.
4. Title and Subtitle Closed-Cycle Gas Dynamic Laser Design Investigation		5. Report Date January 1977
		6. Performing Organization Code
7. Author(s) W. E. Young, G. W. Kelch		8. Performing Organization Report No. FR-7605
9. Performing Organization Name and Address Pratt & Whitney Aircraft Group Government Products Division West Palm Beach, Florida 33402		10. Work Unit No. R6862
		11. Contract or Grant No. NAS3-19705
12. Sponsoring Agency Name and Address National Aeronautics and Space Administration Washington, D. C. 20546		13. Type of Report and Period Covered Final Report
		14. Sponsoring Agency Code 5323

15. Supplementary Notes

16. Abstract

The goal of this program was to conduct a conceptual design investigation of a closed-cycle gas dynamic laser to provide definition of the major components in the laser loop. The system potential application is for long range power transmission by way of high power laser beams to provide satellite propulsion energy for orbit changing or station keeping.

The technical effort for this program was organized into three tasks. A parametric cycle optimization was conducted to establish the thermodynamic requirements for the system components. A conceptual design was conducted of the closed-cycle system and the individual components to define physical characteristics and establish the system size and weight. In the final task, technology confirmation experimental demonstration programs were outlined to develop, evaluate, and demonstrate the technology base needed for this closed-cycle GDL system.

17. Key Works (Suggested by Author(s)) Laser Gas Dynamic Laser Closed-Loop GDL	18. Distribution Statement Unclassified - Unlimited		
19. Security Classif. (of this report) Unclassified	20. Security Classif. (of this page) Unclassified	21. No. of Pages 175	22. Price * $3.00

*For sale by the National Technical Information Service, Springfield, Virginia 22151

CONTENTS

PAGE INTENTIONALLY BLANK

ILLUSTRATIONS

ILLUSTRATIONS (Continued)

ILLUSTRATIONS (Continued)

ILLUSTRATIONS (Continued)

TABLES

INTRODUCTION AND SUMMARY

The NASA has been conducting a program to investigate the application of high energy lasers to spacecraft propulsion and power transmission. The Laser Technology section of the NASA-Lewis Research Center is evaluating different types of lasers for these applications. The requirements for the laser system include multimegawatt power, continuous long duration operation, lightweight, and high overall system efficiency. The conventional open-cycle high energy lasers being developed for ground and airborne applications have relatively short run duration requirements, typically less than 60 sec. For the long run duration of the NASA missions (i.e., in excess of 600 sec), even the most efficient of the open-cycle systems would require prohibitively large quantities of reactants.

The NASA, therefore, has been concentrating on closed-cycle devices that, while being heavier and larger than an open-cycle device, do not require resupply or large reactant storage provisions. The NASA has been investigating electric discharge, chemical, and gas dynamic lasers in addition to some more advanced laser types. The study reported herein, conducted under a NASA contract, dealt with a closed-cycle gas dynamic laser. The objectives of the study were to establish the requirements of the major components of the closed-cycle GDL, define the critical components, and define the system.

The effort consisted of the following three tasks:

- The objectives of Task I were to (a) optimize a closed-cycle GDL system at 1, 5, and 10 Mw output power levels for space and airborne applications, (b) establish the design requirements of each component in the closed-loop system, and (c) provide system design tables to be used in the Task II conceptual design phase.

- Task II involved the conceptual design of the closed-cycle system and individual components selected from Task I. This effort included preparation of informal conceptual layout drawings for the hot gas compressor, diffuser, heat exchangers, gas ducts, nozzle/cavity, mirrors, output windows, and a system composite layout.

- In Task III, technology confirmation experimental demonstrations were recommended based on the technology requirements established for the closed-cycle GDL and its components. For each candidate technology demonstration, a program plan was outlined that included the type and size of demonstration test requirements, technology impact, and estimated cost.

Two different closed-cycle systems were evaluated in the study. One, called the baseline system, consisted of the device which includes the nozzle cavity and diffuser, a heat exchanger, and a compressor. Because of the high temperatures desired in the GDL cavity ($\simeq 1500°$K) for optimum performance, this baseline system requires a significant advancement in high temperature compressor technology. The second system employed a heat source between the

compressor discharge and the GDL nozzles so that a low temperature, state-of-the-art compressor would be used. To improve the efficiency of this cycle, a recuperator was incorporated between the compressor inlet and discharge to recover some of the heat that would normally be rejected from the cycle.

The systems were optimized on the basis of 1990 technology for minimum compressor drive power, considering only the components that make up the closed loop. However, to compare the two cycles (i.e., baseline vs recuperator cycles), parametric weight and volume estimates were made for the power and heat sources and the radiator.

The recuperator cycle was found to be the most desirable for both the space and airborne applications. Installation layouts were prepared using the Space Shuttle cargo bay dimensions as an envelope for the space applications, and the C-5A cargo compartment dimensions for the airborne application.

A technology demonstration program was planned, making extensive use of existing components to assemble a complete closed-cycle system. A detailed description of the program effort and its results are presented in the following sections by task.

TASK 1 - PARAMETRIC CYCLE OPTIMIZATION

Closed-Cycle GDL Description

In a typical open-cycle CO_2 GDL (shown in figure 1 as solid lines), a high pressure, high temperature mixture of CO_2, N_2, and H_2O, produced by combustion of a fuel and oxidizer with the addition of N_2, is expanded rapidly through small throat supersonic flow nozzles. This rapid expansion creates the population inversion necessary for lasing action. The laser energy is extracted from the supersonic flow in the optical cavity. The high velocity, low static pressure gas at the cavity exit is recompressed to atmospheric pressure by a diffuser and discharged to the atmosphere.

In a closed-cycle GDL (shown in figure 1 as the broken lines), the gas (a mixture of CO_2, N_2, and H_2O) after leaving the diffuser is reconditioned and circulated back to the nozzle inlet instead of being discharged to the atmosphere. Since the gas at the diffuser exit is at approximately one-third of the nozzle inlet pressure, a compressor is needed to provide the necessary pressure rise. However, the energy added by the compressor is greater than the optical energy removed; therefore, a heat exchanger is required between the diffuser and the compressor to remove the excess heat. The required compressor drive power can be reduced by lowering the compressor inlet temperature through increased heat rejection. However, when this is done, heat must be added downstream of the compressor to raise the gas temperature to the level required at the nozzle entrance. While this approach reduces compressor horsepower, it results in a very large radiator to reject heat. The radiator size can be reduced significantly and the overall cycle efficiency improved by the use of a recuperator that exchanges heat from the diffuser exit to the compressor exit, thereby reducing the heat rejected to space and the heat input from the heat source. A comparison of the base and recuperator cycle schematics is shown in figure 2.

2

OPEN CYCLE
(CLOSED CYCLE)

GAS COMPOSITION, %

CO$_2$ 14 (8)
N$_2$ 85 (91)
H$_2$O 1 (1)

DIFFUSER

OPTICAL CAVITY

NOZZLES

1600°K
800 psia

(1500°K)
(150 psia)

14.7 psia

(47 psia)

HEAT EXCHANGER OR RADIATOR

COMPRESSOR
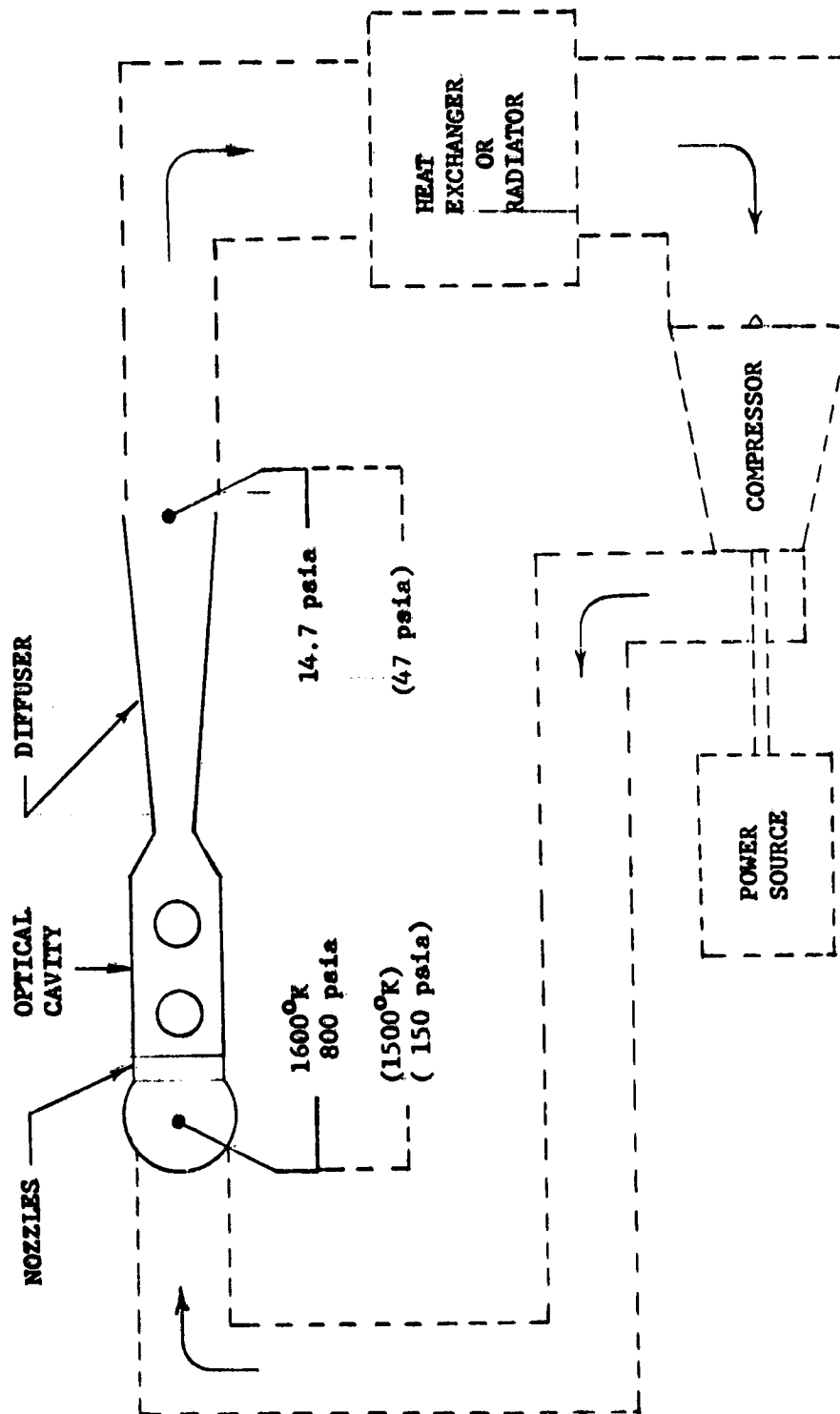
POWER SOURCE

Figure 1. Gas Dynamic Laser Schematic

3
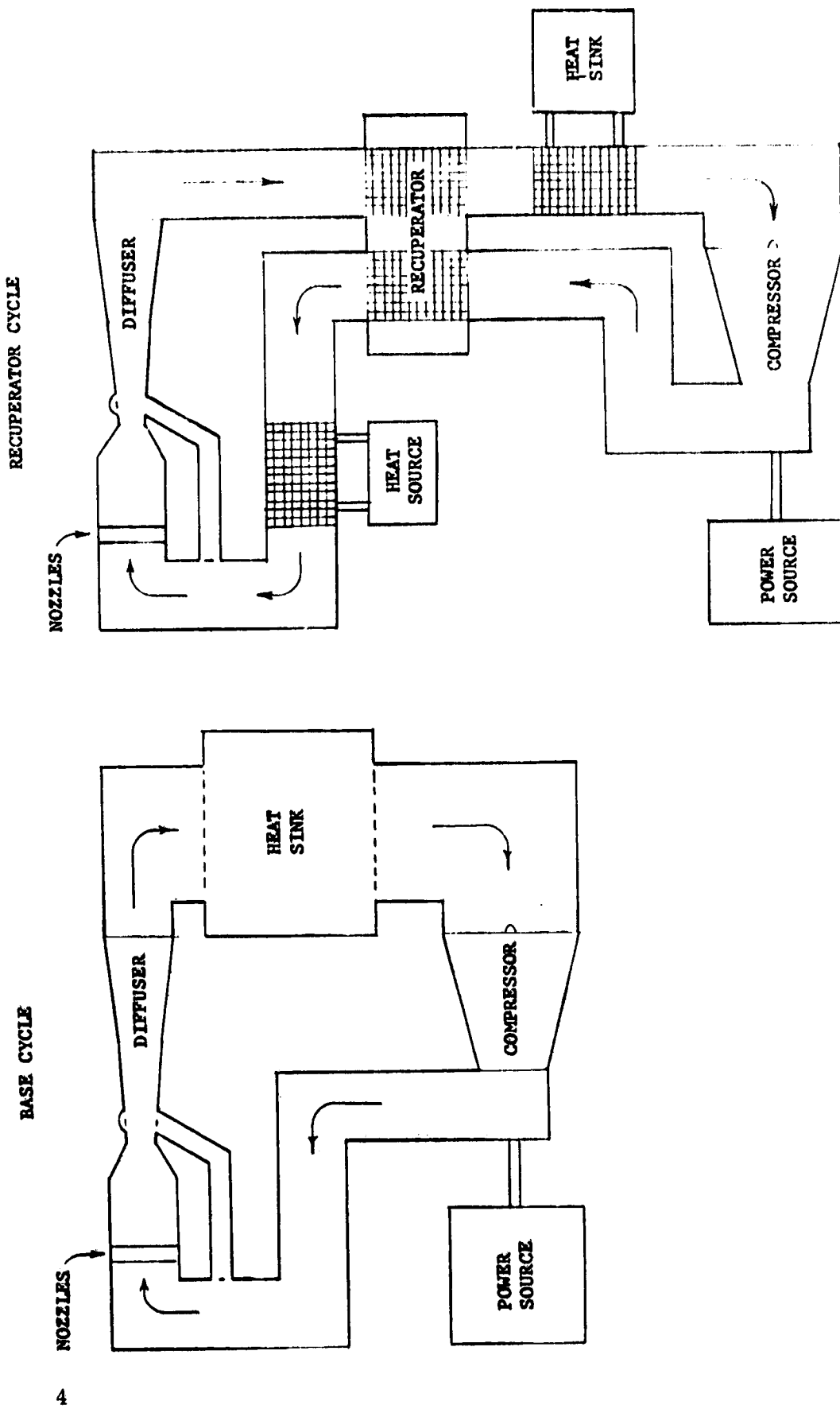
Figure 2. Closed-Cycle Schematics

These closed-cycle configurations can be evaluated or compared using a thermodynamic cycle efficiency and/or a laser/power source efficiency.

The thermodynamic cycle efficiency is defined as the laser output power divided by the sum of the thermal inputs to the laser cycle and to the power system, which supplies the compressor power. For the recuperator cycle this is:

$$\eta_{cycle} = \frac{P_{laser}}{Q_{hs} + \dfrac{HP_c}{\eta_c}}$$

where

$$P_{laser} = \text{Laser output power}$$
$$Q_{hs} = \text{Heat source rate}$$
$$HP_c = \text{Compressor horsepower}$$
$$\eta_c = \text{Compressor efficiency}$$

For the base cycle, Q_{hs} is zero.

The laser/power source efficiency is defined as the ratio of the laser output power to the compressor input power.

$$\eta_{ps} = \frac{P_{laser}}{HP_c}$$

System Optimization Approach

The optimization of the closed-cycle GDL system was performed to establish the thermodynamic requirements for the system components. The technique used to perform this optimization consisted of parametrically characterizing the performance, weight, and volume of each system component. These component characterizations were combined in a system synthesis code, which evaluated each component and performed an energy, flow, and pressure balance for the combined system to establish the cycle data for selecting the optimum design conditions. Minimum compressor drive power was the primary criterion used in the selection of an optimized cycle, with secondary consideration given to the system weight and volume. A logic diagram of this optimization technique is shown in figure 3.

This optimization technique was used on the base and the recuperator cycles for the 1-Mw system for the space application. These same cycles were optimized for the airborne application by modifying the characterization of the affected heat transfer components in the system model. The same system models were used for the evaluation of the higher power (5 and 10 Mw) systems. For these higher power systems, the cavity parameters selected as independent variables were the cavity geometry, beam diameter, optical configuration, and cavity pressure.

5

Figure 3.   Program Logic D

FOLDOUT FRAME 1

eliminary
timum
erature
rmine
tivity
tem to
%, % H_2O

Determine Interaction
of Strong
Variables (T, c, λ)
Holding Weak
Variables Constant
(P_c, % H_2O or H_2)

Sensitivity
Analysis, P_o/hp
for Critical
Parameters

K/T

ε, P_c, λ, %
O or He

T

Base System
Evaluation
(1Mw)
(Closed Cycle
Laser Model)

Design Table
Cycle
Conditions
for Max P_o/hp

Selection
of System
for Conceptual
Design

5 and 10 Mw
Systems
Evaluation

Design Tables
for 5 and 10
Mw Systems

ffuser

M (f c)

Ducting

ΔP
Volume
Weight

Alternate
Systems
Evaluation

Design
Tables for
Alternate
Systems

leed, %

Rey

Figure 3. Program Logic Diagram

The other aerothermodynamic cavity parameters previously optimized for the 1-Mw system were relatively independent of power level and were not changed for the performance evaluation of the higher power systems. The results of the system optimizations were summarized in a design table for each system and were used in the selection of systems for the conceptual design.

A more detailed description of the component characterizations and component performance trades is presented in the following paragraphs, which individually address the selection of each major component.

Component Selection and Characterization

Cavity

The laser cavity performance can be defined as a function of the following variables:

Nozzle Stagnation Pressure, P_c

Nozzle Stagnation Temperature, T_c

Gas Composition, X_i

Nozzle Area Ratio, ϵ

Beam Diameter, D_b

Optical Configuration

The cavity performance (specific power = laser output power/cavity flowrate) was determined by using gas kinetic and power extraction models developed by FRDC and confirmed by experimental data.

To facilitate the generation of a cavity performance map with the inter-action effects of all the above variables, a base point was selected about which the effect of second order variables, like optical configuration, beam diameter, and gas composition, was established. After establishment of these variables, a parametric set of data (maps) was generated as a function of stagnation pressure, nozzle area ratio, and stagnation temperature with cavity specific power as the dependent variable.

Evaluations of various optical configurations and beam diameters were made at the base point conditions given in table I.

Table I.   Cavity Base Point

Nozzle Area Ratio	–	30:1
Nozzle Throat Height	–	0.152 mm
Stagnation Temperature	–	1500°K
Stagnation Pressure	–	17 atm (250 psia)
Gas Composition ($N2/CO_2/H_2O$)	–	91/08/01 mole-%

This base point was selected on the basis of previous studies that showed these conditions provided near optimum performance for a similar application. Later

results indicated this selection of a base point was reasonably close to the optimum point eventually established.

Optical configurations were evaluated to establish the optimum configuration for generation of the parametric specific power map. In unstable oscillator configurations, some output power is coupled back through the cavity to maintain the lasing action. This is accomplished by cutting a hole in the oscillator output mirror (hole coupling mirror) and placing a small convex mirror (convex resonator mirror) in the hole to return a fraction of the power to the cavity. (See figure 4.) The laser output power and beam quality are affected by the size of the coupling hole. The parameter used to describe the size of this hole is the geometric coupling, which is defined as the ratio of the annulus area (output beam area minus hole area) to the total incident beam area.

Hole Coupling Mirror   Nozzle Exit Plane

Convex Resonator Mirror   Concave Resonator Mirror

Flow
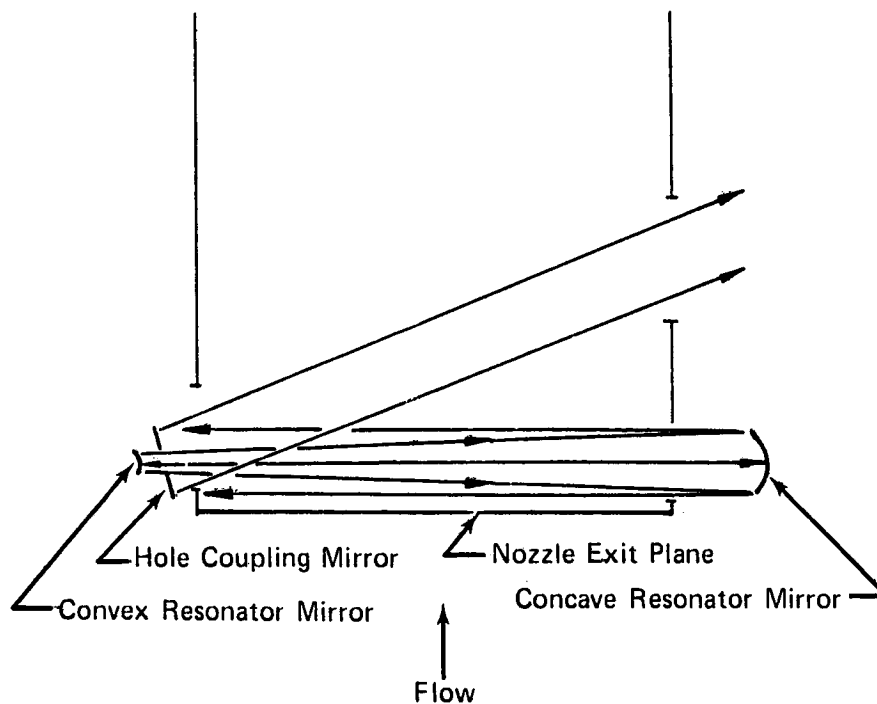
Definition of Geometric Coupling:

d_j d_o (Beam Diameter)
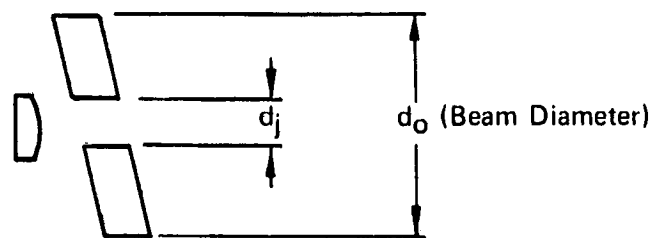
$$GC = \frac{\pi/4 \ (d_o^2 - d_j^2)}{\pi/4 \ d_o^2} = 1 - \left(\frac{d_j}{d_o}\right)^2$$

Figure 4.   Unstable Resonator Configuration

9

Schematics of the optical configurations evaluated are shown in figure 5, and the results of the evaluation as a function of oscillator geometric coupling are shown in figure 6. A beam diameter of 11 cm (cavity width, 12.6 cm) and a cavity length (in the optical direction) of 700 cm were used for this evaluation. This combination results in a power level of approximately 1-Mw. As figure 6 shows, multiple optical passes (UO/3 or 2UO/3)[1] are required to achieve a high value of cavity specific power. The multiple optical passes are required for two reasons: the small signal gain coefficient is relatively low because of the low nozzle area ratio used in the closed-cycle system compared to the area ratio used in an open-cycle system, and the active extraction region (in the gas flow direction) is relatively long (40 cm), so that multiple passes of a small beam are required to sweep the active cavity length. A much larger beam diameter would reduce the number of passes required but would yield lower performance due to low gain of the shorter optical cavity length. The geometric coupling of the oscillator, as shown in figure 6, optimizes at the relatively high value of 0.90. This value provides high beam quality, which is desired.

The 2UO/3 was selected as the closed-loop GDL optical configuration because of its higher performance level.

The performance of a ring resonator would fall between that of a single pass UO and a UO/1 because of its optical length and beam position in the cavity. Since the UO/1 has very low performance, the ring resonator was eliminated from consideration in the generation of the cavity performance map.

A beam diameter investigation was made to assess its effect on system performance. As shown in figure 7, beam diameter can be increased substantially before performance starts to decline. A 15-cm diameter beam was selected for developing the cavity extraction map.

The effect of optical configuration on beam quality (defined as the ratio of far-field power within a given spot size to power out of the laser cavity) has been determined using typical results from the Systems Optical Quality (SOQ) code. The SOQ codes are a generalized, computationally efficient, three-dimensional wave optics analysis tool developed by P&WA under Air Force sponsorship. The code defines beam distortions due to the effects of (1) apertures, (2) mirrors (figure error, thermal loading, and/or misalignment), (3) nonuniform gain (small signal and loaded), (4) refractive index inhomogeneities (due to cavity flow, aerodynamic window, etc.), and (5) thermal blooming.

Detailed determinations of typical beam quality for multiple-pass, co-annular, unstable oscillators of the type selected for this application are available from the above code. These results have been used to determine the approximate far-field performance, which can be expected for this closed-cycle GDL.

---

[1] UO = unstable oscillator
NUO = number of passes of the UO through the cavity.
The number following the slash (/) is the number of amplifier passes.

10

xUO = number of oscillator passes
/a = number of amplifier passes

UO/1

K = 8.4

UO/2

K = 9.9

UO/3

K = 10.5

UO - Ring Resonator

K = 8.4

2UO/1

K = 9.8

2UO/3

K = 11.0
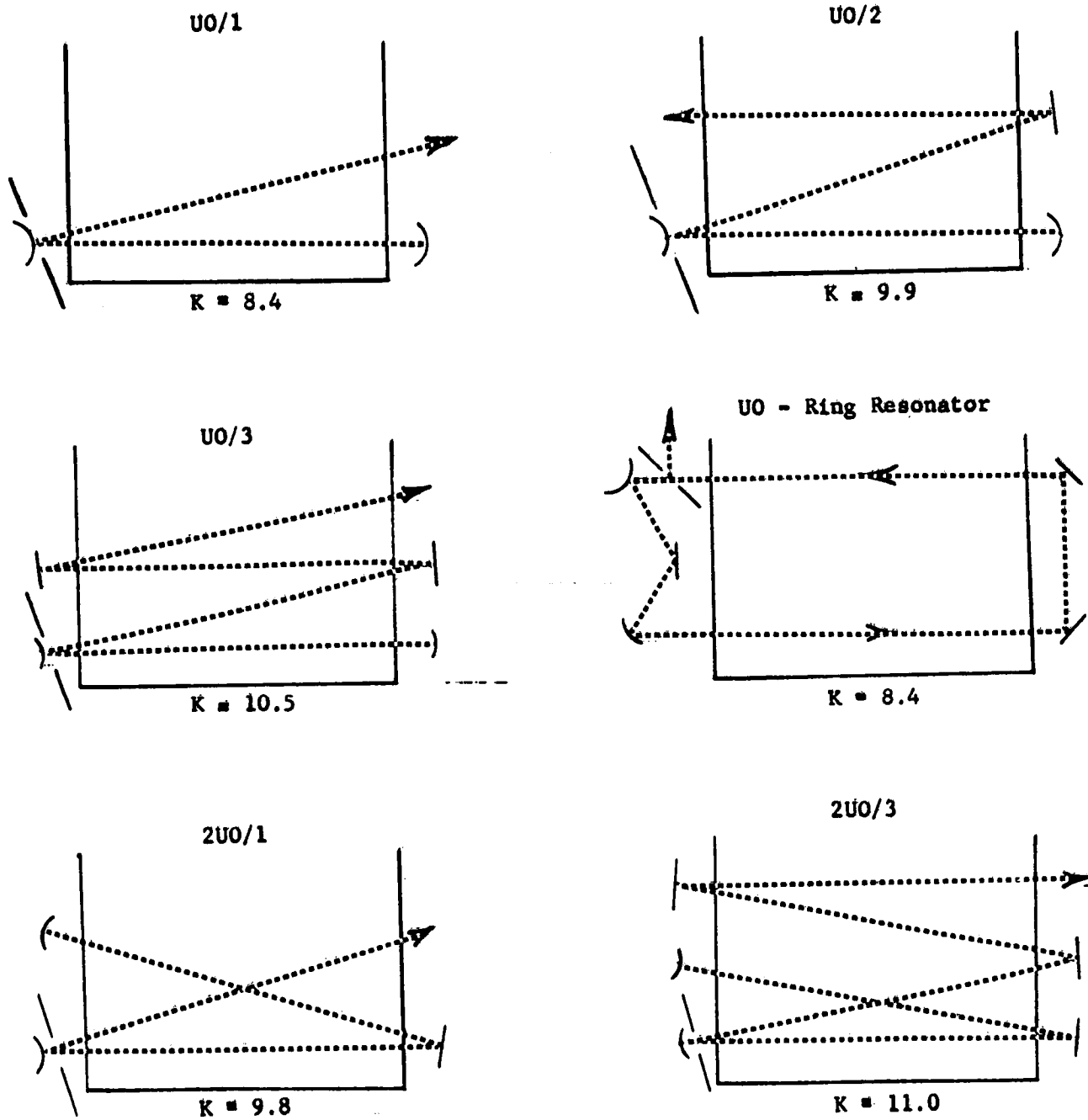
Figure 5.   Optical Configuration Schematics

11
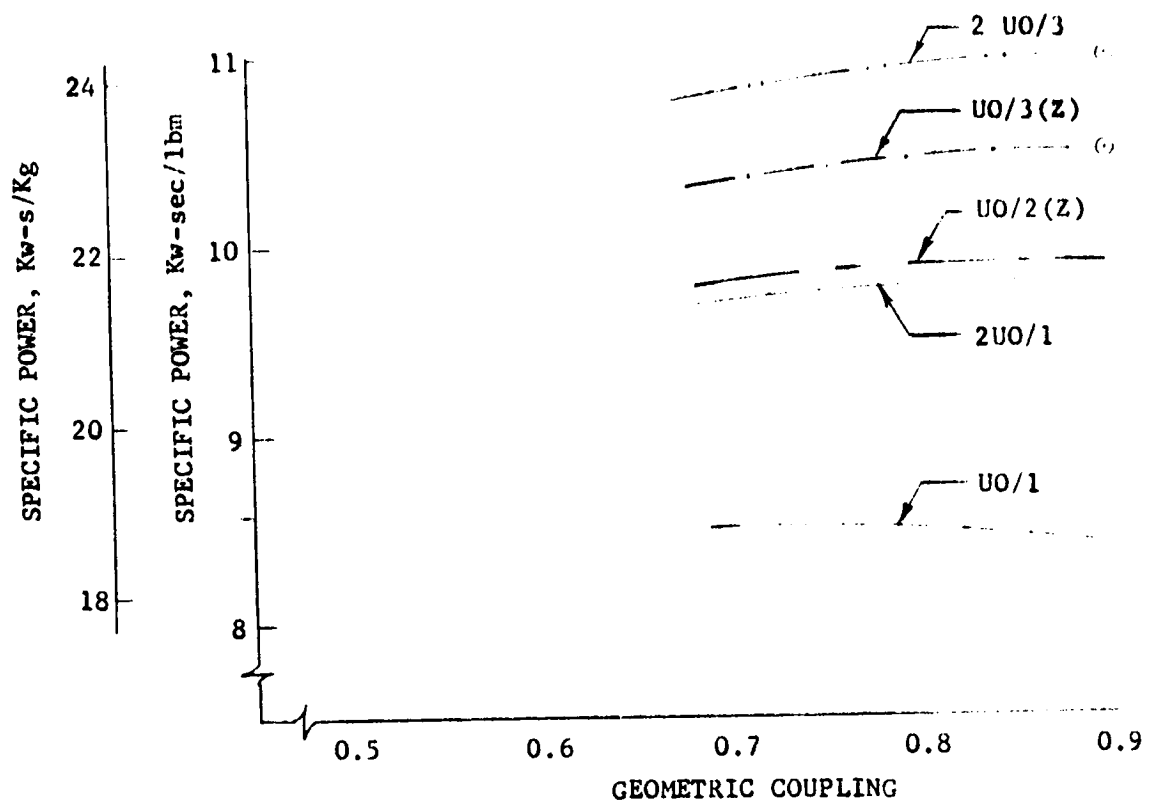
Figure 6.   Optical Configuration Investigation

1 Mw
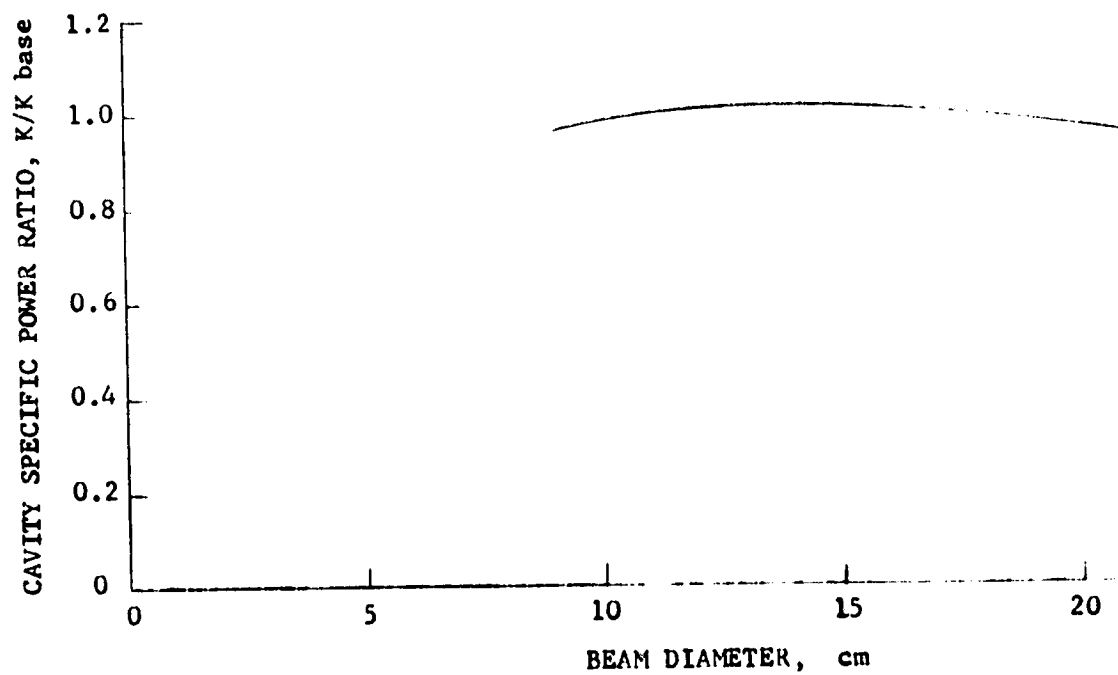
Figure 7.   Beam Diameter Evaluation

12

A comparison of the power available in a nondimensional far-field radius, n, for the ideal and actual vacuum propagation of a co-annular beam with 0.9 geometric coupling is presented in figure 8.

$$n = \frac{rD}{R\lambda}$$

where:

R = Propagation range (m)
λ = Wavelength (m)
D = Output beam diameter (m)
r = Far-field spot radius (m)
n = Nondimensional far-field radius
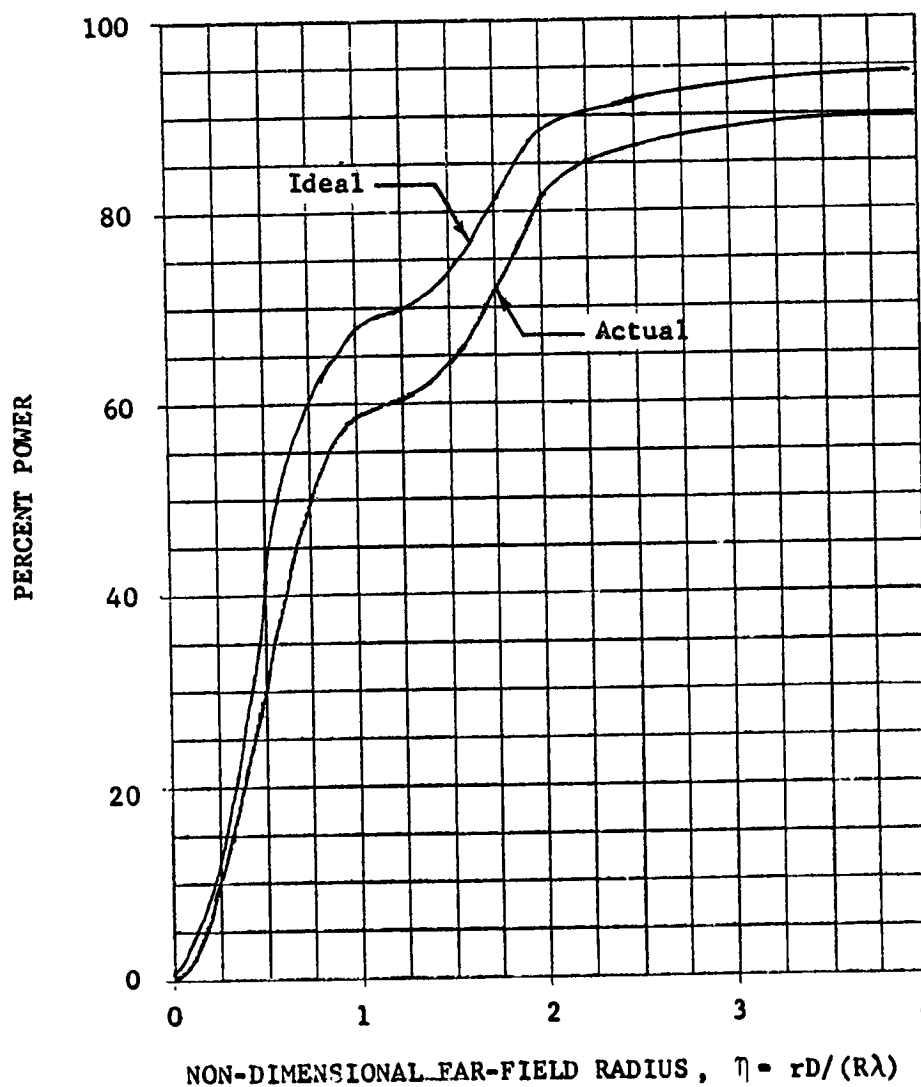
Figure 8. Typical Unstable Resonator Far-Field Performance
at High Geometric Coupling

13

A plot of the far-field nondimensional intensity distribution for the above beam is shown in figure 9. A three-dimensional view of the normalized near-field intensity distribution for this beam is shown in figure 10.

These figures indicate that approximately 60% of the near-field power is recoverable in a far-field spot of 1 $R\lambda/D$, 80% at 2 $R\lambda/D$, and 90% at 4 $R\lambda/D$. The absolute level of near-field power does not significantly affect these results.

The gas composition effect was evaluated by perturbations singularly about the base point, since this parameter has a weaker effect and its interaction with other parameters is minor. The variation in cavity performance with CO_2 and H_2O concentrations is shown in figure 11. These data indicate that the base point selection is near the optimum gas dynamic/nozzle conditions.
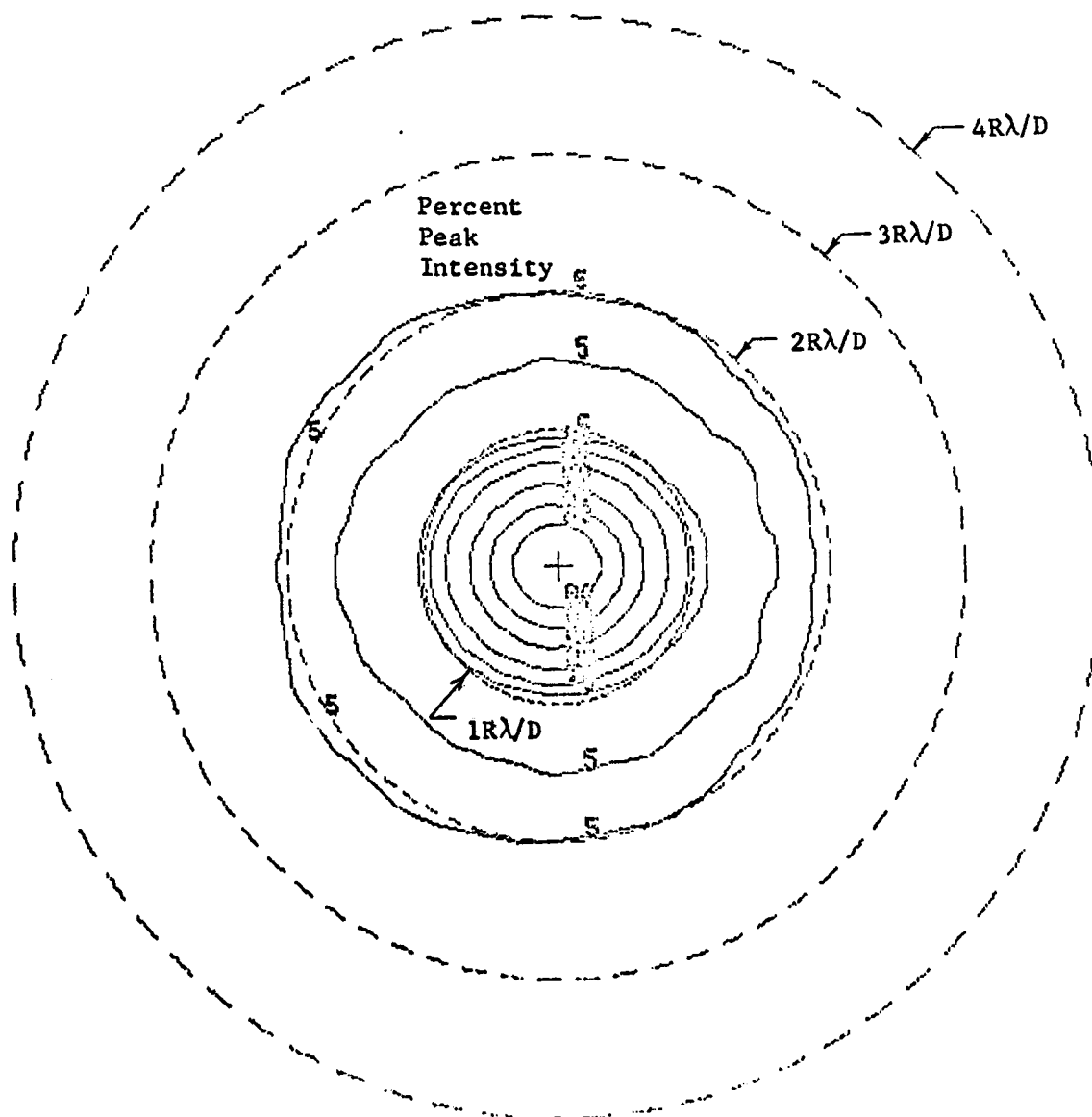
Figure 9. Typical Unstable Resonator Far-Field Intensity Distribution at High Geometric Coupling

14
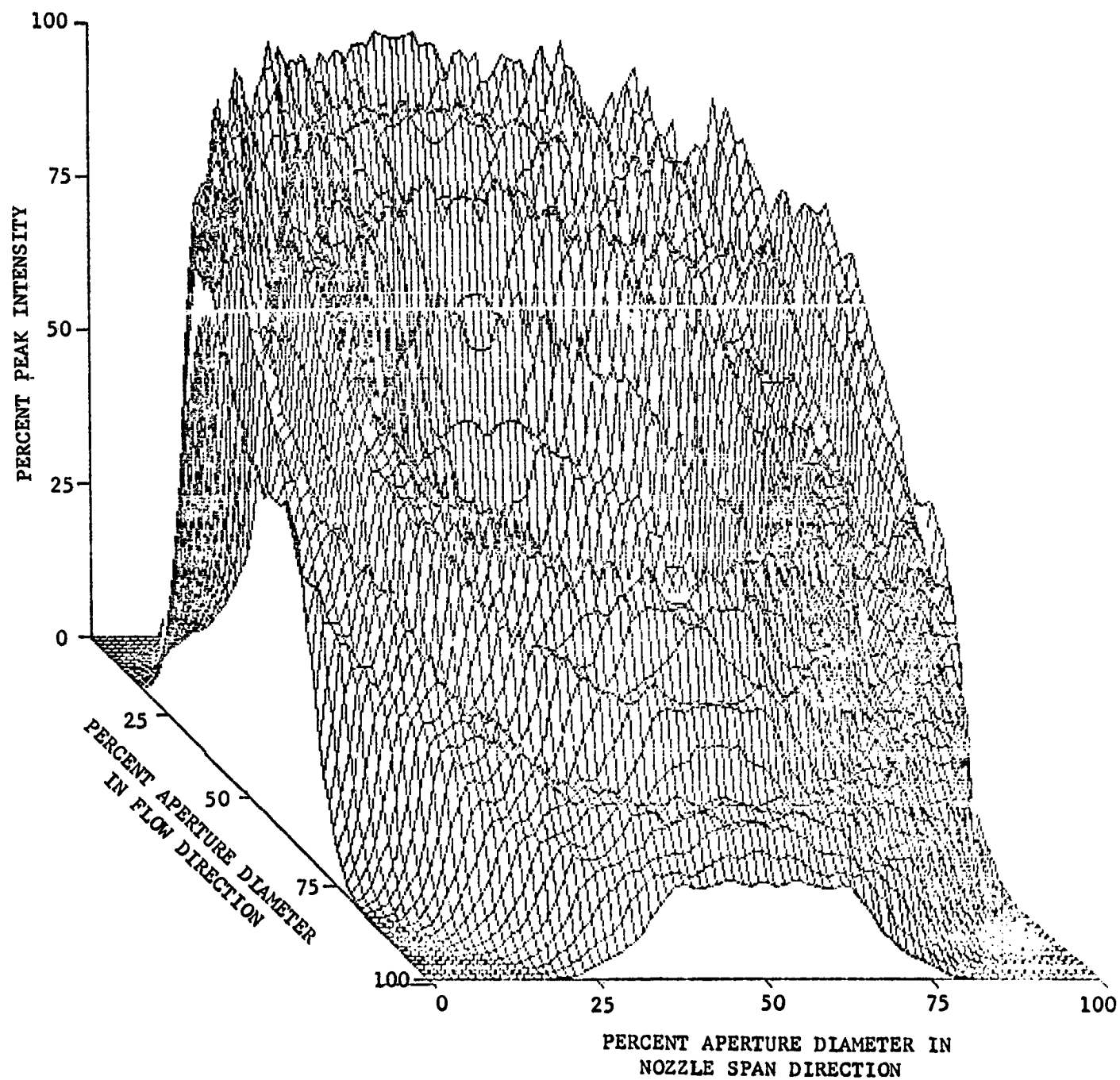
Figure 10.   Typical Normalized Near-Field Intensity Distribution
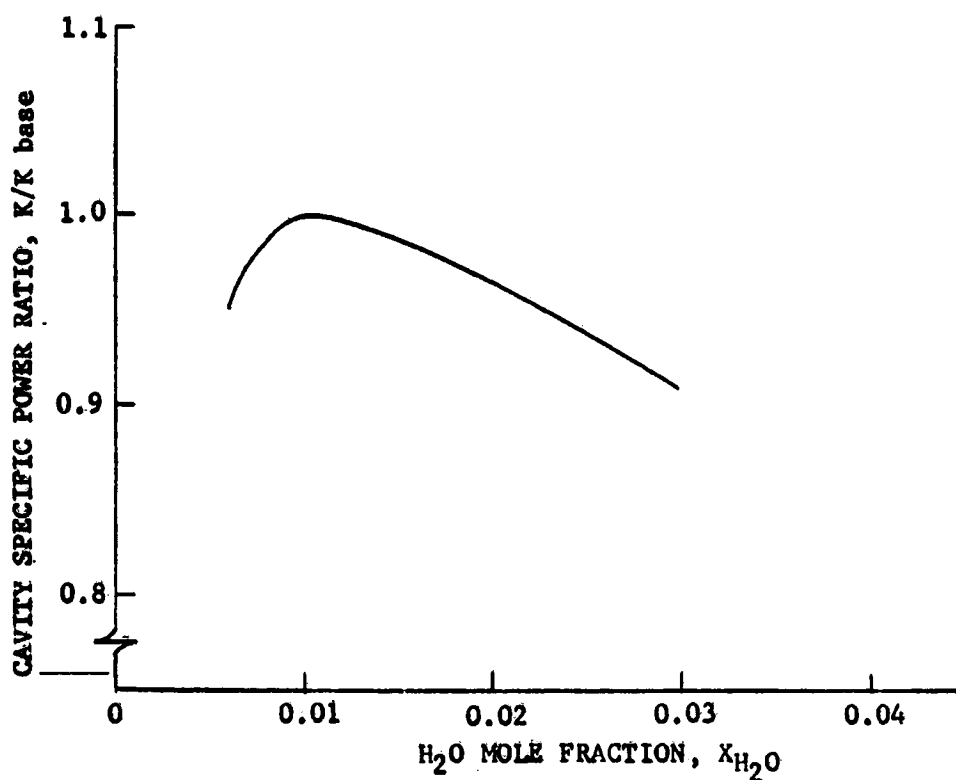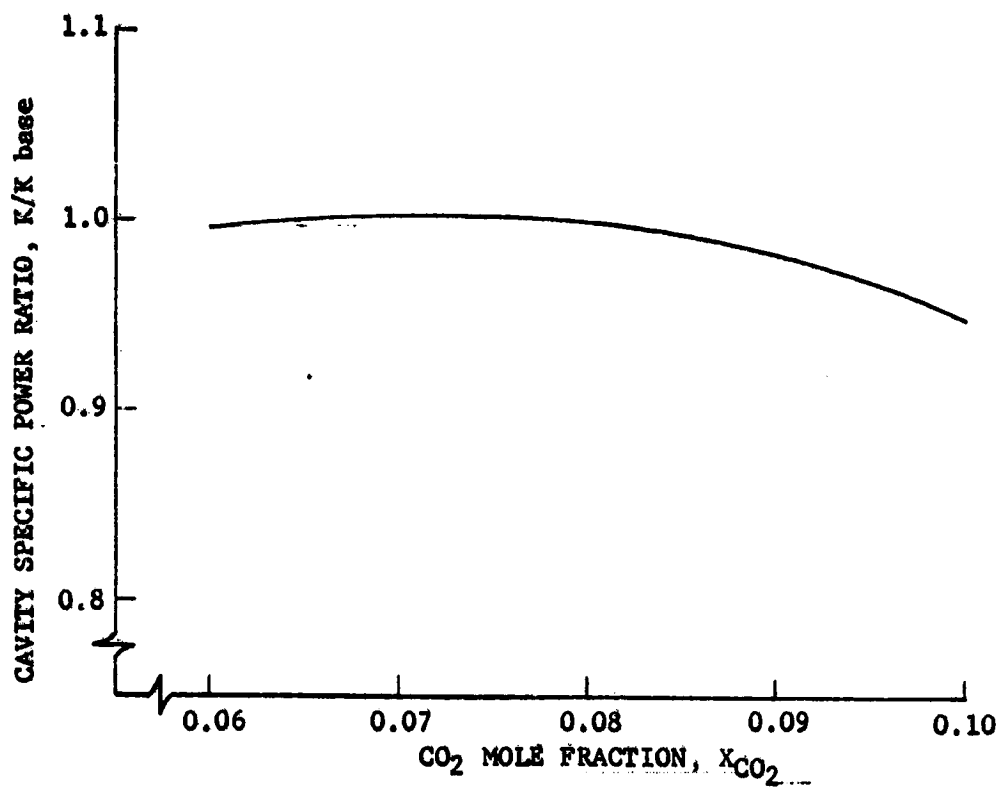
Figure 11. Evaluation of CO_2 and H_2O on Cavity Performance

Extraction analyses were made at different gas-dynamic/nozzle conditions using the 2UO/3 optical configuration, 15-cm beam, and base composition. A full parametric evaluation of stagnation pressure (P_c), stagnation temperature (T_c), and nozzle area ratio (ϵ) over the following ranges was completed.

$$P_c = 0.34 \text{ to } 3.4 \text{ MN/m}^2 \text{ (50 to 500 psia)}$$

$$T_c = 1100 \text{ to } 1600°K$$

$$\epsilon = 10 \text{ to } 40$$

The results are shown in figures 12 and 13 in the form of cavity specific power vs P_c for various area ratios at temperatures of 1600, 1500, 1300, and 1100°K, respectively. From these figures, it may be observed that the maximum specific power for low area ratio systems occurs at lower stagnation pressures. Also, the specific power advantage of high ϵ and P_c combinations decreases as cavity stagnation temperature is reduced.

Additional parameters required for the cavity characterization are the cavity pressure recovery and cavity exit Mach number. The diffuser performance is a function of the cavity exit Mach number and total pressures, which are obtained from the gas kinetics code and are presented as a function of nozzle area ratio in figure 14. The substantial total pressure loss in the cavity occurs because of the energy addition from the frozen vibrational levels to the supersonic flow field. In addition, there is a significant total pressure loss because of the boundary layer in the small grid nozzles.

Diffuser

The compressor power required to recompress the gas to the nozzle stagnation condition in the closed-loop GDL is a direct function of the total pressure recovery of the supersonic flow diffuser. Therefore, to increase the cycle thermal efficiency, it is necessary to obtain the best diffuser performance possible.

Maximum diffuser performance is obtained by compressing the supersonic flow in a converging passage through a series of weak oblique shocks until as low a supersonic Mach number as possible is achieved. Then the flow is further compressed through a series of bifurcated normal shocks in the throat section until subsonic flow is achieved. The subsonic flow is diffused in a diverging passage until a Mach number of approximately 0.2 to 0.3 is reached. Low supersonic Mach numbers from an initially high Mach number (4 to 5 in GDL systems) can be achieved with an area reduction of approximately 4 to 6 from the entrance to the throat.

The major factor limiting diffuser performance is the behavior of the boundary layer flow. Because of the grid nozzle arrays and the high aspect ratio laser cavity (width/height), boundary layer is a significant portion of the flow stream. The boundary layer is a region of relatively low kinetic energy and, consequently, is detrimental to high diffuser pressure recovery. Therefore, boundary layer control devices, such as wall suction or injection, are required to remove or energize the low energy flow.
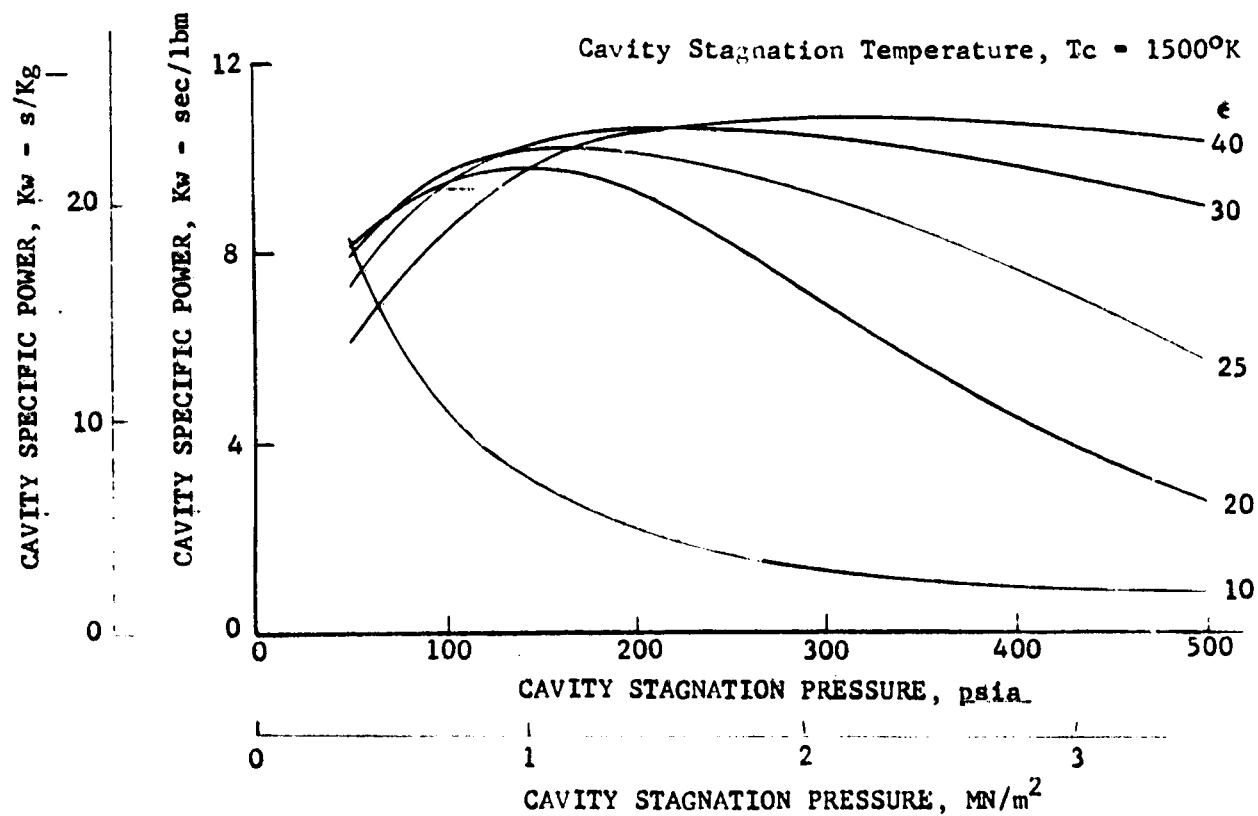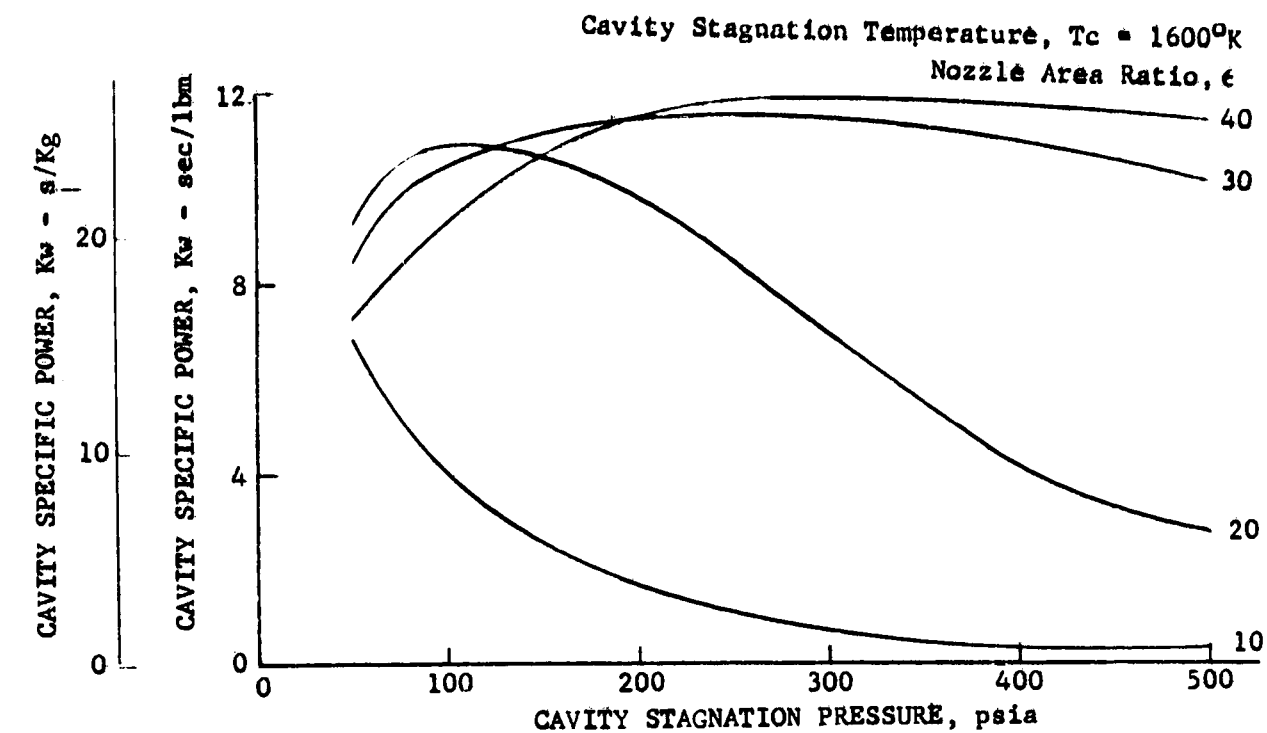
Figure 12. Effect of Cavity Stagnation Pressure on Performance

18
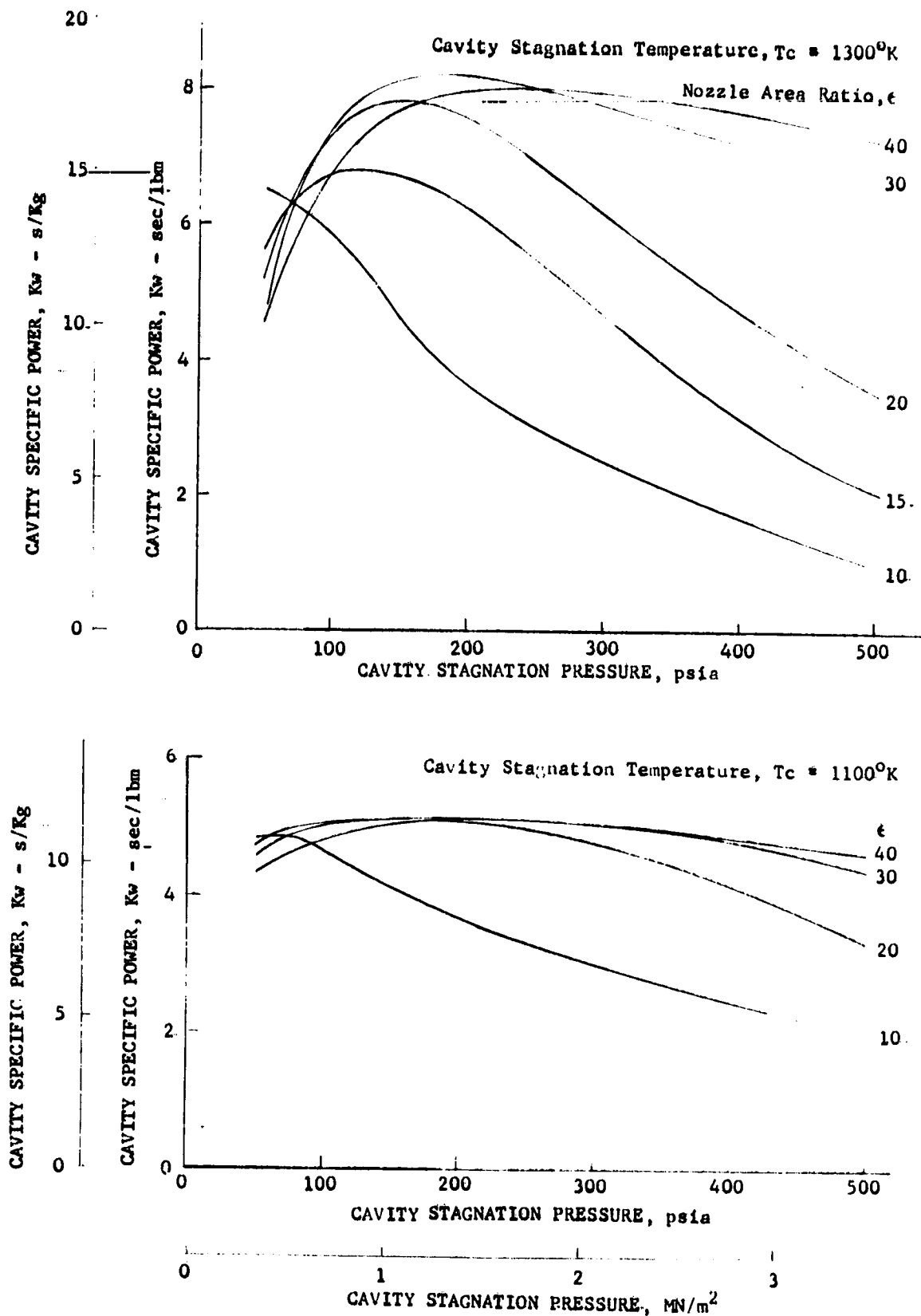
Figure 13. Effect of Cavity Stagnation Pressure on Performance

19
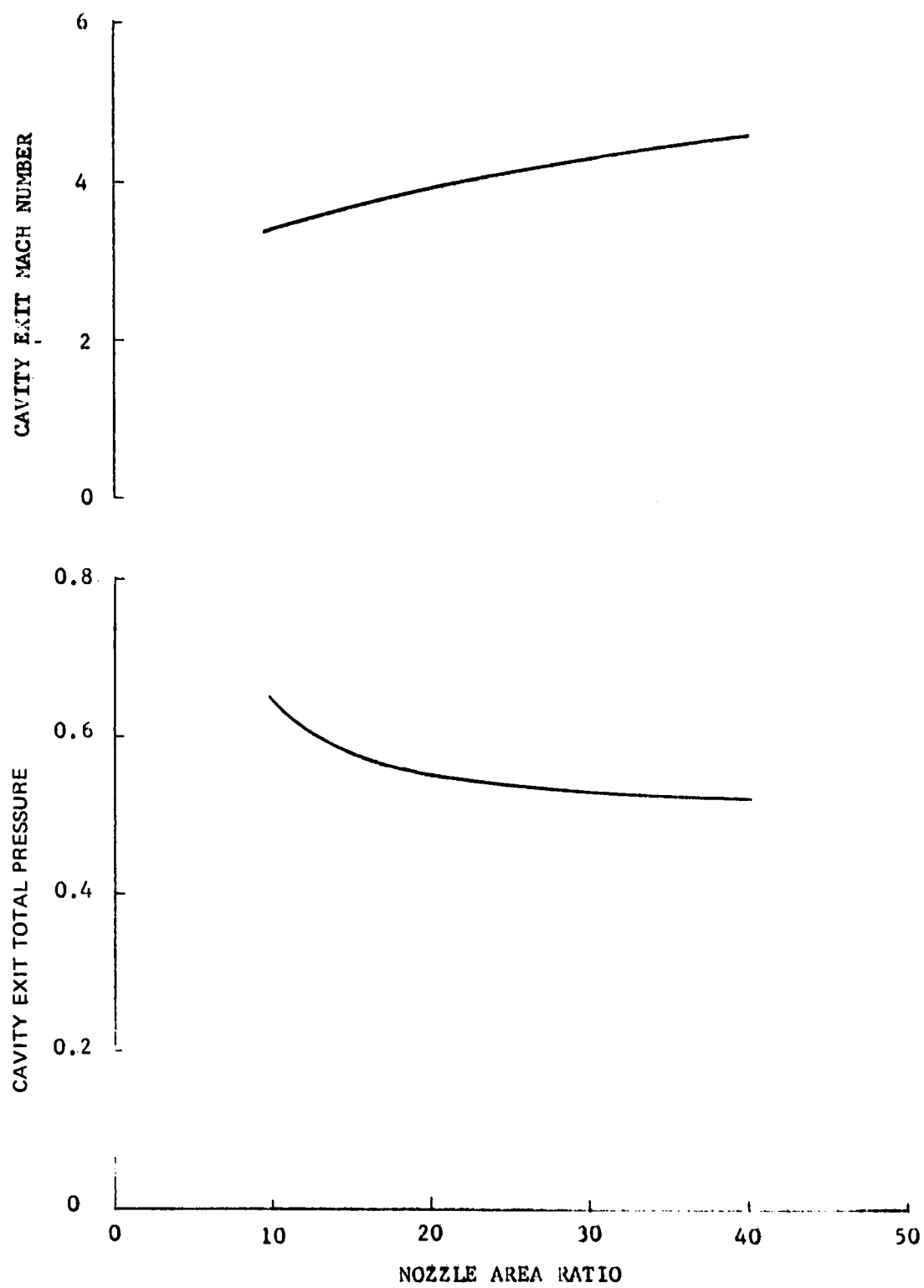
Figure 11. Cavity Mach Number and Exit Total Pressure

20

The Boeing Company, in their closed-cycle GDL Experimental Program (Ref. 1), demonstrated that diffusers with boundary layer bleed can be developed to give acceptable recovery performance for closed-loop application. Their tests were conducted with a nozzle array and cavity upstream of the diffuser. The results of the Boeing study are presented in figure 15 for the nozzle/cavity/ diffuser combination, along with an estimate for the diffuser alone at 5.8% boundary layer bleed. JPL also has tested this type of diffuser with freestream capture of the supersonic flow. Their results are also presented in figure 15. The heavy broken lines are the results of correlating these data into a best fit for 0, 6, and 20% bleed flows with a projection for a 10% increase in performance with additional development.
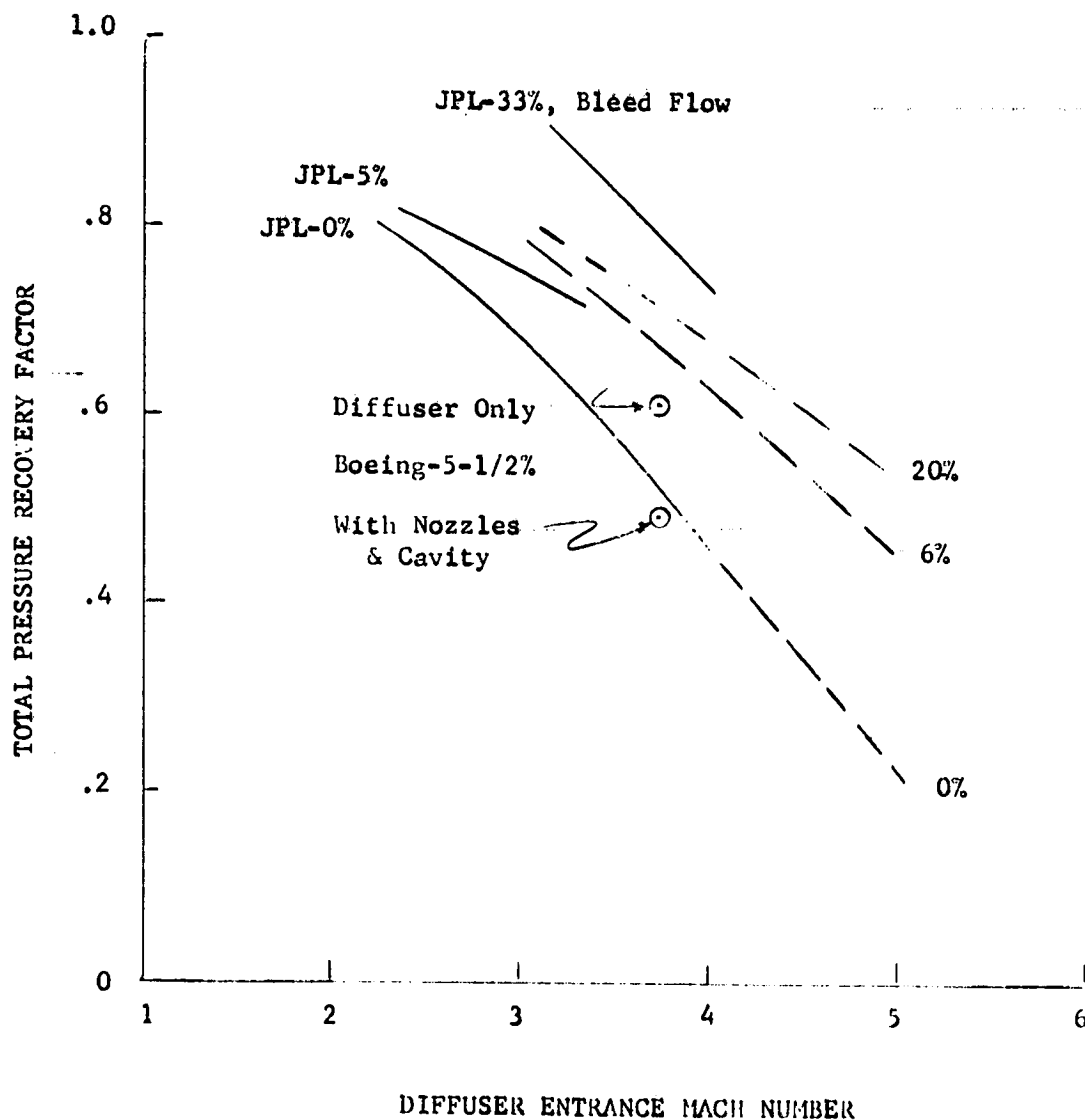
Figure 15. Diffuser Pressure Recovery

Although diffuser wall bleed is an effective method to reduce boundary layer buildup and significantly enhance diffuser performance, this scheme would require an additional compressor and heat exchanger to recondition the bleed flow before it is returned to the main loop. Extensive model testing on low contraction ratio diffusers at UTRC and hot flow GDL cavities at FRDC has shown that endwall and sidewall injection is an equally effective method to energize the boundary layer and improve the diffuser performance. An advantage of the injection method is that the working fluid may be at the same temperature and pressure as the fluid supplied to the nozzle array. This reduces the system complexity by eliminating the need for additional compressors and heat exchangers. The resulting design is simple and within the present state-of-the-art.

The performance capabilities for diffusers with injection flow were assumed equal to that achieved for systems with bleed flow. As discussed in the previous paragraph, this assumption is consistent with hot flow experiments on GDL cavities operating at lower recovery factors; however, this assumption should be experimentally substantiated during the diffuser development program recommended in the technology confirmation section. If the experimental data indicate unacceptable performance is attained with boundary layer injection, then the system can be modified to use boundary layer bleed with the associated added system complexity. The performance levels of diffuser systems with boundary layer bleed are shown in figure 15. The performance level estimated for the injection system has been replotted as a function of injection flow and Mach number and is shown in figure 16.

Although high contraction ratio diffusers result in good steady-state performance levels, the high contraction ratio makes it difficult for the diffuser to "swallow" the starting normal shock. Therefore, some type of variable area system is required to allow starting and provide the efficient transition to steady-state operation.

A movable centerbody is one method of area modulation, but this type of device has severe problems associated with cooling and actuation.

Another method of area modulation is by use of movable sidewalls along the full length of the diffuser. However, this concept requires extensive use of actuators and efficient sealing devices, which result in complexity and weight penalties.

The most attractive method of diffuser area modulation is by means of a bypass bleed door located upstream of the diffuser throat. During the starting sequence, most of the cavity flow is diverted around the diffuser to ensure that the shock is "swallowed" and stabilized in the throat section. The bypass flow eventually reenters the system in the subsonic section of the diffuser through another movable door.

The diffuser configuration selected was a conventional design as shown in figure 17 with provisions for start bypass.

22
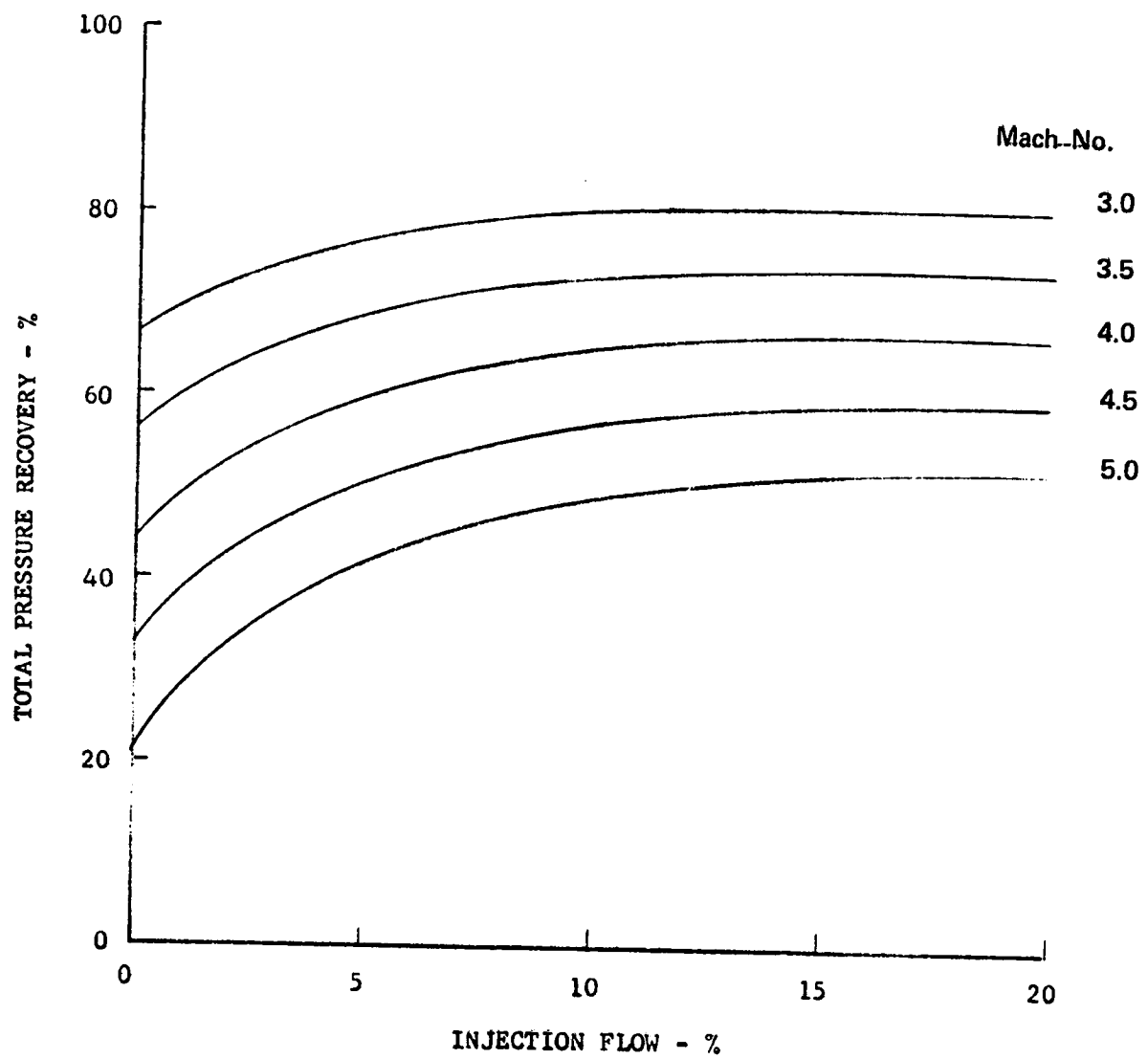
Figure 16. Diffuser Pressure Recovery

23
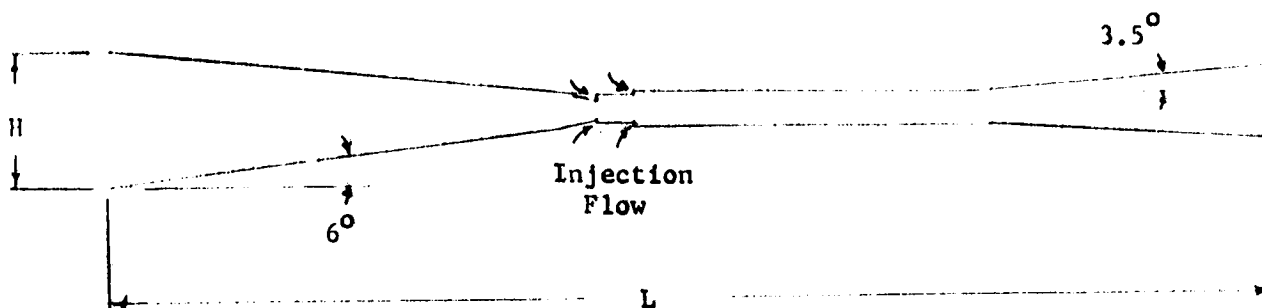
TYPICAL DESIGN CONDITIONS:

INLET MACH NUMBER	3. - 5.
EXIT MACH NUMBER	0.2 - 0.3
CONTRACTION RATIO	4. - 5.
NONDIMENSIONAL LENGTH, L/H	8. - 10.
INJECTION FLOW %	5 - 15

Figure 17. Closed-Cycle Diffuser Design

Compressor

The base cycle requires a compressor discharge temperature of 1500 to 1600°K for optimum laser performance. The operation of a compressor in this environment can be accomplished by using either advanced ceramic materials or advanced turbine alloys with efficient gas cooling. The cooling concept would be similar to that of present air-cooled turbine designs. However, because of the injection of the coolant flow into the main gas stream, compressor efficiency is reduced, as shown in figure 18. This performance penalty results in an increase in compressor horsepower, as shown in figure 19. Based on the performance penalties and possible development risks associated with the cooled compressor, an all-ceramic compressor was selected for characterization for the base cycle. Several ceramic materials are being developed that could meet the requirements for the high temperature compressor, including hot-pressed silicon carbide, sintered silicon carbide, hot-pressed silicon nitride, aluminum nitride, sialon, and Refel. For the compressor study it was assumed that by the year 1990, ceramic technology would have achieved tensile strength capabilities of 276 MN/m^2 (40,000 psi) at 1600°K (2420°F). This stress level was used as the maximum allowable in the compressor rotor.
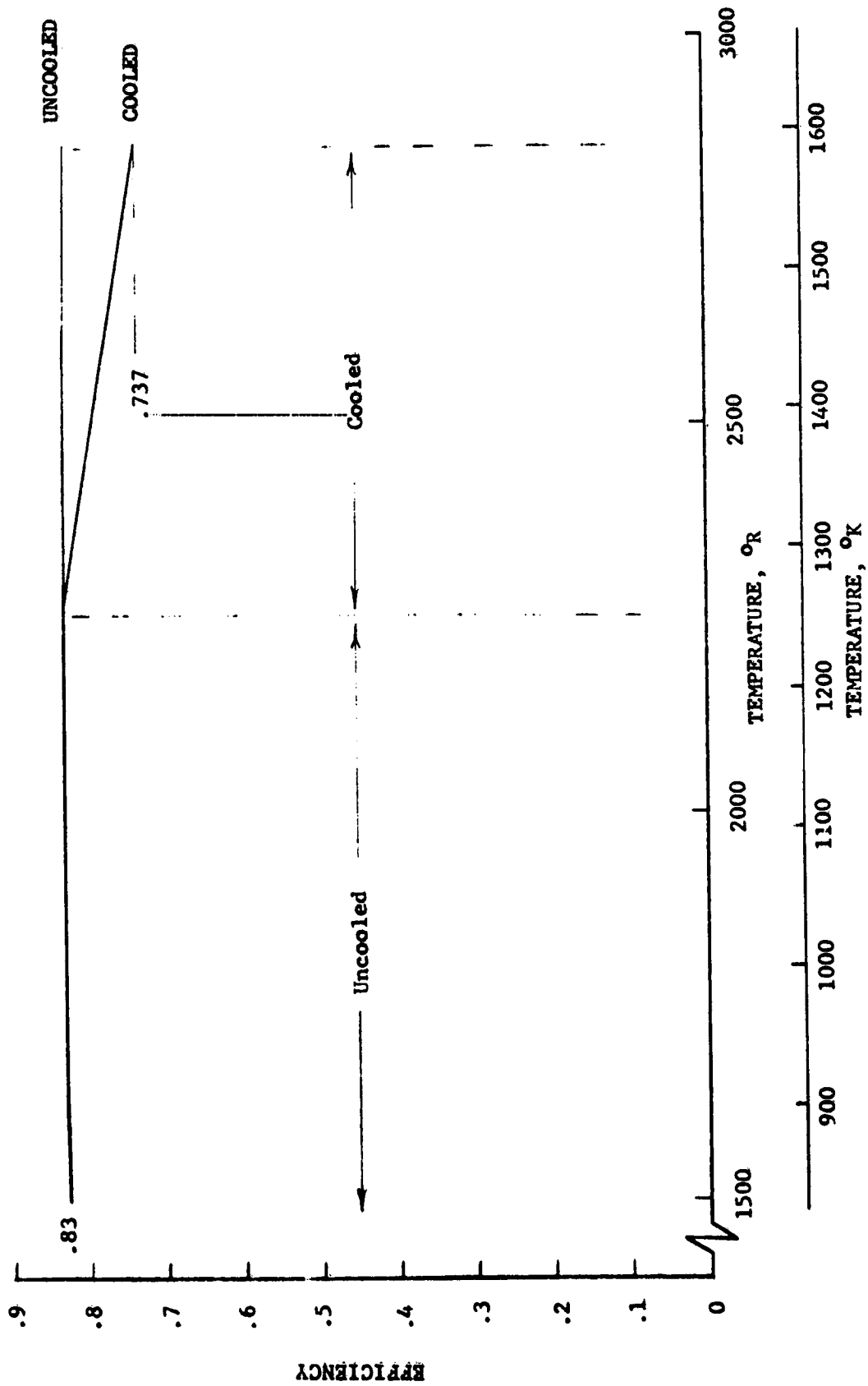
Figure 18. Compressor Efficiency Trades

25
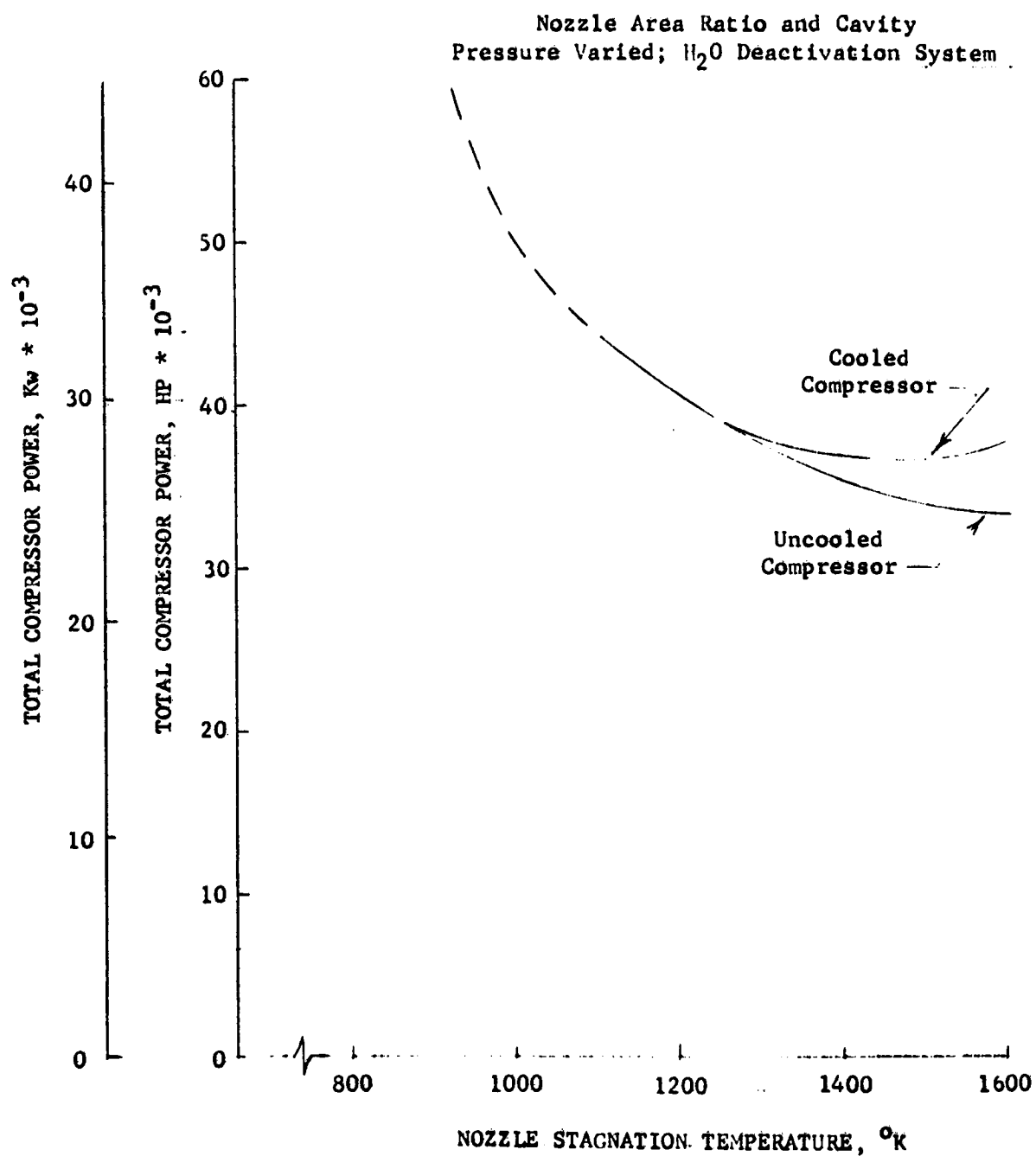
Figure 19. Effect of Compressor Cooling on Optimum
Laser Loop Performance as a Function
of Cavity Temperature

A preliminary design sizing was made for both axial and centrifugal compressors to provide a basis for selection of compressor type. Two flowrates were considered: one at the minimum and one at the maximum limits of the study corresponding to the 1- and 10-Mw systems. An intermediate pressure ratio was used. The results are shown in table II.

Table II. Compressor Configuration Comparison

| | Compressor Type | | | |
	Axial		Centrifugal	
Corrected Flow, kg/s (lb$_m$/sec)	16 (35)	79 (175)	16 (35)	79 (175)
Pressure Ratio, P$_3$/P$_2$	2.6	2.6	2.6	2.6
Compressor Diameter, cm (in.)	41 (16)	91 (36)	132 (52)	297 (117)
Adiabatic Efficiency, %	84	84.5	82	82.5
Rotor Speed, rad/sec (rpm)	1,570.8 (15,000)	701.6 (6,700)	2,094.4 (20,000)	935.1 (8,930)

This preliminary analysis indicated that the axial compressor has performance and size advantages at both flowrates; therefore, this type of compressor was selected.

The axial compressor was characterized for pressure ratios of 2.0, 2.75, and 3.5, which cover the range of anticipated pressure ratios for the base cycle. These characteristics are summarized in table III; plan views of the compressors are shown in figures 20 through 22. From these data, compressor weight, size, and efficiency were correlated as a function of fluid work requirements (figures 23 and 24) for the 1-Mw system. The total compressor weight was established as 30% greater than the sum of the calculated rotor and stator weights to account for bearings, cases, etc. Compressor scaling techniques, developed from extensive gas turbine investigations, were used to extrapolate these data to other flowrates.

Table III. Axial Compressor Parameters

Pressure Ratio	2.0	2.75	3.5
Corrected Flow, kg/s (lb$_m$/sec)	16 (35)	16 (35)	16 (35)
Number of Stages	3	5	6
Adiabatic Efficiency, %	85.2	84.3	83.3
Rotor Speed, rad/sec (rpm)	2,458.8 (23,480)	2,529.2 (24,152)	2,668.3 (25,480)
Disk Maximum Stress, MN/m^2 (psi)	276 (40,000)	276 (40,000)	276 (40,000)
Rotor and Stator Weight, kg (lb$_m$)	32 (71.2)	52 (113.7)	62 (136)

Although the compressor for the recuperator cycle operates at temperatures that do not require advanced materials or cooling, a separate compressor characterization was not generated for the recuperator cycle because the compressor weight and volume are relatively small compared to the total laser loop-weight and volume.

Ducts

A preliminary estimate was made of the duct lengths as a function of the manifold, cavity, and diffuser geometry for the base and recuperator cycles. The pressure drops were characterized as a function of Mach number and friction factor, which is a function of Reynolds number. Weights were based on an uncooled superalloy density of 0.0083 kg/cm^3 (0.3 lb$_m$/in^3) with an allowable stress of 35 MN/m^2 (5000 psi).

Heat Exchangers

The base cycle system has only one heat exchanger which is required to reject the excess heat supplied by the compressor. This heat rejection occurs at a relatively high temperature, and for a space system the simplest heat rejection method is by direct radiation from the gas to the space environment. An intermediate liquid loop system reduces weight for the recuperator cycle, with its much lower rejection temperature.—

Three types of geometry were initially evaluated for the gas ducting in the space radiator:

1. Tubes
2. Tubes with fins
3. Flat duct with web strengtheners.——

Pressure ratio	$P2/P1$		2.0	ND	2.0 ND
Corrected flow	$w\sqrt{\theta}/\delta$		35	lbm/sec	15.9 Kg/s
Rotor speed	N	23,480	RPM		2459 Rad/s
Tip speed	Utip		1602	ft/sec	488 m/s
Temperature inlet	T_1		1800	°R	1000 °K
Temperature exit	T_2		2166	°R	1203 °K
Pressure inlet	P_1		75	psi	0.517 MN/m²
Pressure exit	P_2		150	psi	1.035 MN/m²
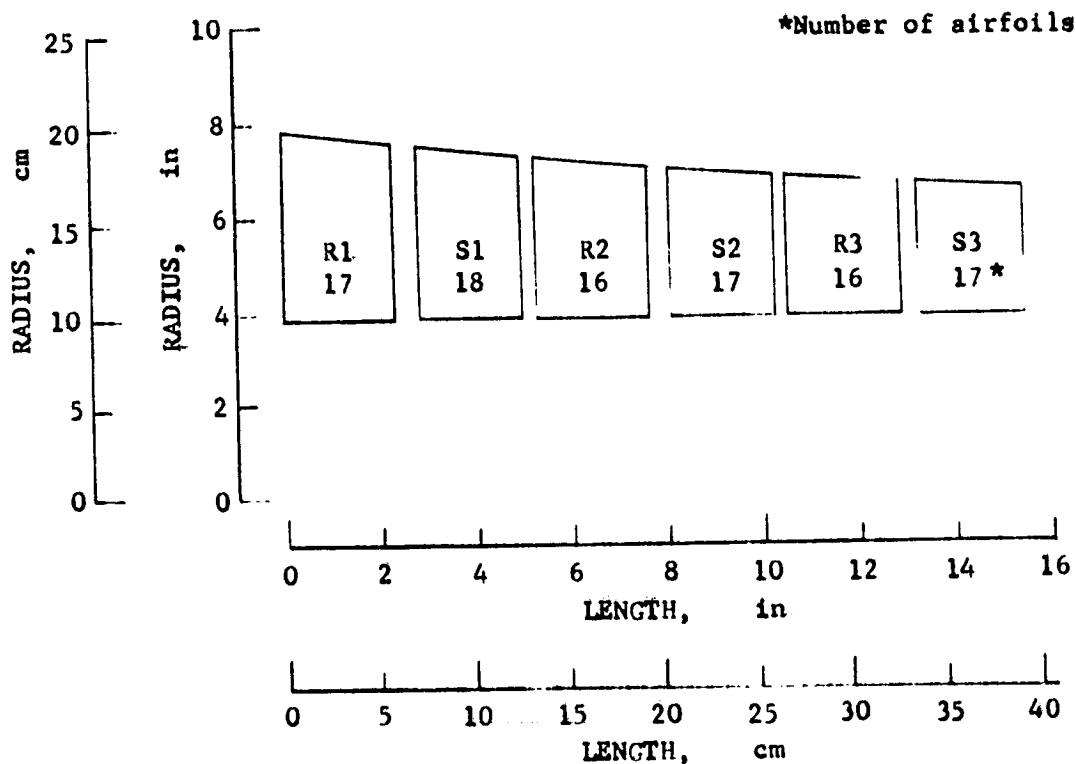
Figure 20. Three-Stage Compressor

Pressure ratio	P_2/P_1	2.75 ND	2.75 ND
Corrected flow	$w\sqrt{\theta}/\delta$	35 lbm/sec	15.9 Kg/s
Rotor speed	N	24,152 RPM	2529 Rad/s
Tip speed	Utip	1648 ft/sec	502 m/s
Temperature inlet	T_1	1950 °R	1083 °K
Temperature exit	T_2	2558 °R	1421 °K
Pressure inlet	P_1	75 psi	0.517 MN/m²
Pressure exit	P_2	206 psi	1.420 MN/m²

*Number of airfoils

R1 17 — S1 18 — R2 16 — S2 17 — R3 16 — S3 17 — R4 15 — S4 16 — R5 15 — S5 14*

LENGTH, in
LENGTH, cm

RADIUS, in
RADIUS, cm

Figure 21. Five-Stage Compressor

29

Pressure ratio	P_2/P_1	3.5 ND	3.5 ND
Corrected flow	$w\sqrt{\theta}/\delta$	35 lbm/sec	15.9 Kg/s
Rotor speed	N	25480 RPM	2668 Rad/s
Tip speed	U tip	1740 ft/sec	530 m/s
Temperature inlet	T_1	2100 °R	1167 °K
Temperature exit	T_2	2945 °R	1636 °K
Pressure inlet	P_1	75 psi	0.517 MN/m^2
Pressure exit	P_2	263 psi	1.814 MN/m^2

*Number of airfoils

Stage	Airfoils
R1	17
S1	18
R2	16
S2	17
R3	15
S3	16
R4	15
S4	16
R5	14
S5	15
R6	14
S6	15*

LENGTH, in

LENGTH, cm

RADIUS, in

RADIUS, cm
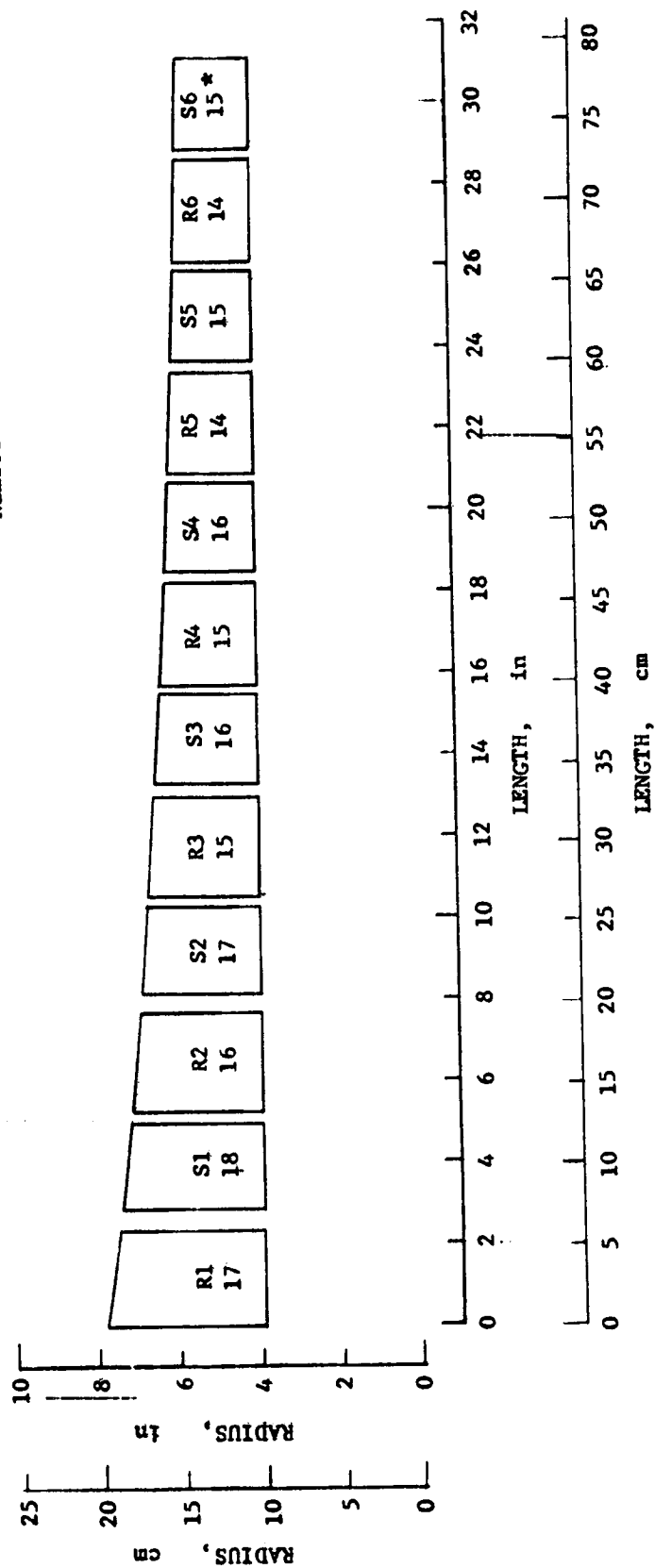
Figure 22. Six-Stage Compressor

30

Scale to different conditions by:

$$W_T \propto (\dot{w}\sqrt{\theta}/\delta)^{1.3}$$

$$L \propto (\dot{w}\sqrt{\theta}/\delta)^{0.5}$$

$$\dot{w}\sqrt{\theta}/\delta = 35 \text{ lbm/sec} = 15.9 \text{ Kg/s}$$
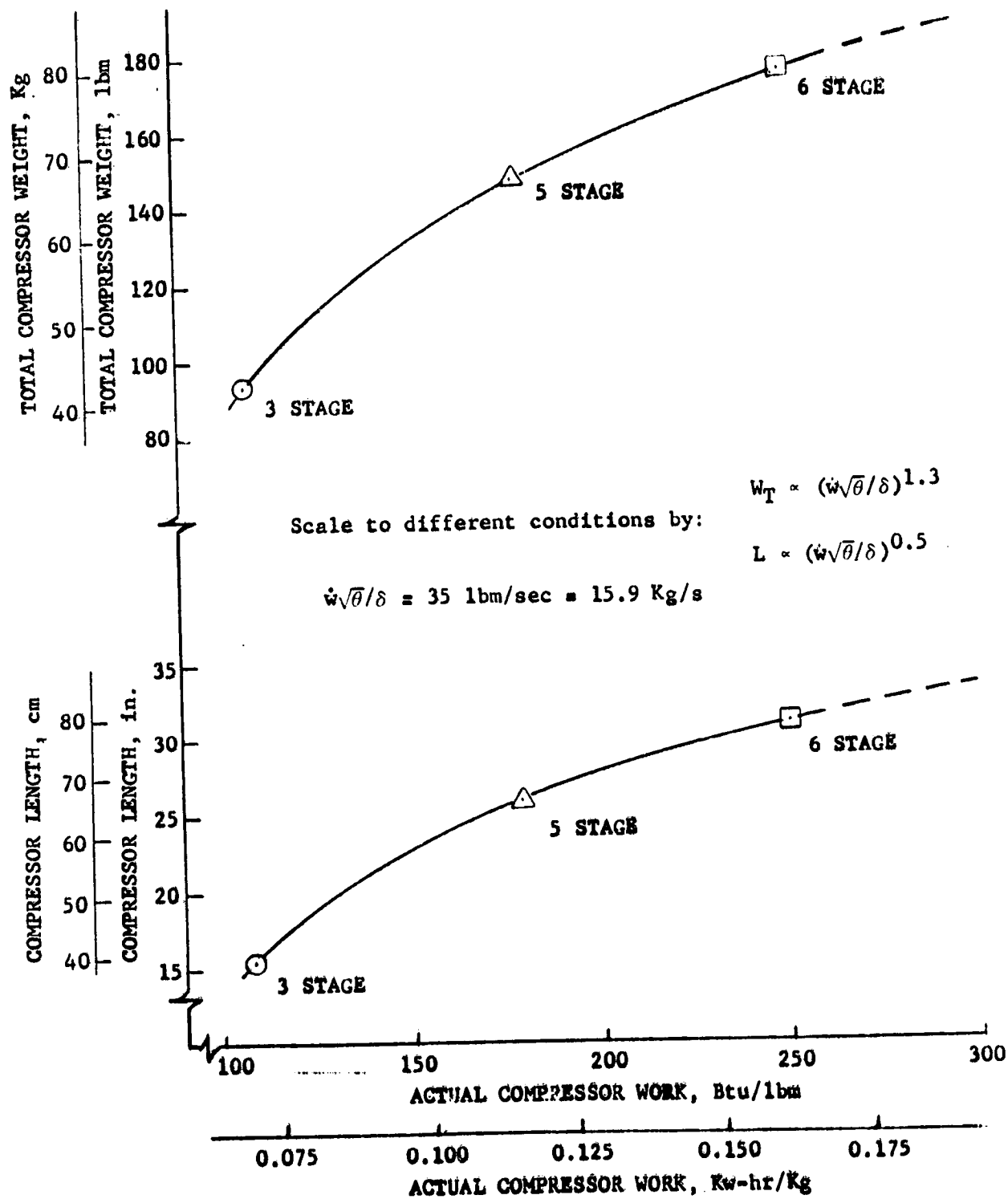
Figure 23. Compressor Weight and Geometry
Characteristics
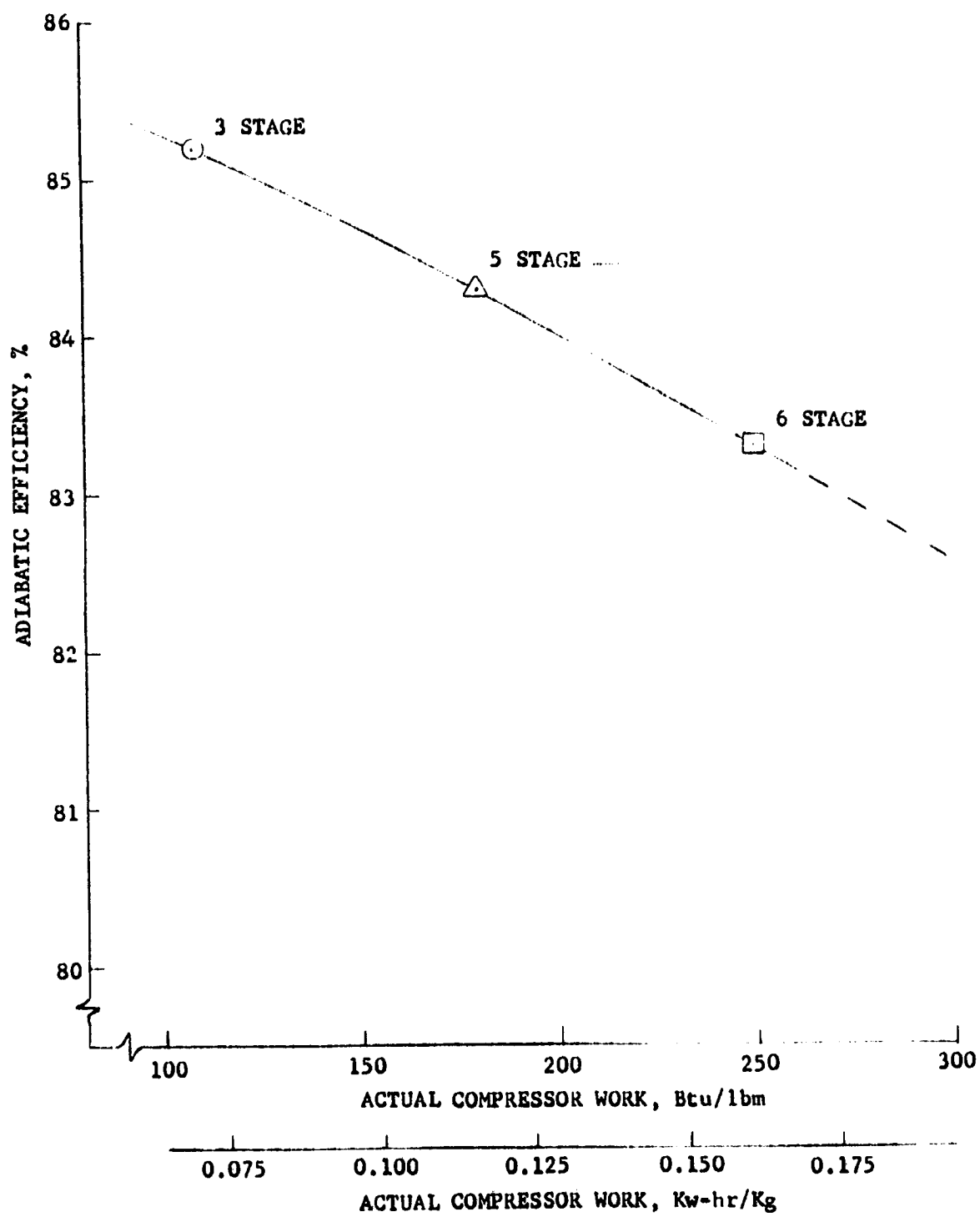
Figure 24. Compressor Efficiency

These are shown schematically in figure 25. The analysis methods developed
by Mackay (Reference 2) were used to evaluate each configuration over a range
of geometric sizes to establish surface area, gas flow length, weight, and
pressure drop. The evaluations were conducted at a gas inlet Mach number
of 0.1 and for typical heat rejection levels for the base cycle. Columbium
was used for the radiator material because of the high gas temperatures.

Cross Sectional Geometry

Tubes
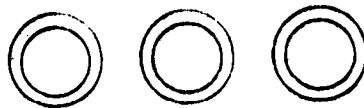
Tubes With Fins
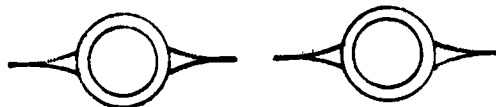
Flat Duct

Figure 25. Space Radiator Concepts

The results of this evaluation indicated that the simple tube arrangement
with no fins and having a tube diameter of 6 cm (2.4 in.) was the optimum con-
figuration. This configuration was characterized by a weight-per-unit area
parameter (W/A_{eff}) of 6.6 kg/m^2 (1.35 lb_m/ft^2) with a pressure drop of 2.3%.
No allowance was made for meteoroid protection.

The effective area of the radiator was characterized using an equation
developed by Glassman and Stewart (Reference 3) which defines the area as
a function of the inlet and exit wall temperatures, film coefficient, sink tem-
perature, and gas flowrate. The weight of the radiator system can thus be
established by the surface area and the W/A_{eff} parameter, $[W/A_{surf} = 6.6 \ kg/m^2$
(1.35 lb_m/ft^2)].

33

Optimization of the recuperator cycle requires that the following additional components be characterized and included in the systems synthesis model:

1. Recuperator

2. Heat sink heat exchanger system (gas-to-liquid heat exchanger and liquid space radiator)

3. Heat source heat exchanger.

Models of the gas-to-gas recuperator, a plate-fin-type heat sink heat exchanger, and a tube-fin-type heat source heat exchanger were established on the bases of effectiveness/exchanger units method developed by Kays and London (Reference 4). The space radiator area was calculated using the method described for the base cycle radiator. While only one configuration for each heat exchanger was included in the systems model and was not necessarily the optimum for the final design, the effects of each component on the overall system could still be determined.

A summary of the design parameters and characterizations of these components is presented in table IV.

Table IV. Recuperator Cycle Component Design Parameters

Heat Sink Heat Exchanger

Type	Plate-Fin (Gas to Liquid)
Effectiveness	0.95
Volume	Reference 4
Pressure Loss, %	Reference 4
Weight	Calculated

Radiator

Area	Reference 3
Weight, kg/m^2 (lb_m/ft^2)	29 (0.6)
Emissivity	0.9
Sink Temperature, °K (°R)	273 (460)

Recuperator

Type	Plate-Fin (Gas to Gas)
Effectiveness	0.9
Volume	Reference 4
Pressure Loss	Reference 4
Weight	Calculated

Heat Source Heat Exchanger

Type	Finned-Tube (Liquid to Gas)
Effectiveness	0.46
Volume	Reference 4
Pressure Loss	Reference 4
Weight	Calculated

Table IV. Recuperator Cycle Component Design Parameters (Continued)

Heat Source

Type	Unshielded Nuclear Reactor
Weight, kg/kw (lb_m/kw)	0.98 (2.17)

Prime Mover

Type	Space Brayton Power Cycle
Weight, kg/kw (lb_m/kw)	30 (66)
Thermal Efficiency, %	25

Heat Source and Prime Mover

Although an analysis of the compressor drive and heat source was not required by the contract Statement of Work, a cursory evaluation was made to permit weight/power comparisons to be made between the base and recuperator cycles. The characterization of the heat source and prime mover is of major importance because their combined weights could be as much as 80% of the total system weight. However, a detailed analysis of these components was outside the scope of this study. An analysis of a Brayton power-conversion module for this type of application can be found in Reference 5. This system uses an unshielded nuclear reactor for the heat source.

The characterizations for the heat source and prime mover used in this parametric study were derived from Reference 5 and are summarized in table IV. The effects of prime mover thermal efficiency on the absolute value of total system weight could be significant, but were not considered in this study.

Optimization of Base Cycle

Using the previously developed component characteristics, a parametric evaluation of the 1-Mw base closed-cycle GDL system was performed. This analysis included performance, weight, and geometry assessment of the system as a function of the major design variables.

The effects of nozzle area ratio, nozzle stagnation temperature, nozzle stagnation pressure, beam diameter, diffuser injection flow, and gas composition on the system weight, volume, and compressor horsepower requirements were calculated using a systems synthesis code. The laser loop weight, calculated by the code, included the laser device (manifold, nozzles, cavity, and diffuser), a direct gas space radiator, the compressor, and the gas flow ducting system. The total system volume is the sum of the box volumes of the aforementioned components. The absolute values of the weights and volumes calculated by the code are not necessarily consistent with the final conceptual design (because of the more detailed analysis), but were considered satisfactory for parametric optimization.

Several second order design parameters were optimized initially using the preliminary cavity operating conditions of nozzle stagnation pressure, P_c 2.07 MN/m^2 (300 psia), nozzle stagnation temperature, T_c ~ 1600°K, and

nozzle area ratio, ϵ 30. The secondary design parameters of beam diameter, gas composition, and diffuser injection flow were selected on the basis of providing the minimum compressor horsepower requirements for the operating conditions. The minimum horsepower condition does not necessarily result in the minimum laser loop weight and volume. However, since the weight and volume for the laser system are small compared to that anticipated for the prime mover, the compressor horsepower was considered the dominant parameter in the system optimization.

The effect of diffuser injection flow on compressor horsepower requirements is presented in figure 26 for a range of flows from 0 to 25%. The effects on laser loop weight and volume are presented in figure 27. Total system weights vary less than 1% over this range, while system volume varies about 10%. The minimum horsepower occurs at 8% injection flow.

The effect of beam diameter on compressor horsepower requirements is presented in figure 28 for a beam diameter range of 9 to 20 cm. The effects on laser loop weight and volume are presented in figure 29. The minimum horsepower occurs at a beam diameter of 13 cm, while the minimum weight and volume occur at beam diameters of 11 and 9 cm, respectively. The selection of a 13-cm beam diameter results in a weight penalty of less than 5% and an estimated volume penalty of approximately 25% for the closed cycle laser system. More detailed volume analysis in Task II indicated that the volume penalty with the 13-cm beam was significantly less than the estimated 25%.

The effect of gas composition on compressor horsepower requirements is presented in figure 30. The minimum horsepower occurs with $N_2/CO_2/H_2O$ mole fractions of 0.91/0.08/0.01, respectively. Since this composition gives the highest specific power (shown previously under cavity characterizations), the minimum weight and volume system also occurs at this gas composition.

Using the selected values of beam diameter, diffuser injection flow, and gas composition, a complete parametric analysis to determine the interactive effects of nozzle stagnation pressure and temperature and nozzle area ratio was completed for the following ranges:

P_c — 0.34 to 3.4 MN/m^2 (50 to 500 psia)
T_c — 1100 to 1600°K
ϵ — 10 to 40

The results, as a function of area ratio and temperature, are presented in figure 31. The chamber pressure, P_c, was selected as the value that gave the highest cavity specific power for a given ϵ. These optimum P_c's at selected ϵ's are indicated in figure 31. The cavity optical length as a function of the major design variables (P_c, T_c, and ϵ) is presented in figure 32 for the area ratios that give minimum horsepower at each temperature. Although the 1600°K and 0.7 MN/m^2 (100 psia) at area ratio of 20 is the optimum condition, the 1500°K, 1.03 MN/m^2 (150 psia) point at area ratio of 20 was chosen as a compromise between the most efficient cavity temperature (1600°K) and the desire to operate at a lower temperature from the structural and metallurgical standpoint. The slightly higher chamber pressure was selected to significantly reduce cavity length with only a minor effect on performance. As shown in figure 31, this temperature results in a 3.9% increase in the compressor power requirements over the 1600°K cavity temperature.

36

Since there is some concern about the corrosion and condensation problems associated with the use of H_2O in the closed-cycle system, an assessment was made of the performance penalties associated with substituting helium for the H_2O to deactivate the lower laser level. The cavity performance was characterized about the nominal base point of:

$N_2/CO_2/He = 57\%/8\%/35\%$
$T_c = 1500°K$
$\epsilon = 20$
$P_c = 1.725$ MN/m^2 (250 psia)

1 Mw	System
2.07 MN/m^2	Cavity Stagnation Pressure
1600 °K	Cavity Temperature
13 cm	Beam Diameter
30 ϵ	Nozzle Area Ratio...

DIFFUSER INJECTION FLOW RATIO, %
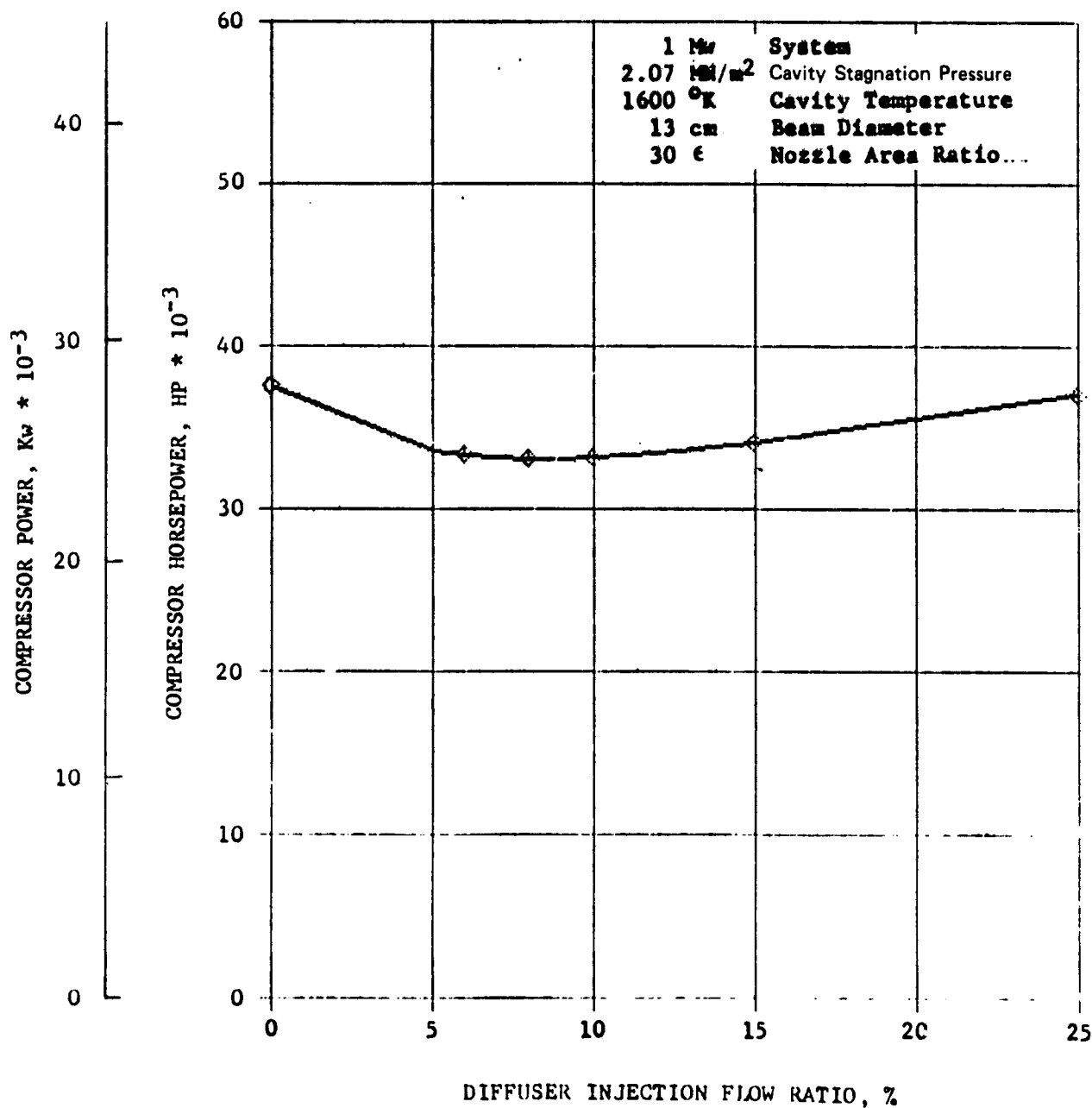
Figure 26. Effect of Diffuser Injection Flow on Compressor Power Requirement

37
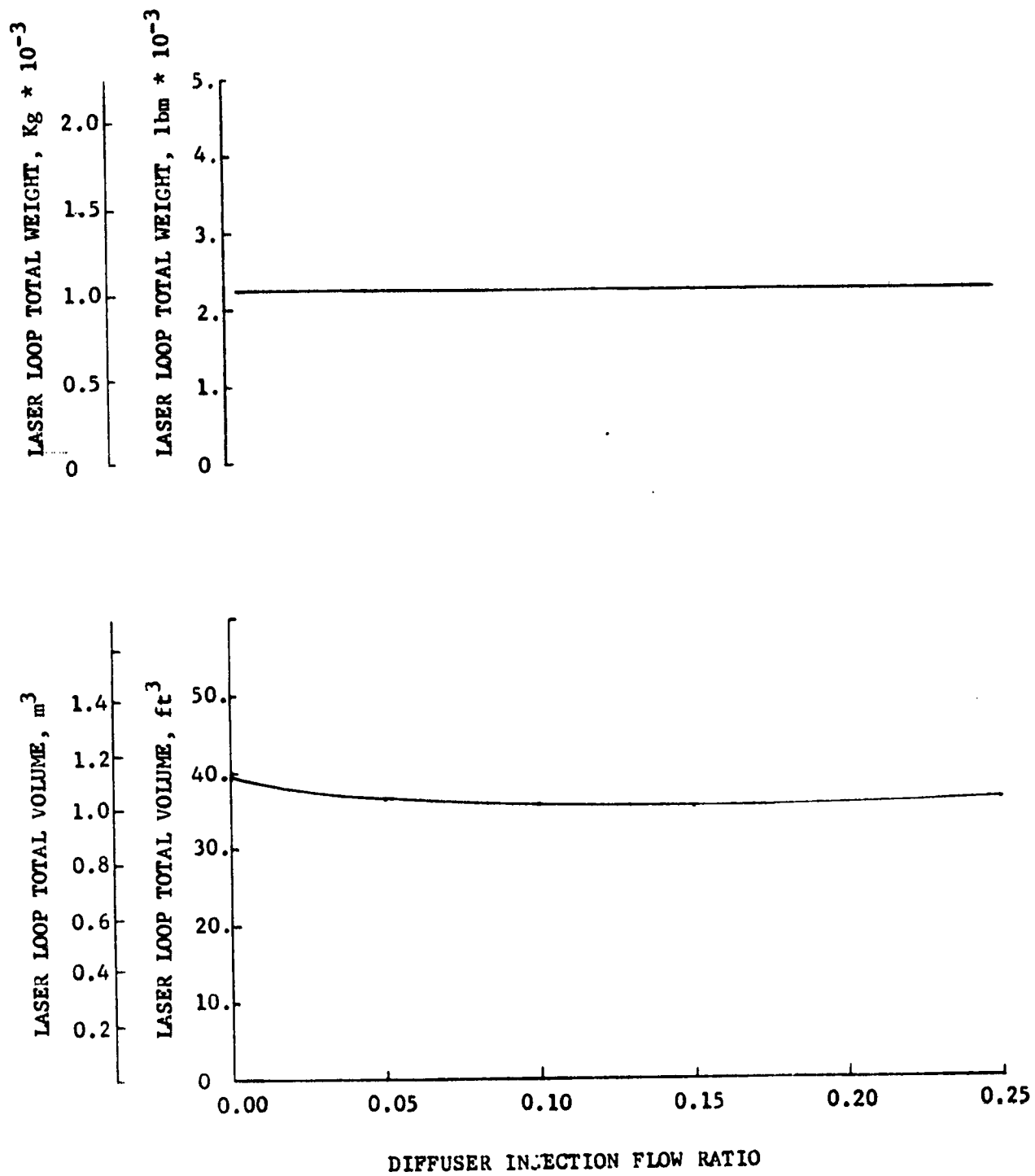
Figure 27. Effect of Diffuser Injection Flow on Laser
Loop Total Weight and Volume

60

40

50

COMPRESSOR POWER, Kw * 10^{-3}

COMPRESSOR HORSEPOWER, HP * 10^{-3}

30

30

40

20

20

10

10

10

0

0

1 Mw	System
2.07 MN/m^2	Cavity Stagnation Pressure
1600 ^{o}K	Cavity Temperature
8 %	Diffuser Injection
30 €	Nozzle Area Ratio

0   5   10   15   20   25
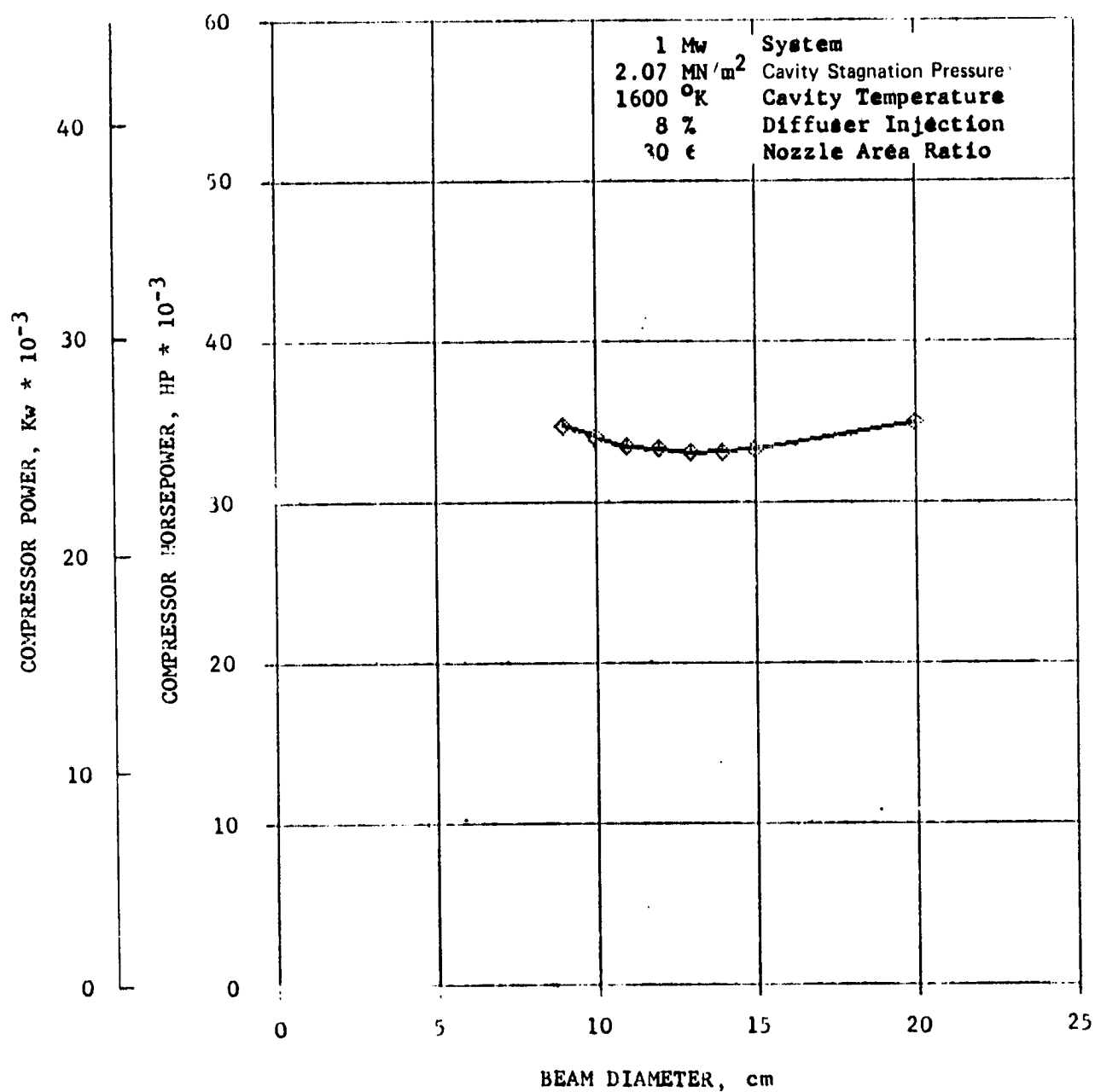
BEAM DIAMETER, cm

Figure 28. Effect of Cavity Beam Diameter on Compressor
Power Requirement
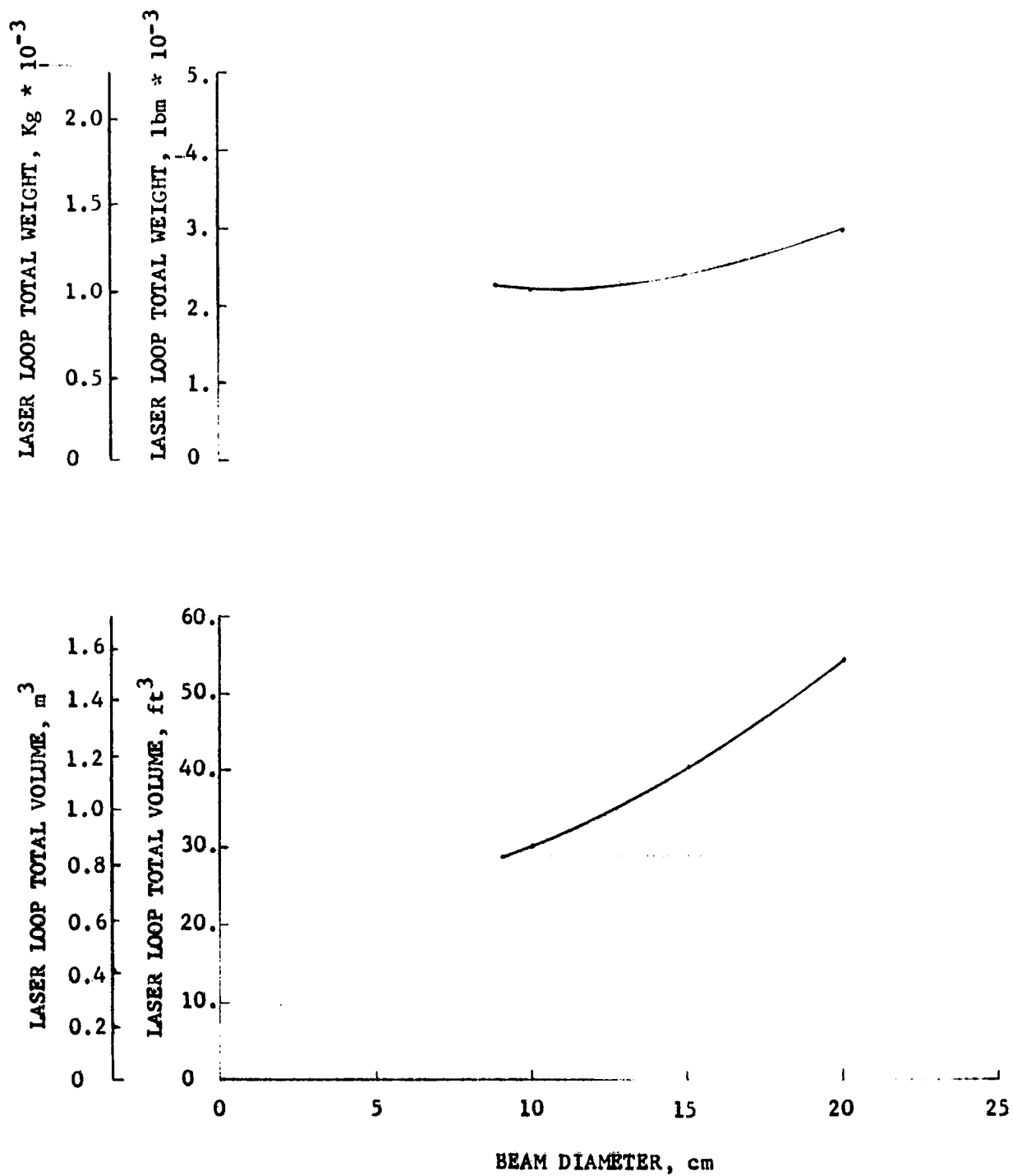
Figure 29. Effect of Cavity Beam Diameter on Laser Loop
Total Weight and Volume
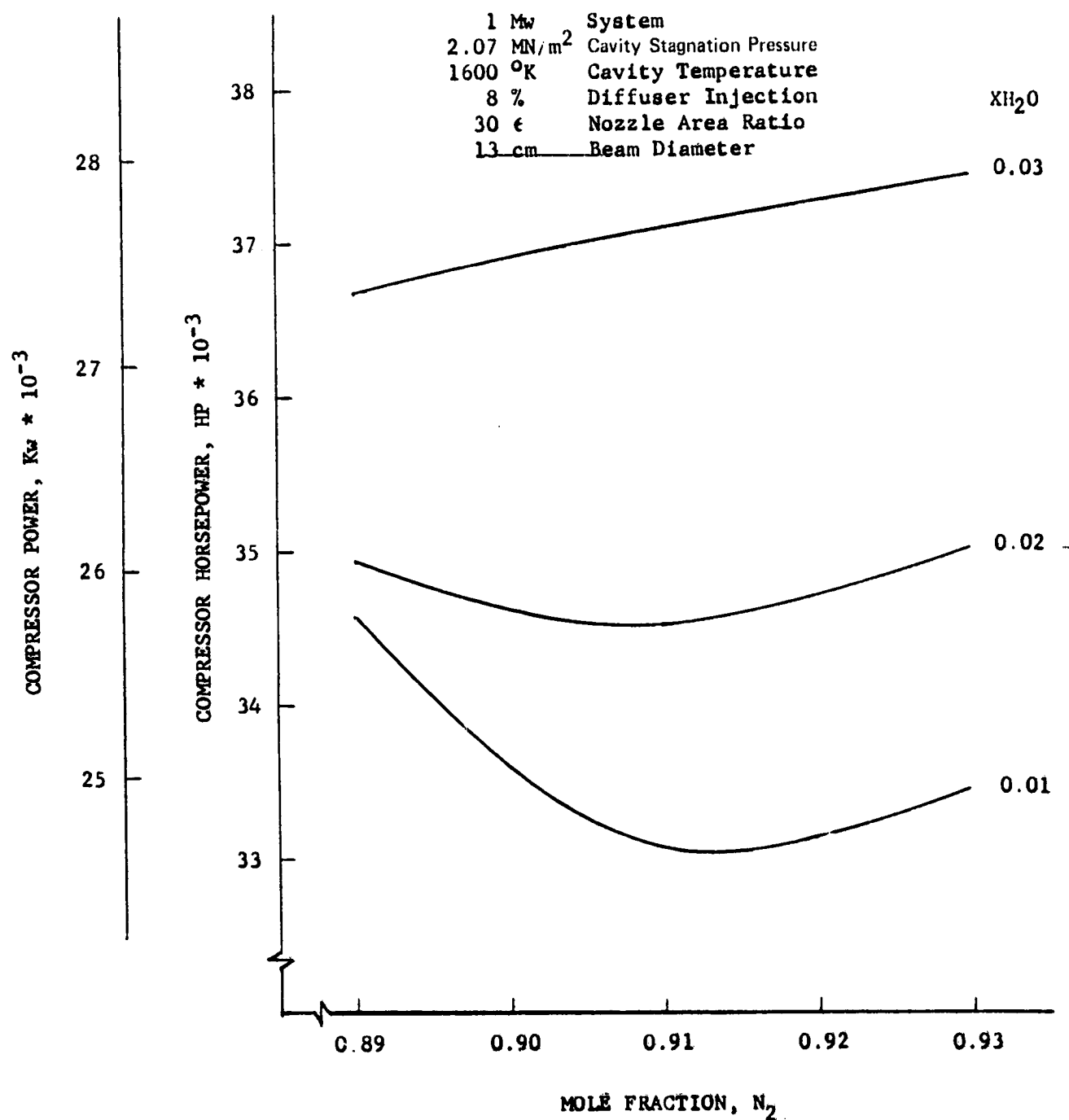
Figure 30. Effect of Gas Composition on Compressor
Power Requirement
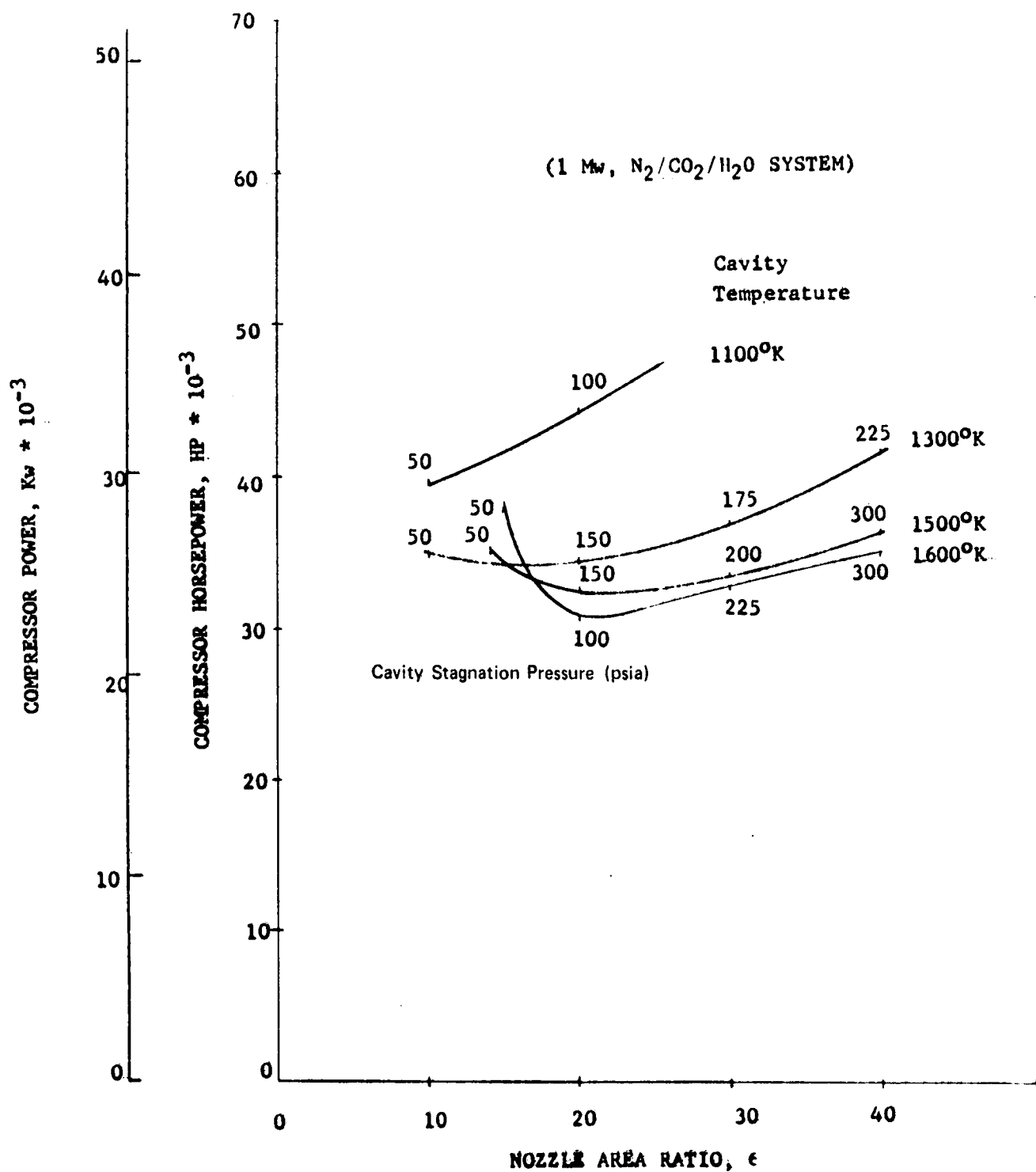
Figure 31. Effect of Nozzle Area Ratio and Cavity
Stagnation Temperature on Compressor
Power Requirement
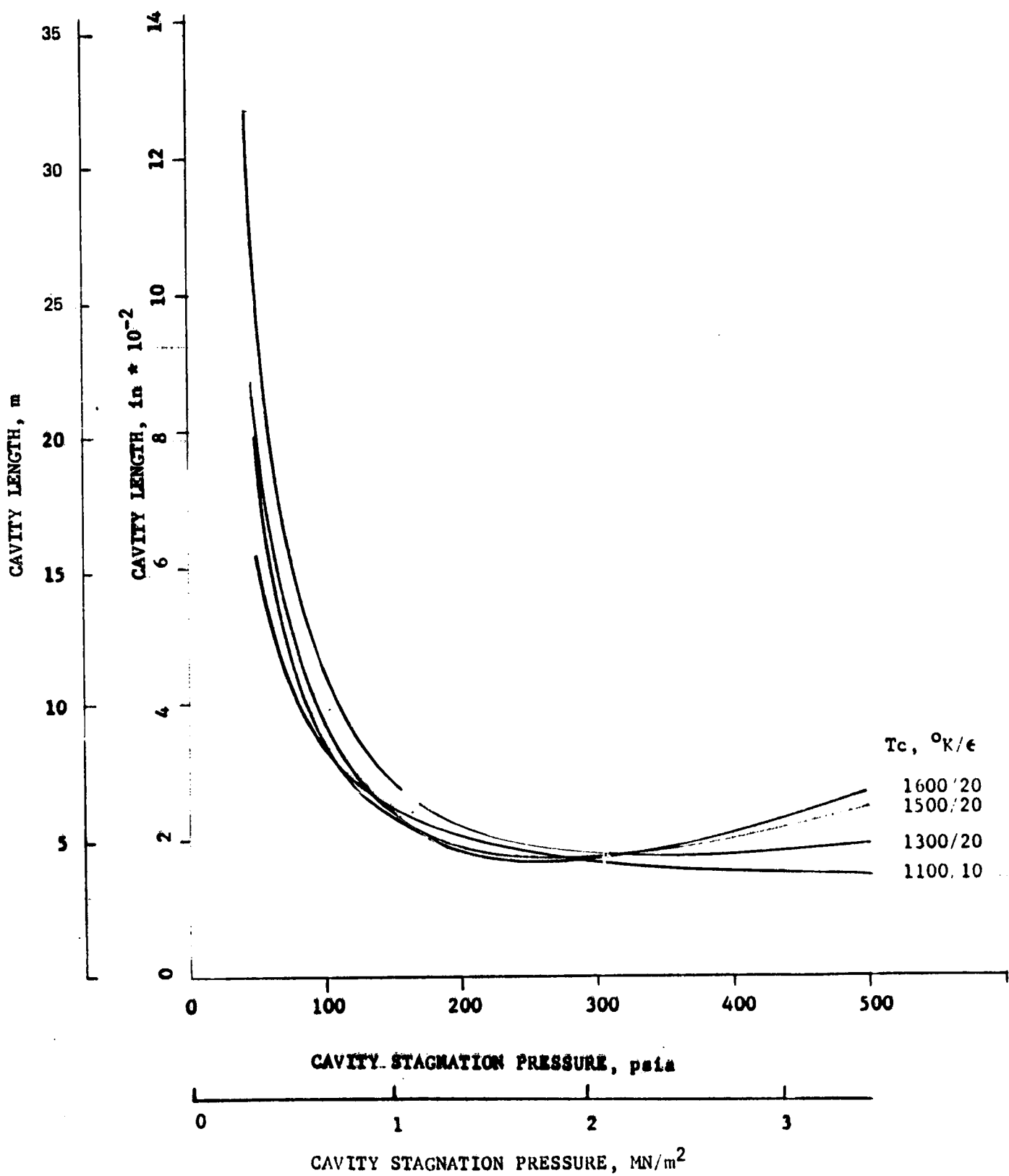
Figure 32. Effect of Cavity Stagnation Pressure and
Temperature on Cavity Length

The results are shown in figures 33 through 35 and indicate that the maximum specific power occurs at ε = 20, with a He mole fraction of 35%. The maximum specific power is some 12% lower than that with H_2O deactivation. A parametric evaluation of the compressor horsepower requirements was performed to determine the optimum composition, cavity stagnation temperature and pressure, and nozzle area ratio.

1 Mw System

Helium Deactivation
$Pc = 1.724$ MN/m^2 (250 psia)
$Tc = 1500^oK$
$XCO_2 = .08$
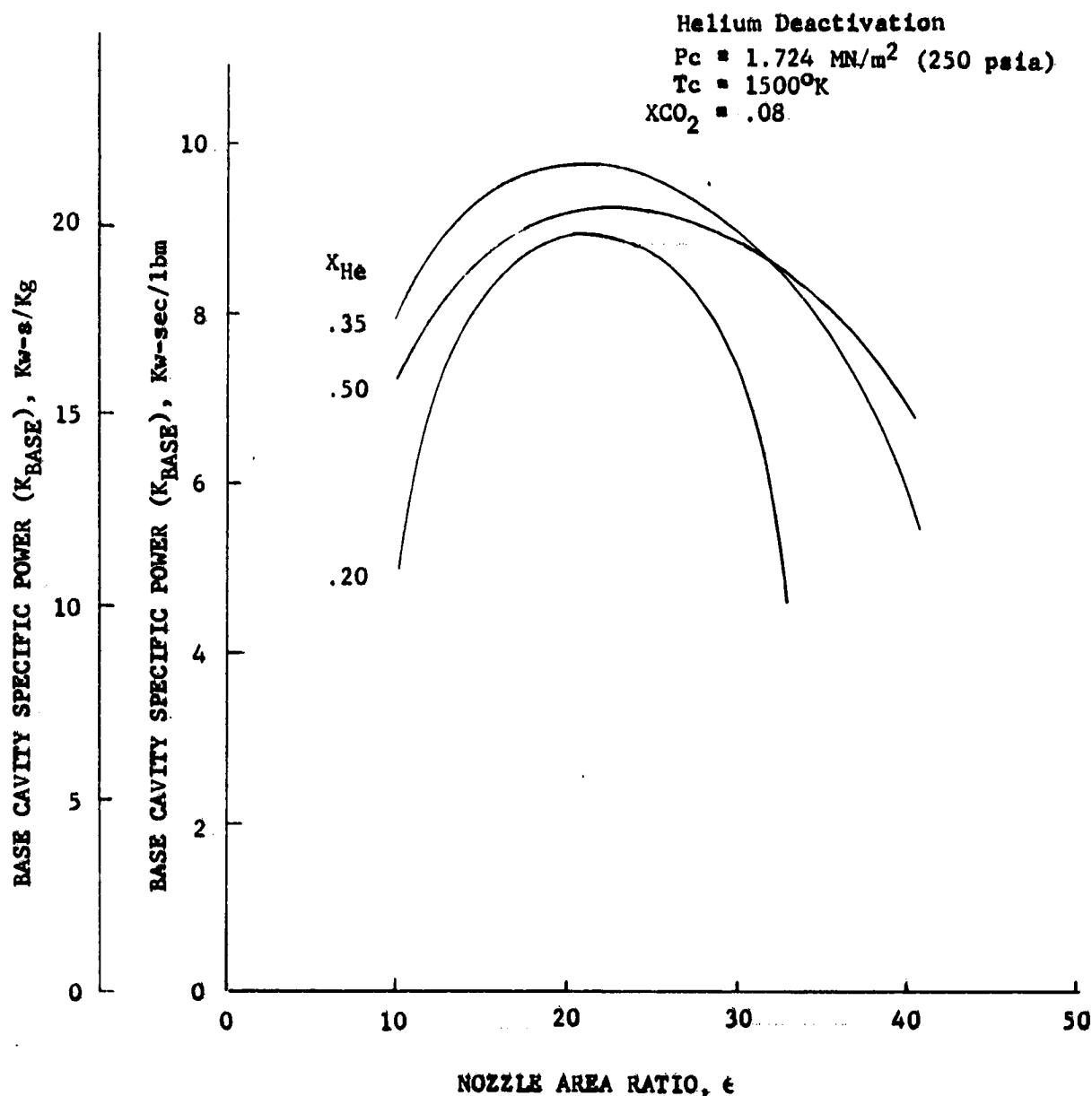
Figure 33. Effect of Nozzle Area Ratio and Helium Mole
Fraction on Performance

44
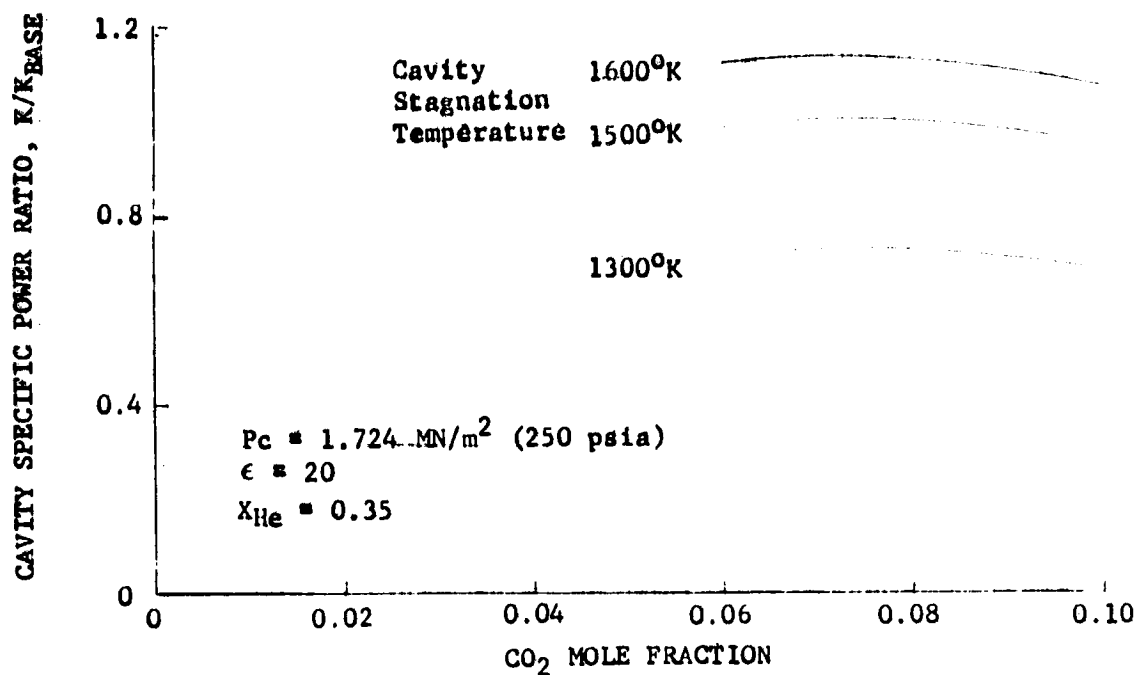
Figure 34. Effect of CO2 Mole Fraction on Performance
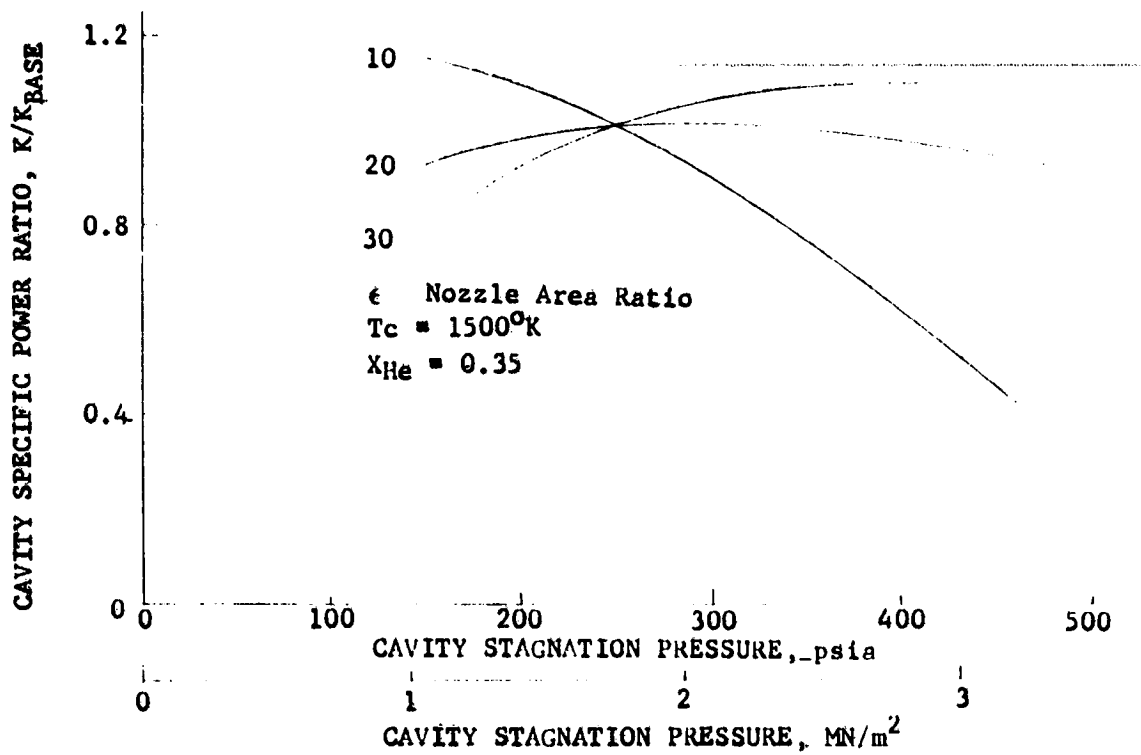
Figure 35. Effect of Cavity Stagnation Pressure on Performance

45

The optimum cavity stagnation pressure for each nozzle area ratio was selected from figure 36. For each optimum P_c/ϵ combination, the compressor power requirements of the 1-Mw helium system, as a function of helium mole percentage and cavity stagnation temperature, were calculated.

These results are presented in figure 36 for the P_c: ϵ combination of 1.03 MN/m^2: 10 (150 psia: 10), figure 37 for the 2.07 MN/m^2: 20 (300 psia: 20) combination, and figure 38 for the 2.93 MN/m^2: 30 (425 psia: 30) combination.

From these curves, the optimum helium mole percentage was selected to reflect minimum compressor power requirements as a function of cavity stagnation temperature. These are presented in figure 39. The minimum horsepower occurs at 35% helium by mole, $P_c = 1.03$ MN/m^2 (150 psia), $\epsilon = 10$, and $T_c = 1600°K$.

The helium system optimizes at a lower area ratio because the ratio of specific heats is higher, permitting expansion to a lower cavity static temperature when compared to H_2O systems at the same area ratio. Table V shows that the same cavity temperature can be obtained at a lower nozzle area ratio for the He system.

A comparison of the minimum horsepower points vs cavity stagnation temperature is presented in figure 40 for the H_2O and He systems. The helium system requires 23% more horsepower at the minimum condition of 1600°K.

If the cavity temperature were reduced to 1250°K, which would permit an uncooled metal compressor instead of a ceramic design, the horsepower requirement would be increased 15% over the minimum value for the H_2O system. The helium system at 1250°K would require 63% more horsepower than the minimum H_2O value.

As figure 40 shows, the use of helium instead of H_2O at the selected design temperature of 1500°K would result in a 20% increase in compressor power requirements. For this reason, gas constituents of N_2, CO_2, and H_2O were used in establishing the conceptual design.

A comparison of the system size and oscillator equivalent Fresnel number is shown in table VI as a function of cavity stagnation temperature for the selected H_2O system.

A low Fresnel number is desirable to provide good mode discrimination and to ensure that only low order modes are established. However, in this case, as shown in table VI, the lowest Fresnel number point is not the optimum from a system performance standpoint.

A summary of the selected base cycle design point is given in table VII, along with a schematic of the 2UO/3 optical configuration. This configuration was selected because it provided the highest cavity specific power, as discussed previously. The oscillator geometric coupling is 0.9 to provide good beam quality for long distance transmission.
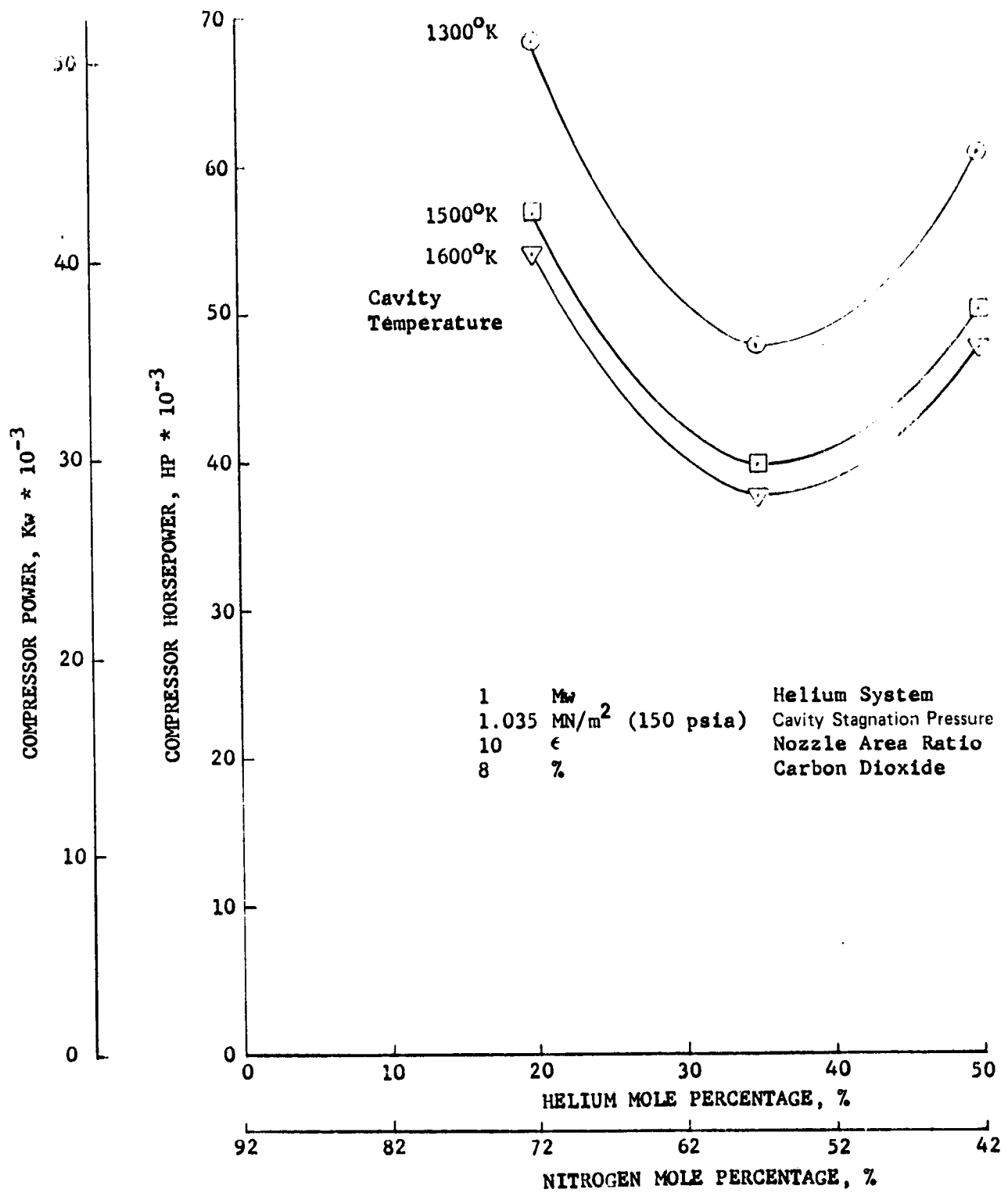
Figure 36. Effect of Helium Mole Percentage and Cavity
Stagnation Temperature on Compressor Power
Requirement

47
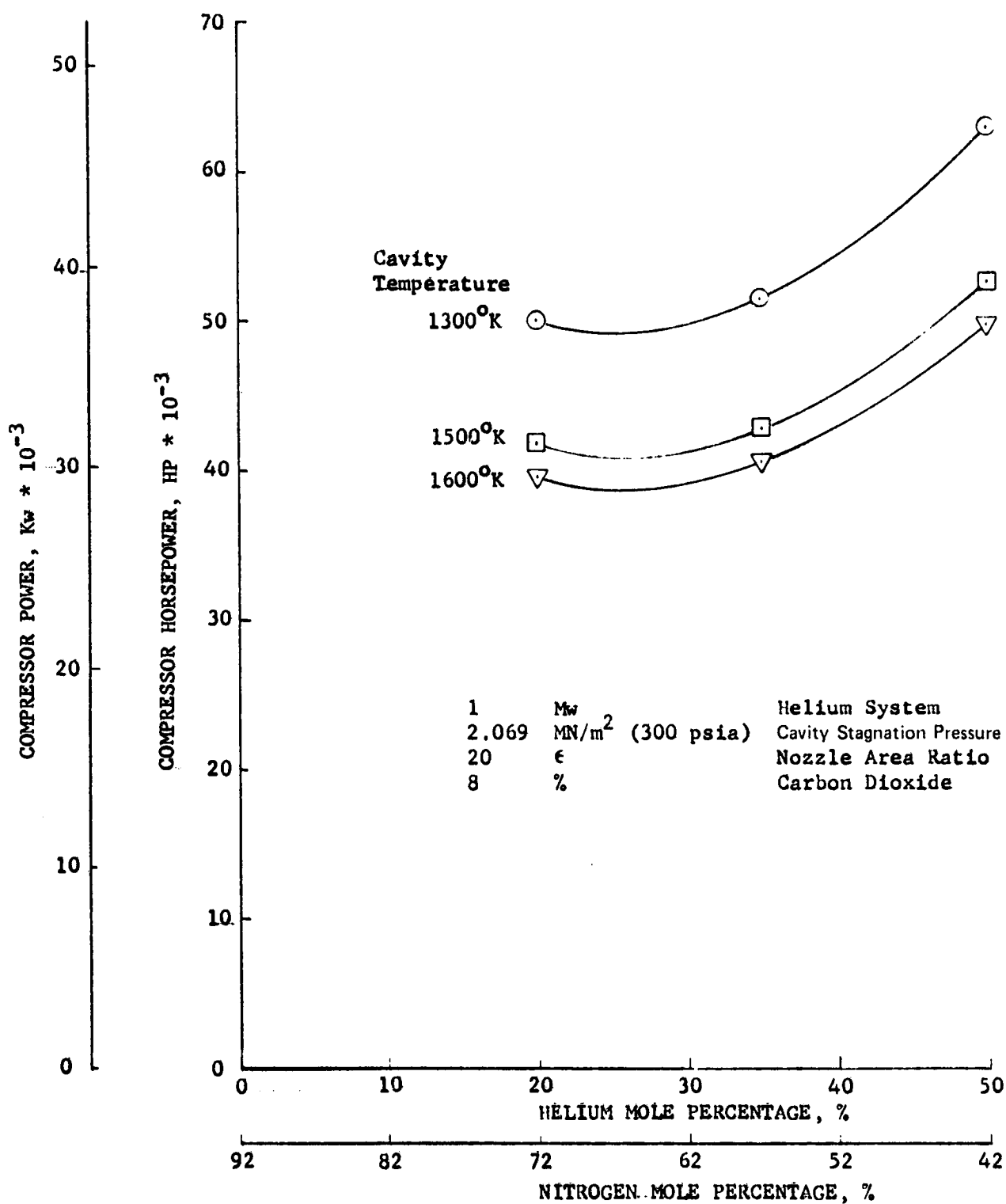
Figure 37. Effect of Helium Mole Percentage and Cavity
Stagnation Temperature on Compressor Power
Requirement

COMPRESSOR POWER, Kw * 10^{-3}

COMPRESSOR HORSEPOWER, HP * 10^{-3}

1300°K

1500°K
1600°K
Cavity
Temperature

1	Mw	Helium System
2.93	MN/m^2 (425 psia)	Cavity Stagnation Pressure
30	ϵ	Nozzle Area Ratio
8	%	Carbon Dioxide

HELIUM MOLE PERCENTAGE, %

NITROGEN MOLE PERCENTAGE, %
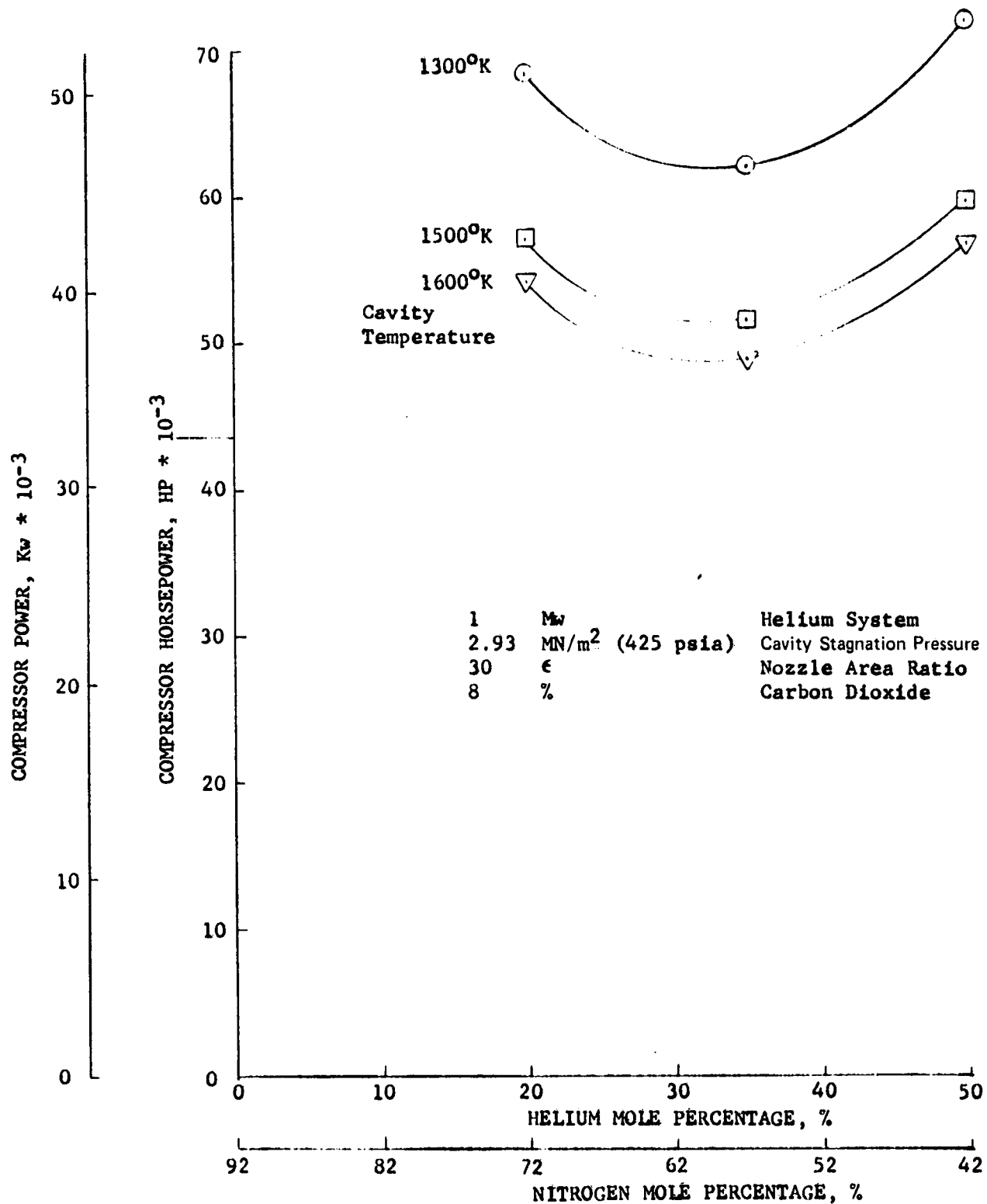
Figure 38.   Effect of Helium Mole Percentage and Cavity
Stagnation Temperature on Compressor Power
Requirement

49

(Minimum Power - Helium Mole Percentage, Cavity Pressure/Nozzle Area Ratio)
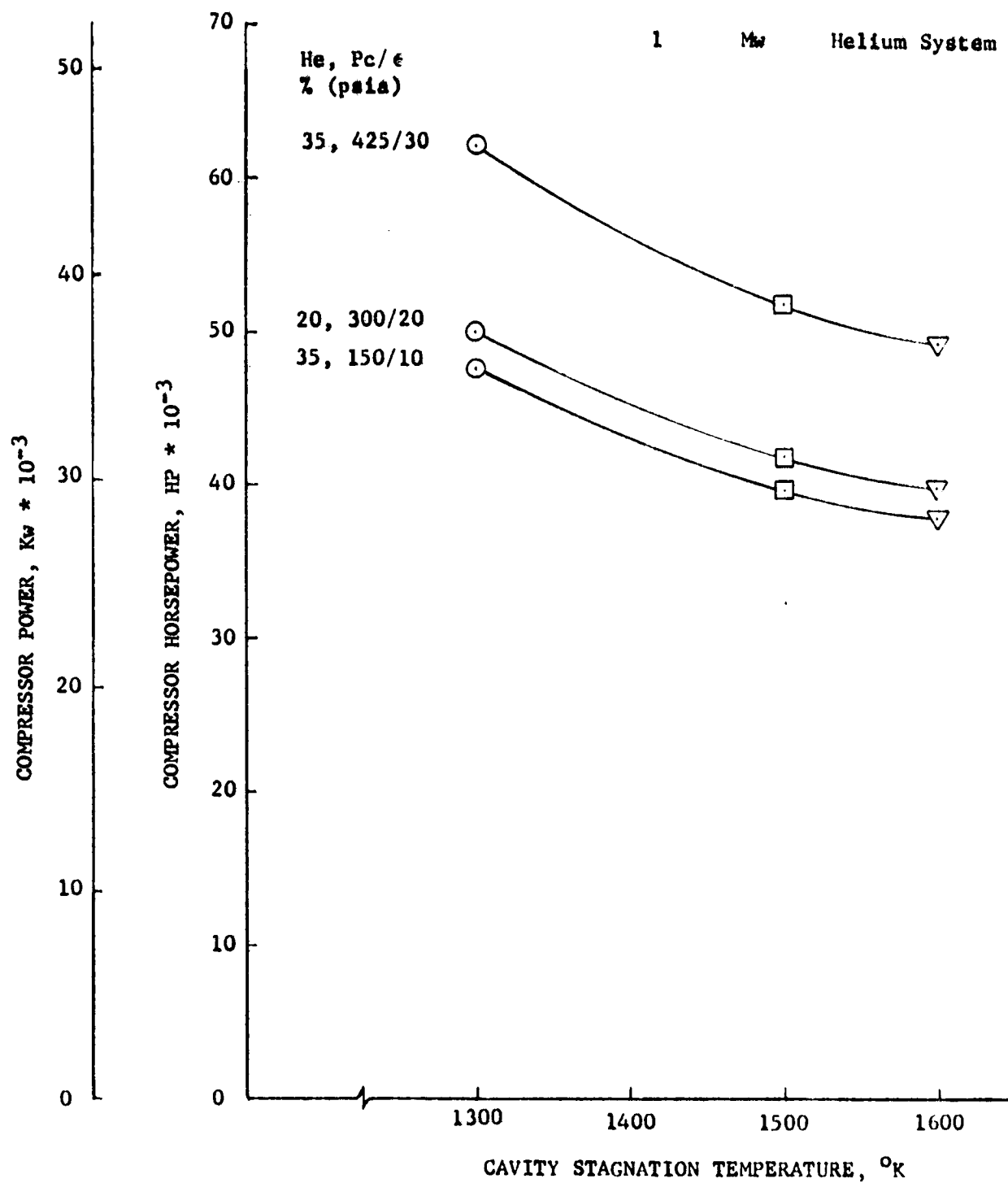
Figure 39. Effect of Cavity Stagnation Temperature and
Pressure on Compressor Power Requirement

Table V. Comparison of He and H_2O System
Cavity Static Temperatures

Effect of Area Ratio on Cavity
Static Temperature, °K

System Parameters

$X_{he} = 35\%$ vs $XH_2O = 1\%$
$P_c = 1.725$ MN/m^2 (250 psia)
$T_c = 1500°K$

Area Ratio	Cavity Static Temperature, °K	
	He	H_2O
10	406	491
20	306	389
30	258	340
40	223	309
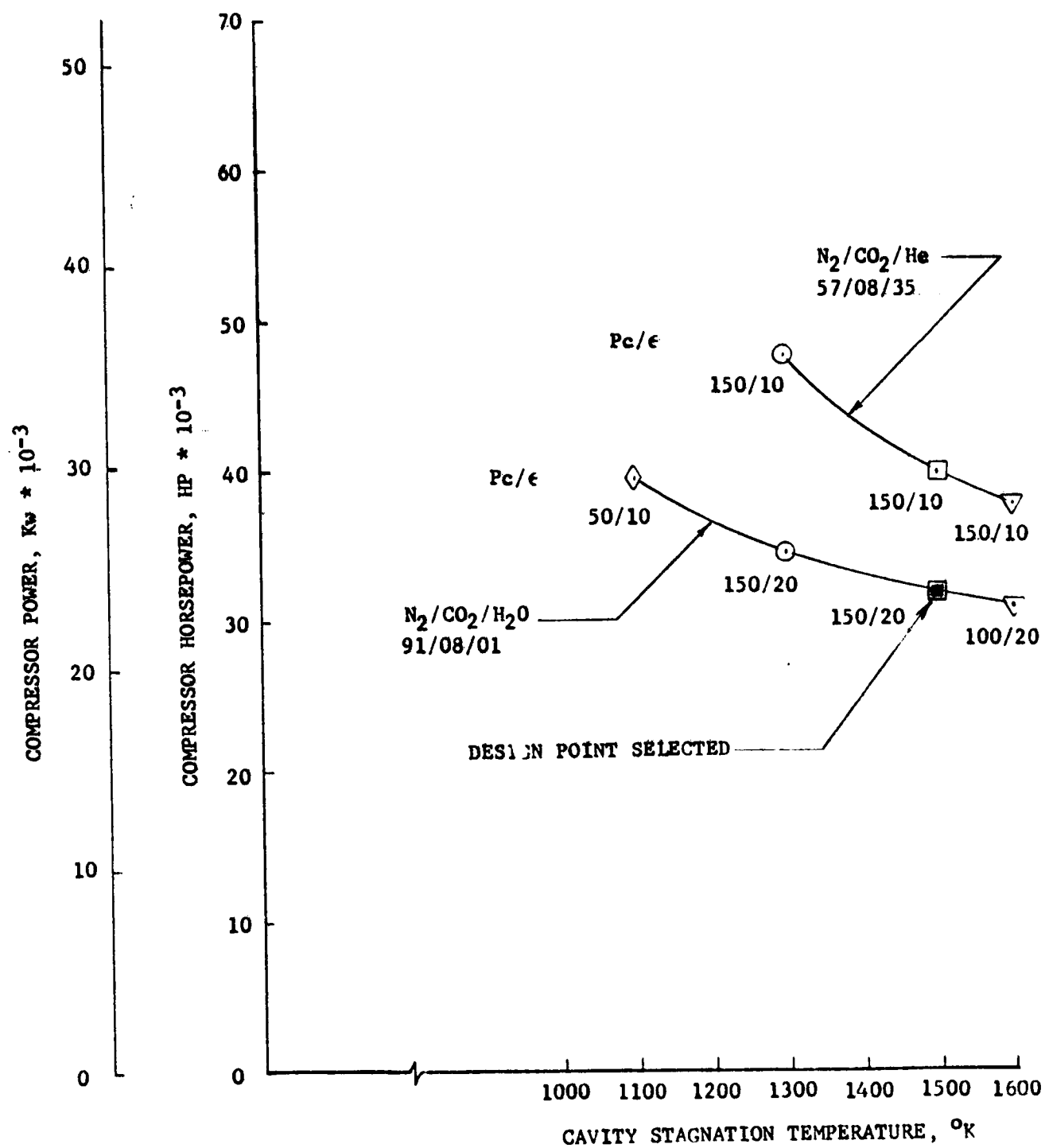
Figure 40. Comparison of Helium and Water Systems
(1-Mw System)

52

Table VI. System Characteristics Comparisons

Cavity Stagnation Temperature	Compressor Power	Cavity Length	Equivalent Fresnel Number
^{o}K (^{o}R)	Kw (HP)	m (ft)	$\frac{(M-1)}{2M^2} \frac{a^2}{\lambda L}$
1600 (2880)	22,968 (30,800)	8.38 (27.5)	2.57
1500 (2700)	23,862 (32,000)	6.35 (20.8)	3.39
1300 (2340)	25,727 (34,500)	7.11 (23.3)	3.03
1100 (1980)	29,381 (39,400)	15.75 (51.8)	1.37

M = magnification = 3.16
a = beam radius = 6.5 cm
L = length of oscillator

53

Table VII. Base Closed-Cycle Design Point

Power,	Mw	1.	
Cavity Specific Power,	Kw-s/Kg (Kw-s/1b)	22.9	(10.4)
Compressor Horsepower,	Kw (HP)	23723	(31800)
Cycle Thermal Efficiency,	%	1.05	
Laser/Power Source Efficiency,	%	4.22	
Stagnation Pressure,	MN/m^2 (psia)	1.03	(150)
Stagnation Temperature,	^{o}K (^{o}R)	1500	(2700)
$X_{N_2}/X_{CO_2}/X_{H_2O}$,	Mole Fraction	.91/.08/.01	
Nozzle Area Ratio	ϵ	20	
Cavity Flow Rate,	Kg/s (lbm/sec)	43.6	(96.2)
Percent Diffuser Injection Flow	%	8.0	
Compressor Flow Rate, lbm/sec	Kg/s (lbm/sec)	47.1	(103.9)
Beam Diameter,	cm	13.0	
Cavity Length in Optical Direction	cm	618.6	
Cavity Width,	cm	14.86	
Cavity Flow Length,	cm	127.	
Diffuser Length,	cm	66.3	
Optical Configuration,		2UO/3	
Duct Mach No.		0.3	

Optical Configuration Schematic

Gas Flow

A schematic of the base closed-cycle system is shown in figure 41 with appropriate flow, temperature, and pressure conditions. A pressure loss of 1.5% was used for the heat sink heat exchanger, as determined from the direct hot gas radiator optimization.

Diffuser Injection Flow

$\dot{W} = 7.7$

$\dot{W} = 103.9$
$T = 2700$
$P = 47.1$

$\dot{W}c = 96.2$
$Tc = 2700$
$Pc = 150$

Cavity   Diffuser

Heat.Sink
Heat
Exchanger

$\dot{W} = 103.9$
$T = 2700$
$P = 153.9$

Compressor
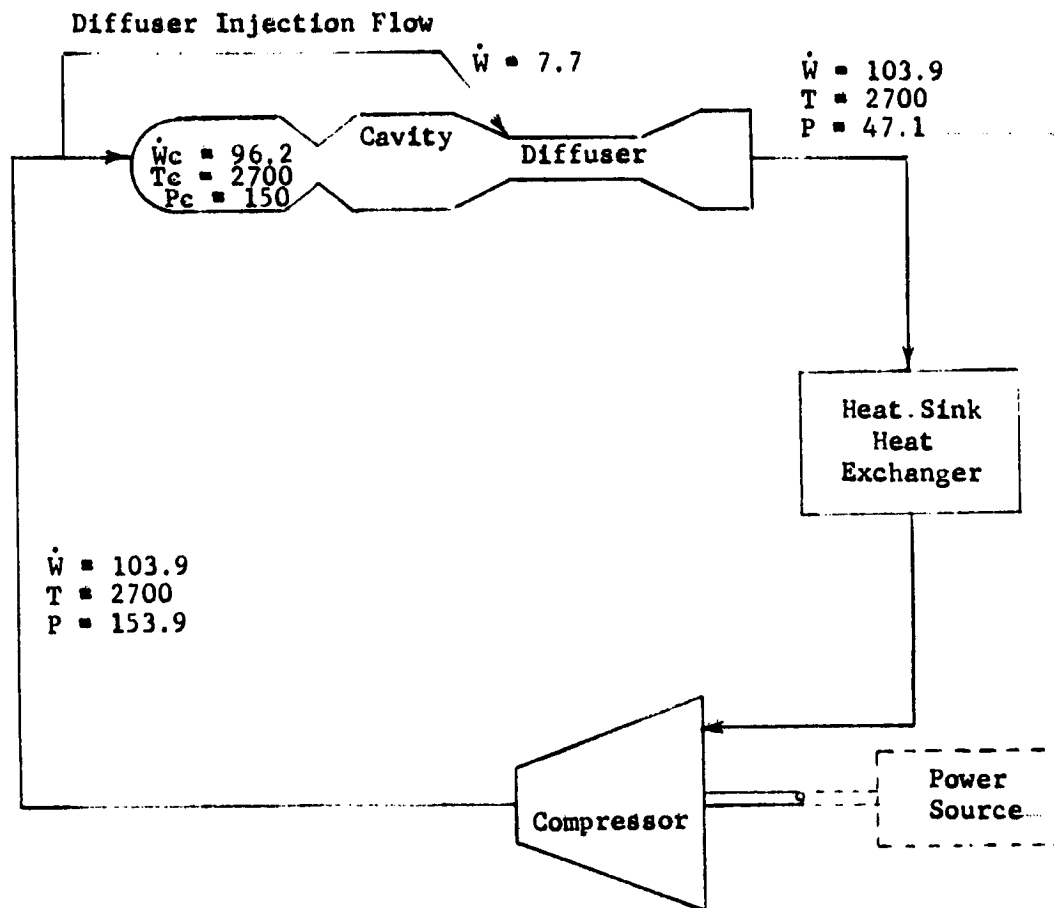
Power
Source

Power, 1 Mw

$\dot{W} \sim$ lb/sec
$T \sim {}^{o}R$
$P \sim$ psia

Cavity Specific Power, 10.4 Kw-sec/lb

Nozzle Area Ratio, 20

Figure 41. Base Closed-Cycle Configuration

Recuperator-Cycle Optimization

The recuperator cycle, shown schematically in figure 42, reduces the horsepower requirements of the compressor from that of the base cycle by reducing the compressor inlet temperature. This is achieved by transferring heat from the compressor inlet side of the gas loop to the compressor discharge with a recuperator, in addition to the overboard heat rejection. Since this heat exchange process is less than ideal, a heat source is required to return the gas to the laser cavity stagnation temperature. .

Because the heat sink heat exchanger is located downstream of the recuperator, the gas temperatures at the heat exchanger are much lower than in the base cycle. The surface area of a direct gas radiator, like the one used in the base cycle, increases significantly as the gas operating temperature approaches the radiator sink temperature. Thus, it becomes impractical to use a direct space radiator in the laser closed loop due to the increase in size and gas side pressure loss.

A gas-to-liquid heat exchanger system, in which an organic fluid such as toluene is used to cool the gas and, in turn, is cooled in a space radiator, provides a lower overall system weight and volume. Both the closed-loop heat exchanger and the space radiator are reduced in size due to the higher density and better heat transfer characteristics of the organic fluid.

The total system was optimized by reducing the compressor exit temperature to lower the horsepower requirements until the total system weight reached a minimum. As explained in the optimization approach, the laser device design conditions for this cycle were the same as those established in the base cycle optimization. The total system weight consists of the laser loop total weight plus the prime mover and heat source weights. The weight characterizations of the prime mover and heat source were described previously. The effect of compressor exit temperature on horsepower, laser loop weight, and total system weight is presented in figure 43. As compressor exit temperature is reduced, compressor inlet temperature approaches the radiator sink temperature and the heat exchanger and radiator sizes increase rapidly offsetting the reduction in compressor drive power source weight. A compressor exit temperature of 556°K (1000°R) was selected for the design point as a compromise between minimum horsepower and minimum total system and laser loop weight.

This low compressor exit temperature allows the use of an uncooled, metallic, state-of-the-art compressor design and eliminates the need for the advanced technology ceramic design which was selected for the base cycle.

A summary of the design parameters for the recuperator cycle is given in table VIII and a cycle schematic, with the gas stream temperatures and pressures given at critical locations, is shown in figure 42.

Cycle Comparison

As shown in tables VII and VIII the recuperator cycle has a thermal efficiency approximately 2.5 times that of the base cycle, and a laser/power source efficiency almost three times greater.

56
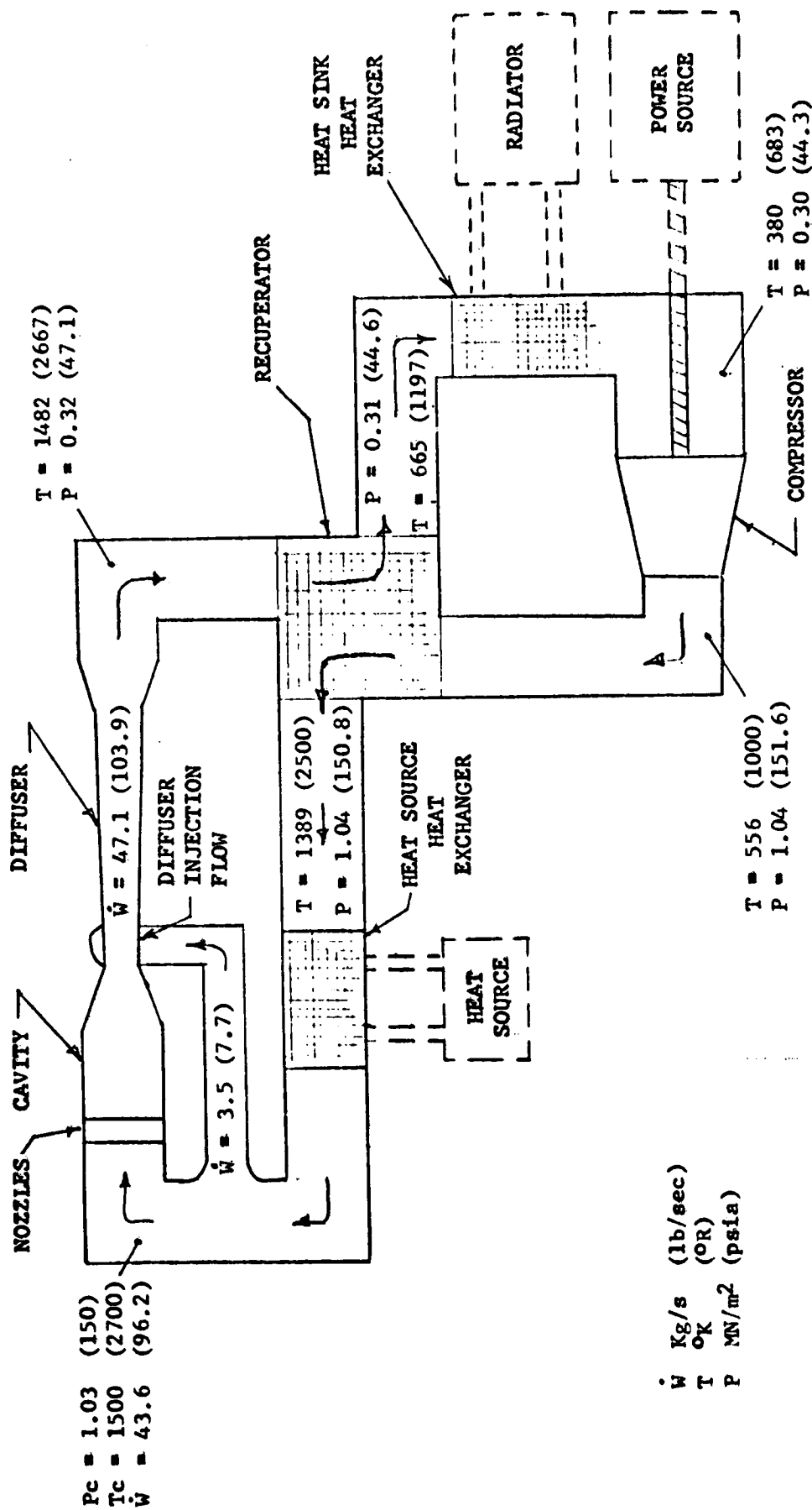
Figure 42. Recuperator Closed-Cycle Schematic
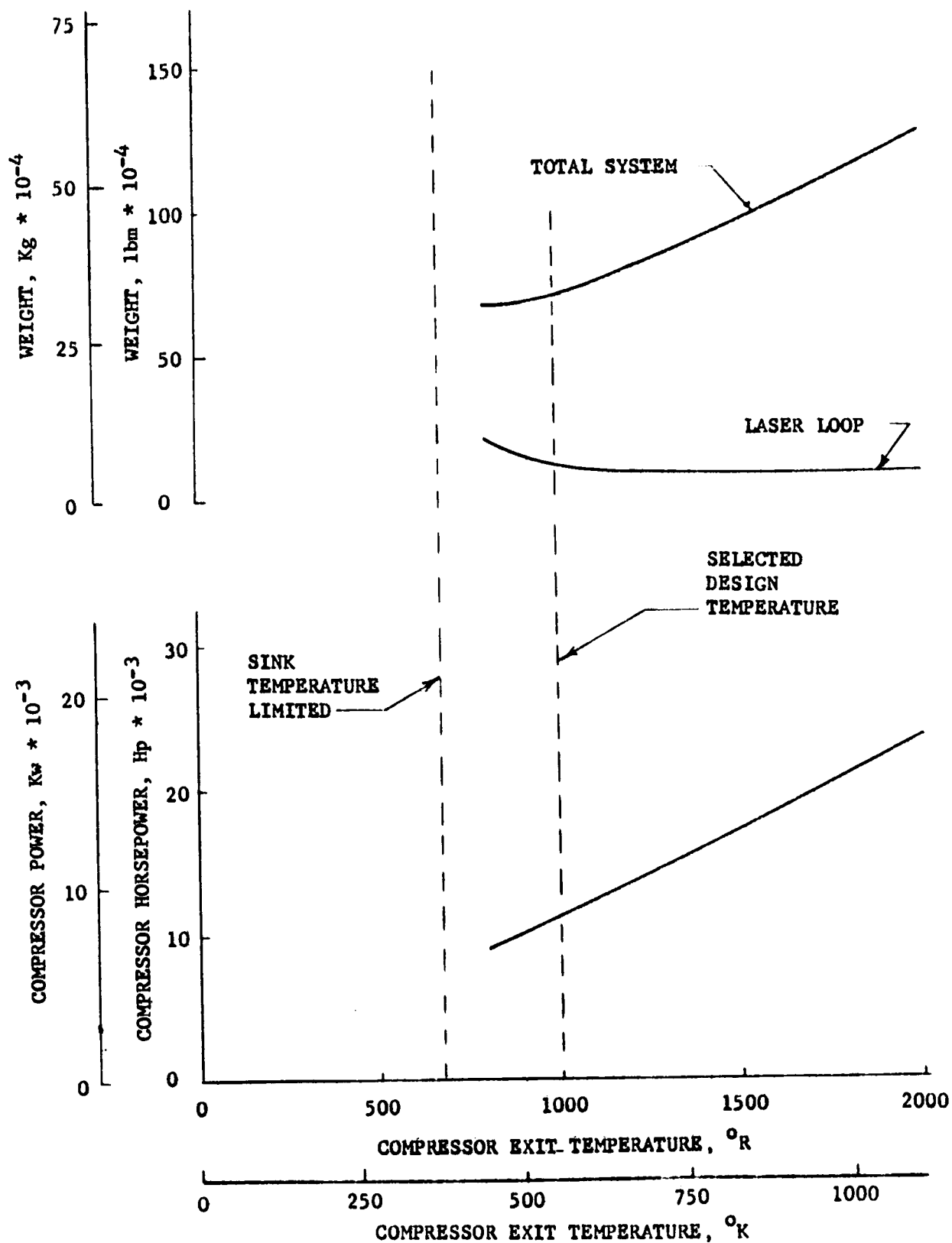
Figure 43. Effect of Recuperator on Space System Performance

Table VIII.   Closed-Cycle Design Point - 1-Mw Recuperator Cycle

Performance Parameters Summary

Power, Mw	1.0	
Cavity specific power, Kw-s/Kg (Kw-sec/lbm)	22.9	(10.39)
Compressor power, Kw (Hp)	8800	(11801)
Heat rejection requirements, KJ/s (Btu/sec)	14,400	(13657)
Heat source requirements, KJ/s (Btu/sec)	6600	(6262)
Stagnation pressure, MN/m^2 (psia)	1.03	(150)
Stagnation temperature, ^oK (^oR)	1500	(2700)
Composition, ($X_{N2}/X_{CO2}/X_{H2O}$)	.91/.08/.01	
Nozzle Area Ratio	20	
Cavity flow rate, Kg/s (lbm/sec)	43.6	(96.2)
Beam diameter, cm	13	
Optical configuration	2UO/3	
Cycle thermal efficiency, % E_{Laser}/E_{Input}	2.40	
Laser/power source efficiency, % $P_{Laser}/P_{Comp \& Hex}$	6.5	
Laser/compressor power efficiency,% P_{Laser}/P_{Comp}	11.4	

Device Parameters

Cavity length in optical direction, cm	619
Cavity width, cm	14.86
Cavity flow length, cm	46.0
Diffuser flow length, cm	127
Cavity recovery	0.47
Diffuser recovery	0.67
Percent diffuser injection flow, %	8.0
Diffuser inlet Mach number	3.81
Diffuser exit Mach number	0.2

Compressor Requirements

Power requirement, Kw (Hp)	8800	(11801)
Pressure ratio	3.42	
Inlet pressure, MN/m^2 (psia)	.30	(44.3)
Exit pressure, MN/m^2 (psia)	1.04	(151.6)
Inlet temperature, ^oK (^oR)	380	(683)
Exit temperature, ^oK (^oR)	556	(1000.)
Efficiency	0.852	(39.55)
Flow rate, Kg/s (lbm/sec)	47.13	(103.9)
Corrected flow rate, Kg/s (lbm/sec)	17.9	(39.55)

59

Table VIII. Closed-Cycle Design Point - 1-Mw Recuperator Cycle (Continued)

Heat Exchanger Parameters

Heat Sink Heat Exchanger

Heat transfer rate, KJ/s (Btu/sec)	14400	(13657)
Effectiveness	0.95	
Gas inlet temperature, $^{\circ}K$ ($^{\circ}R$)	665	(1197)
Gas exit temperature, $^{\circ}K$ ($^{\circ}R$)	380	(683)
Coolant exit temperature, $^{\circ}K$ ($^{\circ}R$)	606	(1092)
Coolant inlet temperature, $^{\circ}K$ ($^{\circ}R$)	364	(656)
Gas inlet pressure, MN/m^2 (psia)	.307	(44.6)
Gas flow rate, Kg/s (lbm/sec)	47.13	(103.9)
Gas pressure loss, %	0.59	
C_{hot}/C_{cold}	0.85	

Radiator

Heat transfer rate, KJ/s (Btu/sec)	14400	(13657)
Inlet wall temperature, $^{\circ}K$ ($^{\circ}R$)	552	(995)
Exit wall temperature, $^{\circ}K$ ($^{\circ}R$)	356	(642)
Sink temperature, $^{\circ}K$ ($^{\circ}R$)	256	(460)
Radiator emissivity	0.9	
Pressure loss, %	---	
Area (both sides), m^2 (ft^2)	8650.	(93108)

Recuperator

Effectiveness,	0.9	
Heat transfer rate, KJ/s (Btu/sec)	45880	(43452)
Hot side inlet temperature, $^{\circ}K$ ($^{\circ}R$)	1482	(2667)
Hot side exit temperature, $^{\circ}K$ ($^{\circ}R$)	665	(1197)
Cold side inlet temperature, $^{\circ}K$ ($^{\circ}R$)	556	(1000)
Cold side exit temperature, $^{\circ}K$ ($^{\circ}R$)	1389	(2500)
Hot side pressure loss, %	5.4	
Cold side pressure loss, %	0.5	
Cold side exit pressure, MN/m^2 (psia)	.31	(44.6)
Hot side inlet pressure, MN/m^2 (psia)	1.04	(151.6)
Mach No. inlet	0.05	

Heat Source Heat Exchanger

Heat transfer rate, KJ/s (Btu/sec)	6600	(6262)
Effectiveness	0.46	
Gas inlet temperature, $^{\circ}K$ ($^{\circ}R$)	1389	(2500)
Gas exit temperature, $^{\circ}K$ ($^{\circ}R$)	1500	(2700)
Gas inlet pressure, MN/m^2 (psia)	1.038	(150.8)
Liquid inlet temperature, $^{\circ}K$ ($^{\circ}R$)	1630	(2934*)
Liquid exit temperature, $^{\circ}K$ ($^{\circ}R$)	1565	(2816*)
Pressure loss, %	.55	
C_{cold}/C_{hot}	0.588	

* Suggested by NASA at Task I review meeting

60

The base cycle compressor requires a drive power of 23,723 kw (31,800 hp) for the 1-Mw system; the recuperator cycle requires only 8,800 kw (11,801 hp). The recuperator cycle laser loop weight is approximately 16 times that of the base cycle due to the additional weight of the recuperator and heat source. However, when the overall system weight (assuming a nuclear heat source and space Brayton power cycle) is considered, the increase in laser loop weight is more than offset by a decrease in power system weight. The net result is a reduction in total system weight of approximately 50% with the recuperator system.

The results of this comparison were presented to the NASA Lewis program monitors at the Task I Review on 4 December 1975. At this time, the recuperator cycle, with an associated heat source, was selected for the space and airborne applications because of its lower compressor horsepower requirements and its state-of-the-art compressor.

Airborne System

A closed-cycle system for airborne operation is essentially the same as for a space application. The differences occur in the heat rejection method and in both the heat and power source systems. The airborne system heat rejection can be accomplished with more conventional methods than with the radiation system required in space. The power source can be a conventional gas turbine instead of a nuclear reactor, and a hydrocarbon burner can be used as a heat source.

The airborne system does not have any components different from the space system that would significantly affect horsepower requirements. Since minimum compressor horsepower was the required optimization parameter, the airborne optimum cycle was the same as that for the space system. The only additional analysis required was in the design of the heat rejection heat exchanger.

To determine the effects of modifying the system for airborne operation, two candidate heat sink systems were considered:

- Gas-to-ram air
- Gas-to-dumped water.

The weight of each system as a function of operating time is presented in figure 44. Except for operating times of less than a few minutes, the ram air system is considerably lighter than the dumped water system. The ram air system was sized to operate with approximately 80% of the aircraft dynamic pressure.

The design parameters for the gas-to-air heat rejection heat exchanger are given in table IX.
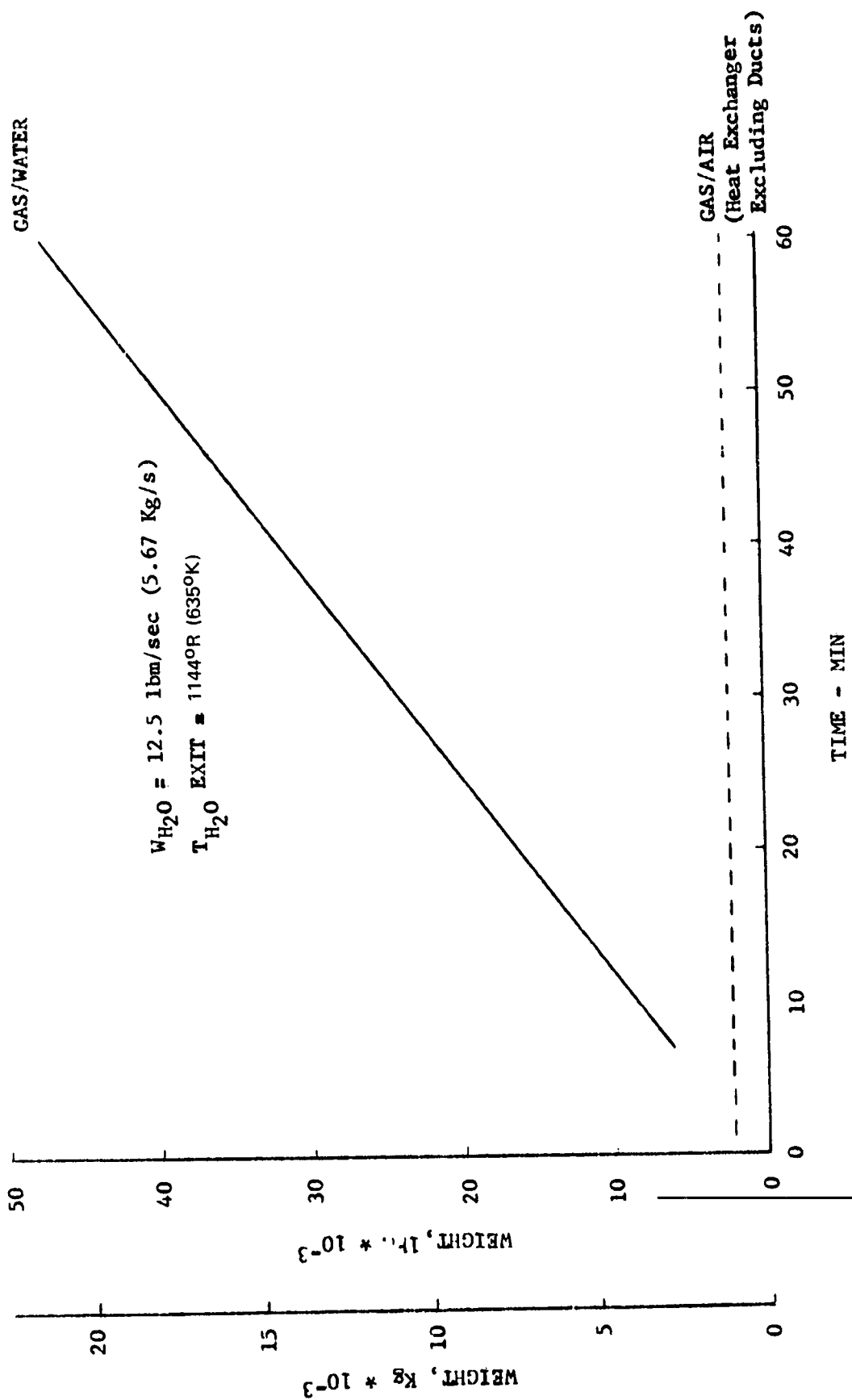
Figure 44. Candidate Heat Sinks for Airborne System

Table IX. Gas-to-Air Heat Exchanger Design

Heat Transfer Rate, kw/s (Btu/sec)	14,400	(13,658)
Gas Inlet Temperature, °K (°R)	665	(1,197)
Gas Exit Temperature, °K (°R)	380	(683)
Coolant Inlet Temperature, °K (°R)	253	(456)
Coolant Exit Temperature, °K (°R)	500	(900)
Coolant	Air	
Gas Inlet Pressure, MN/m^2 (psia)	0.307	(44.6)
Gas Flowrate, kg/s (lb$_m$/sec)	47.13	(103.9

The design conditions for all of the other components for the airborne cycle, with the exception of the power and heat source, are given in table VIII.

Although the recuperator cycle selected for the airborne system does provide minimum horsepower, it is not obvious that it is optimum when total system weight is considered. A preliminary analysis of the power and heat source system for the airborne cycle was conducted even though it was not required for this study. The following listing shows the approximate level of performance that current technology gas turbines should produce at an altitude of 13,716 m (45,000 ft) and a Mach number of 0.8.

shp/wt   -   0.74 kw/kg (0.45 hp/lb$_m$)
Fuel flowrate/shp -   0.22 kg/kw/hr (0.36 lb$_m$/hr/hp)

Therefore, for a run time of 600 sec and a horsepower requirement of 8800 kw (11,801 hp) the total power source weight should be in the range of 11,340 to 13,608 kg (25,000 to 30,000 lb$_m$). This is much less than the power source weight required for the space system. The additional power source weight required to produce the 23,723 kw (31,800 hp) required for the base cycle would be approximately 18,144 kg (40,000 lb$_m$). This extra weight is in the same range as that for the recuperator. Therefore, an additional study, which exceeds the scope of this program, may be warranted to conduct weight trades of the base and recuperator closed-laser loop systems, combined with the prime mover system, to optimize the total airborne system weight.

5- and 10-Mw Systems

As discussed in the Introduction, the objectives of Task I were the optimization of a closed-cycle GDL system at 1-, 5-, and 10-Mw output power levels. The approach to the 5- and 10-Mw system design was to extend the results from the optimized 1-Mw system. This amounted to determining those components whose performance characteristics would change with increased laser output power. These components were then characterized for the effects of the increased power level. With the new performance levels incorporated, the 5- and 10-Mw systems were evaluated. The optimum laser design parameters, such as nozzle area ratio, cavity stagnation temperature, injection flow percentage, etc., were retained from the 1-Mw system, since these optimum values do not change with power level.

The major performance parameter that changed with increased laser power was the cavity specific power. Specific power increased because of the longer cavity optical length and increased beam intensity, which tends to more completely saturate the laser cavity. The cavity is said to be saturated when the laser beam intensity is high enough to stimulate emission in all the excited molecules in the gas flow. It was found that the optical configuration could be simplified and beam diameter increased because of the higher beam power and associated increased intensity. The effects of power level on beam diameter and cavity specific power are indicated in figure 45.

The aforementioned performance effects were incorporated into the system synthesis model, and the effects of higher laser output powers (5 and 10 Mw) on system size were determined. The results from the 1-Mw system optimization indicated that nozzle stagnation pressure can have a significant effect on system weight and geometry. Therefore, the stagnation pressure was varied over the range from 0.34 to 3.4 MN/m^2 (50 to 500 psia) to determine if the value selected for the 1-Mw system was optimum for the 5- and 10-Mw systems. The effect of laser output power and nozzle stagnation pressure on the total system weight is presented in figure 46. The optimum pressure of 1.03 MN/m^2 (150 psia) is the same for the 1-, 5-, and 10-Mw systems if system weight is all that is considered. However, when the physical dimensions of the system, such as cavity optical length, is considered, figure 46 shows that the 10-Mw system components would exceed the dimensions of the space shuttle cargo envelope and the 5-Mw system approaches it. Therefore, a nozzle pressure of 1.38 MN/m^2 (200 psia) was selected as the design point for the 5- and 10-Mw systems. This selection results in only a slight increase in total system weight (2%), as shown in figure 46. A summary of the design parameters for the 5- and 10-Mw space system is presented in table X.

Both the 5- and 10-Mw system weight levels are much greater than the maximum allowable for airborne application, assuming the 99,790 kg (220,000 lb_m) C5A payload capability. Therefore, no additional analysis was attempted on these systems as airborne candidates.
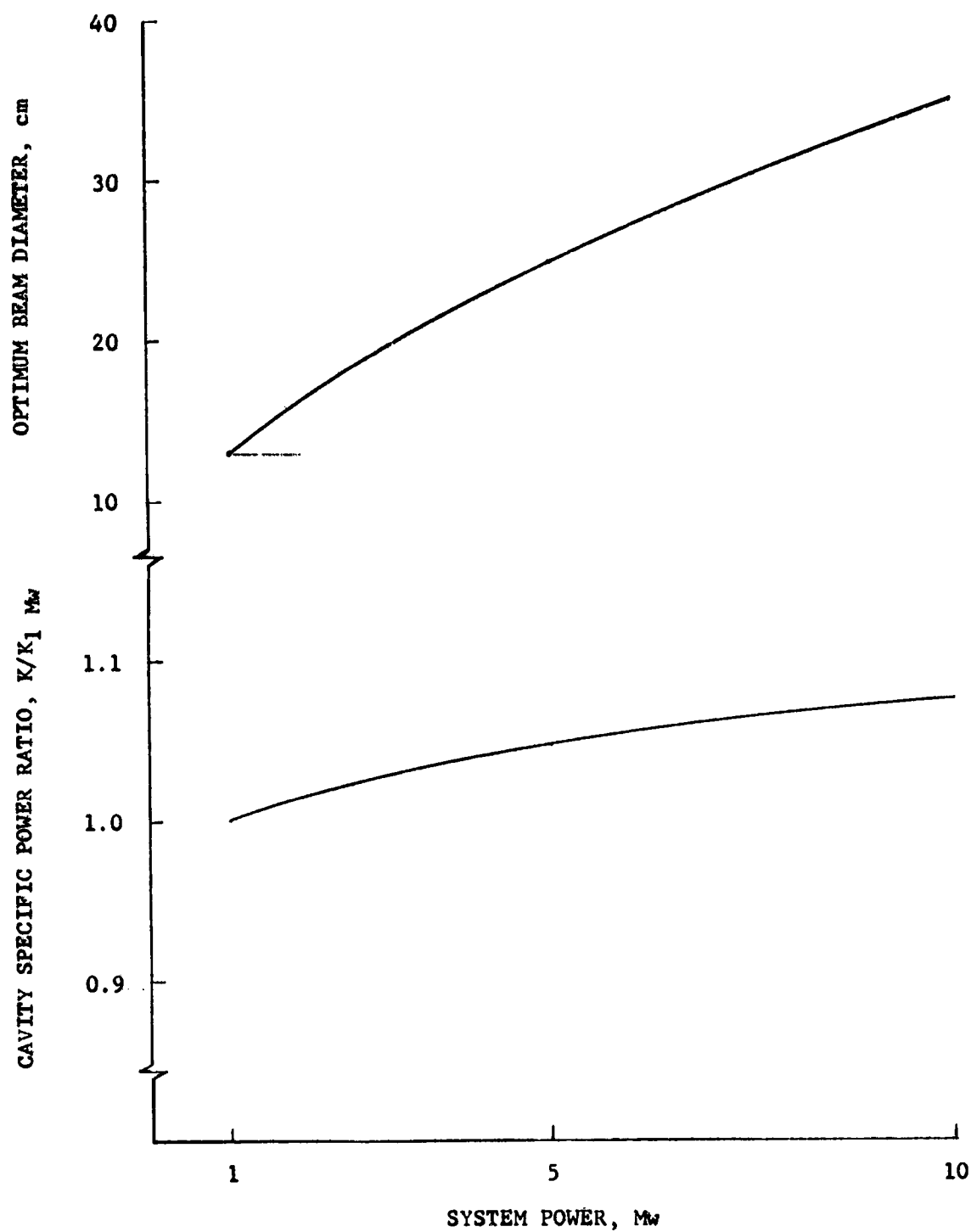
Figure 45. High Power System Performance Evaluation
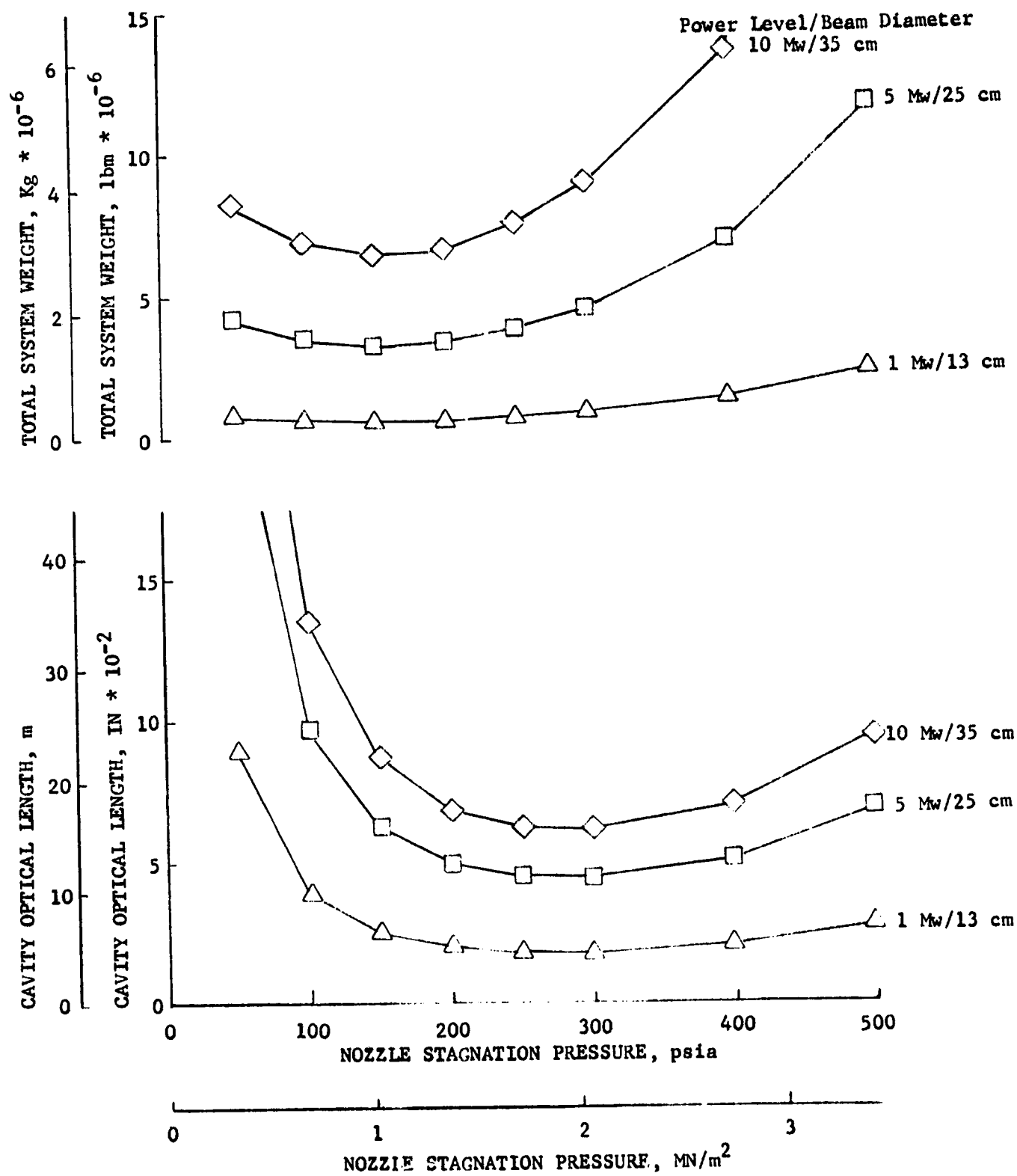
Figure 46. Effect of Laser Power Level and Nozzle
Stagnation Pressure on Total System Weight
and Cavity Optical Length

Table X. Recuperator Closed-Cycle High Power Design Points

Performance Parameters Summary

Power, Mw	5.0		10.0	
Cavity specific power, Kw-s/Kg (Kw-sec/lbm)	22.5	(10.2)	23.1	(10.5)
Compressor horsepower, Kw (hp)	44,500	(59,651)	86,535	(116,000)
Heat rejection requirements, KJ/s (Btu/sec)	72,750	(68,953)	141,650	(134,258)
Heat source requirements, KJ/s (Btu/sec)	33,250	(31,515)	65,115	(61,717)
Stagnation pressure, MN/m^2 (psia)	1.38	(200	1.38	(200)
Stagnation temperature, $^\circ K$ ($^\circ R$)	1500	(2700)	1500	(2700)
Composition, $X_{N2}/X_{CO2}/X_{H_2O}$	.91/.08/.01		.91/.08/.01	
Nozzle area ratio	20		20	
Cavity flow rate, Kg/s (lbm/sec)	221	(488)	431	(950)
Beam diameter, cm	25		35	
Optical configuration,	UO/2		UO/1	
Cycle thermal efficiency, %	2.37		2.43	
Laser/power source efficiency, %	6.4		6.6	
Laser/compressor power efficiency, %	11.2		11.6	

Device Parameters

Cavity length in optical direction, cm	1224	1702
Cavity width, cm	28.5	40
Cavity flow length, cm	82.0	112.0
Diffuser length, cm	244.0	342.0
Cavity recovery,	0.468	0.468
Diffuser recovery,	0.670	0.670
Percent diffuser injection flow, %	8.0	8.0
Diffuser inlet Mach number,	3.81	3.81
Diffuser Exit Mach number,	0.2	0.2

Compressor Parameters

Horsepower requirement, Kw (hp)	44,500	(59,651)	86,535	(116,000)
Pressure ratio,	3.42		3.42	
Inlet pressure, MN/m^2 (psia)	0.407	(59.1)	0.407	(59.1)
Exit pressure, MN/m^2 (psia)	1.393	(202.1)	1.393	(202.1)
Inlet temperature, $^\circ K$ ($^\circ R$)	379	(682)	379	(682)
Exit temperature, $^\circ K$ ($^\circ R$)	556	(1000)	556	(1000)
Efficiency,	0.852		0.852	
Flow rate, Kg/s (lbm/sec)	239	(527.0)	465	(1026)
Corrected, flow rate, Kg/s (lbm/sec)	68	(150.3)	133	(293)

Heat Exchanger Parameters

Heat Sink Heat Exchanger (Gas-to-Liquid) (finned-tube)	5 Mw		10 Mw	
Heat transfer rate, KJ/s (Btu/sec)	72,750	(68,953)	141,650	(134,258)
Effectiveness,	0.95		0.95	
Gas inlet temperature, $^\circ K$ ($^\circ R$)	665	(1197)	665	(1197)
Gas exit temperature, $^\circ K$ ($^\circ R$)	379	(682)	379	(682)
Coolant exit temperature, $^\circ K$ ($^\circ R$)	607	(1092)	607	(1092)
Coolant inlet temperature, $^\circ K$ ($^\circ R$)	364	(655)	364	(655)
Coolant, monoisopropylbiphenyl	MIPB		MIPB	
Gas inlet pressure, MN/m^2 (psia)	0.410	(59.5)	0.410	(59.5)
Gas flow rate, Kg/s (lbm/sec)	239	(527)	465	(1026)
Gas pressure loss, %	0.6		0.6	
C_{hot}/C_{cold},	0.85		0.85	

Table X. Recuperator Closed-Cycle High Power Design Points (Continued)

Radiator

Heat transfer rate, KJ/s (Btu/sec)	72,750	(68,953)	141,650	(134,258)
Inlet wall temperature, $^{\circ}K$ ($^{\circ}R$)	553	(995)	553	(995)
Exit wall temperature, $^{\circ}K$ ($^{\circ}R$)	357	(642)	357	(642)
Sink temperature, $^{\circ}K$ ($^{\circ}R$)	256	(460)	256	(460)
Radiator emissivity,	0.9		0.9	
Pressure loss, %	---		---	
Area (both sides), m^2 (ft^2)	44,108	(474,775)	85,554	(920,900)

Recuperator (plate-fin)

Effectiveness,	0.9		0.9	
Heat transfer rate, KJ/s (Btu/sec)	232,604	(220,614)	452,384	(429,064)
Hot side inlet temperature, $^{\circ}K$ ($^{\circ}R$)	1482	(2668)	1482	(2668)
Hot side exit temperature, $^{\circ}K$ ($^{\circ}R$)	665	(1197)	665	(1197)
Cold side inlet temperature, $^{\circ}K$ ($^{\circ}R$)	556	(1000)	556	(1000)
Cold side exit temperature, $^{\circ}K$ ($^{\circ}R$)	1389	(2500)	1389	(2500)
Hot side pressure loss, %	5.3		5.3	
Cold side pressure loss, %	0.5		0.5	
Hot side inlet pressure, MN/m^2 (psia)	0.433	(62.8)	0.433	(62.5)
Cold side inlet pressure, MN/m^2 (psia)	1.393	(202.1)	1.393	(202.1)

Heat Source Heat Exchanger (finned-tube)

Heat transfer rate, KJ/s (Btu/sec)				
Effectiveness,	33,250	(31,515)	65,115	(61,717)
Gas inlet temperature, $^{\circ}K$ ($^{\circ}R$)	1389	(2500)	1389	(2500)
Gas exit temperature, $^{\circ}K$ ($^{\circ}R$)	1500	(2700)	1500	(2700)
Gas inlet pressure, MN/m^2 (psia)	1.387	(201.2)	1.387	(201.2)
Liquid inlet temperature, $^{\circ}K$ ($^{\circ}R$)	1630	(2934)	1630	(2934)
Liquid exit temperature, $^{\circ}K$ ($^{\circ}R$)	1565	(2817)	1565	(2817)
Hot side fluid,	Lithium		Lithium	
Pressure loss, %	0.6		0.6	
C_{cold}/C_{hot}	0.59		0.59	

TASK II – CONCEPTUAL DESIGN

Objective

The objective of this Task is to supplement the design definition of the closed-loop laser system, selected from the parametric cycle optimization study, by conducting a conceptual design of each major component. The conceptual design provides a technology assessment of critical design areas, identification of component materials and weights, and definition of the system packaging configuration.

Approach

The system conceptual design is the second step in evaluating system feasibility using the data generated in the parametric cycle study. During this Task, a cursory design analysis and component configuration evaluation was performed to assess the criticality of the components that perform the defined thermodynamic functions. The recuperator cycle selected for both space and airborne applications was evaluated by conducting a conceptual design study of each major component. System package arrangements were studied by integrating the respective components into a configuration compatible with the operating environment and with the envelope of typical carrier vehicles.

Ground Rules

The following guide lines were established for the conceptual design study following a review of the results from the parametric cycle optimization.

- The **1-Mw** recuperator cycle was selected for both the space and airborne applications.

- Generate size and weight estimates for the 5 and 10 Mw systems.

- The component design will be based on 1990 technology and component critical aspects will be defined.

- The space system will be arranged for transporting in the space shuttle, with multiple flights if necessary.

- The airborne system will be arranged for the C5A aircraft cargo capacity and containment envelope.

- The heat source and heat sink are extraneous to this system study, with energy supplied or extracted by way of heat exchangers within the loop.

Subsequent subsections of this report present descriptions of the overall recuperator cycle designs for the space and airborne applications and the starting, shutdown, and storage procedures, with the associated equipment required for each. In addition, detailed descriptions of the major component designs are presented.

General Description of the Selected Recuperator Cycle

The Task I parametric optimization study defined the component requirements and general configuration for the closed-cycle GDL system. The optimum cycle selected in Task I was the recuperator cycle with heat source, which includes the following components listed in the order in which they occur in the flowpath:

1. Manifold/nozzle/cavity - provides the flowpath through which the laser gases are expanded to provide a lasing environment and power is extracted

2. Diffuser - converts the kinetic energy of the working fluid coming from the cavity into static pressure

3. Recuperator - transfers some of the diffuser exhaust heat to the compressor discharge

4. Heat sink heat exchanger - rejects the excess heat from the laser gases

5. Multiple-stage, axial-flow compressor - circulates and pressurizes the medium

6. Recuperator - heats the compressor discharge by recovering diffuser exhaust heat

7. Heat source heat exchanger - heats the laser gases to the temperature required at the nozzle inlet

8. Optical system - extracts the laser power using two unstable oscillator passes and three amplifying passes. The system uses five auto aligning mirrors as well as an aerodynamic window, which allows the beam to pass from the low-pressure region of the cavity to ambient pressure.

9. Combination laser gas conservation and start system - includes a vacuum pump, filter, and tank with appropriate valving.

A conceptual schematic showing relative sizes of components is shown in figure 47.

Space System Description

A closed-cycle GDL system for a space application would most likely be ferried into orbit with the space shuttle. Cost considerations make it desirable to minimize the number of trips required to get the total system into space and to limit the amount of assembly work that must be performed in orbit. It would be desirable to send the entire laser closed loop, fully charged and assembled, into orbit in one trip. Special consideration was given in the space system design to achieve these goals within the following constraints and environmental conditions:

1. A space shuttle payload limit of 27,216 kg (60,000 lb_m)

2. A space shuttle payload envelope of 4.6 by 4.6 by 18.3 m^3 (15 by 15 by 60 ft^3)

3. Space vacuum environment

4. Lack of support structure in space

5. Stability of the total system in orbit

6. Nonuniform heating of the device due to solar radiation.

The resulting configuration and conceptual layout for the laser loop portion of the 1-Mw space system is shown in figure 48. The package can be contained within the space shuttle envelope; however, the laser loop total weight of 48,534 kg (107,000 lb_m) exceeds the space shuttle payload capacity. A system weight summary is provided in table XI.
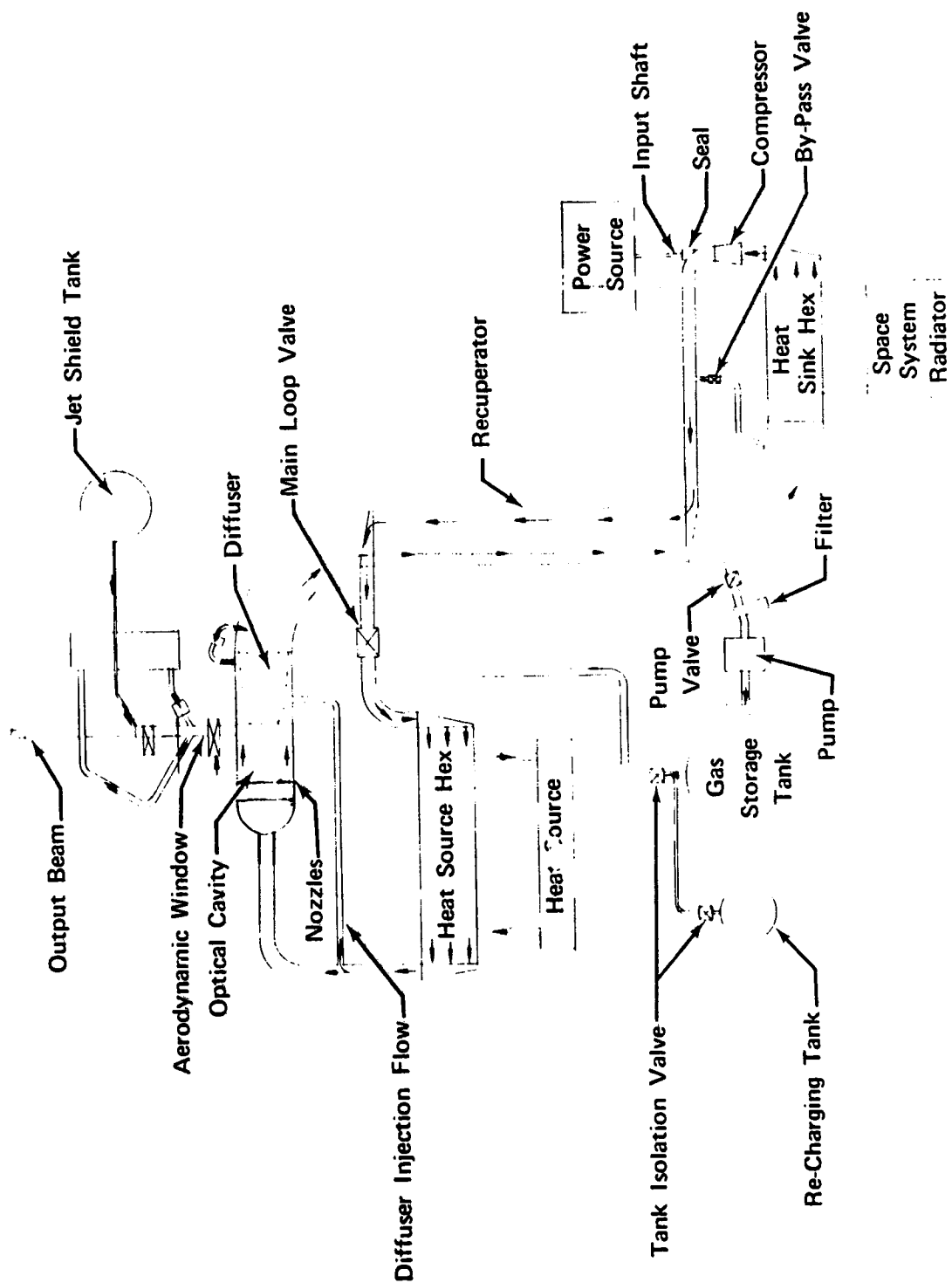
Figure 47. Recuperator Closed-Cycle Schematic (Space and Airborne Application)

71
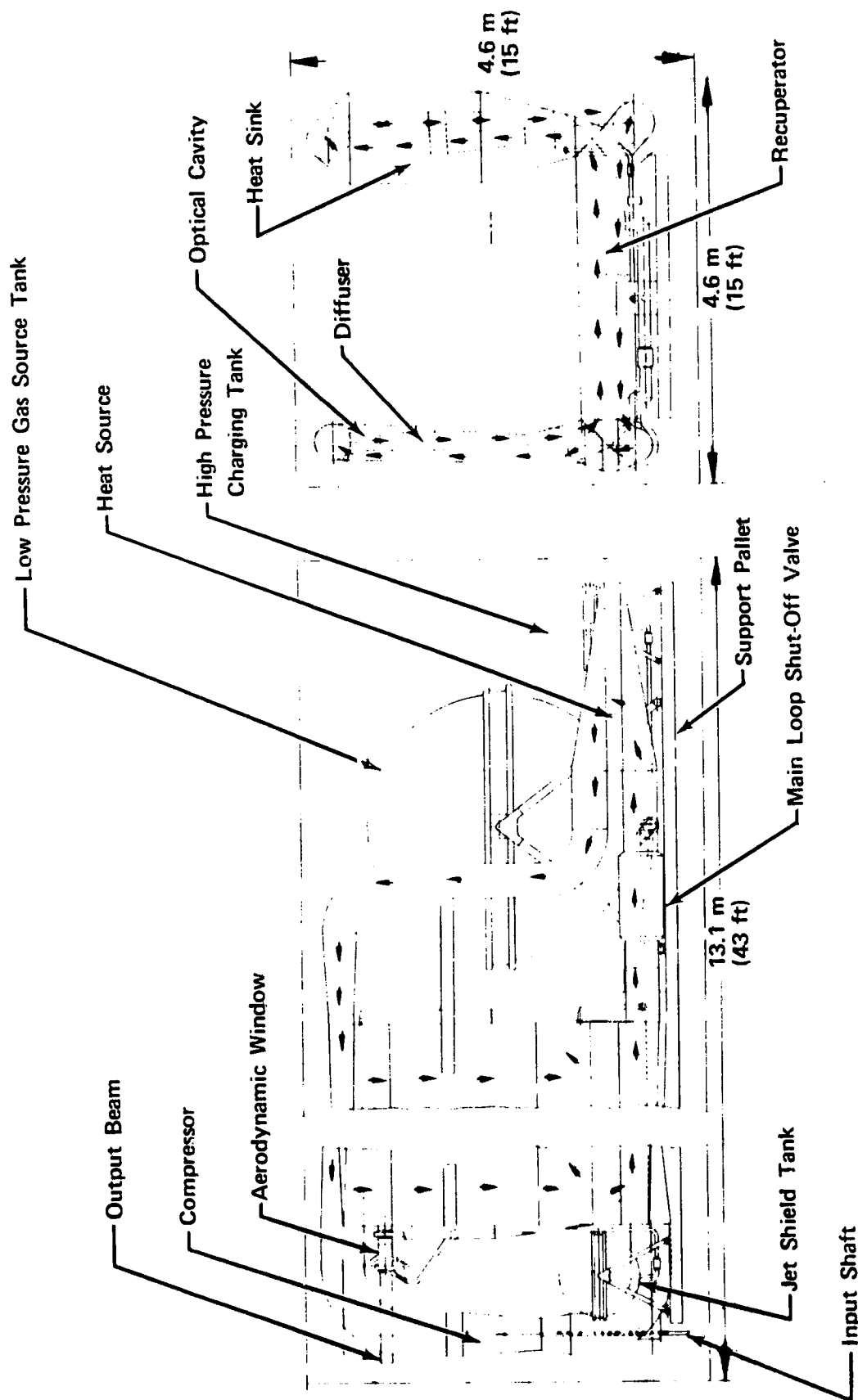
Figure 48. Closed-Cycle GDL (Space Application)

Low Pressure Gas Source Tank

Heat Source

High Pressure Charging Tank

Optical Cavity

Heat Sink

Diffuser

4.6 m (15 ft)

4.6 m (15 ft)

Recuperator

Support Pallet

Main Loop Shut-Off Valve

13.1 m (43 ft)

Output Beam

Compressor

Aerodynamic Window

Jet Shield Tank

Input Shaft

72

Table XI. Closed-Cycle GDL System Effect of Power Level on System Weight

SYSTEM SIZE	POWER LEVEL					
	1 Mw		5 Mw		10 Mw	
units	Kg	(1bm)	Kg	(1bm)	Kg	(1bm)
ITEM						
CNM	753	(1,660)	2,776	(6,120)	5,307	(11,700)
DIFFUSER	6,804	(15,000)	64,410	(142,000)	176,447	(389,000)
RECUPERATOR	25,583	(56,400)	97,296	(214,500)	225,299	(496,700)
HEAT SINK	6,083	(13,410)	33,276	(73,360)	65,045	(143,400)
COMPRESSOR	290	(640)	1,193	(2,630)	2,839	(6,260)
AERODYNAMIC WINDOW	136	(300)	263	(580)	367	(810)
HEAT SOURCE	426	(940)	1,420	(3,130)	2,803	(6,180)
DUCTS	3,606	(7,950)	9,507	(20,960)	13,218	(29,140)
TANKS	4,536	(10,000)	22,680	(50,000)	45,359	(100,000)
OPTICS	318	(700)	939	(2,070)	1,379	(3,040)
TOTAL WEIGHT	48,534	(107,000)	233,759	(515,350)	538,065	(1,186,230)
WEIGHT/Mw	48,534	(107,000)	46,720	(103,000)	53,524	(118,000)

The recuperator estimated weight is 25,583 kg (56,400 lb$_m$), which means that it must be ferried separately. The estimated weight of the remainder of the loop is 22,751 kg (50,600 lb$_m$). As a result, the loop could be ferried into orbit in two space shuttle flights and the recuperator mated with the remainder of the loop in orbit. To facilitate assembly, the loop and recuperator could be evacuated and sealed prior to flight and the laser gas stored in a separate tank from which the loop could be charged for starting. This approach is discussed in more detail in the subsection on starting concepts. If the recuperator and heat sink heat exchanger were built using a more efficient fin and spacing arrangement, the total laser loop weight could be reduced to 23,587 kg (52,000 lb$_m$), as shown later in table XIII. However, the fabrication techniques required for this type of configuration make its availability by the 1990 time period questionable. Therefore, it was not used for the conceptual design.

Structural integration of the space system is provided by mounting the components to a single pallet. It is assumed that system stability to prevent tumbling in space can be provided by the prime mover system since that system is an order of magnitude larger than the laser loop and would itself be stabilized to compensate for fluid dynamic forces.

The space vacuum poses a special problem for the aerodynamic window, since the optical cavity pressure is greater than the ambient pressure. The jet shield, as described in the aerodynamic window design section, is utilized to resolve this problem.

During detailed design, radiation shielding of the device would be provided to isolate critical areas of the device from each other and the prime mover and to prevent excessive thermals due to uneven exposure to solar radiation.

Effect of Power Level on System Size

To determine the effects of increased power level on the closed-cycle GDL system, an estimate was made of the weights and volumes for the 5- and 10-Mw systems. The same design philosophy was employed in the higher power level systems as was used in the 1-Mw system.

A weight summary for the 1-, 5-, and 10-Mw systems is provided in table XI. The size of these larger systems is indicated in table XII, which summarizes the envelope geometries of the 1-, 5-, and 10-Mw systems. A weight summary for a more optimistic system (assuming the development of a more efficient recuperator and heat sink heat exchanger) is provided in table XIII. The effect of higher power levels on the weight and geometry of the individual components is shown in figures 49 through 55 and table XIV.

Starting Concept

The major obstacle in starting the closed-loop GDL is the greater pressure ratio required across the cavity/nozzle/diffuser for starting than for steady-state operation. A starting pressure ratio of approximately 18:1 is required to force a high Mach number normal shock system through the fixed area cavity. This pressure ratio is reduced to 3.2 for steady-state operation. Sizing the compressor to achieve this starting requirement would result in a severe overdesign and compromise performance at the steady-state point. To avoid this problem, a separate gas starting system has been conceived.

The starting concept consists of evacuating the laser loop by tank storage of the gas so that the high starting pressure ratio can be achieved at a relatively low absolute pressure. The components required for starting the system are shown in figure 47. The starting system consists of a main loop shutoff valve inserted just upstream of the heat source heat exchanger to isolate the compressor discharge from the nozzle inlet during the start transient. A compressor bypass loop is provided to prevent compressor stall with the main loop valve closed. A tank and recharging pump are provided for evacuation of the loop and storage of the lasing fluid. The diffuser has provisions for bypassing starting flow, as previously discussed in the diffuser description.

Table XII. Closed-Cycle GDL System Effect of Power Level on System Geometry

ENVELOPE DIMENSIONS	POWER LEVEL		
m (ft)	1 Mw	5 Mw	10 Mw
Width	4.57 (15)	8.23 (27)	12.50 (41)
Height	4.57 (15)	8.23 (27)	12.50 (41)
Length	13.11 (43)	23.77 (78)	35.66 (117)

Table XIII. Closed-Cycle GDL System Effect of Power Level on System Weight With More Efficient Recuperator and Heat Sink

SYSTEM SIZE	POWER LEVEL					
	1 Mw		5 Mw		10 Mw	
units	Kg	(1bm)	Kg	(1bm)	Kg	(1bm)
ITEM						
CNM	753	(1,660)	2,776	(6,120)	5,307	(11,700)
DIFFUSER	6,804	(15,000)	64,410	(142,000)	176,447	(389,000)
RECUPERATOR	3,883	(8,560)	19,006	(41,900)	37,149	(81,900)
HEAT SINK	2,699	(5,950)	14,760	(32,540)	28,853	(63,610)
COMPRESSOR	290	(640)	1,193	(2,630)	2,839	(6,260)
AERODYNAMIC WINDOW	136	(300)	263	(580)	367	(810)
HEAT SOURCE	426	(940)	1,420	(3,130)	2,803	(6,180)
DUCTS	3,606	(7,950)	9,507	(20,960)	13,218	(29,140)
TANKS	4,536	(10,000)	22,680	(50,000)	45,359	(100,000)
OPTICS	318	(700)	939	(2,070)	1,379	(3,040)
TOTAL WEIGHT	23,451	(51,700)	136,953	(301,930)	313,723	(691,640)
WEIGHT/Mw	23,451	(51,700)	27,397	(60,400)	31,343	(69,100)
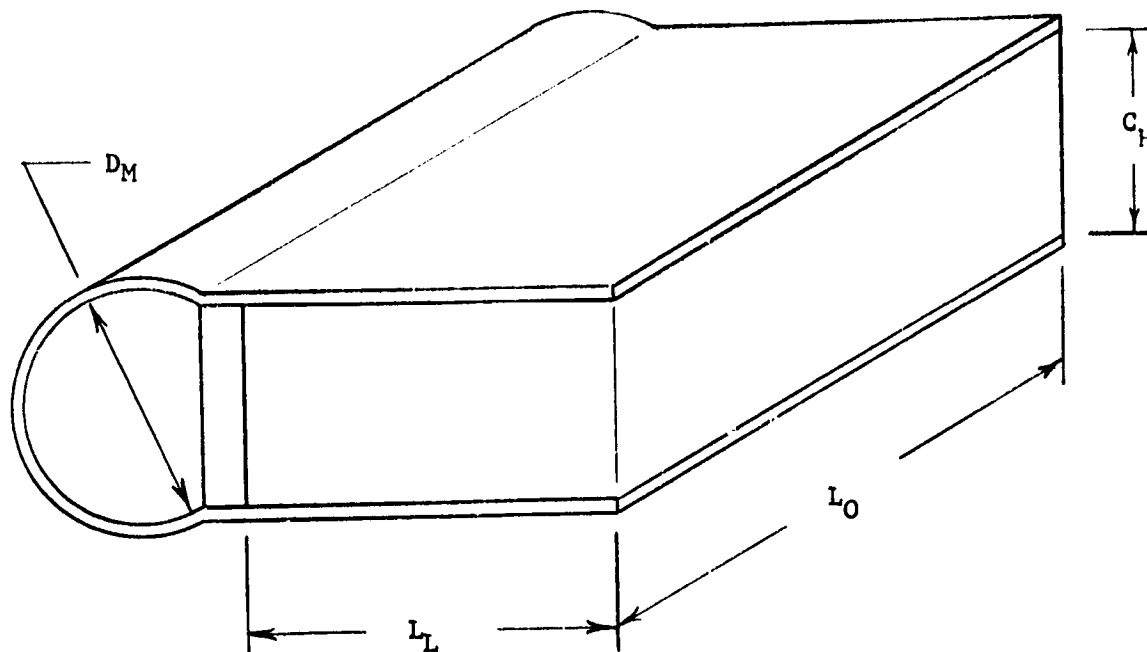
DIMENSIONS	1 MW		5 MW		10 MW	
L_L, cm	46		82		112	
L_O, cm	619		1224		1702	
C_H, cm	14.8		28.5		40	
D_M, cm (in)	40	(15.6)	90	(35.4)	126	(49.5)
W_T, Kg (1bm)	753	(1,660)	2776	(6,120)	5307	(11,700)
W_T/MW	1660	(1,660)	552	(1,240)	531	(1,170)

Figure 49. Effect of Power Level on Manifold/Nozzle/
Cavity Size and Weight
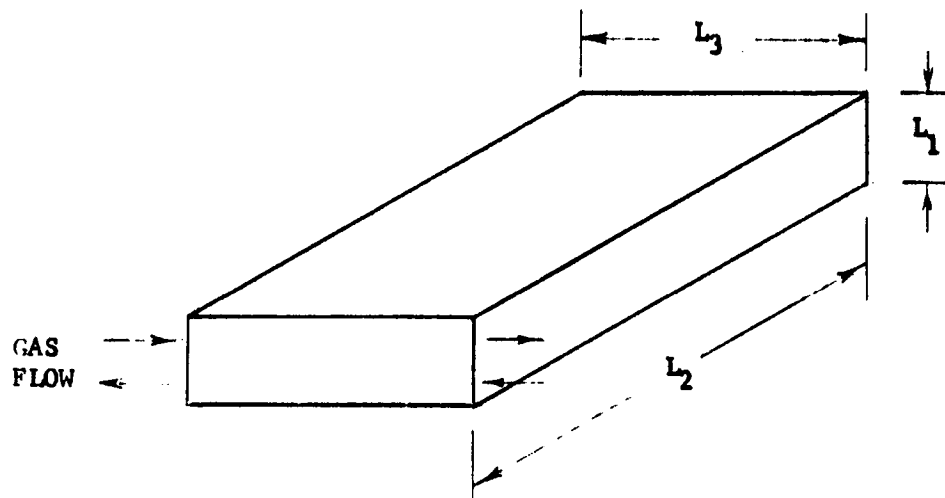
DIMENSION		1 MW	5 MW	10 MW
AF, m^2	(ft^2)	3.87 (41.7)	13.94 (150)	28.89 (311)
Vol, m^3	(ft^3)	11.3 (400)	37.4 (1,322)	86.7 (3,062)
L_1, m	(ft)	0.636 (2.085)	1.143 (3.75)	1.69 (5.55)
L_2, m	(ft)	6.1 (20.0)	12.2 (40.0)	17.1 (56.0)
L_3, m	(ft)	2.92 (9.59)	2.69 (8.81)	3.0 (9.85)
Wt, K_g	(1bm)	25,583 (56,400)	97,296 (214,500)	225,299 (496,700)
Wt/MW		25,581 (56,400)	19,459 (42,900)	22,530 (49,670)

Figure 50. Effect of Power Level on Recuperator Size and Weight - Type 11.1
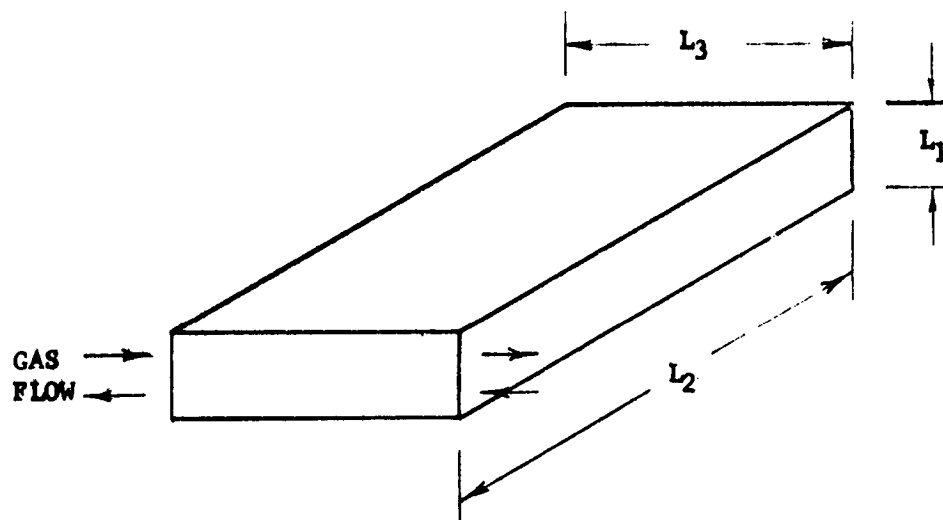
DIMENSION		1 MW	5 MW	10 MW
AF, m^2	(ft^2)	4.85 (52.2)	19.88 (214)	38.74 (417)
Vol, m^3	(ft^3)	1.71 (60.5)	8.38 (296)	16.40 (579)
L_1, m	(ft)	0.796 (2.61)	1.63 (5.35)	2.27 (7.44)
L_2, m	(ft)	6.1 (20.0)	12.2 (40.0)	17.1 (56.0)
L_3, m	(ft)	0.354 (1.16)	0.421 (1.38)	0.424 (1.39)
Wt, Kg	(1bm)	3,883 (8,560)	19,006 (41,900)	37,149 (81,900)
Wt/MW		3,883 (8,560)	3,801 (8,382)	3,715 (8,190)

Figure 51. Effect of Power Level on Recuperator Size
and Weight - Type 46.45T
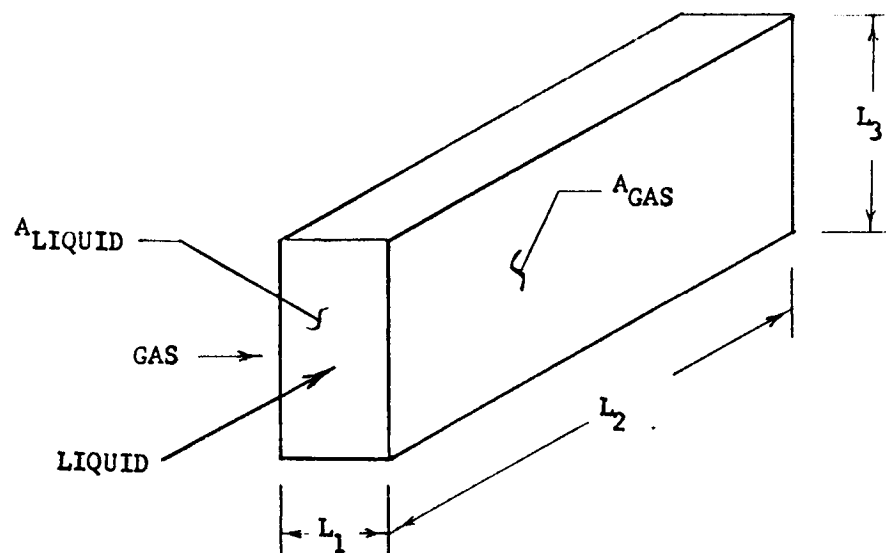
DIMENSION		1 MW	5 MW	10 MW
A_{GAS}, m^2	(ft^2)	1.25 (13.5)	4.24 (45.6)	8.25 (88.8)
A_{LIQUID}, m^2	(ft^2)	0.105 (1.13)	0.409 (4.4)	0.799 (8.6)
Vol, m^3,	(ft^3)	0.22 (7.9)	0.75 (26.4)	1.48 (52.1)
L_1, m	(ft)	0.178 (0.585)	0.176 (0.579)	0.179 (0.586)
L_2, m	(ft)	1.83 (6.001)	1.83 (6.000)	1.85 (6.058)
L_3, m	(ft)	0.589 (1.931)	2.32 (7.60)	4.47 (14.67)
Wt, Kg	(1bm)	426 (940)	1420 (3,130)	2,803 (6,180)
Wt/MW		426 (940)	284 (626)	280 (618)

Figure 52. Effect of Power Level on Heat Source Size and Weight
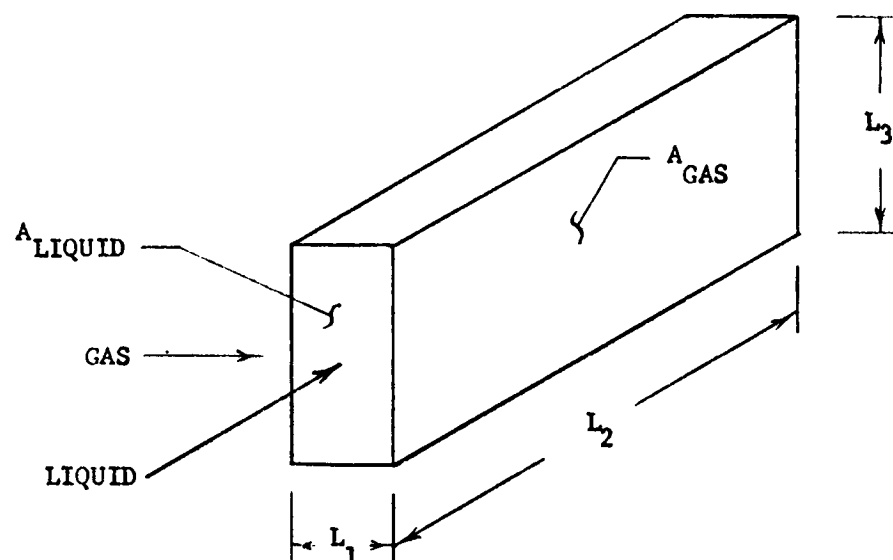
DIMENSION		1 MW	5 MW	10 MW
A_{GAS}, m^2	(ft^2)	6.69 (72.)	28.8 (310.)	56.6 (609)
A_{LIQUID}, m^2	(ft^2)	0.307 (3.3)	1.58 (17.0)	3.02 (32.5)
Vol, m^3	(ft^3)	9.9 (350.)	54.2 (1915)	106.0 (3,744)
L_1, m	(ft)	1.48 (4.86)	1.88 (6.17)	1.87 (6.14)
L_2, m	(ft)	6.46 (21.2)	11.43 (37.5)	11.46 (37.6)
L_3, m	(ft)	1.03 (3.39)	2.54 (8.33)	3.22 (10.57)
Wt, Kg	(1bm)	6,083 (13,410)	33,276 (73,360)	65,045 (143,400)
Wt/MW		6,083 (13,410)	6,655 (14,672)	6,505 (14,340)

Figure 53. Effect of Power Level on Heat Sink Size and Weight
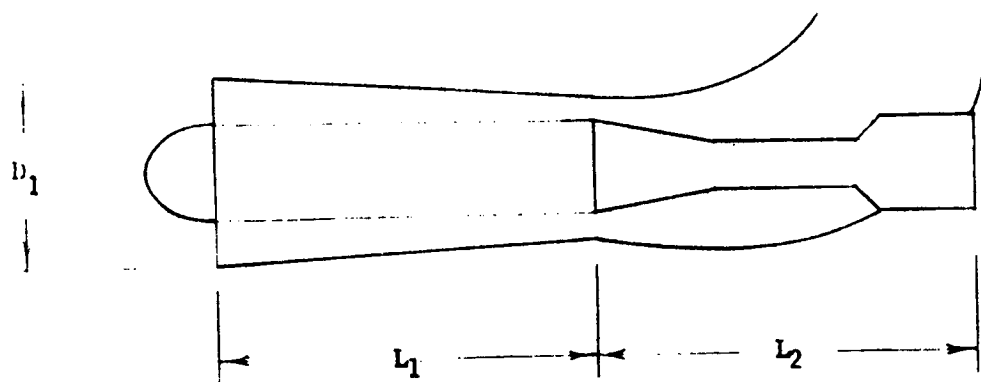
DIMENSION	1 MW	5 MW	10 MW
cm (in)			
L_1	99 (39)	193 (76)	272 (107)
L_2	114 (45)	190 (75)	284 (112)
D_1	48 (19)	84 (33)	117 (46)

Figure 54. Effect of Power Level on Compressor Size
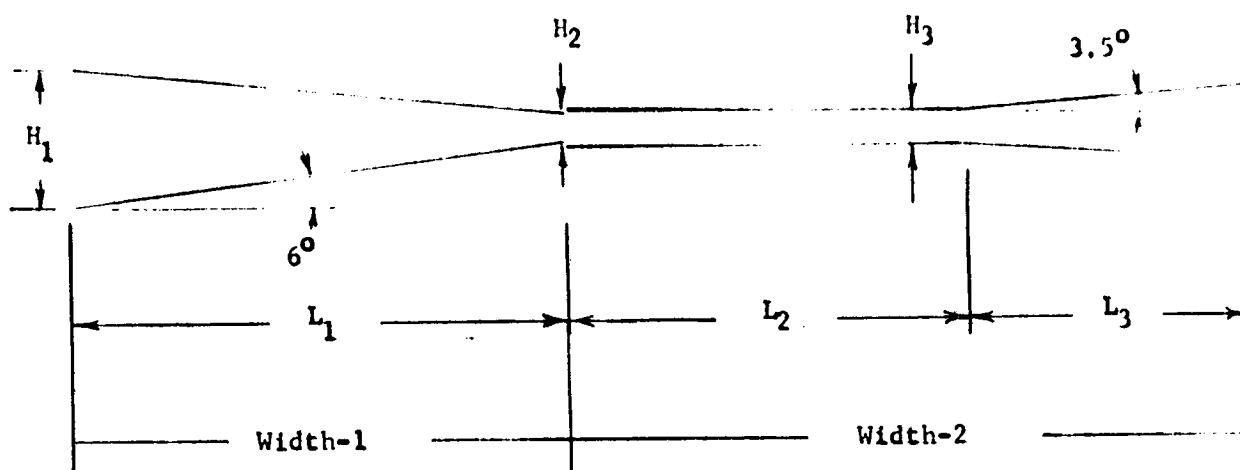
DIMENSION	1 MW	5 MW	10 MW
H_1, cm	14.86	23.5	40.
H_2, cm	3.16	6.06	8.51
H_3, cm	3.42	6.54	9.18
L_1, cm	55.6	106.9	150.
L_2, cm	40.9	78.8	110.6
L_3, cm	30.5	57.7	81.
L_{TOTAL}, cm	127.	243.4	341.6
Width-1, cm	619.	1224.	1702.
Width-2, cm	619.52	1225.	1703.4

Figure 55. Effect of Power Level on Diffuser Size

Table XIV. Effect of Power Level on Miscellaneous Hardware Weight

Wt, Kg (lbm)	1 MW	5 MW	10 MW
Ducts	3,606 (7,950)	9,507 (20,960)	13,218 (29,140)
A/W	136 (300)	263 (580)	367 (810)
Tanks	4,536 (10,000)	22,680 (50,000)	45,359 (100,000)

The starting sequence is shown in figure 56. The system is initially evacuated to a gas pressure of approximately 0.007 MN/m² (0.1 psia). This is achieved by pumping most of the gas out of the system and into the storage tank while the system is dormant. The system is started by bringing the compressor up to its steady-state speed with the compressor bypass valve open and the main loop shutoff valve closed.
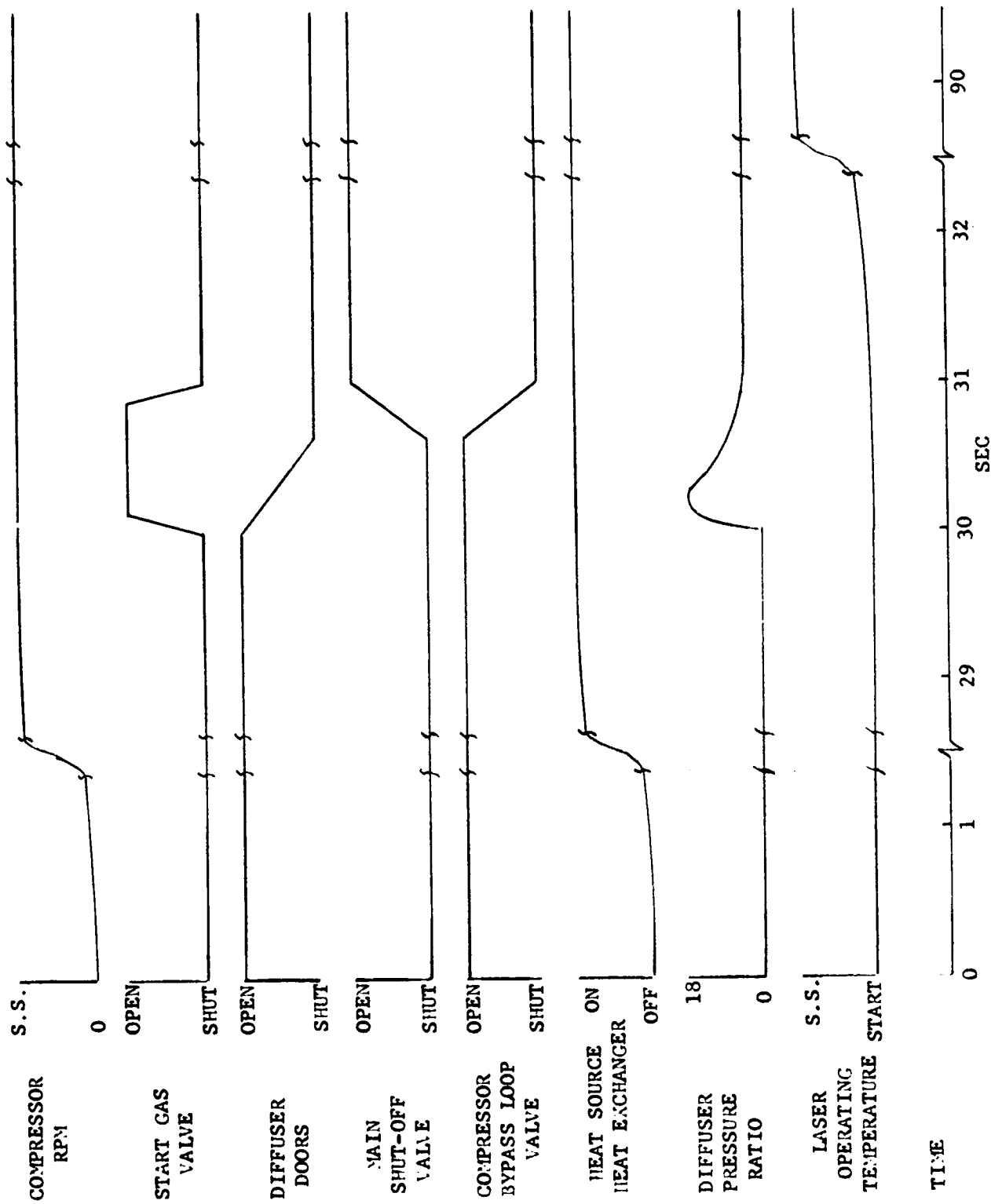
Figure 56. Closed-Cycle GDL Start Parameter Sequence Source

The gas storage system valve is then opened rapidly to pressurize the nozzle plenum. The upstream volume is much smaller than the volume downstream of the diffuser, which results in the downstream pressure lagging the upstream pressure sufficiently to achieve the starting pressure ratio of 18. The heat source heat exchanger is operated to provide hot gas to the nozzles to avoid condensation in the cavity.

Once the diffuser system has started, the system is transitioned to the steady-state operating mode before the overall device pressure ratio (PR) falls below that required for steady-state operation (≈ 3.2 PR). This transitioning consists of closing the compressor and diffuser bypasses and opening the main loop shutoff valve. The gas supply/pump system is used to provide the correct loop pressure as the gas-temperature is increased to its steady-state value.

The total time required for the system to reach steady-state conditions is 70 to 80 sec, with compressor startup requiring approximately 30 sec, valve sequencing at transition about 1 sec, and gas thermal transient 40 to 50 sec.

The compressor startup time was dictated by surge margin requirements. The valve sequencing time was estimated from a simplified transient volume filling analysis considering the system to consist of three separate volumes (gas storage tank, main loop shutoff valve to nozzles, and from nozzles to main loop shutoff valve). The thermal transient time was estimated from a time-dependent energy balance analysis that divided the system into eleven mass units (six ducts, cavity, diffuser, recuperator, heat sink heat exchanger, compressor, and heat source heat exchanger). The mass and surface areas of the components were estimated from the preliminary design drawings.

Structural problems or low cycle fatigue (LCF) and undesirable deformations associated with very fast start transients diminish as transient times increase. Since the above results indicate that the thermal transient for this device is relatively long, many problems are reduced or eliminated. For example, the usual thermal stress or LCF problem in the nozzles is eliminated; the problem of maintaining small blade tip clearances in the compressor is reduced; the thermal loads and deformations in the diffuser can be handled easier; the startup thermal stress levels in the heat exchanger are lower than usual, and there is less thermal shock in the sealed joints that could cause leak problems.

Shutdown Concept

The system shutdown cycle is basically the inverse of the start cycle; however, it is less complicated since it is rather easy to "unstart" the diffuser. The shutdown cycle is performed in the following sequence: (1) the heat source heat exchanger is cycled off; (2) the compressor drive power is gradually reduced, and the system is simultaneously scavenged by opening the pump valve and pumping the lasing fluid into the storage tank (tank isolation valves remain closed); (3) the compressor power is cycled completely off when the nozzle inlet pressure is reduced to 0.35 MN/m² (50 psia); (4) the pump valve is closed and the pump cycled off when the loop pressure reaches 0.0007 MN/m² (0.1 psia); (5) the aerodynamic window jet shield is cycled off and the window shutters closed; and (6) the space radiator is cycled off. The main loop valve and the compressor bypass valve are not cycled during the system shutdown. From this condition, the system can be cycled back to start or dormant storage.

84

Dormant Storage

The only potential problem anticipated during dormant storage involves the water vapor (1% mole fraction) in the loop gas mixture. The equivalent space ambient temperature is about 0°F (256°K) (from a radiation balance with the sun and space) and the water vapor will tend to condense below temperatures of approximately 60°F (289°K), which could cause corrosion and oxidation problems within the loop.

The water condensation during nonoperating periods could be controlled by one of the following methods:

1. During dormant periods, the space radiator can be positioned to receive solar radiation and keep the system temperature above the dew point using a small pump to circulate the lasing fluid.

2. Incorporation of a controlled cold spot in the loop to induce H_2O condensation and freezing at a selected location during the dormant periods.

3. Evacuation of the loop during the dormant period with the gas stored in a controlled environment tank.

The latter method was selected as being most compatible with the start and shutdown procedure.

Airborne System Description

Because of its large payload capability [in excess of 90,718 kg (200,000 lbm)] and cargo area (figure 57), the C5A aircraft was chosen for this study as the carrier for the closed-cycle GDL airborne system. The items considered in the airborne system assembly and installation were:

1. The cargo door envelope

2. Pallets for the device to minimize in-the-aircraft assembly requirements

3. Structural support of the GDL device

4. Compactness

5. Access to the components in the aircraft

6. Orientation of the compressor

7. Provisions for the "prime mover" and heat exchanger

8. Insulating the aircraft from the device.
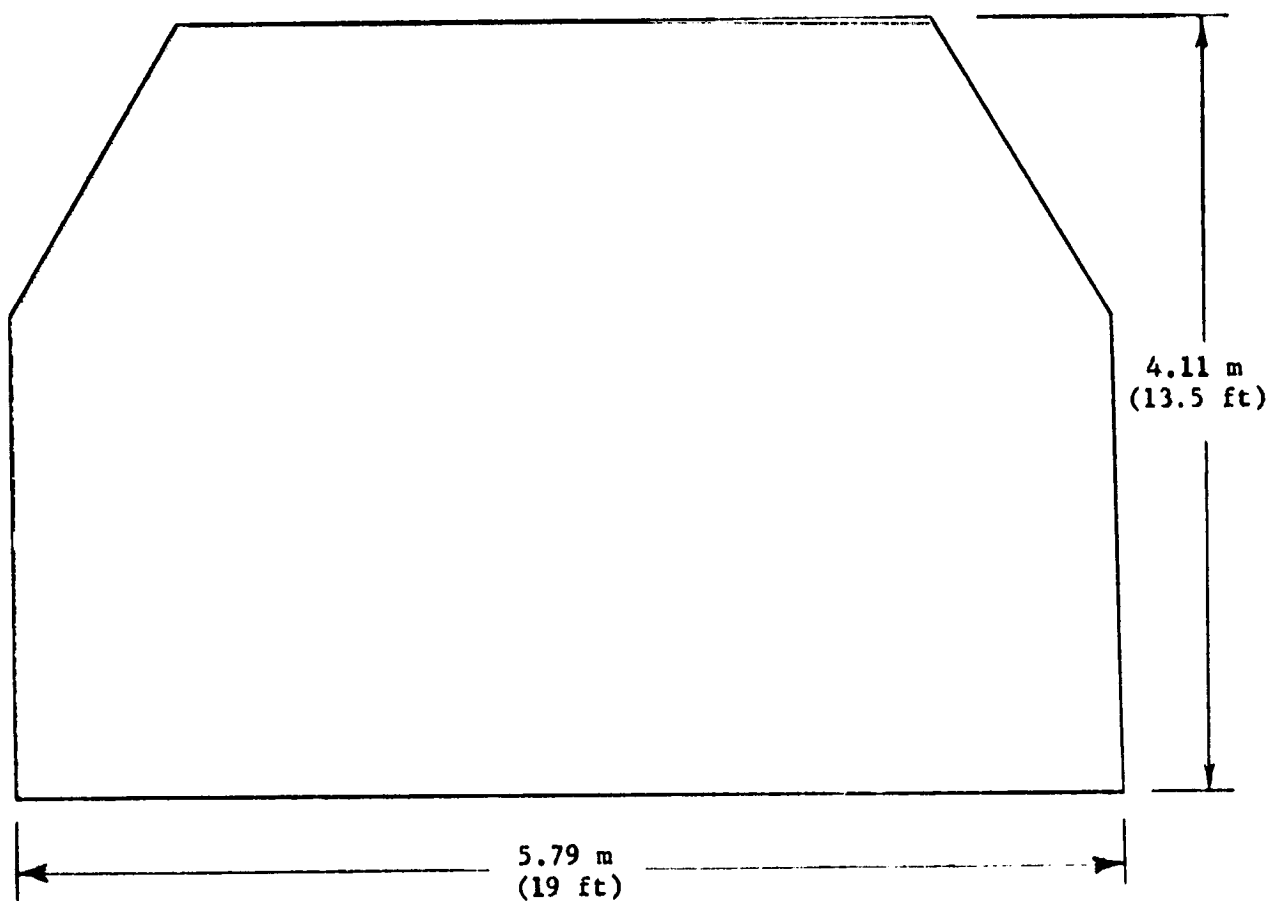
Figure 57. Loading Envelope for C5A Aircraft

The 1-Mw, closed-cycle GDL system package for the airborne application, designed to be compatible with the C5A aircraft, is shown in figure 58. This system package arrangement will fit through the cargo door envelope, and is pallet-mounted to facilitate preassembly outside the aircraft.

Access to the device in the aircraft is optimized by the arrangement as shown in figure 58. This arrangement makes all components readily accessible from either the perimeter walkways or the central platforms, except for the side of the recuperator, which is on the pallet.

The compressor is mounted in a fore and aft direction to minimize the effect of aircraft maneuver and gust loads and to provide device shaft access and prime mover space. Mounting of the compressor in this orientation also provides access for the prime mover and driveshaft connection.

It will be necessary to protect the aircraft from the high temperatures of the device by the use of insulation or baffles. The hot sections of the device will be jacketed or compartmentized with forced air cooling through the jacket to extract the waste heat. An area of concern in the airborne application is the total system weight. The device, as shown, has an estimated weight of 48,534 kg (107,000 lb_m), which does not include the insulation, support structure, electronics, cooling ducts, prime mover, or heat source. Total system weight could easily exceed 90,718 kg (200,000 lb_m).
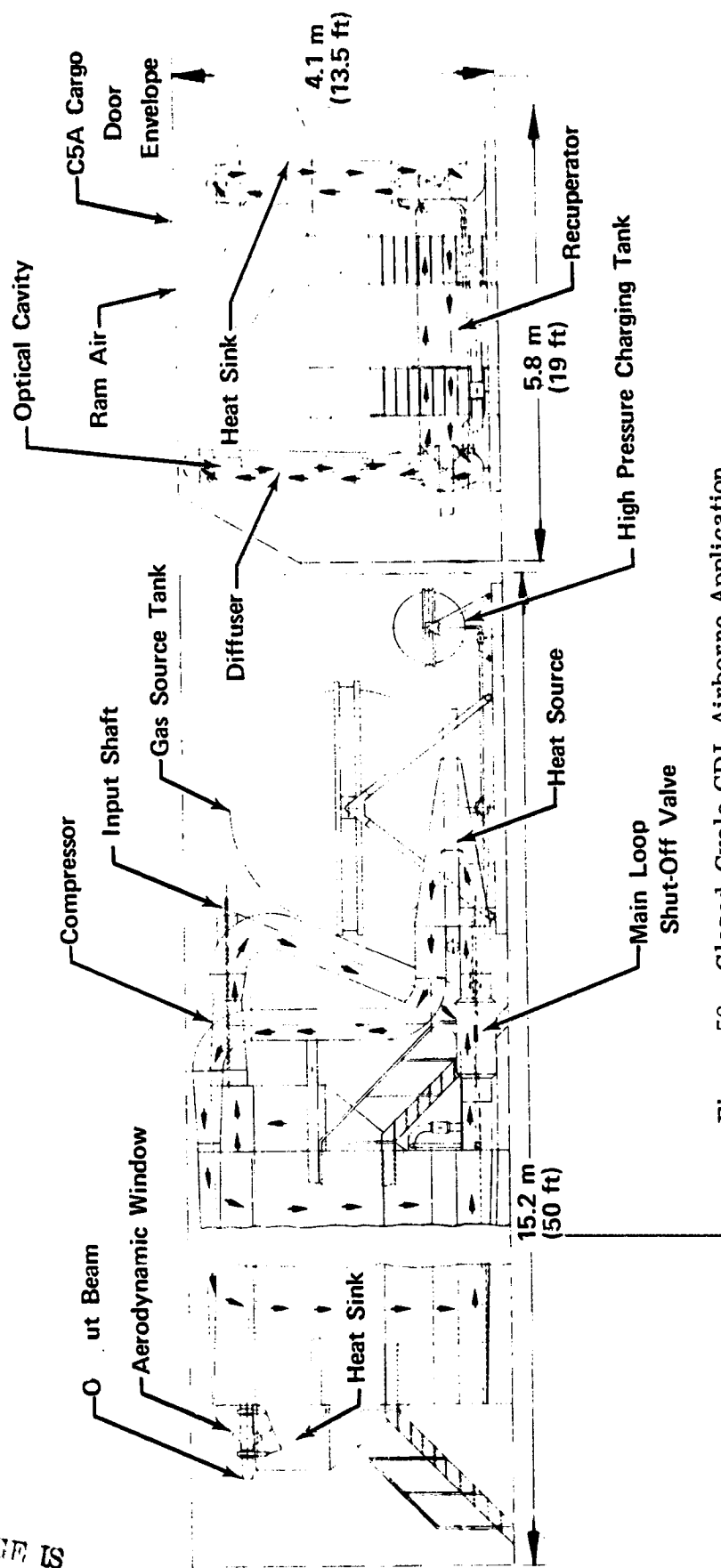
Figure 58. Closed-Cycle GDL Airborne Application

C5A Cargo Door Envelope

4.1 m (13.5 ft)

Optical Cavity

Ram Air

Heat Sink

Recuperator

5.8 m (19 ft)

High Pressure Charging Tank

Diffuser

Gas Source Tank

Input Shaft

Compressor

Heat Source

Main Loop Shut-Off Valve

Output Beam

Aerodynamic Window

Heat Sink

15.2 m (50 ft)

The effect of power on size and weight for the airborne system is essentially the same as that for the space system, since the heat sink heat exchanger is the only component that is different in the laser loop. It is obvious that, due to weight limitations, a closed-cycle GDL greater than 1-Mw is questioned for airborne applications.

The startup concept for the airborne system is the same as that for the space system. The thermal transient will be slightly shorter due to the higher initial temperature of the system.

The dormant storage water condensation problem of the space system should be much less severe for the airborne system, since the ambient temperature is much higher and the device environment more easily controlled.

Component Conceptual Designs

The functions, specifications, critical aspects, and design of each of the major system components are described in the following paragraphs.

Cavity/Nozzle/Manifold

(1) Function

The cavity/nozzle/manifold (CNM) assembly is the major component of the GDL. It provides the flowpath through which the laser gases are expanded to produce an optically active medium from which laser power is extracted. The CNM must be designed to not only expand the gases to the desired Mach number for lasing, but must do so in a manner that will avoid or minimize ordered density gradients, i.e., shocks and expansion waves, which can significantly reduce beam quality through refraction and phase distortion effects.

(2) Critical Aspects

The following critical aspects were addressed in CNM design:

Item	Effects	Solution
Nonuniform Flow Distribution	Density gradients in optical cavity that reduce beam quality	Nozzle inlet configuration contains flow distribution network to establish uniform flow
Nozzle Instability	Nozzle fatigue failure	Leading edges of nozzles are supported. Additional support provided by shrouds near midspan
Leakage	Loss of the lasing medium	Leakage eliminated by integral configuration
Thermals During Startup	Distortion and possible failure of device components	Startup transients minimized by a gradual heating up of the system to steady-state conditions.

88

(3)   Description

The CNM consists of three main components: the distribution manifold, nozzles, and optical cavity. A structural concept was selected for this component that does not contain mechanical joints, such as bolted flanges, thereby eliminating potential fluid leakage. The selected concept provides an integral CNM structure, fabricated by a combination of welding and brazing using high temperature nickel-base alloys.

The distribution manifold consists of a circular duct that runs the length of the nozzle array. The manifold, nozzles, and cavity wall form an integral assembly with no outer structural housing, whereby the nozzles carry the hoop loads from the manifold. (See figure 59.) With this nozzle/manifold concept, the manifold hoop loads can be applied in such a manner as to balance the nozzle gas bending moment to reduce nozzle stresses. Other manifold concepts were considered for this application and found to have no significant advantage for this relatively low pressure system. However, for larger systems with higher cavity pressures, the manifold hoop loads that must be carried by the nozzles become excessive and alternate approaches, such as a dual side mounted manifold, must be considered.

Section A-A
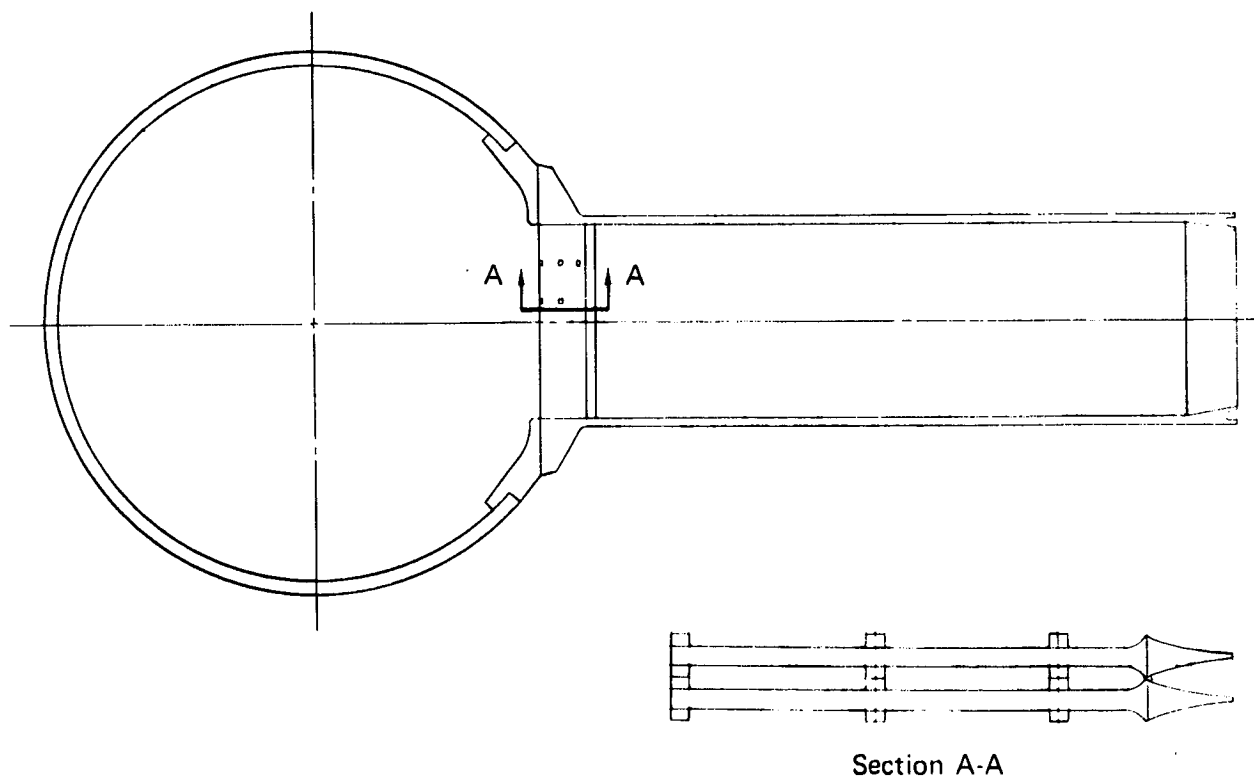
Figure 59.   CNM for Space Application

89

The transonic and supersonic portions of the nozzle are designed on the basis of aerodynamic and kinetic requirements, while the subsonic portion of the nozzle is designed to ensure structural integrity. An iterative design procedure is employed to determine the basic nozzle design parameters: nozzle inviscid area ratio (ϵ), throat height (h_t), and throat radius (r^*), as shown in figure 60. The final supersonic inviscid contour is determined from a method-of-characteristics flow field solution technique, which defines the contour required to ensure shock-free expansion.
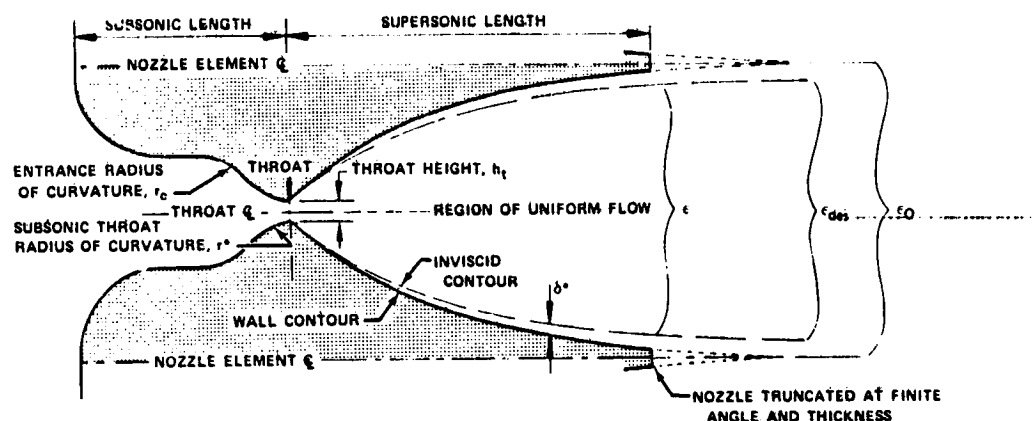
Figure 60. Nozzle Terminology

For peak output power, the nozzles must remain at the design area ratio and the correct aerodynamic contour in the supersonic sections during operation. In addition, spanwise area ratio variations within each nozzle must be limited to eliminate density gradients in the optical cavity that would degrade beam quality.

The nozzle section contains 1873 two-dimensional nozzles of the type shown in figure 61 on a centerline-to-centerline spacing of 0.330 cm (0.130 in.). The nozzles have a throat height of 0.015 cm (0.006 in.), a nozzle area ratio of 20, a supersonic length of 0.665 cm (0.2618 in.), and a height of 14.859 cm (5.850 in.). The nozzle segments are fed from the distribution manifold. (Refer to figure 59, Section A-A.) The individual nozzle segments are bonded together at mating shrouds and end platforms. The network of shrouds is located upstream of the nozzle throat to establish uniform flow and provide additional nozzle stability and control of throat height. The long subsonic length upstream of the nozzle throat is provided to establish a low stress nozzle and uniform flow into the nozzles.

The optical cavity structure is sized compatible with the selected 2UO/3 optical configuration and provides for the extraction of the laser power from the optically active medium. The cavity wall thickness is strongly dependent upon the pressure difference between the cavity pressure and the external environment. A solid cavity wall configuration is selected for the space system, where weight is considered less critical, as previously shown in figure 59. For the airborne system, a lighter weight sheet and stringer cavity wall concept are used, as shown in figure 62. Both configurations employ the integral welded structure concept to eliminate laser fluid leakage.

90

NEP

0.2618 in.

0.1300 in.

Section Showing Two Typical Nozzles   0.006 in.

Flow In

Flow Out
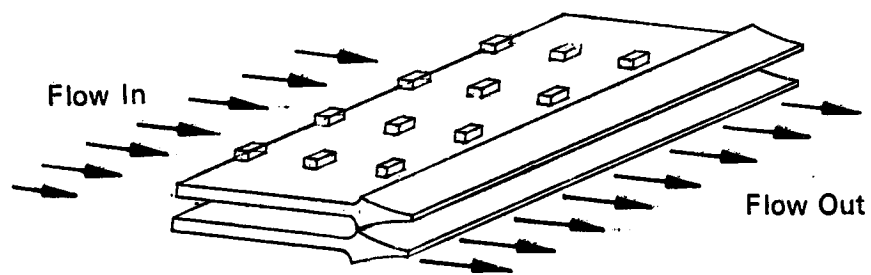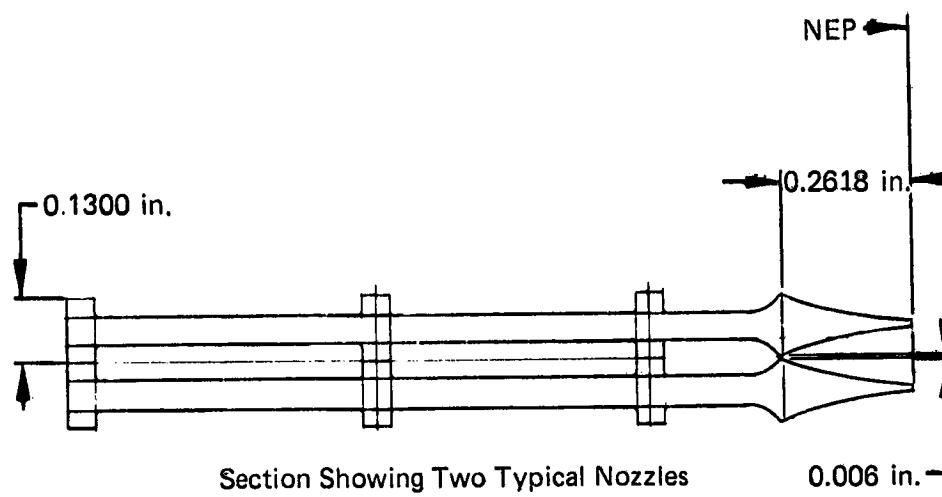
Figure 61. Two Typical Nozzles

91

Section B-B

Section A-A
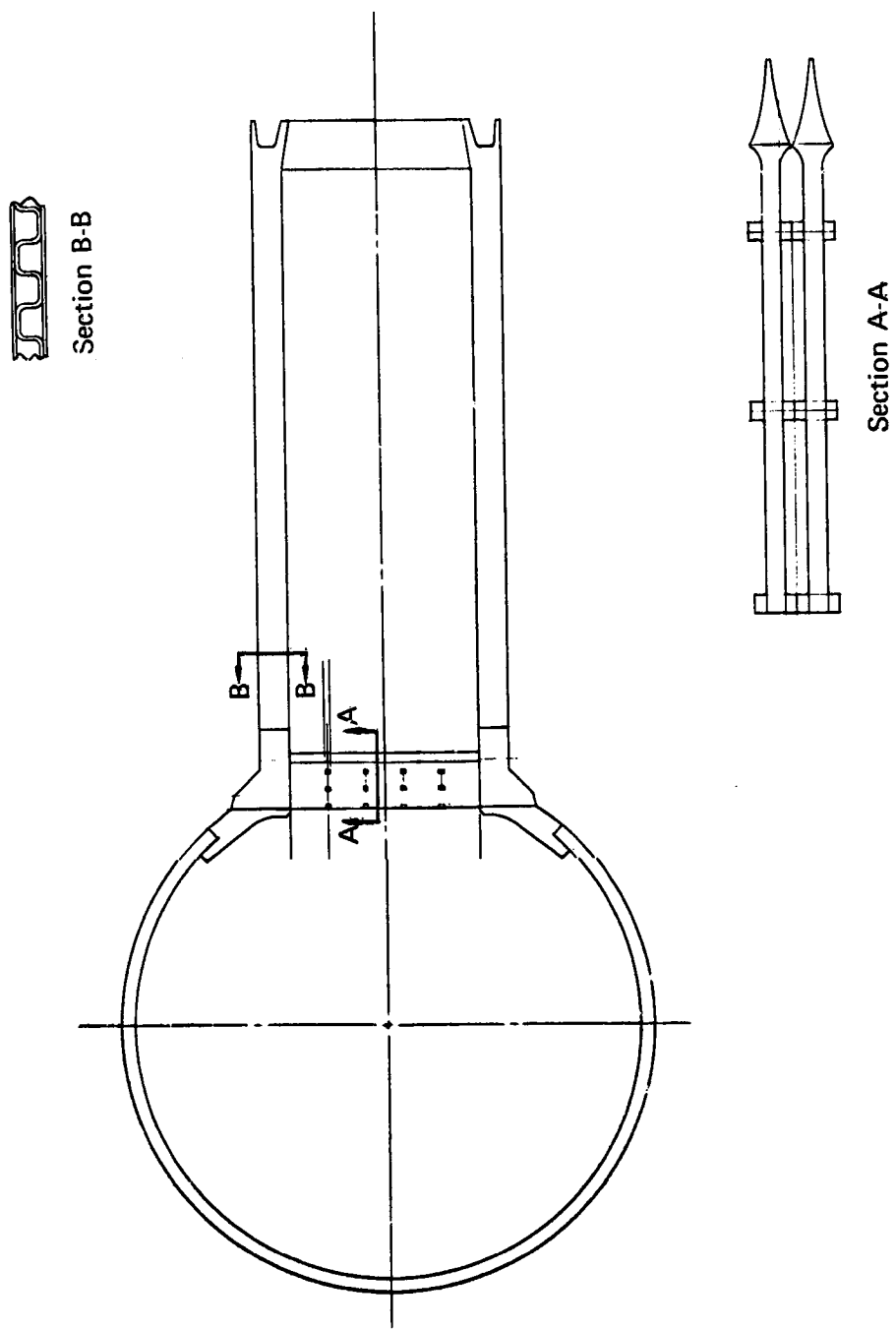
Figure 62. CNM for Airborne Application

92

Optics

(1) Function

The function of the six cavity mirrors making up the 2UO/3 optical configuration (figure 63) is to receive and direct laser radiation at the correct wavelength through the cavity with a minimum of (1) absorbed radiation, (2) induced phase distortion, and (3) beam misalignment. Four of the six mirrors comprise the unstable resonator (UO) which must be optically figured to capture initial spontaneous emission of radiation from the flowing gas and to maintain repeated amplification of that radiation by stimulated emission until the resonating beam dominates all other stimuli competing for the available photons....

In steady-state operation, radiation diverges from the convex mirror, is turned by the opposing flat mirror while maintaining the same divergence angle, is collimated and reflected coaxially by the concave mirror, turned by the same opposing flat, and divided by the hole coupler. The collimated radiation passing through the center of the hole coupler is reflected in a diverging fashion to repeat the "resonating" process. The radiation incident on the hole-coupler mirror surface is reflected through the cavity by two additional turning flats for a total of three amplification passes.

(2) Design Specifications

Substrate Material	SiC
Optical Surface	Multilayer dielectric on metallized surface
Optical Reflectivity	99.9%
Optical Quality	$\lambda_{vis}/50$
Thermal Control	Solid-state thermoelectric
Operating Temperature	295°K ±3° (70°F ±5°)
Storage Temperature	238 to 356°K (−30 to 180°F)
Ambient Pressure	Space vacuum
Alignment (x-y tilt)	Piezoelectric crystal actuators
Alignment Response	2000 Hz
Alignment Stroke	±600 μrad
Alignment Error Sensor	Interferometric/thin film waveguide
Electric Power Source	Solar cells or aircraft supply
Thermal Dump	Space radiator panels or aircraft heat sink

NOZZLE EXIT PLANE
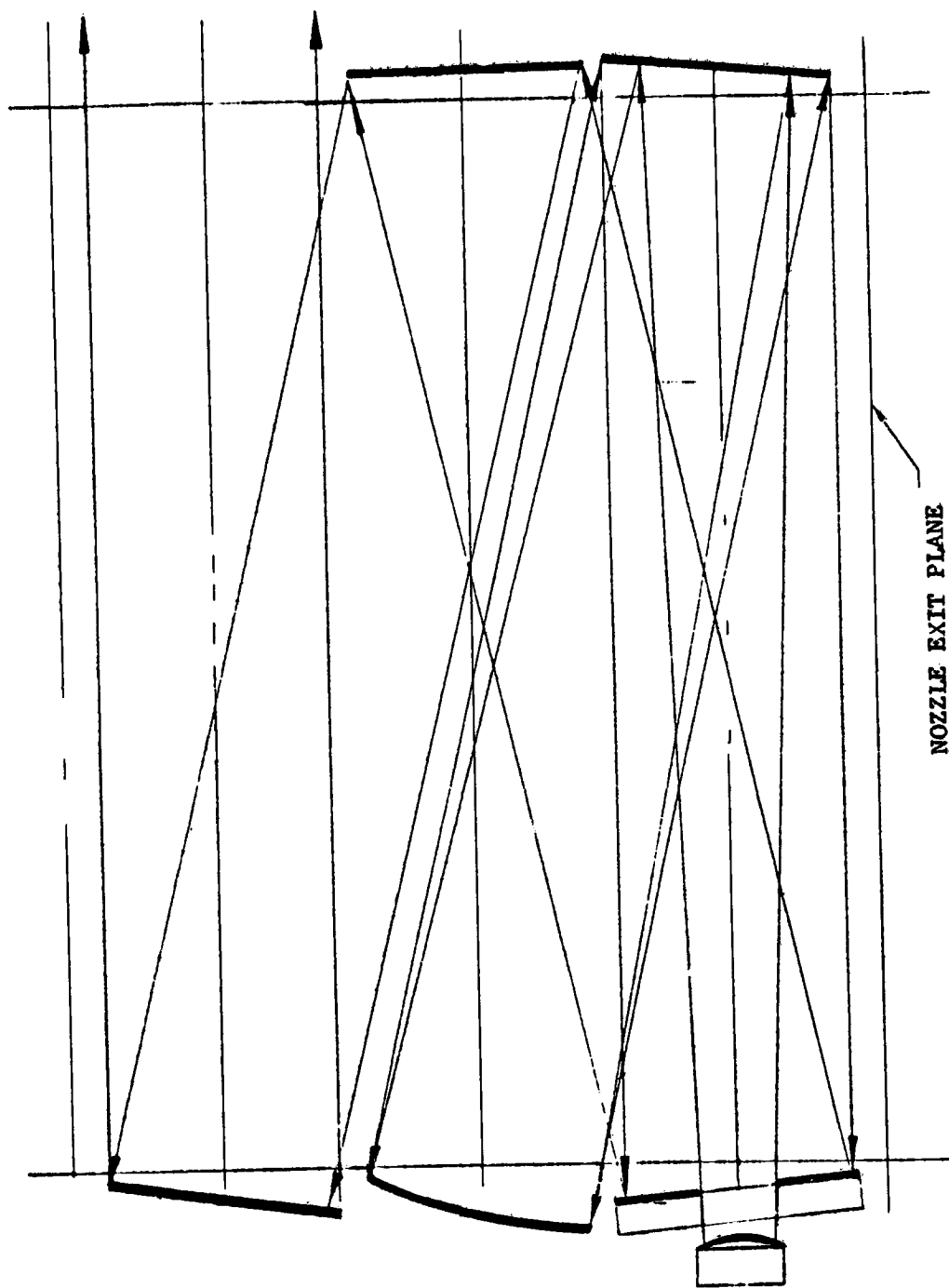
Figure 63. 2UO/3 Optical Configuration Schematic

94

(3)   Critical Aspects

Item	Effects	Solution
Mirror Optical Distortion	Beam phase error and power loss	High reflectivity optical coatings, low thermal expansion mirror material, active mirror thermal conditioning
Optical Reflectivity Degradation	Optical distortion, power loss, increased cooling requirement, catastrophic thermal damage of mirrors	High durability optical coating, oversized cooling system
Liquid Coolant Freezing	Mirror and coolant system structural damage	Continuous coolant temperature conditioning, or solid-state thermoelectric temperature control system
Beam Misalignment	Power loss, component damage	Active mirror alignment system

(4)   Description

The cavity optics system can be divided into the following subsystems for the purpose of discussion.

    1.   Mirrors
    2.   Mount and Alignment System
    3.   Thermal Conditioning System.

These subsystems, as envisioned based on 1990 technology, are discussed below:

(a)   Mirrors

The mirrors will be constructed from a low thermal expansion, high thermal conductivity and lightweight material, such as SiC, currently being used for advanced mirror substrates. The optical surface will be metallized by vapor deposition or plasma spraying, and the metallized surface will be diamond turned to $\lambda_{vis}/50$ optical quality. A multilayer dielectric coating will then be applied to enhance the reflectivity to greater than 99.9%.

The mirror surface will be processed to be fully absorbing outside of the desired beam diameter to eliminate the need for independent beam shaping apertures in the cavity. Excessive temperature rise in the fully absorbing region of a mirror would indicate gross beam misalignment or system malfunction and would be cause for automatic abort.

Current technology in mirror design (i.e., coatings, surface finish, reflectivity) and cooling is adequate to handle the required mirror loadings and can provide an alternative approach. The more advanced concepts employed in the design result in a smaller, lighter, and less complex optical system.

(b)   Mount and Alignment System

Each mirror will be actively aligned during operation by piezoelectric-type actuators with sufficient response to compensate for vibration, and with sufficient stroke to compensate for structural displacement. The complete mirror will be tilted according to the error signal generated by the alignment system. The basic mirror mount structure, against which the actuators react, will be constructed from a nickel alloy capable of operating within the environmental conditions.

A solid-state alignment system will be based on combining integrated optics with integrated electronics for spatial error detection and for error signal generation. The components of the alignment system (figure 64) are mounted on a relatively small, independent, zero-thermal-expansion platform constructed of an advanced version of ULE™or Invar. Actuators that are similar to the mirror piezoelectric actuators actively position the alignment system platform with respect to the optical cavity, and an error signal that is generated by sensing each mirror's position with respect to the alignment system activates the appropriate mirror actuator. Fiberoptics or thin film waveguides embedded in the thermally stable alignment platform will allow interferometric-type spatial measurements for alignment accuracies to fractions of a visual wavelength. Techniques that are based on index of refraction variations of a transparent crystal exposed to varying degrees of compressive stress may improve alignment accuracies still further.

An independent calibration system designed around similar integrated optics/integrated electronics technology could be used on command to automatically zero the alignment system during GDL down periods. In operation, the calibration system would introduce a low power laser beam into the optical train in the reverse or upstream direction. Photosensors would detect the character of the returning radiation to establish a zero alignment error signal by electronic processing for correction of the alignment system's zero position.

(c)   Thermal Conditioning System

Mirror cooling and thermal conditioning will be accomplished using a thermopile dispersed throughout the mirror substrate, and based on the Peltier effect. Thermoelectric cooling or heating will occur locally within the mirror substrate, on demand from temperature sensors also dispersed in the substrate, to maintain the complete substrate at a uniform temperature. Signals from the several sensors will be processed electronically to determine the proper cooling or heating electric current flow to the thermopile's dissimilar metallic conductor junctions. Solar photoelectric panels and space radiator panels could be used, respectively, to provide the electric power and to provide the thermal heat sink for the cold junction of the dissimilar metallic conductors.

(d)   System Design Consideration

Optical components in the 1-Mw airborne system will be the same as those required in the spaceborne system. The electric power source and thermal heat sinks needed to operate the alignment systems and thermal conditioning systems will be different between applications. In the airborne system, a small dynamo and cryogenic heat sink should adequately replace the comparable solar panel and radiation heat sink used in the spaceborne system.

96

Gas Flow

Optical Transponders

Actuator Points

Alignment Mount Structure

Distribution Manifold

Cavity Mirrors
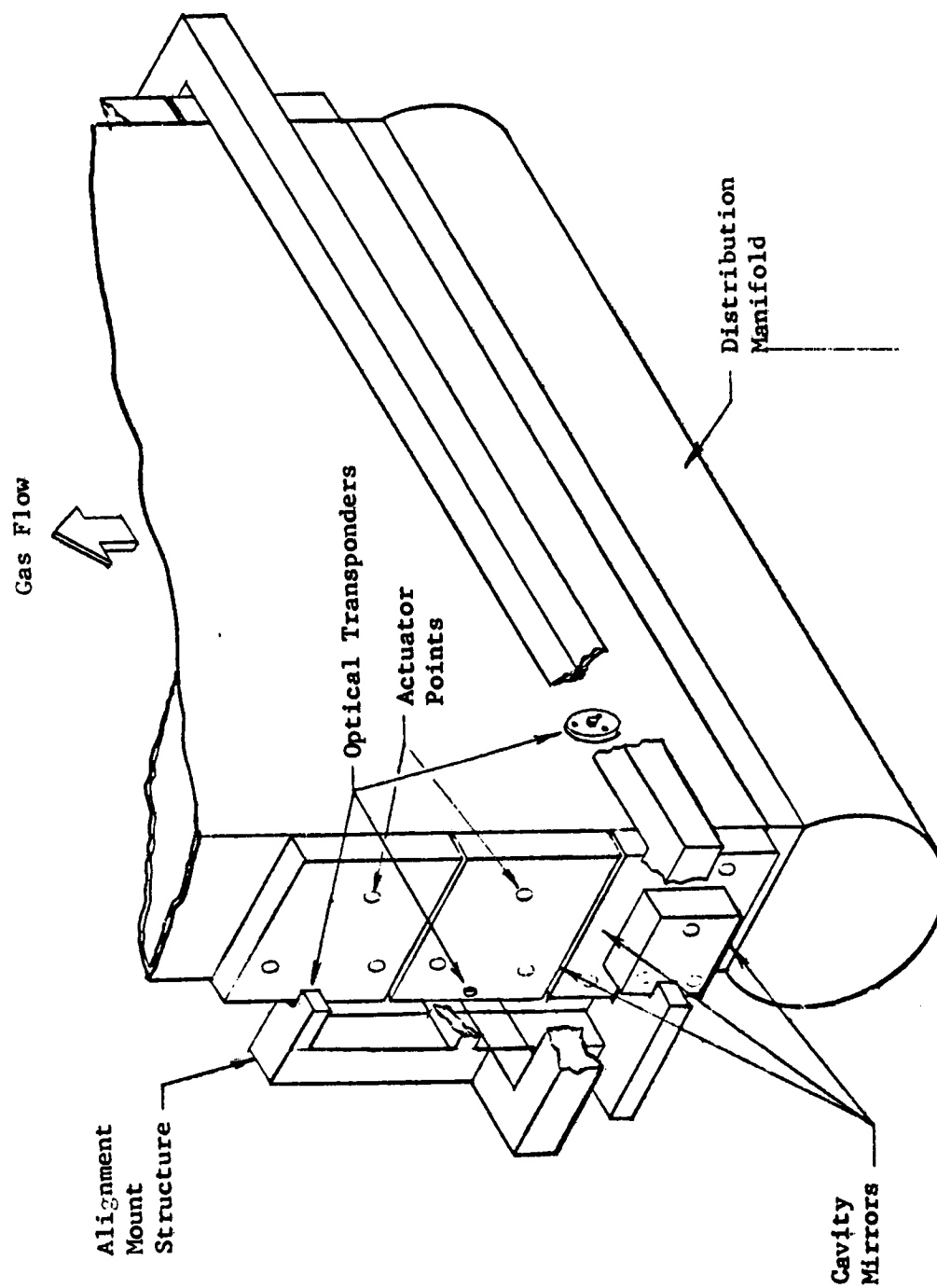
Figure 64. Optical Alignment Scheme

97

Design of structural components associated with the optics will be dominated by the airborne vibrational and g-load forces. Independent design of the structures for the spaceborne system may be desirable to conserve weight.

(e)   Startup and Transients

The startup requirements for the cavity optical systems are (1) stabilize mirror temperatures at 295°K ±3° (70°F ±5°) using the temperature conditioning system, and (2) arm the mirror alignment system. A temperature stabilization period of 1 min is feasible.

(f)   Dormant Storage

The thermoelectric temperature conditioning system will remain active on a continuous basis during dormant-storage modes to control the mirror temperatures within limits, typically 238 to 356°K (-30 to 180°F).

(g)   System Life

The limiting component of the optical system life will be the optical coating on the mirrors. Surface reflectivity will degrade during operation as a result of damage from factors such as thermal cycling and foreign particles. The system will have to be deactivated when the thermal conditioning system can no longer handle the laser beam thermal load.

Output Window

(1)   Function

In the closed-loop gas dynamic laser, a means must be provided for passing the output beam from the low pressure region of the optical cavity into the surrounding environment with minimal degradation in beam quality or loss of lasing fluid. The component that performs this function is called an output window. There are two basic types of output windows known as the aerodynamic and material window. Both of these concepts were considered as candidates for this investigation.

(2)   Critical Aspects

Item	Effects	Solution
Cavity Leakage	Contamination of lasing medium	Minimize leakage of A/W fluid into cavity and use of a compatible fluid in the window loop
Leakage to Ambient	Loss of GN_2 that is operating the space system aerodynamic window	Use shutter doors to keep this leakage to a minimum. A charging tank is used to replenish the system

(3)   Description

Both the aerodynamic window and the material window are discussed in the following paragraphs as design concepts to perform the function of the output window for this system.

The aerodynamic window blocks the flow of ambient air into the output beam duct with a supersonic flow of gas. Early designs for pressure-driven aerodynamic windows depended on the expansion-compression structure of a supersonic free jet to isolate the laser cavity. Acceptable pressure ratios, leakage, and beam quality were achieved, although significant beam jitter (up to 150 μrad) was observed. To reduce the mass flow and beam jitter and improve beam quality, the concept of a centrifugal field aerodynamic window was developed at the United Technologies Research Center (UTRC).

The centrifugal field aerodynamic window uses a two-dimensional supply nozzle, which delivers a supersonic jet suited to large amounts of turning. As the jet flow crosses the duct, it is deflected. It is the momentum change associated with this deflection that balances the ambient-to-cavity pressure difference. The inner nozzle on the cavity side expands the flow to the cavity pressure, while the outer nozzle expands to ambient pressure, and intermediate nozzles expand the flow to intermediate pressures. The multielement centrifugal aerodynamic window (MECA) concept is being employed on the Air Force ALL program and represents a low-risk, near-term technology answer to the requirement for an output window.

Due to the requirement for a nonresupplyable system with a minimum of 600 sec of run time per cycle, it is not feasible to use an open-loop GN_2 pressurized tank supply for the aerodynamic window and simply dump the exhaust overboard. The weight of the tanks and fluid involved becomes prohibitive for the airborne open-loop window (figure 65). Thus, a closed-cycle aerodynamic window will be employed. The closed-cycle consists of a compressor, a heat exchanger, nozzles, two shutter doors, and associated ducting (figure 66). To operate the aerodynamic window at various ambient conditions, a bypass loop is used to direct flow around the window as required. The space system uses a similar closed-cycle aerodynamic window system as shown in figure 67. Note that for the space configuration, the cavity pressure exceeds that of the space environment which deflects the closed-loop window fluid away from the cavity. Also, there is the additional consideration of flow expanding to the near zero pressure of space. An intermediate pressure is created by an expendable jet shield flow to limit the included angle of the expansion fan. The flowrate required for the jet shield, which is leakage overboard, is 0.0077 kg/sec (0.017 lb_m/sec). The power required to operate the closed-loop aerodynamic window compressor is 75 kw (100 hp), and the primary flow for the window is 0.13 kg/sec (0.29 lb_m/sec).
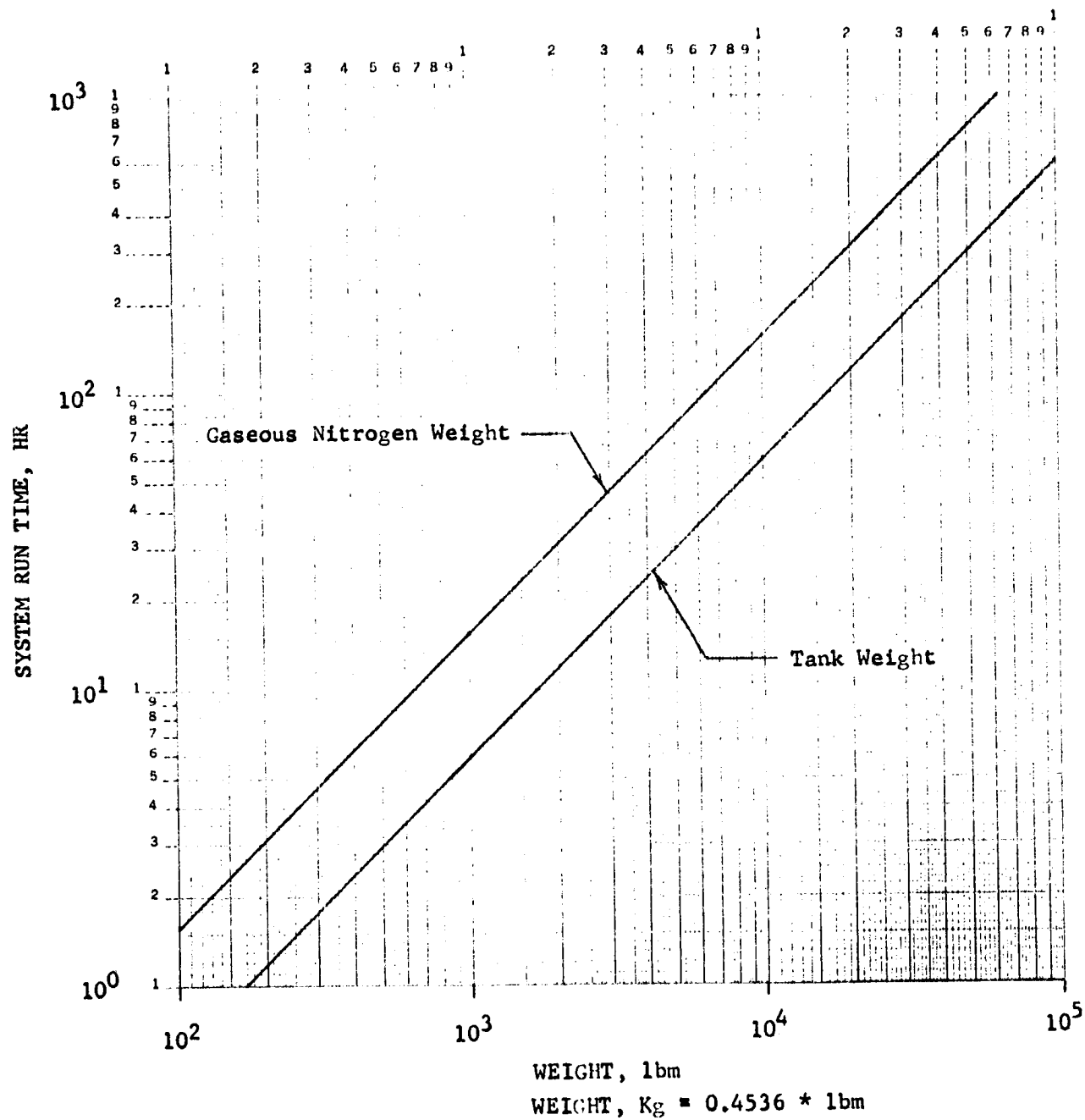
Figure 65. Space System Weight of Tank and Expendable Primary Flow for Aerodynamic Window
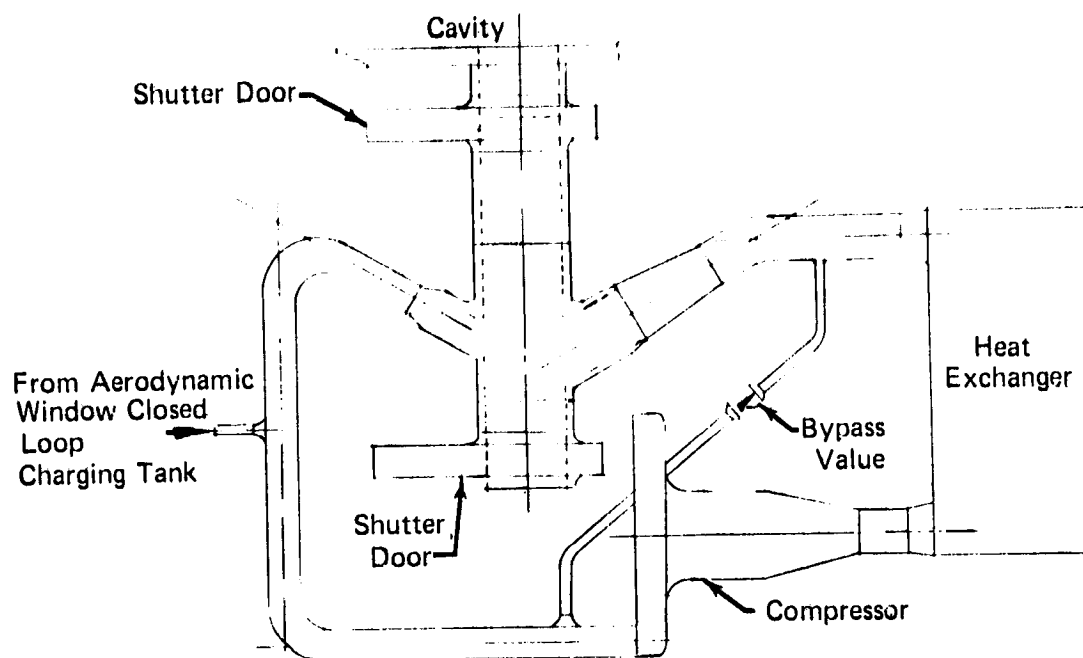
Figure 66. Airborne System Aerodynamic Window Schematic
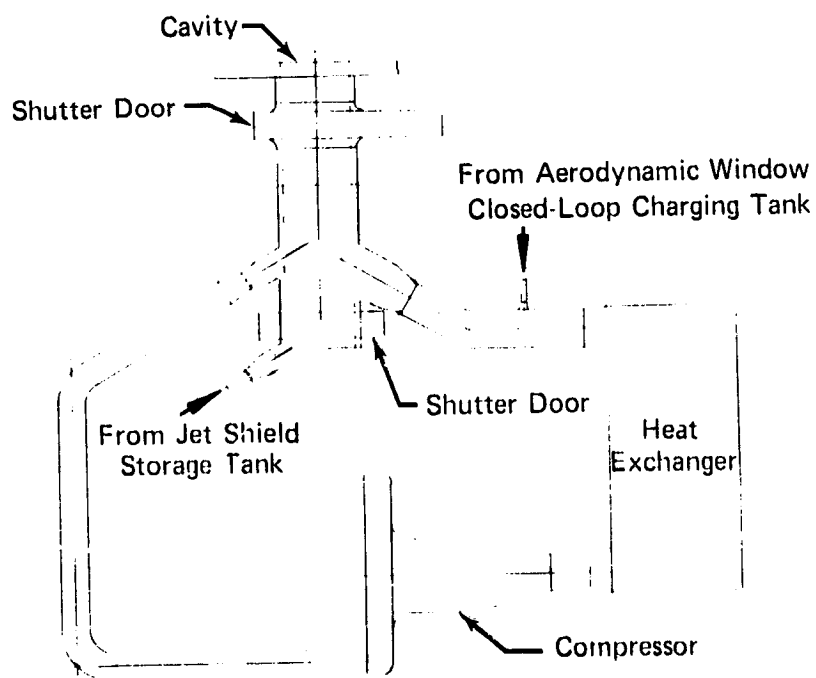
Figure 67. Space System Aerodynamic Window Schematic

The material window is the alternative to the aerodynamic window. The material window has all the advantages in terms of system weight and complexity, but a window material has not been developed that can withstand a high power CW laser beam for long periods of time without severe beam absorption and subsequent window failure. Significant progress has been made in recent years in improving window materials, resulting in the capability of handling greater power levels. In the contingency that an acceptable window material is developed, cavity window mounting concepts were designed and are shown in figure 68. The major concern with the material window is whether the technology will be available by the 1996 time period.
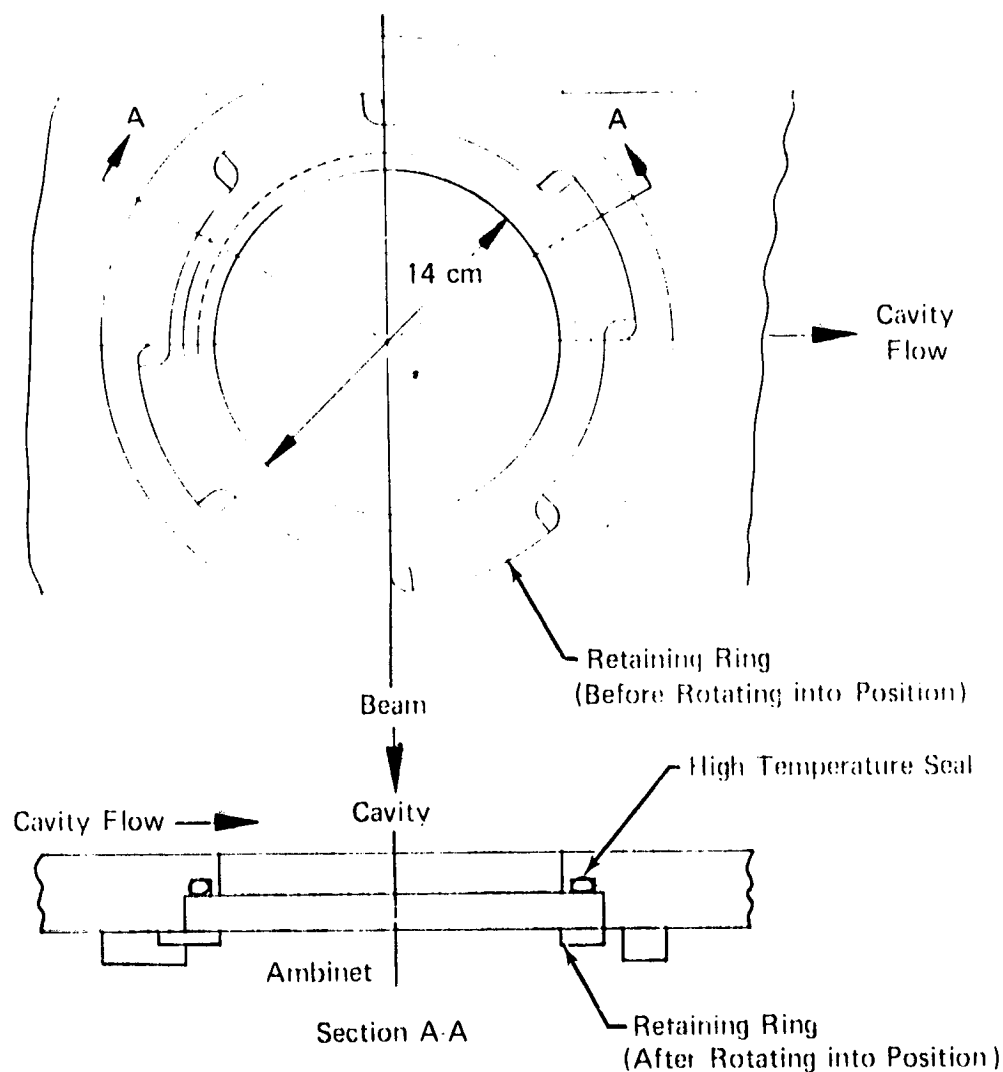
Figure 68. Cavity Window Mounting Concept

Diffuser

(1) Function

A diffuser system is required at the exit of the optical cavity to efficiently convert the kinetic energy of the supersonic flow into a static pressure rise and to establish a relatively low Mach number subsonic flow field that can be ducted to other components with acceptable pressure losses. For example, in the 1-Mw device the diffuser approach Mach number is 3.81 with a corresponding static pressure of 0.0032 MN/m^2 (0.47 psia). Through a series of oblique and bifurcated normal shocks, this flow is diffused until an exit Mach number of approximately 0.2 is reached and the static pressure has increased by a factor of 10.

(2) Design Specification

The following diffuser conditions were established to provide the system parameters defined in the 1-Mw system design table.

Inlet Mach number	3.81
Exit Mach number	0.20
Recovery factor	0.67
Contraction ratio	4.7
Throat length/inlet throat height	13.0
Total length/inlet height	8.54
Injection flowrate, %	8.0
Supersonic contraction half angle, deg	6.0
Subsonic diffuser half angle, deg	3.5
Injector area ratio	5.0
Diffuser minimum run time, sec	600.0
Diffuser overboard leakage	None
Operational environment	Space or airborne

(3) Critical Aspects

Item	Effects	Solution
Uncooled Diffuser Design	High metal temperatures with resultant low allowable stresses	Use sheet and stringer or composite design with thermal isolation of outside structure
High Internal Flowpath Pressures	Large load for diffuser structure	Use sheet and stringer or composite design with internal struts to provide stiff structure
Flowpath Geometry Variations	Flowpath distortions will adversely affect diffuser performance	Use struts to control flowpath shape accurately

103

Item	Effects	Solution
Bypass Duct and Doors	Doors would recirculate flow into diffuser upstream of throat	Use loaded ledge-type seal for operation at 2270° F and return vent bleed duct to supply tank
Bleed Door Actuators	Slow actuators will prevent start	Use rapid response pneumatic system actuators for door actuation in less than 2/3 sec
Sidewall Injection System	Establish boundary layer control	Injection system throat gap controlled to be 0.025 cm (0.010 in.)

(4)   Description

(a)   Diffuser Performance Trades

Extensive model testing at UTRC has resulted in numerous design concepts and performance trades that were considered in the selection of a diffuser for this closed-cycle GDL. The diffuser configurations that have been investigated include the conventional fixed geometry, various strut segmented arrangements, and numerous variable geometry supersonic aircraft inlets (Reference 6). In addition, a high-contraction-ratio conventional diffuser with boundary layer bleed provisions (Reference 6) was considered. These test programs have investigated the performance trades associated with the following parameters:

1.   Diffuser length
2.   Boundary layer control devices
3.   Laser cavity leakage
4.   Supersonic contraction ratios
5.   Struts
6.   Endwall precompression
7.   Injector base step heights
8.   Straight section lengths
9.   Subsonic area ratios

The presence of mirror boxes in the laser cavity results in a significant buildup of endwall boundary layer upstream of the diffuser section. The boundary layer is a region of relatively low kinetic energy and is detrimental to high diffuser static pressure recovery. Boundary layer control devices, such as flow deflectors, vortex generators, wall suction, and injection, are important to energize the boundary layer and enhance pressure recovery.

Based on extensive GDL diffuser model testing conducted at UTRC, the baseline diffuser pressure recovery levels without boundary layer control devices should be approximately 45% of normal shock. Obviously some sort of augmentation, such as blowing, boundary layer bleeding, or vortex generators, will be required to ensure adequate diffuser performance for the closed-cycle application.

Extensive model testing at UTRC has shown that endwall and sidewall injection is an effective method to energize the boundary layer and improve the diffuser performance. Reference 6 documents that near-normal shock recovery, based on diffuser inlet Mach number, can be realized with small amounts of injection as long as (1) the throat section is sufficiently long to contain the normal shock system and ensure adequate mixing of the boundary layer with the mainstream flow, and (2) leakage into the optical cavity is controlled to a low level.

Based on the general trends shown in Reference 6, an injection flowrate of 8% was selected to ensure adequate boundary layer control. The injector flow nozzles will be spaced along the full perimeter at the inlet to the diffuser straight sections. Boundary layer buildup will be significantly greater on the narrow endwalls due to the presence of the mirror boxes and shutters. Thus, endwall injection flowrates will be twice as high per unit of perimeter length as compared to the sidewall injectors. Model testing, however, will be required to confirm this flow split to ensure adequate boundary layer control.

(b)   Startup Cycle

The starting sequence requires that the nozzle pressure ratio be increased until the critical pressure ratio is reached and the nozzle throat becomes choked. An additional increase in pressure ratio will cause a normal shock to move downstream of the nozzle throat and into the optical cavity section. Additional movement of the shock into the diffuser will require the diffuser throat area to be approximately 85% of the cavity exit area. This increase in area could be provided by one of several techniques discussed in the following paragraph. After the shock has been swallowed and becomes stabilized in the diffuser throat section, the diffuser effective throat area is decreased, resulting in a corresponding increase in pressure recovery.

The diffuser throat area can be modulated by the following techniques. Diffuser area scheduling involves using a movable center plug. This technique was initially considered, but rejected due to severe problems associated with cooling and actuation. Another method to provide area modulation is by use of movable sidewalls along the full length of the diffuser. This concept is similar to variable geometry supersonic wind tunnels and requires extensive use of actuators and efficient sealing devices. As with the movable plug, this concept was considered but later rejected due to the complexity and weight penalties. The most attractive method is by means of a bypass bleed door upstream of the diffuser throat. During the starting sequence, a substantial amount of cavity flow is diverted around the diffuser to ensure that the shock is swallowed and stabilized in the throat section. The bypass flow reenters the system in the subsonic section of the diffuser through another movable door. The advantages to this concept are minimized seal surfaces, modest actuator forces, and no additional problems.

Thus, the requirement for a variable geometry diffuser to ensure reliable starting and high pressure recovery has led to the selection of a conventional diffuser design with provisions for start bleed and boundary layer control. This design offers high performance as demonstrated by model testing when compared to vaned or centerbody diffusers.

(c)   Selected Concept

The selected diffuser configuration and flowpath is shown in figure 69. The single-bypass configuration was preferred over a symmetrical bypass diffuser, based on steady-state performance advantages due to the reduction in leakage and the elimination of an additional set of seals, bypass doors, and actuators. The inlet and exit bypass doors are operated by pneumatic actuators using lasing fluid to prevent contamination of the loop in the event of actuator leakage. The upstream door uses a "flex" hinge to provide a perfect seal at the convergent section of the diffuser. The bypass doors are contained within the all-welded envelope containing the lasing fluid flowpath for positive leakage control. The bypass loop is vented to the supply tank return system to scavenge any door leakage from the ledge-type seals that could recirculate into the diffuser and degrade performance during supersonic operation.

The diffuser structure uses a sheet and stringer-type design configuration. The transient and steady-state pressure loads are resisted by the external beam-like structure. The primary and bypass gas flowpaths are stabilized by connecting stringers and cross pieces supported by the external structure and by internal struts. Sufficient thermal isolation is provided between the gas flowpath and the external structure to prevent the outer portion of the structure from reaching the main stream temperature.

Compressor

(1)   Function

A compressor is required in the closed-cycle GDL system to recirculate the laser medium and maintain the pressure ratio and flow parameters necessary to sustain the flow of an optically active medium from which laser power is extracted. In essence, the compressor is the major source of energy being transferred to the active medium with the only other source being by way of the heat source heat exchanger. Thus, the compressor must compensate for all pressure losses in the system.

Compressor efficiency is a major parameter affecting system performance because the primary parameter to measure system performance is the ratio of extracted laser energy to supplied energy. Due to the steady-state nature of this GDL system, the compressor can be designed for high efficiency at a single design point, as opposed to some applications that require compressor performance trades to operate over a range of conditions. ...

For the purposes of this study, the compressor package includes the compressor aerothermodynamic flowpath, compressor exit duct diffuser, exit turning duct, rotor shaft bearings, power shaft housing, power shaft, and power shaft seals.

106
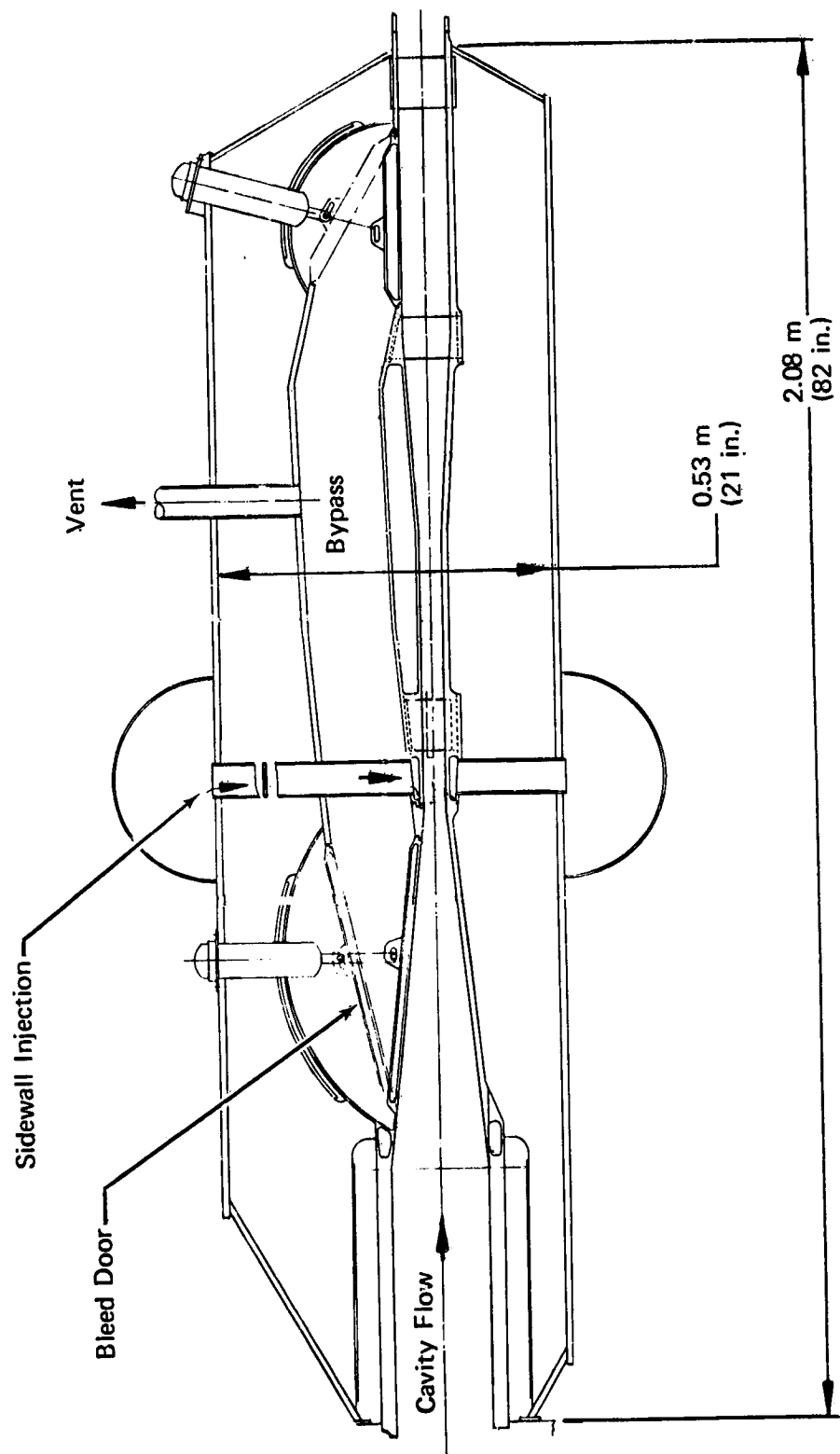
Figure 69. Diffuser

107

(2)   Design Specifications

The following requirements were established for the compressor package.

1. The configuration must be compatible with the system parameters defined in the 1-Mw system design table.

2. High efficiency shall have primary importance with weight and size considered as secondary.

3. The compressor shall have a minimum 10% stall margin.

4. The compressor design shall be an uncooled metal configuration within the technology projected for the year 1990.

5. The compressor must be compatible with the space or airborne environment.

6. The compressor must be capable of operating for a minimum of 600 sec per cycle.

7. The compressor drive shaft shall not impart axial thrust loads to the prime mover.

8. The power shaft seal shall have long life and zero leakage.

9. The compressor cases and ducts shall have zero leakage.

(3)   Critical Aspects

Item	Effects	Solution
Compressor Stalls	Stalls cause violent vibrations of the rotor assembly. This can cause performance deterioration and structural damage	Maintain a minimum of 10% stall margin
High Rotor Speeds	Possible structural failure due to critical speed limitations	Decrease rotor speed without sacrificing performance by increasing the number of stages
Compressor Length	Compressor length increases rotor flexibility. This can cause performance deterioration and possibly structural damage	Shorten the compressor by using fewer stages or use additional shaft bearings
High Efficiency	Performance and stall margin are inversely related	Design accurately to the 10% stall margin limit

Item	Effects	Solution
Transients (Startup/ Shutdown)	Transients can force the compressor into stall and can create thermal gradients which cause rubs between moving and stationary parts	Design compressor clearance to increase during the transient and control operation to avoid stall.
Start/Stop Transients and High Speed Bearing Rubs	Surface damage; technology requirement for improved surface coatings. Solid film lubricant is essential	Reference 7 recommends development of sputtered hard coatings of silicon nitride (Si3N4) or possibly chrome oxide
Bearing Thermal Distortion	Gas bearings are sensitive to housing/shaft misalignment	Design to ensure that thermal distortion is minimized. No new technology is required
Bearing Foil Material	Heat generation unknown	Run tests to determine heat generation. Inco 718 appears to be best material for temperatures up to 811 to 922°K (1000 to 1200°F). Bearing housings are cooled with compressor fluid
Radial Clearance	Compressor tip clearance affects performance	The tip clearances can be small since the maneuver loads are low and there is only one steady-state design point. The only clearance required is for surge loads.
Dynamic Power Shaft Seal	Near zero leakage required	A centrifugal ferrofluidic seal is recommended. This will provide a low-leakage rate seal
Dynamic Seal Heat Generation	If heat generation is too high, the ferrofluid evaporation rate will be accelerated	Cool with fluid from the radiator at 367°K (200°F)
Static Power Shaft Seal	A near-zero leakage static seal is required to prevent the loss of fluid	A ferrofluidic magnetic seal is recommended. This provides low leakage, while providing a means to retain the fluid from the dynamic seal in static condition

Item	Effects	Solution
Static Seal Evaporation	Static seal fluid evaporation to space environment	A carrier fluid must be selected for the ferrofluid, which has a very low vapor pressure, such as polyphenylether or diester. Also provide a reservoir to give replenishment capability
Compressor Thrust Balance	Rotor has large thrust unbalance because the compressor is not balanced against the drive turbine	A thrust balance disk is provided on the power shaft outside the flowpath

(4) Description

(a) Aerothermodynamic Flowpath

A parametric study was conducted to evaluate the compressor efficiency trades based on compressor correlations substantiated by the Low-Aspect-Ratio Compressor (LARC) experimental studies (Reference 8). Parameters that were varied in the study included aspect ratio, gas chord ratio, number of stages, and inlet specific flow. The results of the parametric study are summarized in figure 70, which indicates the compressor adiabatic efficiency versus the number of stages with families of curves for constant speed lines, constant compressor length, and constant inlet specific flow. The stall limit line has been superimposed on these data. The five-stage compressor with a specific flow of 16 kg/sec (35 lb_m/sec), which has a relatively high adiabatic efficiency of 0.908%, was selected for evaluation in the conceptual design.

The conceptual design of this uncooled compressor contains a low-aspect-ratio drum rotor with cantilevered stators (figure 71). In this application, cantilevered stators with low tip clearance offer a performance advantage relative to shrouded stators. Conditions are favorable for low tip clearance because the system has a single steady-state design point, the rotor is relatively stiff, and adequate surge margin (10%) has been provided.

The compressor inlet distortion is intentionally minimized by positioning the input power shaft on the compressor exit, because high performance is a primary goal and it is advantageous to operate with a low surge margin. The power shaft is enclosed in a housing in the turning duct and exit vane case. The turning duct is a 90 deg elbow with a bend radius of two times the diameter. The exit vane case is also a 2:1 area ratio diffuser that reduces the fluid Mach number and friction losses prior to entering the turning duct.

Constant Inlet
Specific Flow
Kg/s-m² (lbm/s-ft²)

122 (25)

146 (30)

171 (35)

152 (60)

127 (50)

102 (40)

Constant
Length
Lines
cm (in)

Proposed Design

Stall Limit Line
(10% Stall Margin)

Constant
Speed
Lines, RPM 14,000

16,000

18,000

NUMBER OF AXIAL COMPRESSOR STAGES

COMPRESSOR ADIABATIC EFFICIENCY, η

94

93

92
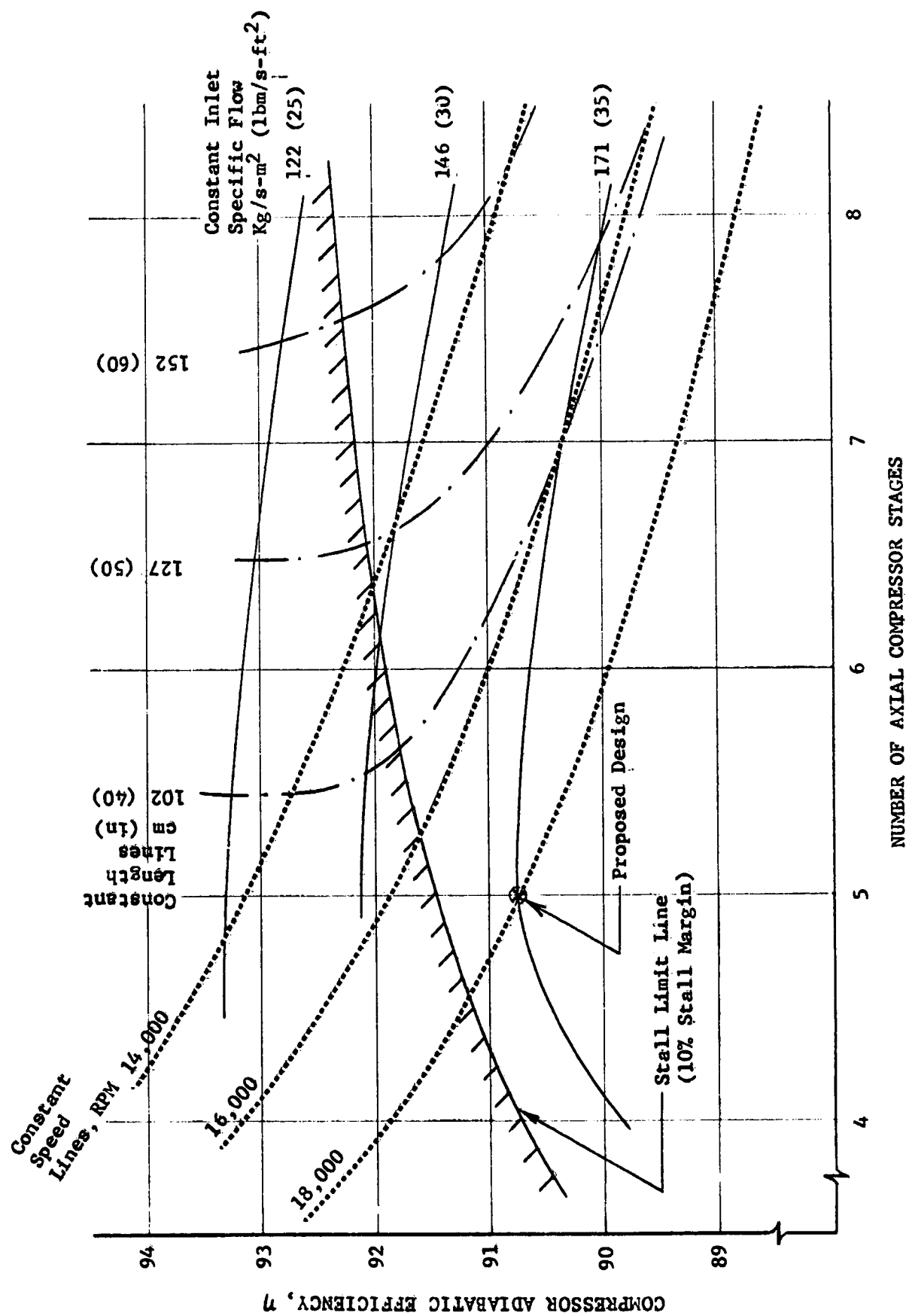
91

90

89

4   5   6   7   8

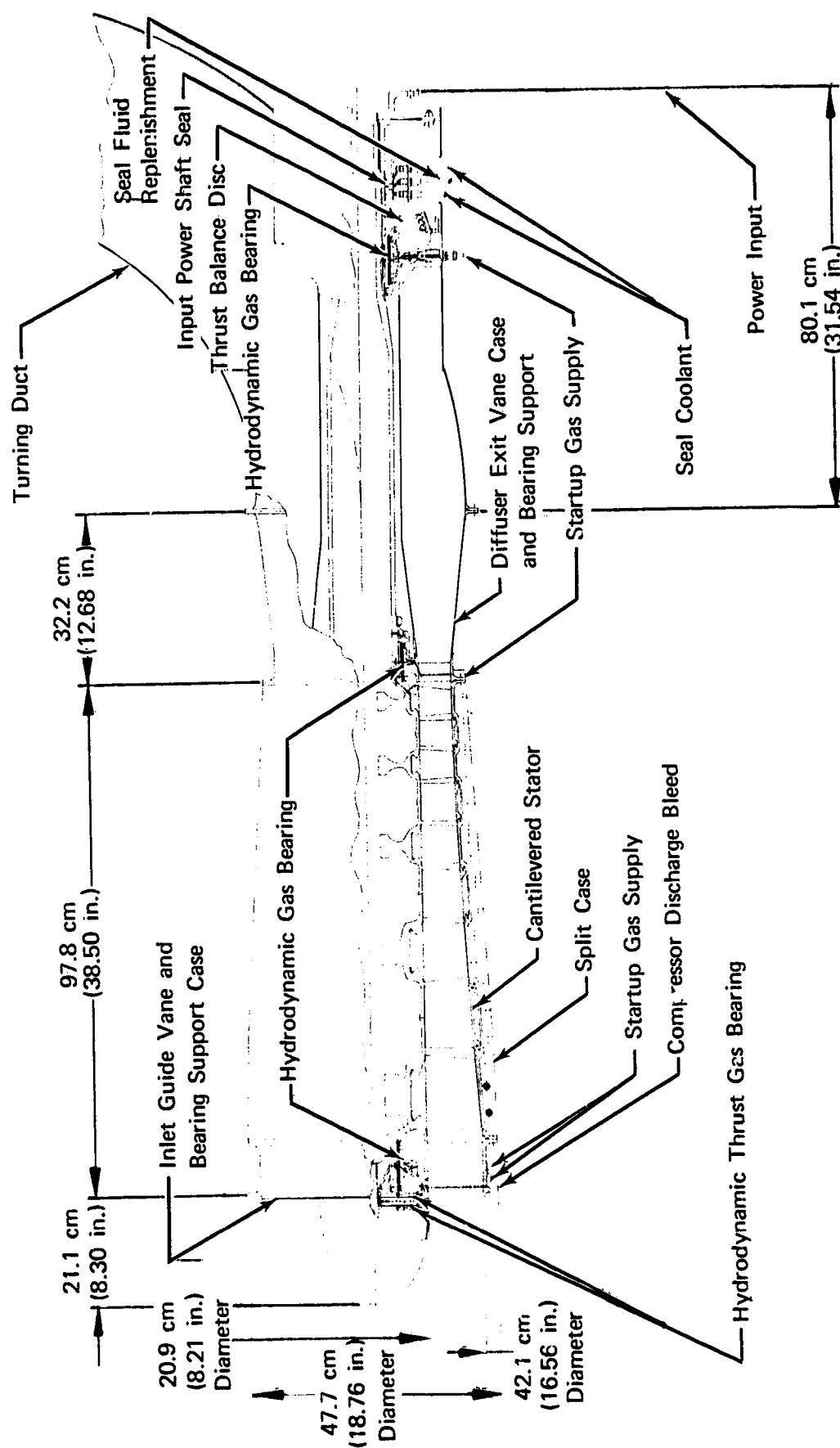Figure 70. Compressor Performance for Recuperator GDL Cycle

Figure 71. IMW Compressor

112

(b)   Bearing Consideration, Selection, and Concept

Three basic types of bearing concepts were considered for the compressor: a conventional rolling element bearing, a hydrodynamic gas bearing, and an unconventional rolling element bearing. The advantages and disadvantages of these concepts are presented in table XV. The foil-type hydrodynamic gas bearing was selected for primary consideration because it eliminated (1) the potential of contaminating the lasing fluid with the bearing coolant and (2) the requirement for separate seals, lubrication, and cooling systems (figure 72). The foil-type hydrodynamic gas bearing has the following advantages over other gas bearing concepts:

1.   Greater load capacity at low supply pressures
2. _   Higher bearing stability margin
3. .   Tolerance to rotor and housing distortions
4. .   Ease of assembly and installation
5.   Low fabrication cost.

The compressor conceptual design contains four gas bearings, as shown in figures 73 through 75. Three are journal bearings, one located at each end of the drum rotor and one at the end of the input power shaft. The fourth is a double-acting thrust bearing located at the front of the compressor. The front and thrust bearings are supported by the inlet guide vane case. The rear rotor bearing is supported by the exit vane case. The compressor will be supported from these two locations. Because weight is not critical, these bearing supports and mount rings will be made stiff. This is desirable to control rotor deflections and critical speed. Also, an additional bearing can be added in the center of the rotor if the detail design indicates it is needed for critical speed considerations. The power shaft bearing is supported by a ring where it protrudes from the turning duct. This ring can carry bearing loads directly to a support mount. The journal bearings were sized to take a 3g radial load while running, based on a unit loading of 0.24 MN/m^2 (35 psi) (Reference 7). The thrust bearing can accommodate the 3g axial load with either a nickel or titanium alloy rotor, based on a unit loading of 40 psi.

There is a wide range of materials available for the compressor in the recuperator cycle because it is not subjected to a high temperature environment. Candidate materials include all the nickel-base, titanium, and stainless steel alloys. The freedom of the final selection should remain open until the detailed design is performed so the selection can be based on the results of the detailed thermal and stress analyses to achieve proper clearance during the cycle transients.

(c)   Thrust Balance

This compressor rotor has a large thrust unbalance of 31,138 to 40,034 N (7,000 to 9,000 lb$_f$) because it is not balanced against the prime mover. A thrust balance disk on the power shaft was selected as the most desirable technique to balance this force (figure 75). The disk uses labyrinth seals with leakage of less than 0.14 kg/sec (0.3 lb$_m$/sec) that will have little effect on performance. The following is a discussion of thrust balancing concepts that were considered and rejected as less desirable. A gas bearing was excluded

because the thrust load was considered too large, requiring an eight-stage stacked bearing that imposed excessive manufacturing tolerances and assembly problems. A grease packed bearing could not tolerate the heat generation. A lubricated ball bearing, located outside the flowpath seal, would position the shaft axially from the bearing location, but would induce a thermal growth problem between the case and the rotor during transients.

Table XV. Bearing Concept Considerations

Advantages	Disadvantages
Conventional Rolling Element Bearing	
With conventional cooled lubrication compartment	
Proved design technology	Separate lubrication and cooling system required
High load carrying capacity	Bearing compartment leakage will contaminate lasing fluid
With grease pack lubrication	
Proved design technology	Heat generation too high for 600 sec or longer run without cooling
High load carrying capacity	
No separate lubrication and cooling system required	
Hydrodynamic Gas Bearing	
Lubricated with lasing fluid (no separate system required)	Limited experience
No high temperature limit beyond that of the structural and surface materials	
Not life limited when operating on a full-hydrodynamic film	
Unconventional Rolling Element Bearing (Unlubricated Silicon Nitride Ball Bearing)	
Lower heat generation than steel bearings (Reference 9)	Little experience (considered too risky for this application)
No separate lubrication and cooling system	
Higher temperature capability	

114
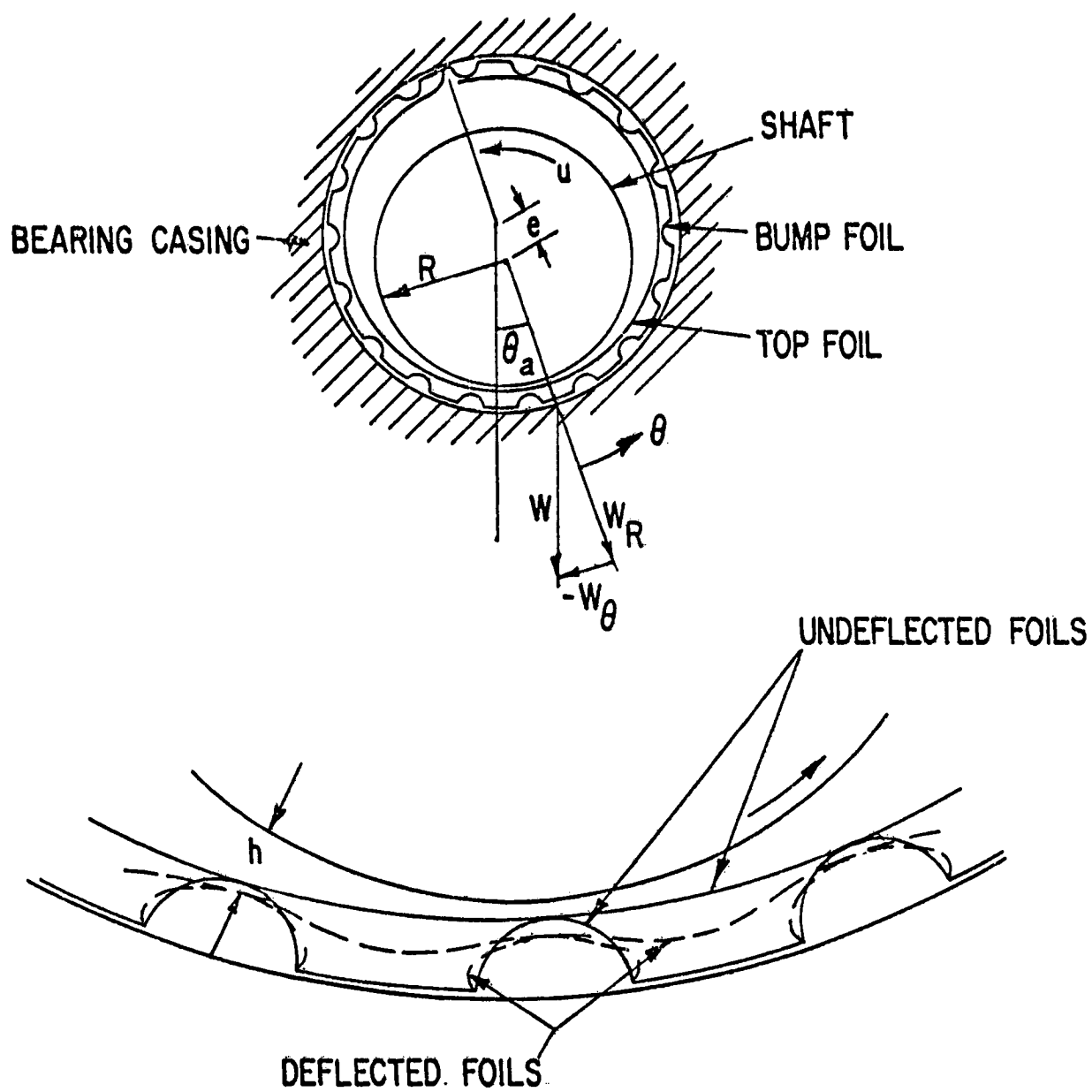
Figure 72. Journal Bearing Schematic
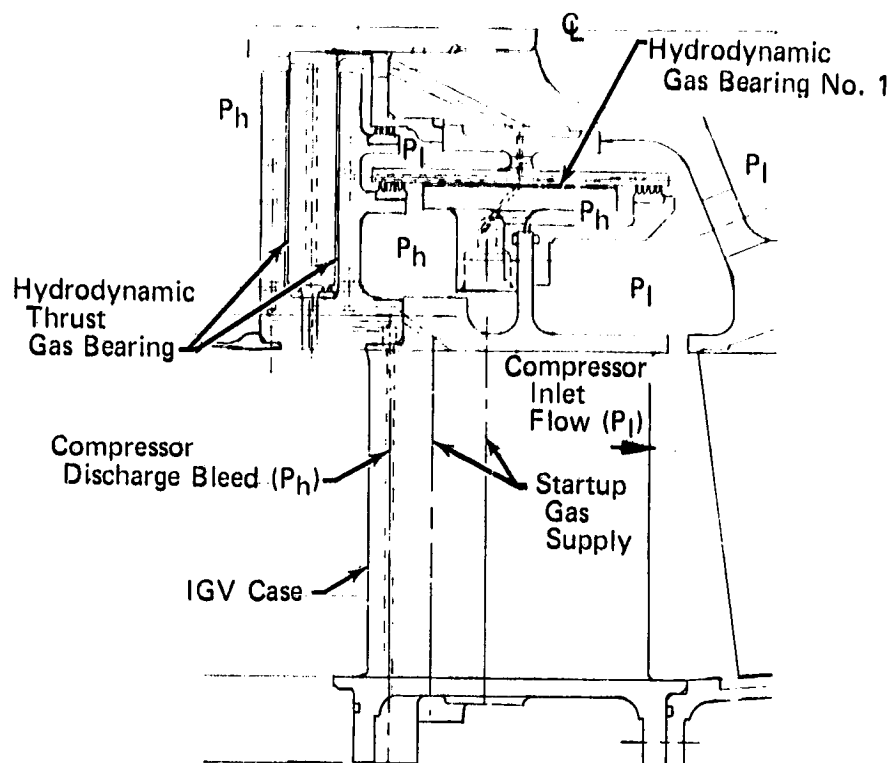
Figure 73. Hydrodynamic Thrust and No. 1 Journal
Gas Bearings
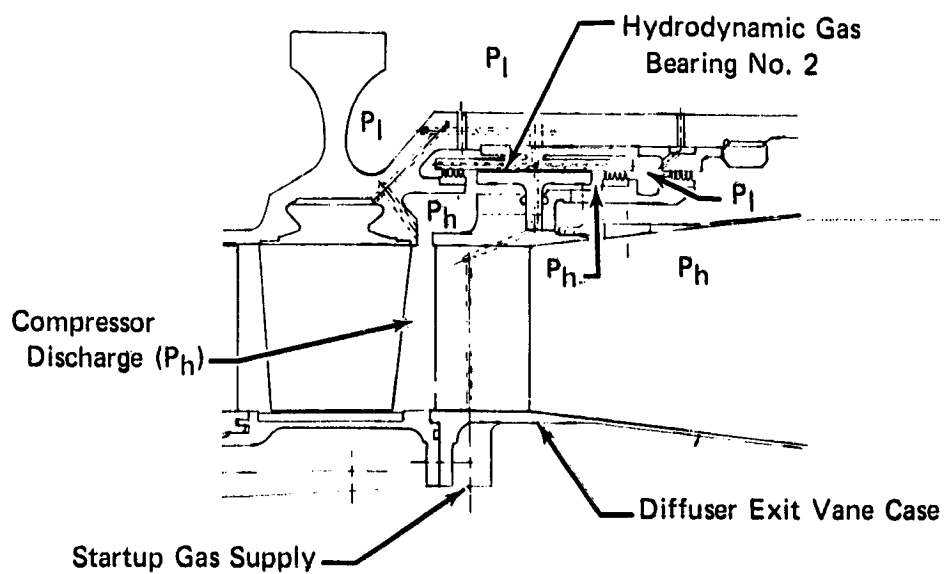
Figure 74. Hydrodynamic No. 2 Journal Gas
Bearing
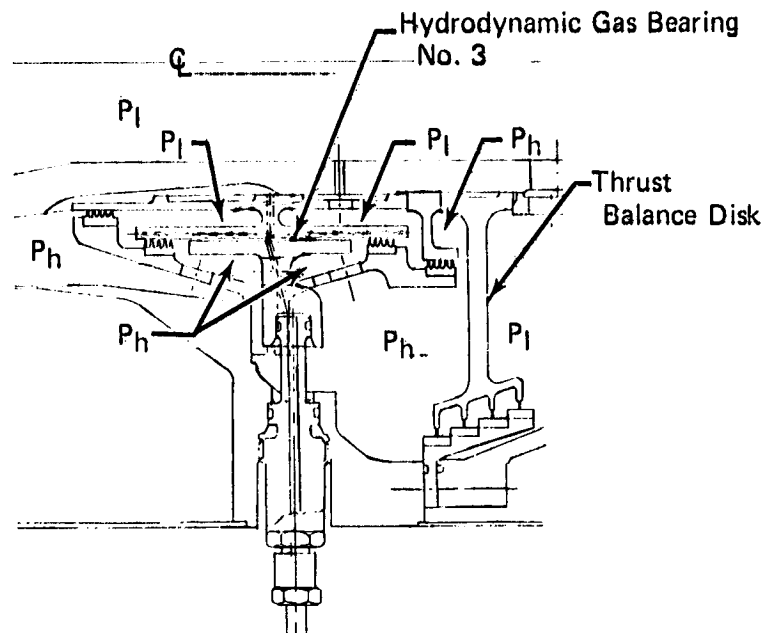
Figure 75. Hydrodynamic No. 3 Journal Gas
Bearing and Thrust Balance Disk

(d)   Seals

The power shaft must have a dynamic and static seal with near-zero
leakage for containment of the lasing fluid. The centrifugal ferrofluidic seal was
selected for this application because it had demonstrated zero leakage capability
(Reference 10). This seal functions as a centrifugal seal during dynamic operation
and as a magnetic seal for static conditions. This seal package is shown with
cooling provisions in figure 76. A face seal was also considered for this applica-
tion and rejected because of its leakage rate of 0.0009 kg/sec (0.0019 lb_m/sec).

The cases and other connections for the airborne system can use
Viton or Kelrez O-ring seals. Kelrez has a long life operating temperature
range of 280 to 560°K (-65 to 550°F). For the nonserviceable or resupplyable
space system, the split case and mating "tee" joints can be permanently sealed
by welding or brazing.

Recuperator

(1)   Function

The recuperator's function in both the space and airborne GDL is to
increase the system's thermodynamic efficiency by recovering energy from the
diffuser exhaust and returning it to the laser medium downstream of the com-
pressor. The recuperator is located downstream of the diffuser. In the design
of the recuperator, primary attention is directed to achieve the thermal effective-
ness goal with secondary priority given to volume, weight, cost, and structural
material considerations.

117
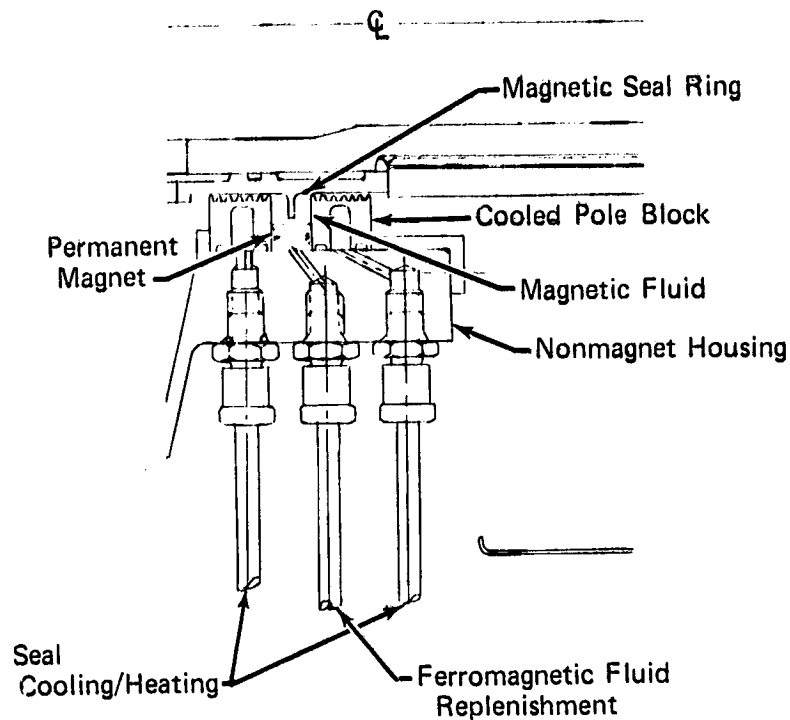
Figure 76. Centrifugal Ferrofluidic Shaft Seal

(2)   Critical Aspects

Item	Effect	Solution
Columbium Material Recuperator	Possible laser medium material reactions	Use a protective coating for columbium, or use lower strength nickel-base alloys
Complex Heat Exchanger Surfaces	Small passages make coating of metal difficult	Use simpler, less efficient surfaces or gas passivation coating
	Difficulty in manufacturing the recuperator	Use brazed construction
Thermals During Startup	Distortion and possible failure of device components	Startup transients minimized by a gradual heating of the system to steady-state condition

(3)   Description

The recuperator concept was selected on the basis of a parametric design analysis of core geometry configurations. The high thermal efficiency that is required of this heat exchanger limits the core configuration to either a counter-flow or multipass cross-counterflow heat exchanger. The core geometries considered for this device were mainly plate-fin surfaces because these surfaces are

especially efficient when both fluids are gases. With the plate-fin design, a large heat transfer area per unit volume can be achieved. The types of plate-fin surfaces considered for the recuperator were plain plate-fin (rectangular and triangular) and a louvered plate-fin. The louvered-fin design has fins that have been bent into the gas stream, thus reducing boundary layers and increasing heat transfer conductances. Also, one finned-tube, multipass, cross-counterflow design was considered. The major advantage of the finned tube is its ability to withstand high pressure differentials between the hot and cold sides. These core configuration descriptions are summarized in table XVI.

Table XVI. Heat Exchanger Core Configurations

Designa-tion	Description	Fin/Per		Plate Spacing,	
		cm	(in.)	cm	(in.)
A	Plain plate fin (rectangular)	28.2	(11.1)	0.63	(0.25)
B	Plain plate fin (rectangular)	13.5	(5.3)	1.19	(0.47)
C	Plain plate fin (rectangular)	15.7	(6.2)	0.65	(0.256)
D	Plain plate fin (triangular)	118.0	(46.45)	0.25	(0.10)
E	Plain plate fin (triangular)	43.1	(16.96)	0.65	(0.256)
F	Louvered plate fin	15.4	(6.06)	0.63	(0.25)

A comparison of volumes for these core configurations of table XVI is shown in figure 77 plotted versus reduction in recuperator pressure loss from the base design. The data in this figure indicate that the recuperator size is significantly more sensitive to core configuration than to pressure loss.

Recuperator conceptual designs were performed with core configurations A and D, as shown in figure 78. Configuration D was selected as a core with relatively large fin spacing that can be fabricated and coated with technology projected for the year 1990. Configuration A represents a recuperator that would require a significant advancement in core fabrication and could only be coated by gas passivation. To achieve the counterflow plate-fin recuperator configuration, triangular end sections on the core are used to manifold the hot and cold gases into the core.

The type of structural material used in the recuperator is of primary concern. A material such as columbium appears to be a natural choice for its high temperature strength and relatively high thermal conductivity. However, at elevated temperatures, the reactivity of columbium with the lasing medium is not known and may cause corrosion or embrittlement. The use of a coating to protect columbium probably is required and would reduce the thermal conductivity, increase cost, and perhaps impose limitations on the core geometry to accommodate the coating process. Other materials candidates include the dispersion-hardened nickel-based alloys. The sensitivity of the most efficient recuperator core configuration (surface D) to changes in metal thermal conductivity is shown in figure 79.

119

The protective coatings for columbium alloys consist primarily of the silicide coatings which may be applied by either a slurry or a vapor phase technique. Silicide coatings of this type are good up to around 1925°K (3000°F).

The recuperator is an integrated brazed assembly for fluid leakage control. Candidate braze materials for refractory materials are listed in table XVII, from Reference 11.
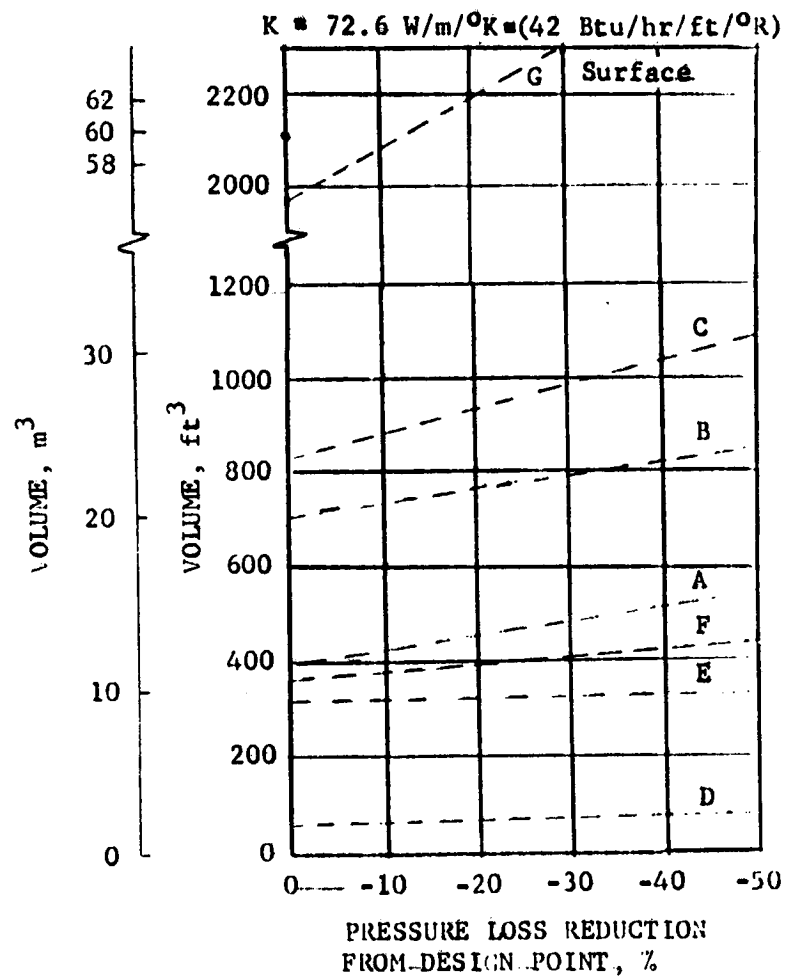
Figure 77. Effect of Pressure Loss on 1-Mw System Recuperator Volume

120

SECT B-B
1/4 SIZE

VIEW C
1/4 SIZE

COLD SIDE
IN

HOT SIDE
OUT
C

292.1
(115)

VIEW A

HOT SIDE
IN

85.1
(33.5)

OUT
COLD SIDE
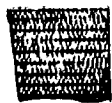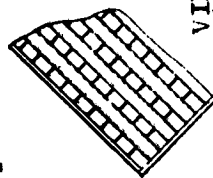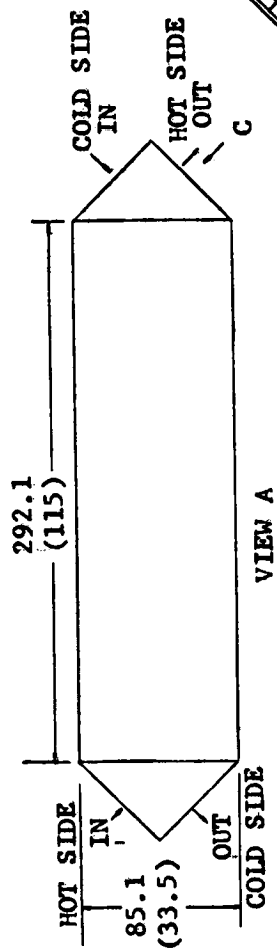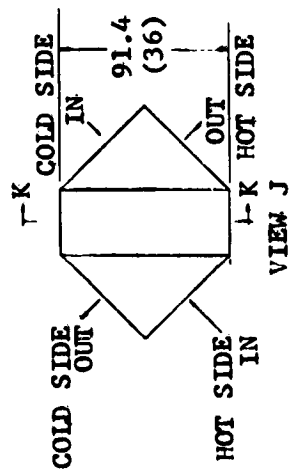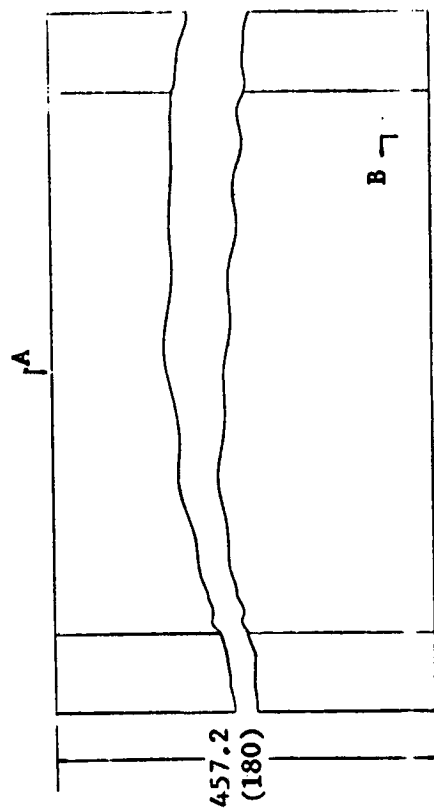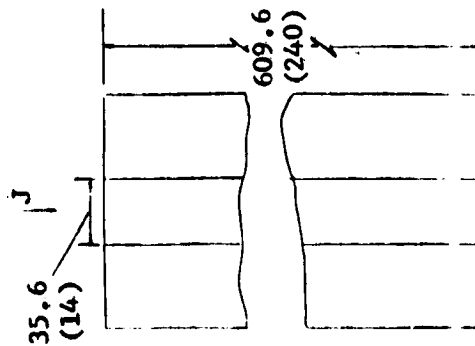
COLD SIDE

RECUPERATOR #1
MAT'L: COLUMBIUM (COATED)

457.2
(180)

A

B

B

NOTE: ALL DIMENSIONS, cm (in)

Figure 78. Recuperator

SECT K-K
1/2 SIZE

91.4
(36)

K   COLD SIDE
IN

OUT
HOT SIDE

COLD SIDE
OUT

K   HOT SIDE

HOT SIDE
IN

VIEW J

J

609.6
(240)

35.6
(14)

VIEW H
RECUPERATOR #2

121
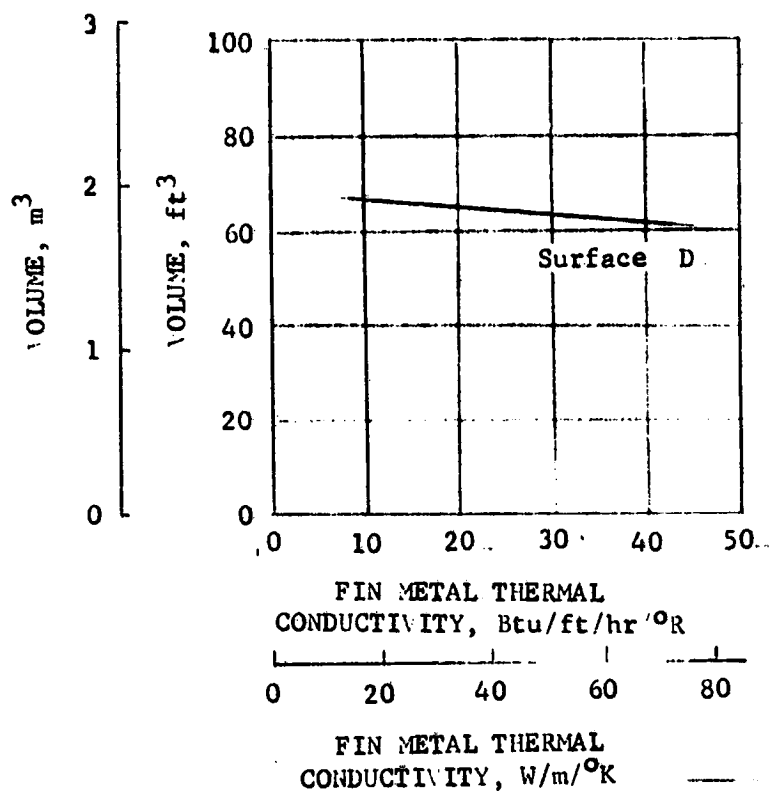
Figure 79. Effect of Core Material Thermal
Conductivity on 1-Mw Recuperator
Volume

Table XVII. Brazing Materials for Refractory Metals

Flow Points of Selected Filler Metal Compositions for Brazing Refractory Metals[101]			Results of Brazing Filler Metal Remelt Study[013]			
				-Temperature, °F--		Approximate melting point rise
Alloy composition, wt %	Flow point-- F	°C	Filler metal composition, wt %	Brazing	Remelt	
Ta - V - Cb			25Ta - 50V - 25Cb	3400	4530	1130
30Ta - 65V - 5Cb	3400	1870	30Ta - 40V - 30Cb	3500	3630	130
5Ta - 65V - 30Cb	3300	1920	30Ta - 65V - 5Cb	3400	4170	770
10Ta - 80V - 10Cb	3400	1870	5Ta - 65V - 30Cb	3300	4170	870
30Ta - 30V - 40Cb	3550	2010	30Ta - 65V - 5Ti	3350	4350	1000
30Ta - 40V - 30Cb	3500	1930	25Ta - 55V - 20Ti	3350	3990	640
25Ta - 50V - 25Cb	3400	1870	20Ta - 50V - 30Ti	3200	4350	1150
5Ta - 90V - 5Cb	3400	1870	10Ta - 40V - 50Ti	3200	4350	1150
20Ta - 60V - 20Cb	3400	1870				
Ta - V - Ti						
10Ta - 40V - 50Ti	3150	1750				
15Ta - 25V - 60Ti	3000	1650				
5Ta - 20V - 75Ti	3000	1650				
10Ta - 20V - 70Ti	3000	1650				
30Ta - 35V - 35Ti	3100	1705				
20Ta - 50V - 30Ti	3200	1760				
30Ta - 65V - 5Ti	3350	1845				
25Ta - 55V - 20Ti	3350	1845				

Heat Sink Heat Exchanger

(1) Function

The heat sink's function in both the space and airborne GDL system is to reject excess heat from the lasing medium. This excess heat results primarily from the adiabatic inefficiency of the compressor, which supplies more heat than the lasing action extracts. The heat sink is located downstream of the recuperator "hot side" outlet, as illustrated in the recuperator cycle schematic. The space cycle heat sink uses a liquid coolant loop through a radiator to dump waste heat, whereas the airborne heat sink uses external air as a cooling source. In the design of the heat sink, primary importance was assigned to achieving the cycle thermal effectiveness, with secondary considera-tion given to such factors as volume, weight, cost, and structural material.

(2) Critical Aspects

Item	Effect	Solution
Aluminum Base Material for Heat Sink	Possible large strength fall-off with higher tem-perature excursions	Use nickel-base alloy if required
Space Heat Sink Coolant	Possible decomposition of MIPB at high temperatures	Substitute other organic working fluids, such as toluene
Thermals During Startup	Distortion and possible failure of components	Startup transients minimized by a gradual heating of the system

(3) Description

The heat sink heat exchangers were investigated by means of a para-metric evaluation of core configurations for both the space and airborne systems. The two systems use different heat sink fluids, which affect the core configurations. The space cycle uses an organic liquid coolant such as Monoisopropylbiphenyl (MIPB), Humble 3152, or toluene to exchange the laser fluid heat to the radiator, whereas the coolant fluid for the airborne system is air.

The gas-to-liquid space heat sink can be either a finned-tube or plate-fin core configuration. However, for the gas-to-liquid combination, the finned-tube core normally provides a better match of heat transfer coefficient and surface area and simplifies the construction of a leak-resistant core. The surface con-figurations studied for the space system are listed in table XVIII.

123

Table XVIII. Space System Heat Sink Core Configurations

Designa- tion	Description	Fin per cm	Fin per (in.)	Tube OD cm	Tube OD (in.)	Plate Spacing cm	Plate Spacing (in.)
A	Finned flat tube	28.75	(11.32)	0.25 x 1.87	(0.1 x 0.737)	-	-
B	Finned circular tube	19.69	*(7.75)	1.72	(0.676)	-	-
C	Finned circular tube*	20.32	*(8.0)	1.02	(0.402)	-	-
D	Finned circular tube	22.99	(9.05)	1.97	(0.774)	-	-
E	Finned circular tube	21.15	(8.72)	0.97	(0.38)	-	-
F	Finned circular tube	22.10	(8.7)	1.64	(0.645)	-	-
G	Plain plate-finned	28.19	(11.1)	-	-	0.64	(0.25)
H	Plain plate-finned	117.98	(46.45)	-	-	0.25	(0.10)

*Continuous fins

All of these cores contain a multipass cross-counter flow configuration to provide high thermal efficiency. A comparison of volumes for the core configurations in table XVIII are plotted versus reduction in gas side pressure loss from the base design in figure 80. These data indicate that the heat sink volume is significantly more sensitive to core configuration than pressure loss. Core configuration C was selected for the space system heat sink based on the following considerations: (1) configuration C is the most compact finned circular tube core evaluated and has advantages relative to manufacturing simplicity, reliability of sealing, lighter weight, and lower cost; and (2) configuration II and A were rejected even though they were more compact because the heat sink size was not a major factor and these cores were judged more difficult to manufacture and less reliable. The conceptual design of the space system heat sink is shown in figure 81.

A similar parametric study was conducted for design of the airborne heat sink. The core geometries considered for this heat sink are plate-fin surfaces, since these surfaces are especially efficient when both fluids are gases. Large heat transfer area per unit volume can be achieved with the plate-fin design. The types of plate-fin surfaces considered are shown on table XIX.

The core volume comparison for the cross-flow configurations in table XIX is presented in figure 82 as a function of pressure loss. Configuration I was selected for the airborne heat sink core because it provided manufacturing simplicity and the relatively small size of this heat exchanger did not warrant the complexity of a more compact core. The conceptual design of the airborne heat sink is shown in figure 83.

The primary material selected for the heat sink heat exchanger was an aluminum alloy. The superior properties of this material that made it a prime candidate for low temperature heat exchangers were its high thermal conductivity and low density. In the event the cycle temperatures were increased beyond the acceptable temperature strength of aluminum alloys, then nickel-base alloys could have been substituted in this heat exchanger with an associated penalty in conductivity and weight.

124
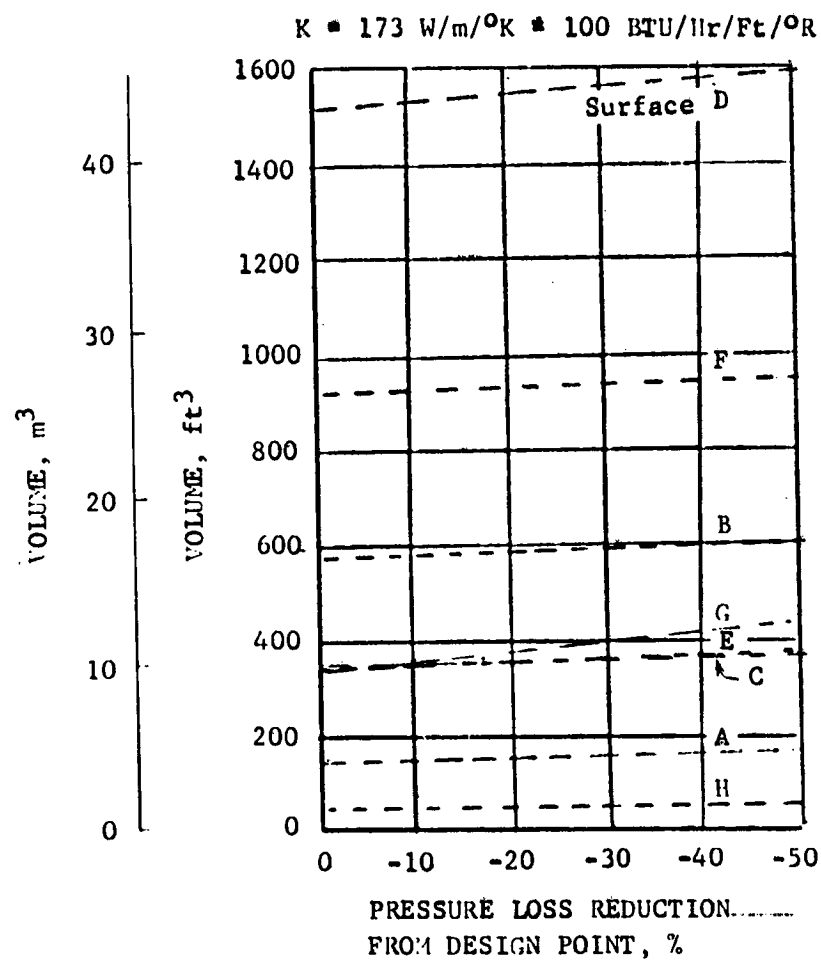
Figure 80. Effect of Pressure Loss on 1-Mw Space
System Sink Heat Exchanger Volume

146.3
(57.6)

104.9
(41.3)

GAS IN
→P

VIEW L

GAS OUT

COOLANT IN   L

457.2
(180)

GAS IN

GAS COLLECTION
MANIFOLD

COOLANT OUT

SPACE HEAT SINK
MAT'L: ALUMINUM

COOLANT IN

COOLANT FLOW   VIEW M   COOLANT FLOW

N

GAS FLOW →

VIEW N

COOLANT IN
(7 PASSES)

GAS IN →   → GAS OUT

COOLANT OUT

SPACE HEAT SINK SCHEMATIC

COOLANT IN

VIEW P

COOLANT OUT →

NOTE: ALL DIMENSIONS, cm (in)
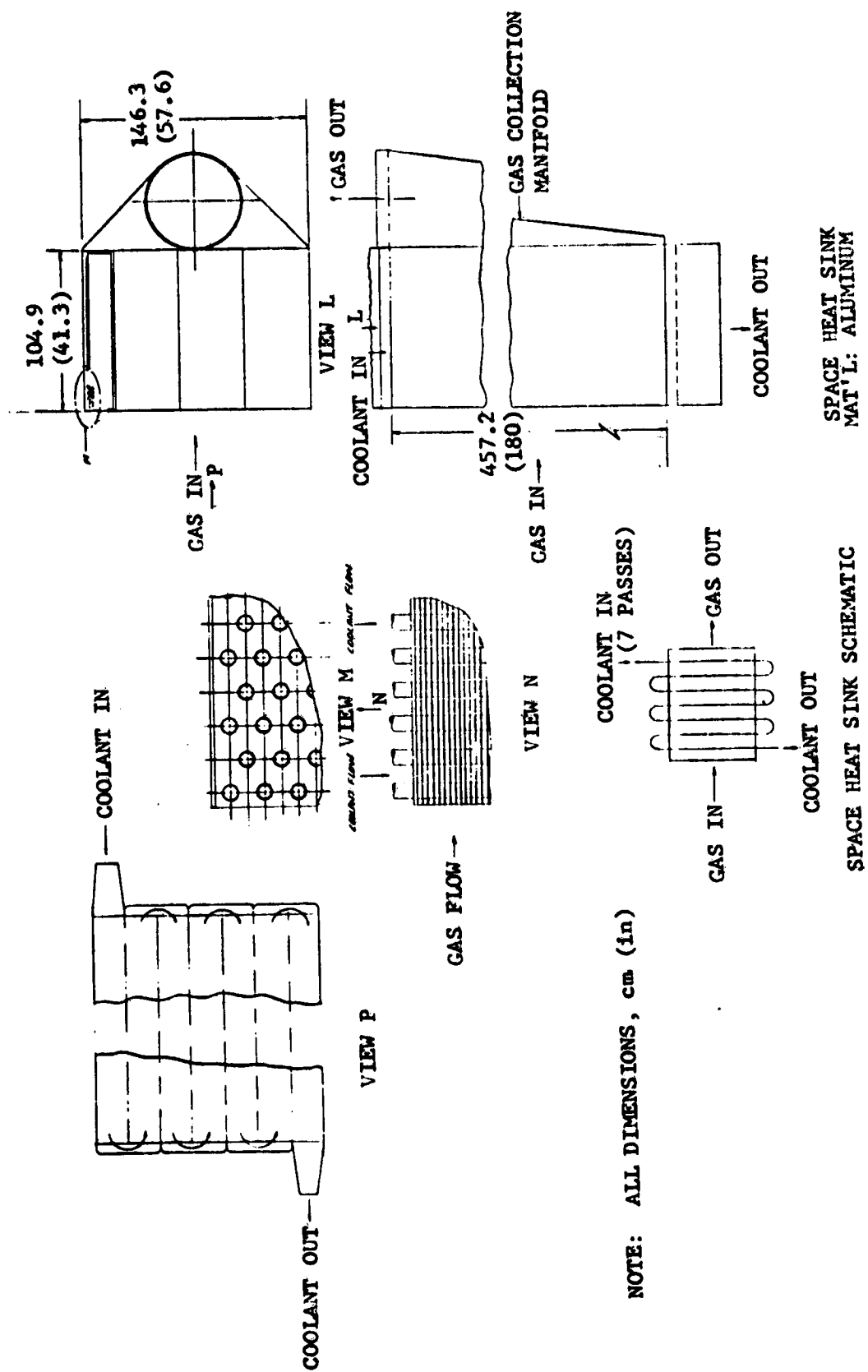
Figure 81. Space Heat Sink

126

Table XIX. Airborne System Heat Sink Core Configurations

Designa-tion	Description	Fin per		Plate Spacing	
		cm	(in.)	cm	(in.)
I	Plain plate fin	28.19	(11.1)	0.64	(0.25)
J	Plain plate fin	117.98	(46.45)	0.25	(0.10)
K	Louvered plate fin	15.39	(6.06)	0.64	(0.25)

K = 173 W/m/°K = Btu/Hr/ft/°R

PRESSURE LOSS REDUCTION
FROM DESIGN POINT, %
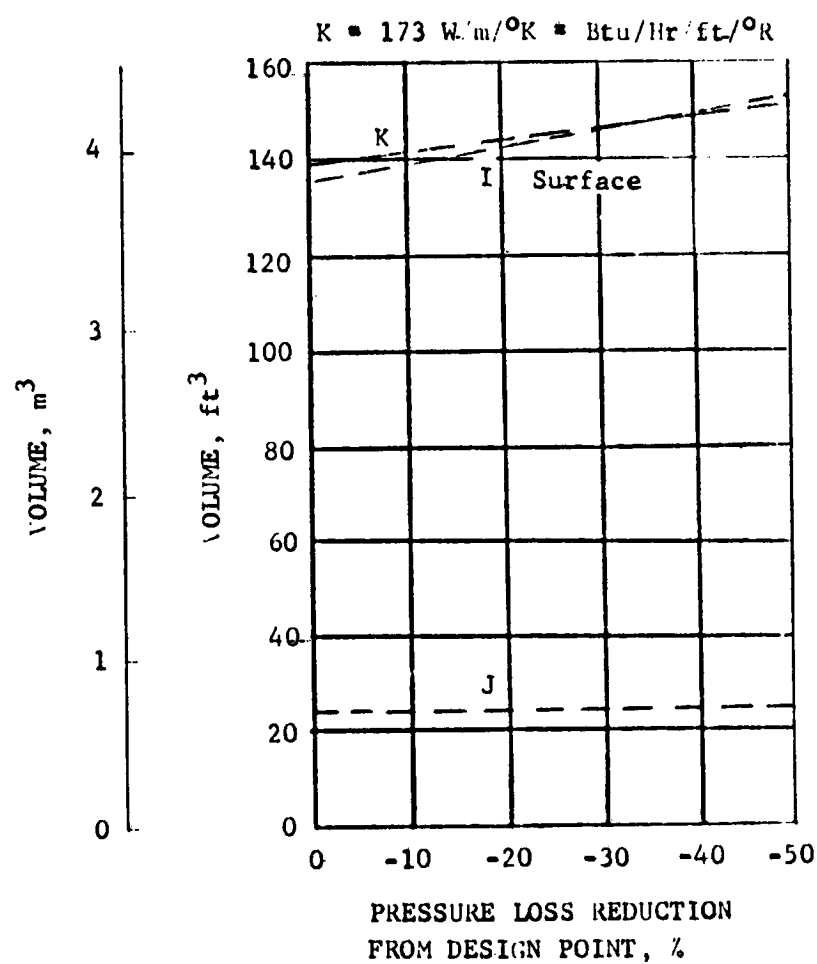
Figure 82. Effect of Pressure Loss on 1-Mw Airborne
System Heat Sink Heat Exchanger Volume

127

VIEW V
1/2 SIZE

V

AIR IN

U → GAS
IN →

54.6
(21.5)

90.2
(35.5)

VIEW T

VIEW U
1/2 SIZE

T

778.8
(306.6)
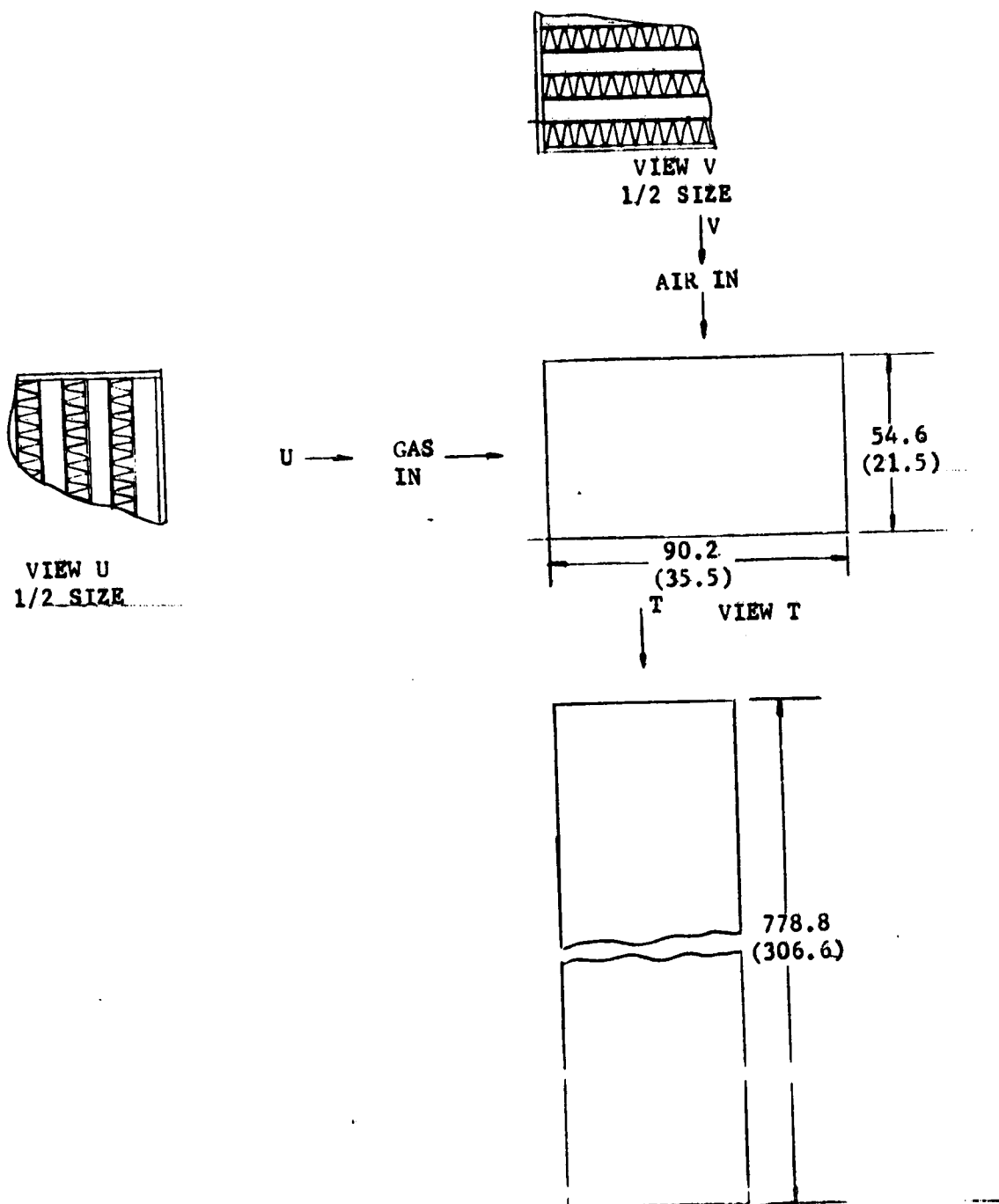
AIRBORNE HEAT SINK
MAT'L: ALUMINUM

NOTE: ALL DIMENSIONS, cm (in)

Figure 83. Airborne Heat Sink (Cross Flow)

Heat Source Heat Exchanger

(1) Function

The function of heat source heat exchangers in the space and airborne GDL is to replace the heat loss in the device and the loss due to the efficiency limitation of the recuperator. The heat is added by cycling liquid lithium at 1750°K through a heat source and a heat source heat exchanger, which is located downstream of the recuperator "cold side" exit, as previously shown in figure 47.

(2) Critical Aspects

Item	Effects	Solution
Columbium Material for Heat Source Heat Exchanger	Possible laser medium material reactions	Use protective coating
	Reduced strength at liquid lithium temperatures	Change material to higher strength tantalum
Complex Heat Exchanger Surfaces	Makes coating of metal surfaces, if required, difficult	Use a more simple core
	Makes fabrication difficult	Use brazed construction
Thermals During Startup	Distortion and possible failure of device components	Startup transients minimized by gradual heating

(3) Description

The heat source heat exchanger core geometry was evaluated by parametric design analysis. Due to the relatively low thermal efficiency required of this heat exchanger, only single-pass, cross-flow configurations were evaluated. Finned-tube core geometries were studied for this device since this configuration normally provides the best balance of heat transfer coefficient and surface area for liquid-to-gas systems. Also, the finned-tube arrangement simplifies the containment of the liquid lithium. The core configurations studied for the heat source exchanger are listed in table XX. The core volume comparison for the configurations in table XX is presented as a function of pressure loss in figure 84. These data indicate that the heat source will be small regardless of which core configuration is selected. Core configuration C was selected for compactness and because it contained circular tubes that have a manufacturing simplicity and reliability advantage over the flat tube configuration. The conceptual design of the heat source heat exchanger is shown in figure 85.

Table XX. Heat Source Heat Exchanger Core Configurations

Designation	Description	Fin per cm (in.)	Tube OD, cm (in.)
A	Finned flat tube	28.8 (11.32)	0.25 by 0.95 (0.1 by 0.373)
B	Finned circular tube	19.7 ('7.75)	1.72 (0.676)
C	Finned circular tube	20.3 ('8.0)	1.02 (0.402)
D	Finned circular tube	22.2 (8.72)	0.97 (0.38)

'Continuous fins
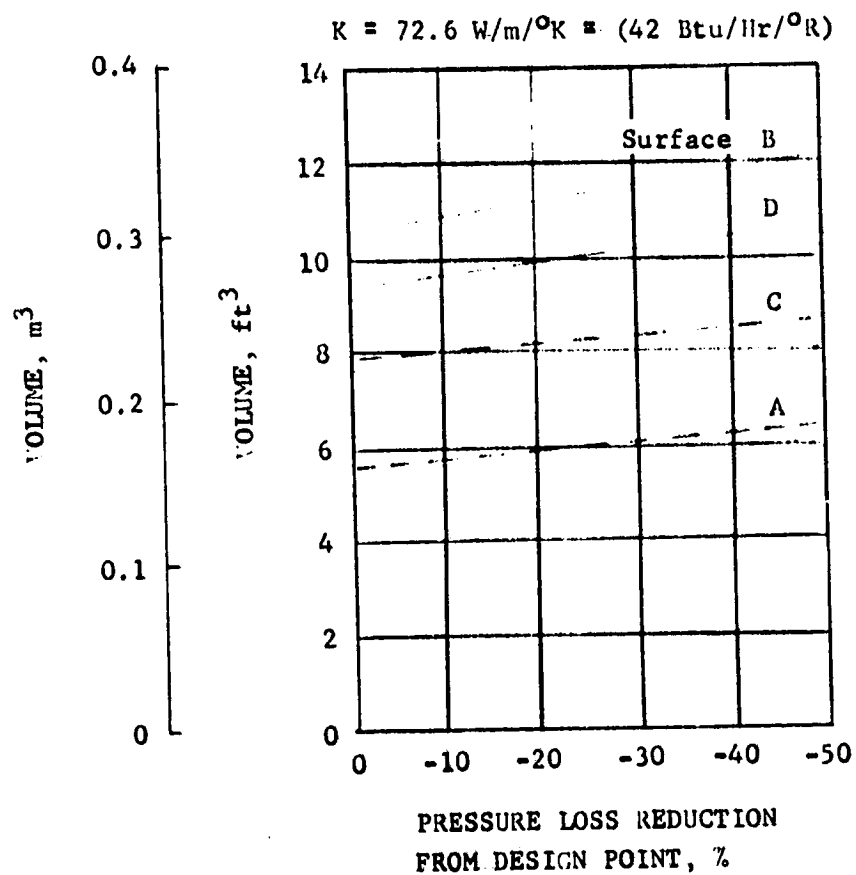
Figure 84. Effect of Pressure Loss on 1-Mw
System Heat Source Heat Exchanger
Volume

24.4
(9.6)

19.1
(7.5)

VIEW Q

SECT S-S
1/2 SIZE

COOLANT IN

S   S

R

Q   GAS OUT

VIEW R
1/2 SIZE

518.2
(204)

GAS IN

COOLANT IN

GAS IN   GAS OUT

COOLANT OUT

HEAT SOURCE SCHEMATIC

HEAT SOURCE

MATERIAL: COLUMBIUM (COATED)
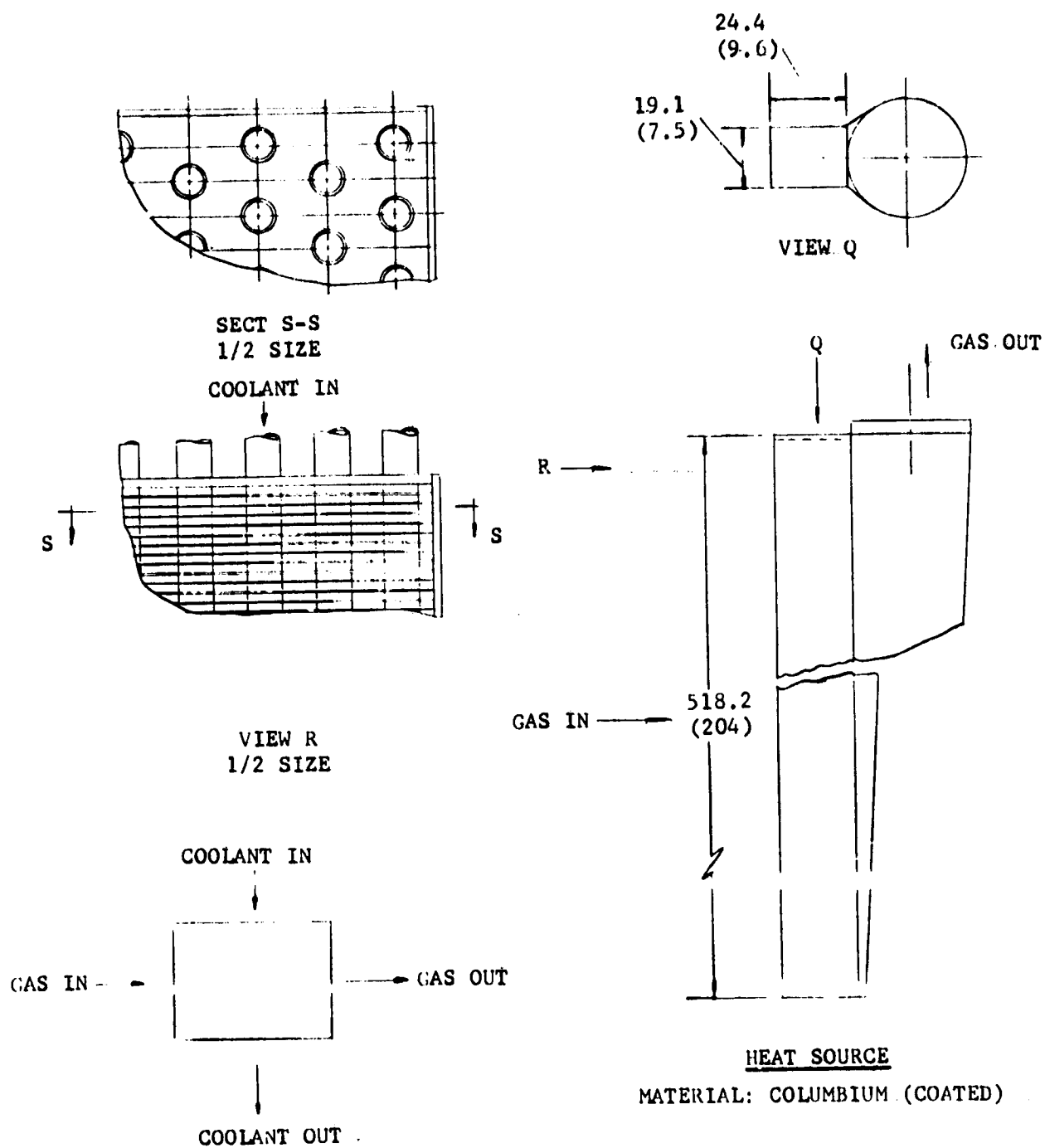
NOTE: ALL DIMENSIONS, cm (in)

Figure 85. Heat Source

The materials in the heat source heat exchanger are subjected to a severe environment and must resist attack by liquid lithium at 1750°K (3159°R), and operate in the 1500°K (2700°R) lasing fluid. Material candidates are columbium (niobium) and tantalum, which show good resistance to attack by the alkali metals. However, columbium and tantalum are subject to nitrogen embrittlement at high temperatures. The severity of the problem, which is time and temperature dependent, should be experimentally evaluated. Both materials can be protective coated if required. Columbium is preferred for this heat exchanger from a consideration of thermal conductivity and density; however, the final material selection between columbium and tantalum should be based on the results of an experimental environmental compatibility evaluation.

This heat exchanger is an integrally brazed assembly for fluid containment control. Candidate braze materials for refractory materials were previously presented in table XVII.

Ducting

    (1)   Function

The function of the ducting is to contain and direct the lasing fluid between components with acceptable pressure losses and zero leakage. The ducting must also provide for a smooth flow transition between rectangular and circular shapes and for providing low loss fluid turning, such as between rectangular diffuser exit and the circular shapes and for providing low loss fluid turning, such as between rectangular diffuser exit and the circular recuperator inlet.

    (2)   Critical Aspects

Item	Effects	Solution
Duct Pressure Losses	Increased requirements on the compressor	Size ducts for a low Mach number flow of 0.2 or less to keep pressure losses low
Leakage	Loss of lasing medium to ambient	Use welded ducting wherever possible to minimize leak paths
High Temperature Seals	Leakage to space	Develop high temperature seals to minimize leakage

    (3)   Description

The general physical characteristics of the closed-cycle GDL system ducting were evaluated to provide data for the system assessment of complexity, weight, and size. The study has been organized by separating the ducting into categories relative to the type of joint and duct contour. The results of the study are summarized in the table on figure 86, which indicates the type, diameter, and material of each duct. The respective location of each duct is denoted on the cycle schematic (figure 86). The ducts have been defined as types A, B, or C for which conceptual sketches are depicted in figures 87 through 89.

132

Figure 86. Closed-Loop GDL Recuperator Cycle Schematic

Duct Schedule

Line No.	Line Type	Nominal Diameter Inside Diameter, cm	Nominal Thickness t, cm	Maximum Temperature °K	Material
1	C	N/A	N/A	650	Stainless Steel
2	A/B	53.3	0.051	383	Stainless Steel
3	A/B	13.0	0.089	556	Stainless Steel
4	B	40.6	0.635	1406	Nickel
5	A/B	40.6	0.635	1500	Nickel
6	A	11.4	0.178	1500	Nickel
7	A	40.6	0.635	1500	Nickel
8	C	N/A	N/A	1489	Nickel
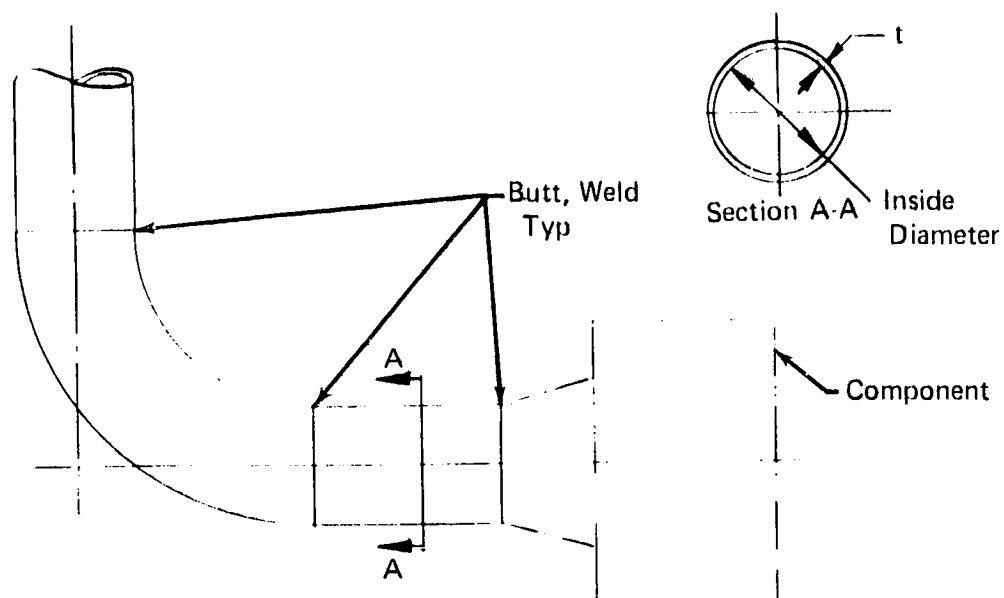
Figure 87. Type A Duct
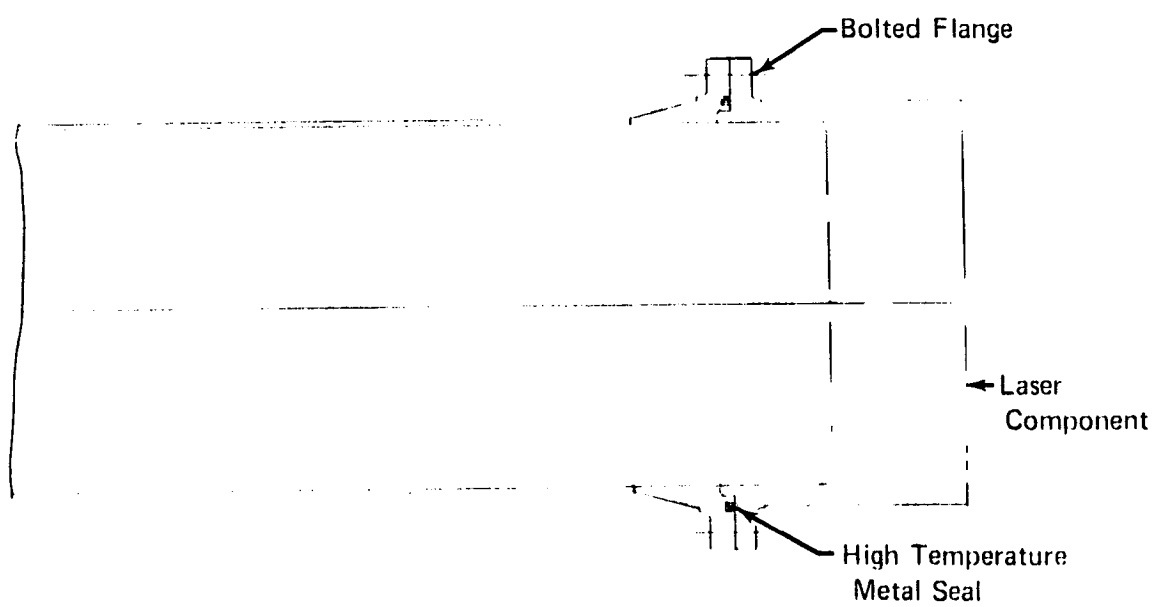
Figure 88. Type B Duct

View C   View D
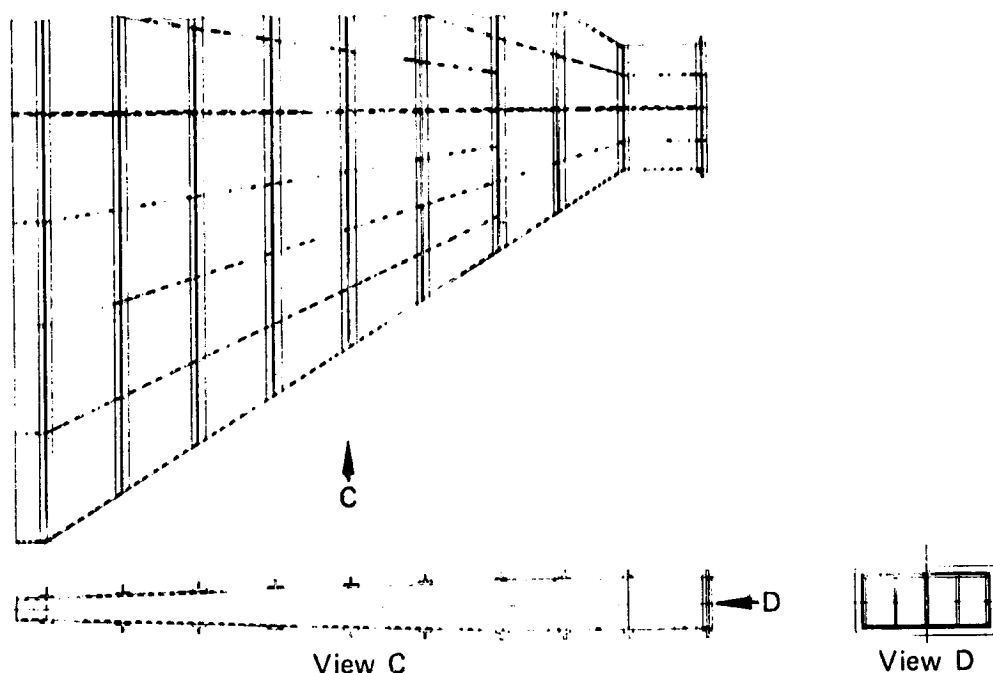
Figure 89. Type C Duct

Type A ducts connect components of similar materials. These ducts are welded to the components they connect and offer no potential leak paths.

Type B ducts connect components of dissimilar materials, or components, which require a bolted connection. These ducts use a seal at the joint to minimize leakage. The development of a high temperature zero-leak seal is an item subject to development and experimental verification.

A type C duct is a rectangular transitional duct between two components of a different cross section, such as the duct from the diffuser exit to recuperator inlet. Ducts of this type, with large plane surfaces, require external ribs and internal struts for structural support.

TECHNOLOGY CONFIRMATION

The objective of this Task was to assess the technology requirements of the components for the recuperator closed-cycle GDL for space and/or airborne operation and to define component demonstration programs that can be used to develop and/or evaluate the feasibility of the closed-cycle GDL.

A general assessment of the extent that the individual component technology exceeds current engineering s'ate-of-the-art technology was made based on the judgment of engineers working in the GDL field and knowledgeable in the related theory, component design, material properties, and fabrication concepts. The results of this assessment are summarized in table XXI. This table was devised as a guide to provide a general indication of the extent that the component technology exceeds currently available hardware to establish which components are candidates for experimental demonstration programs.

135

Table XXI. Individual Component Technology Assessment

Laser Components	State-of-the-Art (No Verification Required)	New Configuration (Should Be Demonstrated)	Advanced Technology (Demonstration Required)
Nozzle/Cavity		X	
Optics			X
Diffuser			X
Recuperator			X
Heat Source Heat Exchanger			X
Heat Sink Heat Exchanger	X		
Compressor		X	
Ducts	X		
Outside Scope of Study			
Space Radiator			X
Controls		X	
Prime Mover:			
Airborne System		X	
Space System			X

The most direct approach to arrive at a closed-loop GDL system demonstration, is to develop each of the major components individually to the requirements of the closed-loop and construct and test the system using these components. The system, and the components developed for it, can be scaled to reduce cost and lead time. However, even in a reduced scale, this approach is expensive and time consuming.

An alternate approach, which would significantly reduce the cost and lead time required to achieve a closed-cycle demonstration, involves the use of existing components where possible to construct a closed-loop GDL. The scale of the demonstrator could be selected to be compatible with existing hardware, such as a cavity/nozzle/manifold assembly, a compressor test rig, and facility heat exchangers.

New components would be provided to supplement existing rigs where necessary. A closed-loop system of this type would have certain limitations compared to a new scaled system; however, this approach could provide answers to many of the technical questions associated with closed-loop operation. The test unit could be upgraded as new components are developed.

The following four technology confirmation experimental demonstration programs are recommended to develop and substantiate the technology base needed for closed-cycle GDL application. The first program covers the establishment of a closed-loop system that will be used to investigate system effects and to evaluate components that have completed preliminary development. The other three programs are for individual components and cover the diffuser, recuperator, and optics.

The priority of the component development programs was established on the basis of the criticality of the technology for the closed-cycle GDL system. The diffuser development is assigned the highest priority because the unique requirements of the closed-loop diffuser and the achievement of an acceptable diffuser pressure recovery have a major influence on the compressor horsepower requirement and thus the overall cycle efficiency. Thus, a new specifically designed and developed diffuser is required for the closed-loop GDL test system — The recuperator development has the potential of significantly reducing the overall loop weight and is therefore assigned the second priority. The optics were assigned third priority because this technology area is currently undergoing intensive research and since existing optics can be used in the closed-loop demonstrator, it would be prudent to review the technology advancements in this area later in the program. The organization and phasing of these three development programs into a closed-loop GDL development plan is summarized in figure 90; the timing of this plan is flexible and can be varied to match the availability of funding.

	Cost				

Closed-Loop GDL Test System
  Scaled Model Design
  Fabricate Scaled Model
  Conduct Closed-Loop Test
    Program
	3.0M				

Diffuser Development
  Subscale Model Evaluation
  Subscale Model Demonstration
  Closed-Loop Test
	1.2M				

Recuperator Development
  Core Material and Coating
    Evaluation
  Core Configuration Evaluation
  Scaled Prototype Closed-Loop Test
	0.6M				

Optics Development	0.8M				

Years From Initiation

Figure 90. Technology Confirmation Program Summary

Closed-Cycle GDL System Experimental Investigation

The goal of this program is to experimentally investigate the system and component integration effects of the closed-loop GDL. Specifically, this program will combine components to provide a closed-loop system test bed that will be used to investigate such characteristics as system starting, dynamics, controls, stability, component performance, and performance degradation.

This plan is formulated to start closed-loop testing (with a low initial expenditure) by using as many existing components as possible to perform the preliminary testing. This approach will provide early definition of the system aspects that require further development and will provide the flexibility to direct research consistent with available resources.

137

A three-Task program is recommended to provide the facility and perform the experimental investigation of the closed-loop system, as shown in table XXII. Task I involves a design study of the system to establish the loop operating conditions and configuration. From this study a system size will be selected that permits the use of as many existing components as possible without compromising the technical objectives. Facility design layouts will be prepared for the selected system. Task II consists of the fabrication of the new and mating hardware, the assimilation of available hardware and of components from the demonstration programs, and the assembly of the test system, and will conclude with a checkout of this facility. Task III consists of conducting the closed-loop test program.

Table XXII. Closed-Cycle GDL System Experimental Investigation

---

TASK I - SCALED MODEL DESIGN

Perform Scaled Model Design and Cost Trade Study
Select Model Scale, Components and Configuration
Conduct Facility Design

TASK II - FABRICATE SCALED MODEL

Fabricate New Components and Mating Hardware
Prepare Closed-Cycle Test Facility
Assemble Test System
Perform Facility Checkout

TASK III - CONDUCT CLOSED-LOOP TEST PROGRAM

Substantiate Closed-Loop Feasibility
Establish Closed-Loop Control
Demonstrate Diffuser Operation

The test program will be planned to investigate the following aspects of closed-cycle GDL operation.

1. The feasibility of sustained closed-loop operation will be determined. The cavity small signal gain will be monitored to verify that system performance does not deteriorate with time.

2. The performance of components that have completed preliminary development will be evaluated in the closed-loop system.

3. A control technique will be designed and developed for the operation of this closed-loop system. The experience and data derived from the operation of this system will assist in the development of a control system for a possible future full-scale, closed-loop system.

4. The diffuser starting concept and performance will be evaluated in the closed-loop system.

138

System Discussion

The closed-loop GDL test system will be designed for economic as well as technical considerations. The 1-Mw system flowrate should be scaled into the range of a 1/20 to 1/10 scale model to fit existing components. The nozzle and diffuser pressure ratios of the full-scale system should be retained. However, the cavity absolute pressure could be shifted if necessary to improve the flow match of available components. The cavity temperature can be reduced initially to approximately 1200°K to simplify the material/structural requirements and to reduce component expense.

Component test rigs and facility support equipment are available at FRDC that could be combined to provide two-thirds of the major components of the closed-loop test system, as presented in the following paragraphs. However, no single test stand currently exists that contains a combination of these components. Thus, a relatively extensive effort is required to combine this equipment into a single facility. The closed-loop GDL contains six major components:

1. Cavity/Nozzle/Manifold
2. Diffuser
3. Recuperator
4. Heat Sink Heat Exchanger
5. Compressor
6. Heat Source Heat Exchanger.

Equipment is currently available that could be used for four of these components.

Preferably, the cavity/nozzle/manifold would be of the design selected specifically for this application. However, preliminary testing could be started with an existing structural test rig known as the STR 1 with Mod 6 nozzles. This rig contains a single distribution manifold configuration and individual nozzle plates clamped together to provide a 20:1 nozzle area ratio. The support structure would be limited to approximately 30 sec runs at 1200°K and 1.03 MN/m^2 (150 psia) nozzle inlet conditions. This CNM would be used in the closed loop for preliminary tests to evaluate the diffuser starting characteristics and the lasing fluid stability. Fluid stability would be evaluated by conducting successive tests with the same fluid to evaluate the effect of longer run times. It would be preferable to replace this component relatively early in the test program with a CNM of the selected design.

The diffuser system should be the specific configuration that evolves from the diffuser demonstration program to permit the system performance and starting characteristics to be investigated. Thus, no existing diffuser is recommended for this component; but rather the closed-loop investigation would be phased to follow Tasks I and II of the diffuser development program so that the final diffuser evaluation would be performed as a part of the closed-loop testing.

The recuperator function could initially be performed with an existing heat exchanger connected in a reverse flow configuration. A heat exchanger is available manufactured of stainless steel (AISI 347) and containing ≈ 2000 tubes, 34 ft long of 1/4 in. diameter. Material temperatures would be limited to approximately $1115°K$ ($1600°F$) which is consistent with a cavity temperature of approximately $1200°K$. Later in this program, when it is desirable to go to higher temperatures, a recuperator fabricated to the configuration that evolves from the recuperator development program would be substituted for this component.

The heat sink could be provided by another existing stainless steel heat exchanger similar to that utilized for the recuperator. Water would be used in the outer jacket of this heat exchanger to dispose of the waste heat.

The compressor for the test loop could be either of two existing centrifugal compressor rigs. The Small Turbine Advanced Gas Generator (STAGG) compressor rig would provide a flowrate of approximately 5 lb/sec, the flowrate required for a 1/20 scale system. The ST9 compressor rig provides a flow of approximately 15 lb/sec, part of which could be bypassed to provide a 1/10 scale system and to avoid compressor stall. However, prior to selecting either of these compressors, the economics of using a commercially available compressor and drive system should be considered as part of the system design study. The expense of setting up either one of these experimental compressor rigs and a drive system may exceed the cost of an "off-the-shelf" unit that would efficiently perform this function.

The heat source heat exchanger requirement is not easily provided by adapting existing hardware. This component function for the closed-loop test bed can be provided by an electrical resistance heated Inconel tube bank. This type of heater is a relatively simple device that is well within current state-of-the-art technology and would not involve development or a major expense. The tube bank heater will consume 150 to 300 kw of electrical power for a 1/20 to 1/10 scale system. Later in the program, when it is desirable to evaluate a scaled prototype heat source heat exchanger, the resistance heater could be replaced.

It is estimated that the cost to establish a scaled test loop facility and to conduct the initial closed-loop test program would be approximately $3 million over a 3-year period.

Diffuser Development

The variable-geometry GDL diffuser is a significant step forward from the present day fixed geometry diffusers. The high-pressure recovery goal of this diffuser will require active boundary layer control with the boundary layer energized by injected flow. The supersonic diffuser performance is dominated and limited by the ability of the boundary layers to negotiate adverse pressure gradients. Diffuser development normally must use an empirical approach, because the analytical prediction of the boundary layer characteristics is not reliable near the conditions of separation.

The supersonic diffuser for this closed-loop system should be model tested and developed to assure an acceptable performance level. The largest pressure loss in the laser system loop occurs in the diffuser; thus this component has the most significant influence on the compressor horsepower requirement.

140

The closed-cycle, high-recovery, variable-geometry diffuser will require development to achieve an acceptable compromise between the mechanical and aerodynamic requirements to provide:

- Acceptable pressure recovery
- Rapid transition
- High-temperature operation
- No fluid leakage.

Diffuser pressure recovery is enhanced with boundary layer control to inhibit flow separation of the low momentum fluid at the diffuser walls. Scaled tests of the diffuser boundary layer control concept should be performed to optimize the energizing fluid blowing parameters and minimize injection flowrate, determine boundary layer injection location(s), evaluate stability of the boundary layer control concept, and establish the diffuser recovery factor.

The diffuser must be capable of providing a rapid transition during the start cycle that minimizes the time required to "swallow" the starting shock wave and to establish the steady-state flow field. The start cycle is initiated with the lasing loop evacuated so that the pressure ratio of approximately 18 across the nozzle/cavity/diffuser can be established at an upstream absolute pressure level less than the steady-state design pressure. After the starting shock wave is swallowed, the diffuser bypass doors must be closed before the backpressure increases sufficiently to "unstart" the diffuser. This flow transient must be completed in less than 1 sec. The reaching of thermal equilibrium and the stabilization of the absolute pressure level can be achieved at a much slower rate.

The high-temperature operational environment of the diffuser imposes severe structural design problems. The structure has relatively large flat plate surfaces and mating bypass doors that must be restrained to close dimensional accuracy in the presence of both pressure and thermal loading.

A three-Task diffuser demonstration is recommended. (See figure 91.) It is estimated that the cost to perform the first two Tasks of this program would be approximately $1.2 million, including engineering, hardware, facilities, and tests. The cost to conduct Task III is included in the program to investigate the scaled closed-loop GDL system.

Task I - Basic Flow Rig Parametric Evaluation

The goal of this task is to develop boundary layer control and geometry variation techniques to achieve the diffuser pressure recovery levels required for the closed-loop system.

Subscale cold flow tests will be planned and conducted to evaluate approximately nine diffuser boundary layer control configurations that vary control fluid blowing parameters and injection location. A range of blowing parameters shall be studied by varying both injection geometry and flowrate. The test shall be designed to monitor the diffuser recovery factor and stability. The diffuser configuration that provides an optimized system performance as a function of recovery factor, control fluid flowrate, and stability shall be selected for evaluation in the following Task.

141

Task I

Sub Scale Model Test
Steady-State

Evaluate
Blowing Parameter
Flowrate
Injection Location
Stability
Recovery Factor

Control Configuration Selection

Task II

Subscale Model Test
Start Transient
Evaluate
Transient Characteristic
Demonstrate Control
Stability and Repeatability
Recovery Factor

Task III

Closed-Loop Test

Demonstrate
Start Characteristic
Recovery Factor
Stability
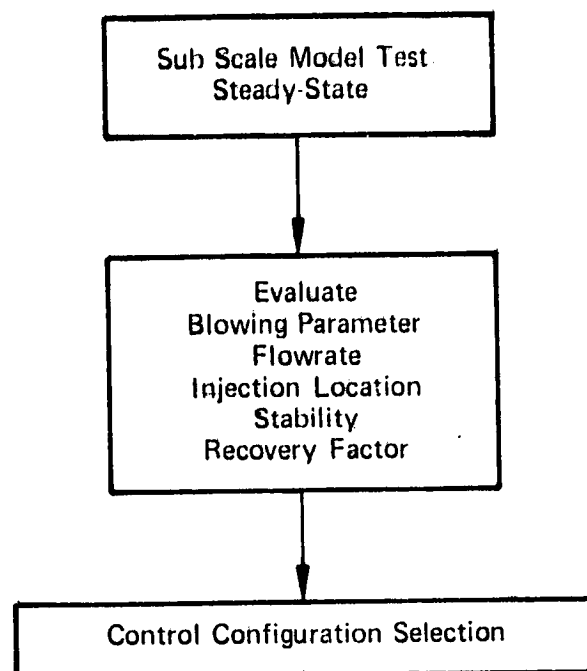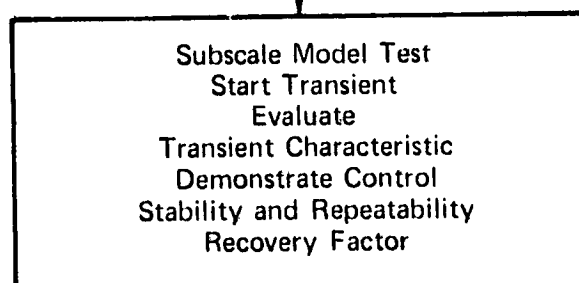
Figure 91. Diffuser Development Program

Task II - Scale Diffuser Evaluation

The goal of this Task is to demonstrate the diffuser configuration developed under Task I in hot flow tests.

A diffuser shall be designed and fabricated that contains the selected boundary layer control configuration and a starting bypass door configuration compatible with the closed-loop system. Hot tests of this diffuser system will be conducted to investigate its transient characteristics. An open-loop test facility will be used which provides a diffuser discharge pressure that simulates the pressure characteristics of the closed-loop start transient. The test program shall be conducted to develop and/or demonstrate:

1. That a system, sequence, and valve schedule has been established that will provide diffuser control

2. That the diffuser transient response rate and bypass door cycle are compatible with the system response
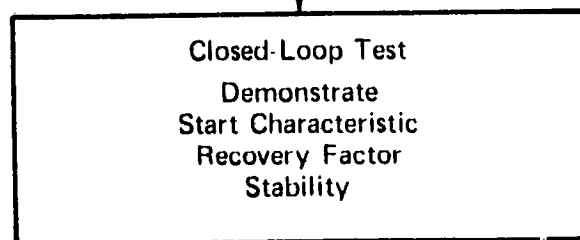
3. That the diffuser system can achieve repeatable and stable operation

4. That the diffuser provides the steady-state recovery factor required for a closed-loop system.

Task III - Scaled Diffuser Closed-Loop Evaluation

The goal of this Task is to demonstrate the operation of the diffuser in the closed-loop GDL device.

The diffuser developed in Task II shall be installed in the closed-loop laser test bed. Tests shall be conducted to demonstrate that the system can be started and steady-state operation established without inducing compressor stall. The diffuser stability and steady-state recovery factor shall be evaluated.

Heat Exchanger and Recuperator Development

The closed-loop system investigated in this study is very dependent on efficient energy transfer via heat exchangers. In fact, heat exchangers comprise three key components of this system, performing vital functions in the heat source, heat rejection, and recuperator. These components have a significant influence on the system performance and represent two-thirds of the laser loop weight for the 1-Mw system. Analysis of compact heat exchanger configurations indicates that the recuperator weight could be reduced by nearly a factor of seven with a fin and plate geometry that exceeds current manufacturing technology. An advancement of this magnitude in compact heat exchanger design would reduce the weight (without degradation of performance) of the system to within the space shuttle payload limit. The attainment of this weight goal has the obvious advantage of system preassembly and transportation to orbit via a single space shuttle flight.

The goal of the heat exchanger/recuperator development program is to investigate advance compact heat exchanger core concepts, determine material compatibility with lasing fluid environmental conditions, select core material, select protective coating if required, and conduct an evaluation of a scaled prototype neat exchanger. This evaluation shall provide data to indicate heat transfer and pressure loss characteristics, physical geometry, weights, and overall component integrity.

Approach

A technology development program is recommended for the heat transfer components. This program is designed to advance the technology of compact heat exchanger concepts and to evaluate the most promising concept in a scaled prototype model evaluation.

This program is oriented primarily for the development of the recuperator since this component has the largest potential for weight reduction; however, the concepts developed for the recuperator would also be applicable to the other heat exchangers in the system.

To improve performance, the trend in compact heat exchanger designs has been to increase the ratio of internal surface area per unit of heat exchanger volume. For example, the recuperator in this study would have a weight reduction from 25,583 to 3,883 kg (56,400 to 8,560 lb$_m$) if the core configuration utilized a 0.005 cm (0.002 in.) fin thickness on a 0.05 cm (0.020 in.) fin spacing. However, a core geometry this small exceeds current state-of-the-art manufacturing practice. (Refer to figure 92, B value ≈ 1350 from Reference 12.) In addition, the recuperator core maximum temperature will approach 1478°K (2200°F) in the lasing fluid environment with a 0.59 MN/m^2 (100 psia) differential pressure. This environment imposes severe restraints on the material selection.

A three-Task program is planned to evaluate the recuperator/heat exchanger technology. (See figure 93.)

Task I - Material Selection

The goal of this task is to select a minimum of two candidate recuperator core materials for further evaluation in Task II.

Candidate core materials will be evaluated to determine their compatibility with the lasing fluid at the core operating temperatures. Candidate core materials evaluated should include (but not be limited to) columbium, TD nickel, TD nickel chrome, and TD NICRALOY. The evaluation will determine thin specimen susceptibility to nitrogen embrittlement, oxidation, and corrosion. In the event of material degradation in this environment, protective material coatings will be evaluated by similar tests of coated specimens. Material coating techniques will be limited to those concepts that can be applied to the recuperator core configuration. For example, most slurry coating application techniques are not compatible with the small passages and sharp radii encountered in the fin configuration of compact heat exchangers, although gas passivation and fluid application techniques can be compatible.

144
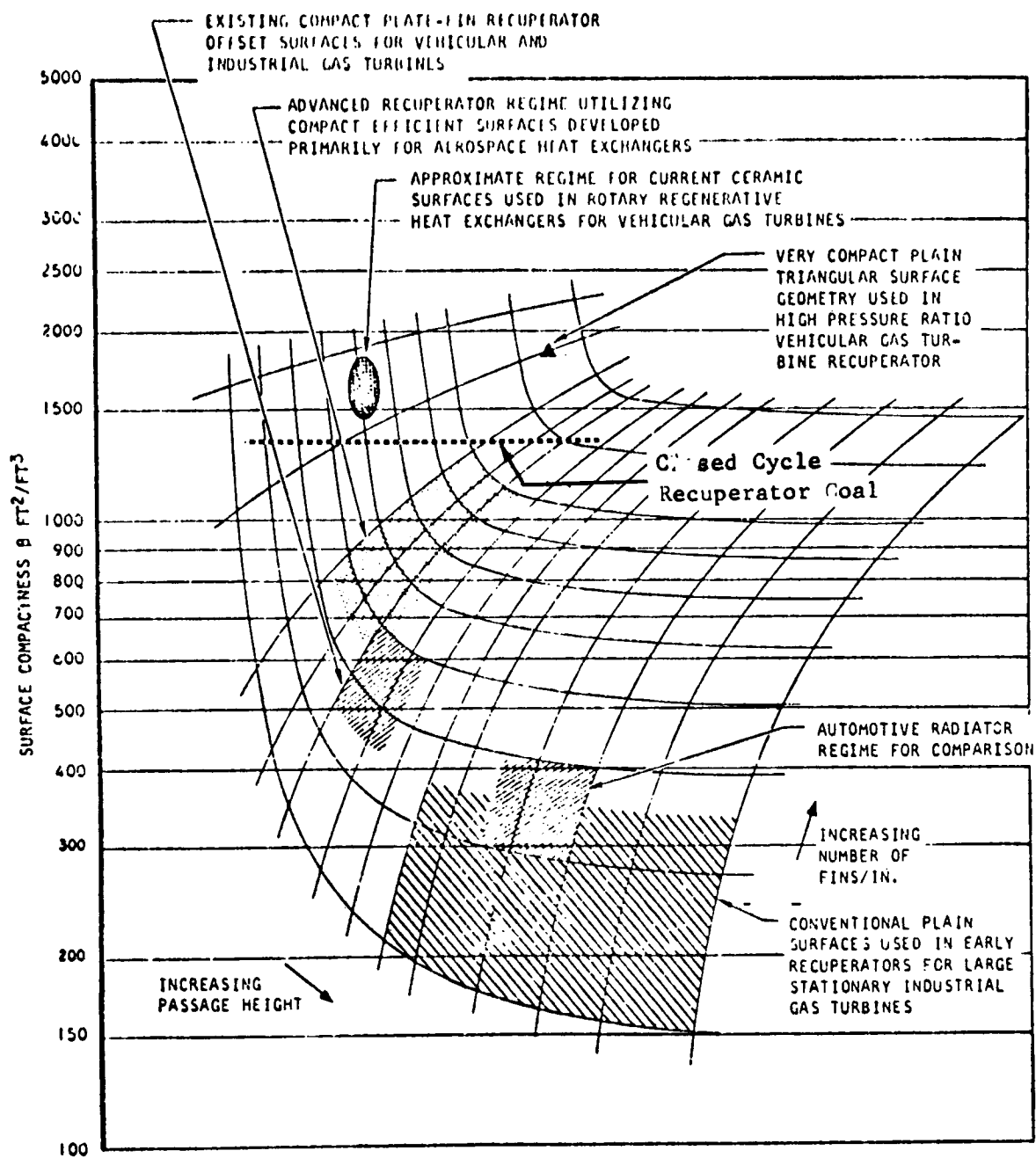
Heat exchanger surface compactness spec-
trum for plate-fin recuperator geometries

Figure 92. Recuperator Compactness

145

Task I

Core Material and Coating Evaluation and Selection

Select Candidate Core Materials

Manufacture Thinwall Specimens:

Columbium
TD Ni
TD NiCr
TD Nicraloy
Material - A
Material - B

Coat Specimens

Nitrogen
Embrittlement
Test

Oxidation
Corrosion
Test

Stress-Rupture Life Evaluation:
Metallurgical and Weight Examination

Material Selection
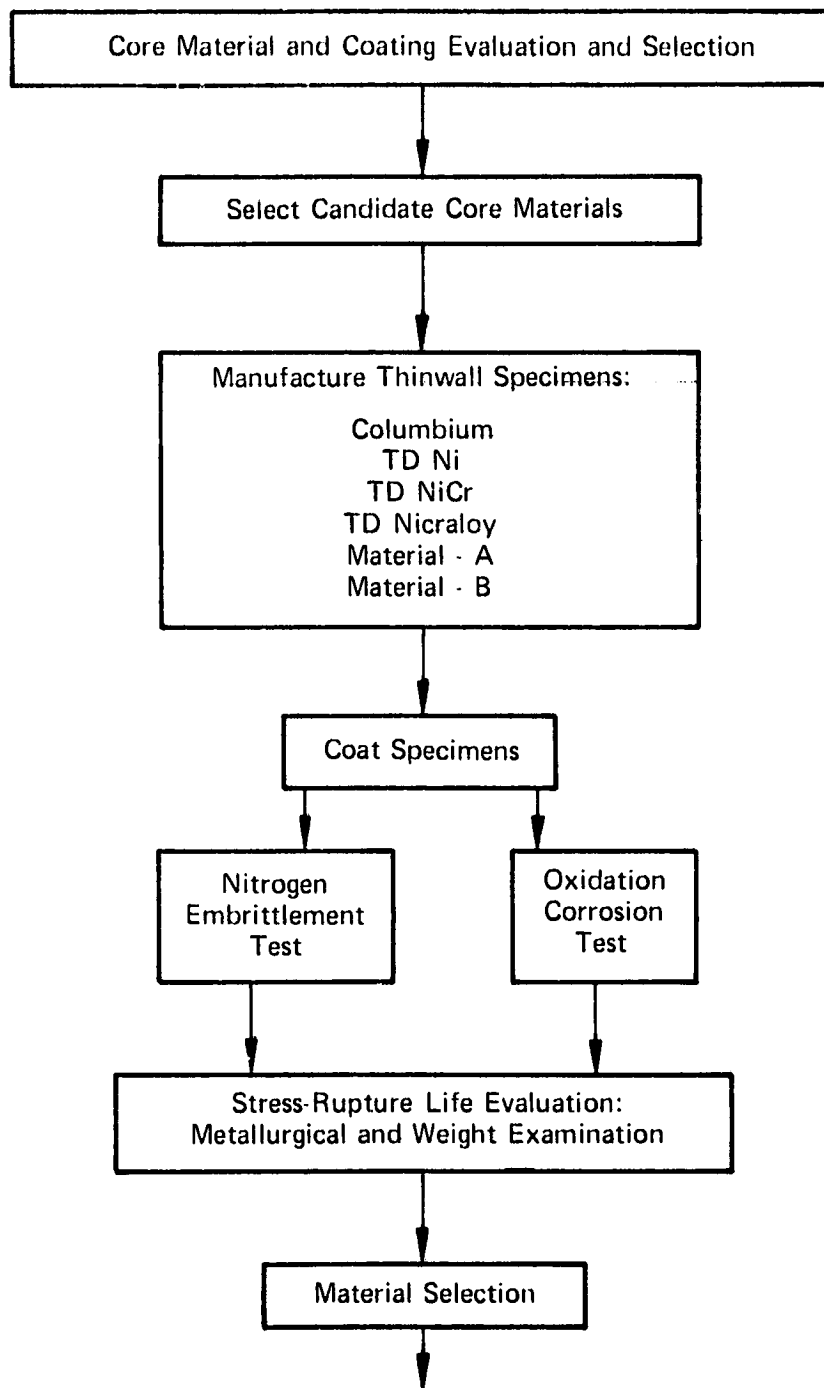
Figure 93. Recuperator Development (Sheet 1 of 2)

Task II

Baseline Core Configuration:

Experimental Fabrication Study and
Definition of Minimum geometry

Design and Fabricate Core Configurations
With Porous Metal Matrix

Candidate Matrix Includes:

Feltmetal
Woven Mesh
Sintered Power Metal
Sintered Metal Chips

Core Specimen Testing

Thermal Effectiveness, Pressure Loss, Physical Properties

Data Correlation and Selection

Baseline and Advance Cores

Task III

Scaled Prototype Recuperator:
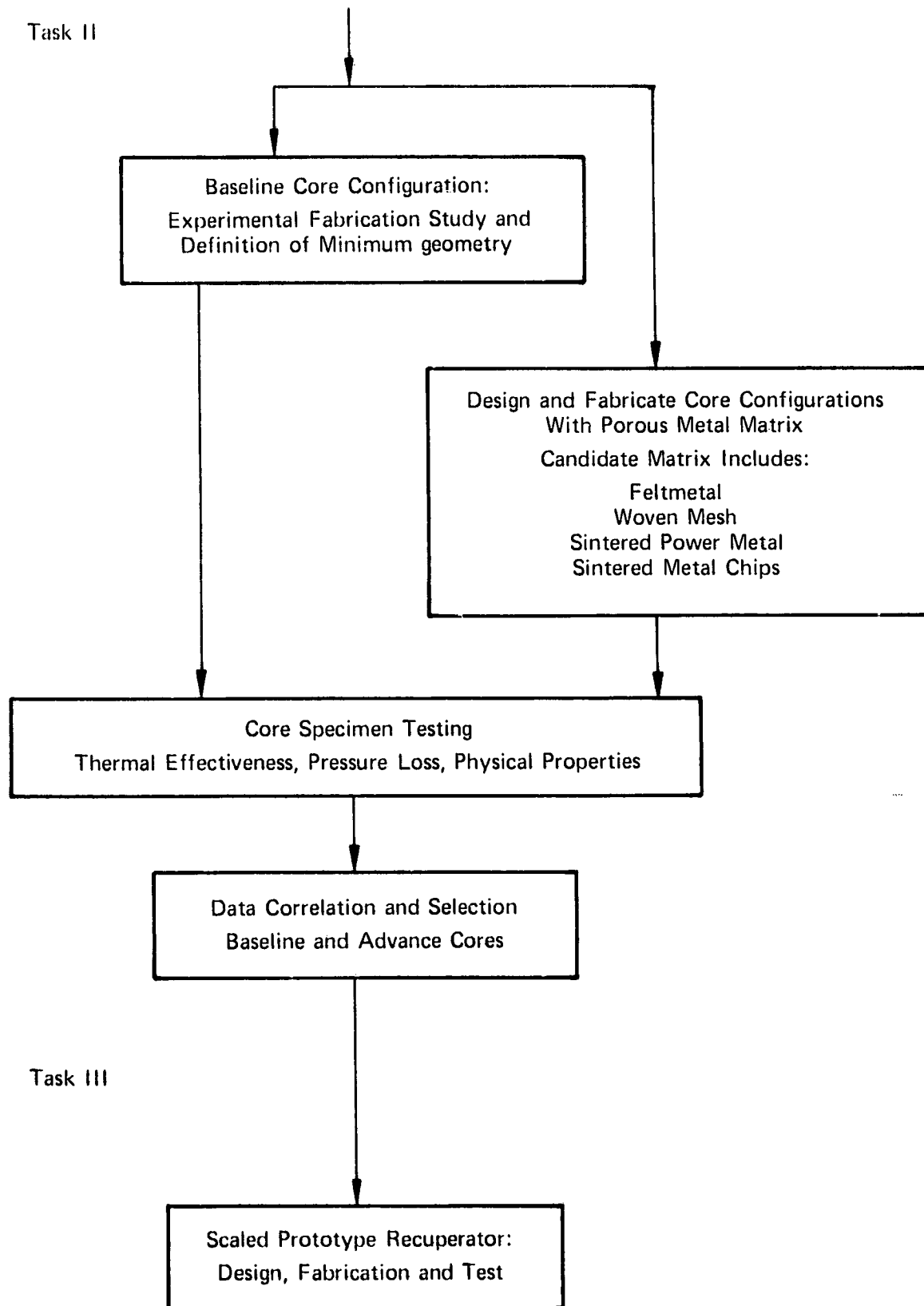
Design, Fabrication and Test

Figure 93. Recuperator Development (Sheet 2 of 2)

The candidate materials, with and without coatings, •... be ranked relative to their ability to withstand degradation in operational environment exposure tests. The criteria for defining material degradation will be based on metallurgical examination, loss of weight, and stress rupture life.

Task Ii - Recuperator Core Development and Substantiation

The goal of this task is to screen several candidate recuperator core configurations and to select the best configuration for this application based on performance, weight, size, and integrity.

Basically, the recuperator core consists of the conventional plate and fin configuration. This geometry consists of a matrix of plates that form intermittent layers separating two fluids. The surface area of each plate is effectively extended by a fin consisting of a thin sheet folded parallel to the flow direction and attached to adjacent plates. (See figure 94a.) A compact heat exchanger incorporates a heat-transfer surface having a high area density per unit of volume. Core compactness can be increased by reducing fin thickness and spacing until a fabrication or strength limitation is approached. Thus, the core compactness of this conventional core configuration should be experimentally evaluated considering the material restriction defined in Task I.

Advancements in core compactness should also be investigated. The trend to advance compactness by increased area density per unit volume suggests that the next generation in recuperator core technology may be possible by replacing the folded fin concept with a porous metal matrix bonded between the plates. (See figure 94b.) Candidate metal matrices are feltmetal, woven meshes, sintered power metal, and sintered metal chips. The manufacture of these matrices can be varied to control porosity, Reference 13.

The design and fabrication feasibility study would perform the following recuperator core configuration investigation.

(1)   Baseline Evaluation

Using the best two materials selected in Task I, conduct design and experimental fabrication studies to determine the minimum core geometry practical for the conventional plate and fin configuration. Construct core specimens and demonstrate, by way of heat transfer tests, the core thermal effectiveness, pressure loss coefficient, and physical characteristics of the core.

(2)   Advanced Concept Evaluation

Design and fabricate core configurations using porous metal matrices of approximately 6 to 12 configurations that in theory offer potential advancement in core compactness and performance. Subject core specimens of each configuration to identical heat transfer tests conducted on the conventional core, as described in previous paragraph.

148
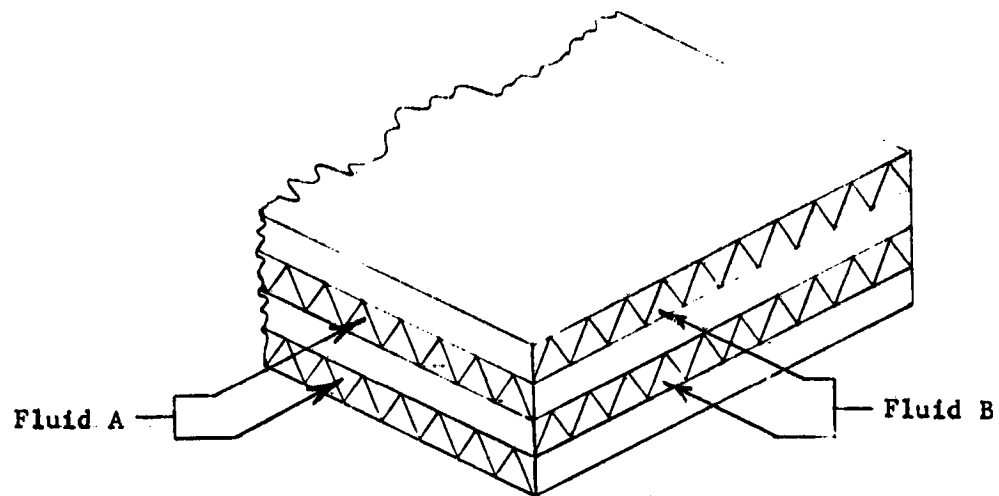
a. Conventional Plate/Folded-Fin Configuration
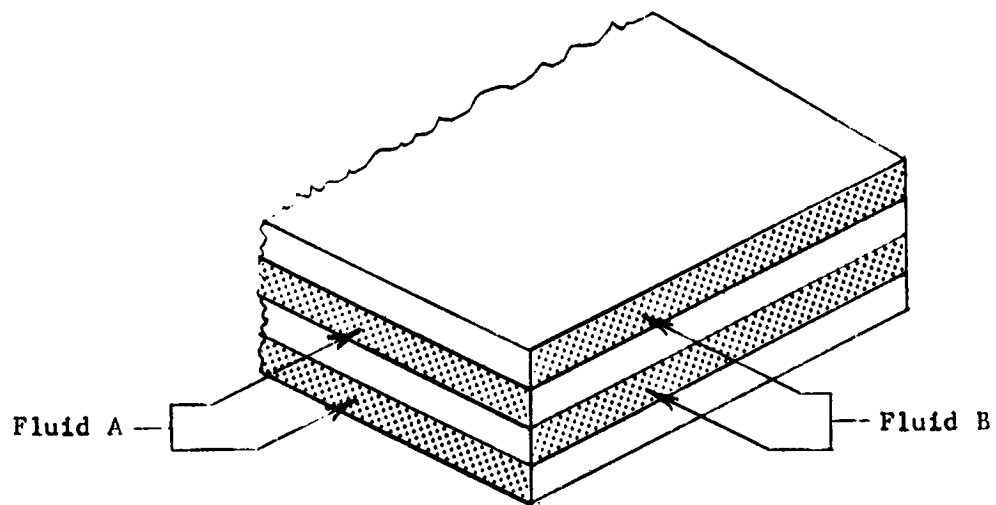
b. Plate/Porous Material Configuration

Figure 94. Recuperator Core Surface Geometries

(3)   Concept Correlation

Correlate merits of baseline and advance core specimens based on thermal effectiveness, pressure loss, compactness, weight, volume, and structural integrity. Recommend a concept most compatible with laser system requirements for scaled prototype evaluation.

Task III - Scaled Prototype Recuperator

The goal of this task is to design, fabricate, and test a scaled recuperator using the core configuration selected in the preceding task.

Based on a scale factor selected for the closed-loop cycle GDL investigation, the design of a prototype recuperator will be performed. The design performance parameters for the recuperator will be defined from the design table established for the scaled closed-loop GDL system. The design will use the same core thermal effectiveness, pressure loss coefficient, material, configuration, and manufacturing technique that would be utilized for full-scale prototype manufacture. Thus, the core flow area is scaled without scaling the core configuration or altering the heat transfer and fluid transport characteristics.

The recuperator will be manufactured and tested as a component of the scaled closed-loop GDL test unit. Data will be taken to determine thermal effectiveness, pressure loss coefficient, and transient thermal response.

It is estimated that the cost to perform this three-Task program would be approximately $600,000. This estimate is based on performing the Task III design of the scaled prototype recuperator in this recuperator development program. The expense of the fabrication and testing of the recuperator is included in the program to investigate the scaled closed-loop GDL system.

Cavity Optics

A cavity optics system could be designed based on present state-of-the-art technology but would be heavy, complex, and of questionable durability in a space environment. To improve the optics system significantly, several areas of technology development are required, including (1) mirror substrate, (2) optical coating, (3) alignment system, and (4) thermal control system. Suggested programs to develop and demonstrate technology in the areas mentioned above are given in the following paragraphs.

Mirror Substrate

Lighter weight, optically stable material development for mirrors will relax alignment system and thermal control system requirements. Technology development in this area is currently in progress under both independently funded and Government-funded programs. The emphasis of such a program based on the closed-cavity GDL requirements would be placed on manufacturing integral alignment and thermal control elements. Material such as SiC and graphite-epoxy composite are attractive candidates because of their high stiffness (for optical stability) and lightweight characteristics.

150

A technology confirmation program for mirror substrates would consist of:

1. Candidate Material Review
2. Optimum Material Selection
3. Manufacturing Technology Development and Demonstration
4. Performance Testing

   a. Optical Finishing Quality
   b. Thermally Induced Distortion
   c. Long-Term Structural Stability
   d. Environmental Durability.

Optical Coatings

Existing optical coatings have exhibited high reflectivities in the range of 99.8% under moderate flux levels. It is anticipated that current technology efforts will improve reflectivity to above 99.8% and will result in development of a coating suitable for high flux level operation. The emphasis for the closed-cycle GDL technology confirmation program would be to evaluate candidate coatings for durability when exposed to long-term storage in a space environment. Although coating reflectivity will reach such a level that active cooling during operation would appear unnecessary, the slightest defect (either inherent or externally inflicted) will result in increased absorption and local heating. It is imperative that any such local heating be accommodated by the thermal control system to prevent progressive destruction of the mirror. Design performance of the thermal control system is consequently set by this requirement.

Testing of candidate optical coatings would include:

1. Reflectivity (gross)
2. Scatter
3. Flux Level Tolerance
4. Thermal Cycle Durability
5. Abration Resistance
6. Degradation Due to Space Vacuum
7. Environmental Temperature Limits
8. Compatibility With Substrate.

Alignment System

The mirror alignment system is based on sensing the spatial error between points on the mirror and a reference surface. Present technology development effort towards deformable mirrors (COAT system) should provide sufficient technology fallout to design adequate actuator and electronic signal processing components. Error sensing and structural design demonstrations are required. A breadboard design should be adequate for experimental technology confirmation.

The alignment system development program would consist of the following tasks:

1. Literature search for candidate optical waveguides, photo sensors, optical transponders, electronics, etc.

2. Selection of components to be tested in a breadboard system

3. Hardware design of a breadboard system

4. Procurement of components

5. Assembly

6. Testing.

Design and testing of the breadboard system is envisioned to consist of driving an optical transponder to simulate the vibration and structural displacements of the laser cavity. A subscale alignment system bench supported by piezoelectric actuators would follow the perturbations of the transponder based on electronic processing of the spatial error signal generated by optical sensors attached to the bench. Similar optical components would link a second transponder to the system bench to simulate a mirror. This second transponder would be actively positioned by its own actuator, and its ability to follow the perturbations of the initial transponder would be assessed.

Environmental and life cycle tests of all candidate components would be included.

Thermal Conditioning System

The development of a solid-state thermal conditioning system for the mirrors will require improved flux level capability for thermoelectric elements. An investigation of various material combinations for conductor junctions should result in improved performance. The greatest gains are anticipated by development of a combination of heat pipe and thermoelectric techniques. The heat pipe has the capability to receive high flux levels over a small area and to distribute it at a low flux level over a large area.

Technology development would proceed as follows:

1. Conceptual Design Study
2. Experimental Design, Construction, and Testing of Samples
3. Prototype Mirror Design and Construction
4. Prototype Mirror Testing:
    a. Flux Capability
    b. Cyclic and Storage Life
    c. Environmental Durability.

152

DISCUSSION OF RESULTS

The Task I parametric optimization involved the use of generalized mathematical models of components to determine the effect of their design parameters on the overall GDL system performance. The primary goal of Task I was to select an efficient thermodynamic cycle with acceptable physical characteristics based on a first approximation of component weight and size. In Task II, an extensive physical evaluation of the selected thermodynamic cycle was performed to more accurately assess component weight, size, and configuration. Refinement to the thermodynamic cycle analysis to reflect the additional definition provided by the Task II conceptual design is normally accomplished during a subsequent Preliminary Design task. Although the scope of this program did not include a Preliminary Design, some of the results from the conceptual design impacted the selected cycle and are discussed in the following paragraphs.

The compressor characterization used in the Task I parametric optimization was originally established for a high temperature, uncooled, ceramic design with an efficiency level of 85%. The selection of the recuperator cycle with its low compressor temperature requirements eliminated the need for this advanced technology design. Instead, an uncooled, metallic, state-of-the-art compressor was used, which resulted in a compressor design with an efficiency level of approximately 90%. However, the use of air bearings in this design resulted in a 5% flow recirculation with a corresponding horsepower penalty of 5%.

The recuperator characterization used in the Task I parametric optimization had equal flow areas on the hot and cold sides. This resulted in a very low Mach number and pressure loss for the cold side. Results from Task II indicated that this type of design produced a large and heavy recuperator, which dominated the complete laser loop system weight, causing it to exceed the Space Shuttle capacity. A recuperator design with equal Mach numbers into the hot and cold sides results in a smaller package, but a larger pressure loss with increased compressor horsepower requirements.

The revised compressor efficiency and redesigned recuperator were incorporated into the system model to determine the net effect on the total system. A comparison between the revised cycle and the one from Task I is presented in table XXIII, with the impact on the 5 and 10 mw loop weights also shown.

The redesigned recuperator is approximately 39% smaller and lighter, resulting in a total laser loop weight reduction of approximately 20%. This is not enough to allow the entire closed-loop, fully charged and assembled, to be transported into orbit in one Space Shuttle trip; however, use of a more light-weight, closely spaced, plate-fin configuration, as described in the Task II conceptual design, might make this possible.

The effect of the increased compressor efficiency is more than offset by the air bearing and the increased recuperator pressure losses. The result is an increase in compressor horsepower requirements of 3%.

The increased power requirement and the decreased laser loop weight combined to result in total system weight decrease of less than 0.5%.

Table XXIII. Comparison of Baseline Recuperator Cycle
With Revised Task II Cycle

	Baseline Recuperator Cycle From Task 1	Revised Recuperator Cycle With Task II Results
Compressor Efficiency, %	0.852	0.908
Recuperator Total ΔP, %	5.9	9.8
Recuperator Weight, kg (lb$_m$)	25,583 (56,400)	15,717 (34,650)
Recuperator Volume, m^3 (ft^3)	11.3 (400)	6.9 (245)
Compressor Horsepower, kw (hp)	8,800 (11,801)	9,053 (12,140)
Laser Loop Weight, kg (lb$_m$)	48,534 (107,000)	38,669 (85,250)
Total System Weight, kg (lb$_m$)	317,515 (700,000)	316,154 (697,000)
5 mw Laser Weight, kg (lb$_m$)	233,759 (515,350)	186,100 (410,850)
10 mw Laser Weight, kg (lb$_m$)	538,065 (1,186,230)	428,700 (946,070)

CONCLUSIONS AND RECOMMENDATIONS

Based on the results of the closed-cycle GDL study, the following conclusions have been reached:

1.   The closed-cycle GDL concept that incorporates a recuperator
      and supplemental heat source results in the smallest and
      lightest overall system, when the prime mover and heat sink
      are considered, and is, therefore, the most attractive for both
      the space and airborne applications.

2.   Because the compressor power source and space radiator are
      the dominant factors in the overall system weight and volume,
      any improvements in component or system performance that
      reduce compressor horsepower or heat sink requirements
      will pay large dividends.

3.   The space application will require multiple space shuttle
      flights and assembly in space. The airborne system, using
      the closed cycle developed in this study, will be limited to
      less than the 2 megawatt power level with the C-5A as a carrier.
      However, alternate approaches, such as the following, might
      be considered to improve system power:

      a.   In the recuperator closed-cycle GDL system, 85% of
            the loop weight is contained in the diffuser and heat
            transfer components. Significant weight reductions
            should be possible by advancing heat exchanger tech-
            nology and investigating a lighter weight diffuser
            structure.

154

b. The complete airborne system, including a well de-fined prime mover, should be optimized by varying the degree of recuperation, to arrive at a minimum system weight and volume.

c. The open-loop multistage bireactant (i.e., only two reactants, N_2O and a hydrocarbon fuel, are used) GDL should be considered. The high specific power obtained with this concept may make it an attractive alternative.

Conclusions

To permit a more in-depth evaluation of the closed-cycle GDL as a candidate for the NASA power transmission applications, the following efforts are recom-mended:

1. Initiate the diffuser technology development and closed-cycle demonstration programs outlined in the Technology Confirma-tion section.

2. Investigate through more-detailed studies the alternate approaches for the airborne system discussed above.

DEFINITION OF SYMBOLS

A	Area, cm^2, m^2 ($in.^2$, ft^2)
a	Beam radius, cm (in.)
AF	Frontal area, m^2 (ft^2)
BD	Beam diameter, cm (in.)
CNM	Cavity/nozzle/manifold
D	Diameter, cm (in.)
d	Diameter, cm (in., ft)
D	Dimensional
GC	Geometric coupling
H	Height, cm (ft)
HP.	Horsepower or power, kw (hp)
K	Specific power, kw/kg/s ($kw/lb_m/sec$)
L	Length, cm, m (in., ft)
M	Mach number
M	Magnification
N	Speed, rad/s (rpm)
n	Nondimensional far-field radius
NEP	Nozzle exit plane
P	Power, Mw, kw (hp)
P	Pressure, MN/M^2 (psi)
Pr	Pressure ratio
Q	Heat flowrate, kw (Btu/sec)
R	Range, (m)
r	Radius, cm (in.)
T	Temperature, °K (°R)
UO	Unstable oscillator
Vol	Volume, m^3 (ft^3)
W	Weight, kg (lb_m)
$\dot{W}$	Flowrate, kg/s (lb_m/sec)
X	Gas composition mole ratio
Δ	Differential increment
δ	Total pressure ratio to standard sea level
ϵ	Nozzle area ratio

156

Subscripts

η	Efficiency
θ	Temperature ratio to standard sea level
λ	Wavelength
B	Beam
c	Cavity
c	Compressor
eff	Effective
HS.	Heat source
HS	Heat sink
i	Inside
o	Outside
ps	Power source
surf	Surface
T	Total
t	Throat
1	Inlet
2	Exit

REFERENCES

1. "Closed Cycle Development Program Diffuser Development, Materials Evaluation and Gas Composition Effects," The Boeing Company Program, Code No. 9E30, Period of Report, 1 August 1969 to 31 May 1970.

2. Mackay, D. B., Design of Space Powerplants, 1st ed, 1963.

3. Glassman, A. J. and W. L. Stewart, "Thermodynamic Characteristics of Brayton Cycles for Space Power," J. Spacecraft, Vol 1, No. 1, January 1964.

4. Kays & London, Compact Heat Exchangers.

5. Kerwin, P. J., "Analysis of a 35 to 150 kw Brayton Power Conversion Module for Use with an Advanced Nuclear Reactor," NASA TN-DG52S, September 1971.

6. Zumpano, F. R., "High Aspect Ratio Supersonic Diffusers for Gas Dynamic Laser Systems," Report N213757-1, December 1974 (Proprietary)

7. Walowit, Murray, McCabe, Arwar and Mayer, "Gas Lubricated Foil Bearing Technology Development for Propulsion and Power Systems," Technical Report AFAPL-TR-73-92, December 1973. Air Force Aero Propulsion Laboratory.

8. Cheatham, J. B., J. D. Smith, and D. L. Wright, "Single-Stage Experimental Evaluation of Low Aspect Ratio, Highly Loaded Blading for Compressors," Part IX Final Report, Stage F and Stage G, Vol I, Contract NAS3-11158 NASA CR-134993-4.

9. Reddecliff, "Silicon Nitride Ball Bearing Demonstration Test," May 1975, Naval Air Propulsion Test Center, Contract N00140-75-C-0382.

10. Moskowitz and Ezekiel, "Non-Wearing Ferrofluidic Seals," September 1975, SAE 750851.

11. Pattee, H. E., "High-Temperature Brazing," Bulletin No. 187, September 1973, Welding Research Council.

12. McDonald, "Gas Turbine Recuperator Technology Advancements," ASME publication 72-GT-32.

13. Rannie, J. B., "Investigation of Methods for Transpiration Cooling Liquid Rocket Chambers," NASA Final Report, Contract NAS8-21135, conducted by Pratt & Whitney Aircraft.